N° d'ordre: 2021LYSE1004 Année 2021

THESE EN COTUTELLE

en vue de l'obtention des grades de

DOCTEUR DE L'UNIVERSITE DE LYON

ET

DOCTEUR EN SCIENCES DE L'INGENIEUR DE L'UNIVERSITE DE LIEGE

soutenue publiquement le 07 01 2021

par

Mr Francesco Lorenzo GALUPPO

Design, optimization and control by condensation pressure manipulation of an ORC based waste heat recovery system in heavy-duty trucks

devant le jury composé de

Mr	Pierre DEWALEFF,	Examinateur, Prof., Univ. de Liège
Mr	Pascal DUFOUR,	Directeur de thèse, Maître de Conférences, Univ. Lyon 1
Mr	Lars ERIKSSON,	Rapporteur, Prof., Linköping Univ.
Mr	Sotirios KARELLAS,	Rapporteur, Prof., National Technical Univ. of Athens
Mr	Vincent LEMORT,	Directeur de thèse, Prof., Univ. de Liège
Mme	Céline MORIN,	Examinateur, Professeur, Univ. Polytechnique Hauts- de-France
Mme	Melaz TAYAKOUT-FAYOLLE,	Examinateur, Prof., Univ. Lyon 1
Mme	Alina VODA,	Examinateur, Maître de Conférences, Univ. Grenoble Alpes

et en présence de

Mme	Madiha NADRI WOLF,	Membre invité, co-directeur de thèse, Univ. Lyon 1
Mr	Thomas REICHE,	Membre invité, Encadrant VOLVO GTT, Lyon

Abstract

The new European regulation about the CO_2 emissions of long-haul heavy duty trucks pushed the manufacturers to study and implement solutions that can limit the CO_2 emissions by reducing the fuel consumption of the vehicle. Considering the limited efficiency of the internal combustion engines and the thermal losses that are encountered, the waste heat recovery technologies have gained much interest in the heavy-duty trucks industry; in particular thermodynamic bottoming cycles, as the Organic Rankine cycle, are considered suitable to reduce the fuel consumption and, consequently, the CO_2 emissions. However, several obstacles are encountered in the implementation of a safe system that can ensure high standards of performance as long as possible, reducing the total cost of ownership of the vehicle. In the last decade, a large scientific community studied intensely this topic related to the working fluid selection, component modeling and testing, control and optimization. Another important aspect of this application derives from the fact that the heat is recovered from an heat source characterized by a transient behavior. This is taken into account in the system architecture definition, as well as in the implementation of suitable control strategies, intended to the maximization of the performance.
In this thesis the exhaust gas and the engine coolant flow are investigated as heat sources; in both cases modeling and control strategies are implemented, in the latter an experimental campaign is performed. Although the heat source is often considered as the main secondary fluid in the Rankine system, the heat sink is often characterized by a transient behavior as well, that can limit the performance of the system and pushes to further control development in the cold side of the system. In this thesis, the control problems related to the working fluid conditions at the inlet of the expander (the controlled variable is called superheat) and the pump (the controlled variable is called subcooling) are addressed, studying the dynamics of the evaporator and condenser, in specific selected operating points, chosen by means of a specific algorithm (published in Galuppo et al. 2018a). For both the heat sources that have been analyzed, the manipulation of the condensation pressure is shown to be not only recommendable, but it is necessary, in order to ensure component safety and high standards of performance of the system. The utilization of the condensation pressure as and additional manipulated variable leads to the definition of a MISO (Multiple Input Single Output) problem to control the subcooling at the inlet of the pump and, consequently, to improve performance (published in Galuppo et al. 2021). Another potential control improvement is identified in the utilization of a deep neural network, trained on-line, to replace the weighting estimators and determine, in an adaptive way, a representative model to design the controller (published in Peralez et al. 2020).

Keywords

Waste heat recovery, Organic Rankine cycle, automotive, modeling, operating points selection, model-based control, weighting estimators, condensation pressure manipulation, model-based real-time optimization, artificial intelligence.

Scientific and technical production issued from the thesis

1 article in international journal with review committee

- Galuppo, F., Reiche, T., Lemort, V., Dufour, P., Nadri, M. (2020). Organic Rankine cycle based waste heat recovery modeling and control of the low pressure side using direct condensation and dedicated fans. *Energy*, 119074, Vol. 216, 2021.

4 international conferences with review committee and proceedings

- Galuppo, F., Dufour, P., Nadri, M., Reiche, T., and Lemort, V. (2018a). Experiment Design for Waste Heat Recovery Modeling in Heavy Duty Trucks. *Proceedings IFAC AAC*, 51(31):726–731, Changchun, China, sept. 20-22, 2018.
- Galuppo, F., Nadri, M., Dufour, P., Reiche, T., and Lemort, V. (2019b). Evaluation of a Coupled Organic Rankine Cycle Mild Hybrid Architecture for Long-Haul Heavy-Duty Truck. *Proceedings IFAC E-CoSM'18*, 52(5):478–483, Orléans, France, june 23-27, 2018.
- Galuppo, F., Lemort, V., Nadri, M., Dufour, P., and Reiche, T. (2019a). Assessment of Rankine Waste Heat Recovery Potential on Heavy Duty Trucks Using Direct Condensation. *Proceedings of the 5th International Seminar on ORC Power Systems*, 1(36):1–10, Athens, Greece, sept 9-11, 2019.
- Peralez, J., Galuppo, F., Dufour, P., Wolf, C.,and Nadri, M.. (2020). Data-driven multi-model control for a waste heat recovery system. *59th IEEE Conference on Decision and Control (CDC)*, Jeju Island, Republic of Korea, pp. 5501-5506, 2020.

2 international workshops

- Galuppo, F., Reiche, T., Lemort, V., Dufour, P., Nadri, M., Galuppo, F., Reiche, T., Lemort, V., Dufour, P., Nadri, M., Galuppo, F., Reiche, T., Lemort, V., Dufour, P., Nadri, M., and Huin, X. (2018b). Waste heat recovery (WHR) assessment in complete

truck simulation environment. *Proceedings SIA Powertrain*, Rouen, France, may 16-17, 2018

- T. Reiche, F. Galuppo, N. Espinosa (2018), Waste Heat Recovery Potential on Heavy Duty Long Haul Trucks – A Comparison, *Energy and Thermal Management, Air-Conditioning, and Waste Heat Utilization, 2nd ETA Conference, November 22-23, 2018, Berlin, Germany, 141-153*

Nomenclature

Acronyms

AI Artificial intelligence

BDC Bottom dead center

BTE Break thermal efficiency

CaC Charge air cooler

CC Colchester

CO Cut-off ratio

CO_2 Carbon dioxide

CRF Capital recovery cost

CV Controlled variable

$EATS$ Exhaust after treatment system

ECU Electronic control unit

EGR Exhaust gas recirculation

EPC Electricity production cost

FB Feedback

FF Feedforward

FK Frankfurt-Koblenz

$FOFOPTD$ First order plus first order plus time delay

$FOPTD$ First order plus time delay

FV Finite volume

GHG Greenhouse gases

GWP Global warming potential

$HCFC$ Hydrochlorofluorocarbures

HD Heavy duty

HEX Heat exchanger

HT High Temperature

HTC Heat transfer coefficient ($\mathrm{W/m^2}/K$)

IAE Integrated absolute error

IBC Inverted Brayton cycle

ICE Internal combustion engine

IMC Internal model control

ISE Integral squared error

$LCAPECs$ Life-cycle air pollution externality costs

$LCCs$ Life-cycle costs

LCG Lyon-Chambery-Goncelin

$LCGHGs$ Life-cycle greenhouse gases

LT Low Temperature

$MISO$ Multiple input single output

$MMPID$ Multi model based proportional integral derivative

MPC Model predictive controller

MV Manipulated variable

$NMPC$ Non-linear model predictive control

$NPSH$ Net positive suction head

NTU Number of transfer unit

ODP Ozone depletion potential

ORC Organic Rankine cycle

PID Proportional integral derivative

PP Pinch point (K)

PR Pressure ratio

PTO Power take-off

RAM Ram Air intake

RTO Real time optimization

SH Superheat

$SISO$ Single input single output

SO Second order

SP Set point

TCO Total cost of ownership

TDC Top dead center

TEG Thermo-electrical generators

TV Total variation

US United States

Greek letters

α Heat transfer coefficient ($W/m^2/K$)

β Density of the heat transfer surface area (m^2/m^3)
ϵ Effectiveness ($-$)
η Efficiency ($-$)
λ Heat conductivity ($W/m/K$)
μ Dynamic viscosity ($Pa.s$)
Ω Engine speed (rpm)
ω Angular velocity (rad/s)
ϕ Pump speed reduction factor (-)
ρ Density (kg/m^3)
σ Standard deviation
τ Time constant (s)
τ_c SIMC tuning parameter($-$)
θ Lag (s)
ε Heat exchanger efficiency ($-$)
T Torque ($N.m$)

Latin letters

$\dot{m}$ Mass flow (kg/s)
$\dot{Q}$ Heat flow rate (W)
$\dot{V}$ Volume flow rate (L/s)
$\dot{W}$ Power (W)
A_c Minimum flow area (m^2)
C Pump displacement (m^3)
C_c Cubic capacity (m^3)
c_p Specific heat ($J/kg/K$)
D_h Hydraulic diameter (m)
E Energy (J)
e Modeling error ($-$)
f Friction factor ($-$)
F_p Fin pitch (m^2)
G Static gain ($-$)
H Enthalpy (J)
h Specific enthalpy (J/kg)
J cost function ($-$)
j Colburn number ($-$)
K_p Proportional gain ($-$)
K_{eq} Equivalent throat diameter (m^2)
L_p Louver pitch (m^2)
M Mass (kg)
N Rotational speed (rpm)
N_{vol} Number of volumes (-)
Nu Nusselt number ($-$)
p Pressure (Pa)
p_{red} Reduced pressure ($-$)
Pr Prandtl number ($-$)
q Quality ($-$)
Re Reynolds number ($-$)
s Entropy ($J/kg/K$)
T Temperature (K)
t Time (s)
$T0$ Ambient temperature (K)
T_i Integral time ($-$)
U Internal energy (J)
u Input ($-$)
u_c Velocity in the minimum flow area (m/s)
U_{fluid} Fluid heat transfer coefficient ($\frac{W}{m^2K}$)
U_{gas} Gas heat transfer coefficient ($\frac{W}{m^2K}$)
U_{glob} Global heat transfer coefficient ($\frac{W}{m^2K}$)
V Volume (m^3)
v Speed (m/s)
w Weight ($-$)
x State ($-$)
y Output ($-$)

Subscripts

2Φ Two phase state
air Air
amb Ambient
bay Bayesian
$brake$ Brake
C Cold
c Controller
$cond$ Condensation
$conv$ Convection
$coolpack$ Cooling package
$cool$ Coolant
$cooler$ Cooler
$cross$ Cross section
$cycle$ Cycle
dev Developed
eff Effective
egr EGR gas
$elec$ Electrical
eng Engine
eq Equivalent

ev	Evaporator	min	Minimum
ex	Exit	out	Output
exh	Exhaust gas	p	Plant
exp	Expander	pot	Potential
$expe$	Experimental	$pump$	Pump
ext	External wall	rec	Recovery
f	Working fluid	sat	Saturation
fan	Cooling fan	sim	Simulated
$filt$	Filter	sp	Single phase
$heat$	Heat source	su	Suction
in	Input	th	Theoretical
int	Internal wall	$turb$	Turbine
is	Isentropic	vap	Vapor state
k	Current time	veh	Vehicle
kin	Kinetic	vol	Volumetric
liq	Liquid state	w	Heat exchanger wall
max	Maximum	wf	Working fluid

List of Figures

Acknowledgements

This cotutelle PhD thesis is a collaboration between:

- Laboratoire d'Automatique de Génie des Procédés et de Génie Pharmaceutique (LAGEPP) UMR 5007 CNRS-UCBL1, 43 boulevard du 11 Novembre, 69100 Villeurbanne, France
- LABOTHAP, University of Liege, Campus du Sart Tilman Bat. B49, B4000 Liege, Belgium
- Volvo Trucks Group Trucks Technology, 1 av Henri Germain 69800 Saint Priest, France

The French ministry of higher education and research is acknowledged for the financial support of this CIFRE PhD thesis 2016/1205.

Personal acknowledgments

I would like to thank firstly my supervisors for the patience, support and time that they dedicated to me: Pascal Dufour and Madiha Nadri from the University of Lyon 1, Vincent Lemort from the University of Liege and Thomas Reiche from Volvo. All contributed in a massive way to the success of this work and they taught me a lot about technical aspects, commitment and methodology. During the three years together I could also notice their humanity, that has been another important aspect of the path that we shared.
I would like to acknowledge the two reviewers Lars Eriksson and Sotirios Karellas for the time they have devoted for reviewing this work and the precious advice they have given. Finally, I would like to express my gratitude to all the members of the jury: Céline Morin, Alina Voda, Melaz Tayakout and Pierre Dewaleff.
I would like to give a special thanks to all the people I have collaborated with during these three years: Nicolas Espinosa (Volvo Trucks), Olivier Dumont, Antoine Parthoens and Nicolas Leclercq (University of Liege) and Johan Peralez (University of Lyon 1) helped me in several technical aspects and contributed in the improvement and richness of this thesis.
I would also like to mention my fantastic friends, that I always feel close to me from all around the Europe, in particular Raffaele, Roberto, Alberto, Enrico, Vittorio, Alessandro, Damien, Janett.
Finally, my family, Mom, Dad, Laura and Gianni who had to deal with my bad mood especially in the last year related to the thesis and not. I am proud of us and the fantastic family that we are.

Résumé en langue Française

De nos jours, les problématiques environnementales ont un impact primordial sur notre société. L'intérêt croissant pour le réchauffement climatique et la pollution conduisent à approfondir les recherches sur les économies d'énergie, les énergies renouvelables, l'amélioration de l'efficacité des procédés. L'Union Européenne a établi une nouvelle législation sur les émissions des poids lourds long-courriers, fixant la réduction attendue pour 2025 à 15% par rapport à la référence de 2019. Ce nouvel objectif ambitieux a poussé les constructeurs à accélérer la mise en œuvre de nouvelles solutions qui peuvent réduire les émissions de CO_2 directement, en utilisant un carburant qui réduit les émissions, en réduisant la consommation de carburant.
Au cours des dernières années, l'évolution du secteur des transports vers l'électrification s'est fortement accélérée et l'électrification des voitures particulières est une réalité solide. Quant au domaine des camions, le processus est plus lent, mais les villes utilisent déjà des camions à ordures électriques et des camions légers pour les livraisons urbaines. Dans le même temps, malgré des inconvénients connus liés au coût et au poids, l'industrie des camions lourds a étudié massivement l'hybridation. En particulier, l'hybridation "mild-hybrid" et, par conséquent, l'électrification du compresseur de climatisation, de la pompe EGR, du ventilateur de refroidissement par exemple, ont gagné un intérêt important, en raison d'une réduction du poids et du coût, de l'amélioration du rendement de la machine électrique et du stockage dans la batterie. D'autres propositions, qui pourraient contribuer à la réduction de la consommation de carburant et, en d'autres termes, à l'augmentation de l'efficacité thermique (Break Thermal Efficiency, BTE), sont liées à la combustion (surface isolée des pistons, température du liquide de refroidissement plus élevée) et au système de carburant (injecteurs à haut débit).
De la même manière, et c'est ce qui nous intéresse dans cette thèse, la récupération de l'énergie résiduelle est généralement considérée parmi les technologies susceptibles de contribuer au respect des nouvelles limites d'émission de CO_2. Les fabricants estiment que la récupération de la chaleur résiduelle des gaz d'échappement et du fluide de refroidissement peut permettre d'atteindre une économie de carburant de 4 à 5%. La technologie consiste en un système de cycle organique de Rankine, qui récupère la chaleur perdue d'une source de chaleur spécifique (dans la plupart des cas, le flux de gaz d'échappement) et la transfère à un fluide de travail mis sous pression par une pompe; puis le fluide transfère une partie de la chaleur résiduelle à un fluide à basse température dans le condenseur. Le fluide de travail s'évapore dans l'échangeur de chaleur et est donc détendu dans une machine de détente (un détendeur à déplacement positif ou une turbine), qui convertit la différence d'enthalpie en puissance mécanique ou électrique (dans le dernier cas une machine électrique est intégrée dans la machine de détente). L'exploration de cette technologie était, au départ, basée sur la fourniture et les essais des composants; ensuite, les principaux sujets de recherche et développement ont évolué vers le contrôle, l'optimisation du système et l'intégration du système dans le véhicule. De plus, la taille et le poids du système sont également considérés comme extrêmement importants dans la conception, car ils peuvent avoir un impact négatif sur la consommation de carburant du véhicule, malgré la récupération de l'énergie perdue.
Il est donc nécessaire d'estimer les performances de ce système dans un environnement réel de véhicule, en tenant en compte des interactions du système avec les autres sous-systèmes. Pour cette raison, la modélisation du système Rankine, ainsi que la modélisation des conditions environnemen-

tales et des principaux sous-systèmes du véhicule est extrêmement importante. Dans la plupart des cas, la définition de l'architecture Rankine (architecture et taille des composants) est nécessaire afin de prendre en compte les avantages et / ou les inconvénients que l'on ne rencontre pas avec d'autres architectures. A titre d'exemple, l'architecture de condensation directe a l'avantage de ne pas impacter le fonctionnement du système de refroidissement du véhicule, mais d'autre part, nécessite d'une modélisation du condenseur et du ventilateur dédié, afin d'évaluer le débit d'air de refroidissement au condenseur à une vitesse de rotation du ventilateur spécifique. Dans cette thèse, une fois la modélisation validée dans différentes conditions de fonctionnement avec des résultats expérimentaux, elle peut être utilisée efficacement pour évaluer le potentiel de la technologie, en comparant d'autres fluides de travail, les architectures Rankine ou d'autres technologies.
Le système de récupération de la chaleur basé sur cycle de Rankine devrait fonctionner dans des conditions garantissant le temps d'utilisation maximal possible. La source de chaleur, ainsi que le fluide qui retire la chaleur dans le condenseur, sont des fluides qui changent continuellement de débit massique et de température : par conséquence, afin d'assurer de bonnes performances aussi longtemps que possible, le contrôle a un rôle important. Dans la plupart des travaux publiés, l'état du fluide de travail à l'entrée de la machine d'expansion est contrôlé avec précision afin d'assurer la production d'énergie dans toutes les phases de la mission. Dans cette thèse, de plus, une attention particulière doit est accordée à l'évacuation de la chaleur du Rankine, en particulier dans l'architecture de condensation directe, caractérisée par une faible capacité de refroidissement. Par conséquent, le contrôle des conditions du fluide de travail à la sortie du condenseur doit être contrôlé, ainsi que d'autres actionneurs comme la vitesse de la machine de détente et le by-pass sont activement manipulés afin d'assurer la sécurité et les performances des composants.
Un problème important à résoudre pour la mise en œuvre de ces contrôleurs est la puissance de calcul limitée de l'unité de contrôle électronique (ECU) utilisée dans ce milieu automobile; cela limite fortement la complexité des contrôleurs à utiliser. Afin de limiter l'utilisation d'une forte puissance de calcul, ici, différents modèles linéaires locaux de premier et second ordre ont été étudiés; cette approche flexible permet l'utilisation de contrôleurs PID simples à la place d'algorithmes de contrôle plus compliqués comme la commande prédictive.
Compte tenu du niveau de maturité atteint par les composants en termes de fiabilité et de performances, le contrôle optimal a été considéré ici comme une étape majeure pour l'amélioration des performances du système. Dans cette thèse, une optimisation en temps réel, basée sur un modèle simplifié, a permis d'atteindre de meilleurs résultats que la référence dans différentes conditions routières et ambiantes. À l'avenir, la puissance de calcul croissante de l'ECU pourrait ouvrir la possibilité de mettre en œuvre des stratégies et des contrôleurs plus complexes, par exemple à base d'intelligence artificielle, comme nous les verrons ici.

Contents

Global introduction

Context

Nowadays the environmental problematics have a primary impact on our society. The growing interest in the global warming and pollution leads to further investigation on energy savings, renewable energy, improvement of the efficiency of the processes. The European Union established the new legislation about the emissions of long-haul heavy-duty trucks, setting the expected reduction for 2025 at 15% with respect to the baseline of 2019. This new ambitious goal pushed the manufacturers to accelerate the implementation of new solutions that can reduce the emission of CO2 directly, by using alternative low-carbon fuels or indirectly, by reducing the fuel consumption.
During the recent years, the evolution of the transportation sector towards the electrification has accelerated dramatically and became a solid reality in the industry of passenger cars. As for the truck industry, the process is slower, but cities are already using electric garbage trucks and electric light-duty trucks for deliveries. In the same time, although the known drawbacks related to cost and weight, the heavy-duty trucks industry has massively investigated the hybridization; in particular, the mild-hybridization and, consequently, the electrification of the air conditioner compressor, EGR pump, cooling fan etc, have gained an important interest, as a result of a reduced weight and cost, improvement of the efficiency of the electrical machine and battery storage. Other proposals, that could contribute to the reduction of the fuel consumption and, in other words, to the increase of the Break Thermal Efficiency, are related to combustion (insulated surface of the pistons, higher coolant temperature) and fuel system (high flow injectors).
Contemporary, the recuperation of the waste energy is usually considered among the technologies that can potentially contribute to meet the new CO2 emissions limits ; manufacturers estimate that the recuperation of the waste heat from exhaust gas and engine cooling flow can lead to fuel saving between 4-5% and 1-2 % respectively. The technology consists in an Organic Rankine cycle system, that recovers the residual heat from a specific heat source and transfer it to a pressurized working fluid. The working fluid evaporates in the evaporator and is therefore expanded in an expansion machine (a positive displacement expander or a turbine), that converts the enthalpy difference into mechanical or electrical power (in the case of an electrical machine is integrated into the expansion machine).
The exploration of this technology was, at the beginning, based on the components supplying and testing; afterwards the major topics in the research and development have evolved towards control, system optimization and system integration in the vehicle. Additionally, the size and weight of the system are also considered extremely important in the design, as they can impact negatively on the fuel consumption of the vehicle, despite the recuperation of waste energy.
Therefore it is necessary to estimate the performance of the system in a real vehicle environment, taking into account the interactions of the system with the other subsystems of the vehicle; for this reason, the modeling of the Rankine system, as well as the modeling of the environmental conditions and the main subsystems of the vehicle are extremely important. In most of cases, the definition of the Rankine architecture (layout and size of the components) is necessary in order to consider advantages and/or drawbacks that are not encountered using other architectures.

As an example, the direct condensation architecture has the advantage to not impact the operation of the cooling system of the vehicle, but on the other hand, requires the modeling of the condenser and fan system, in order to evaluate the cooling air flow rate to the condenser at a specific fan rotating speed. In this thesis, the fan-condenser model is validated over different operating conditions according to data supplier and it is used in order to evaluate the potential of the technology, benchmarking other working fluids, Rankine architectures or other technologies and design controllers.
The Rankine based waste heat recovery system should operate within conditions that ensure the maximum possible utilization time. The heat source, as well as the heat sink are fluid that continuously change in mass flow rate and temperature; in order to ensure good performance as long as possible, control has an important role. In particular, the condition of the working fluid at the inlet of the expander machine is generally set and accurately controlled in order to ensure the power production in any phase of the mission. In this thesis, additionally, particular attention is paid to the heat removal from the Rankine, especially in the direct condensation architecture, that is characterized by low cooling capacity; consequently the control of the working fluid conditions at the inlet of the feed pump have to be controlled as well. Other actuators as the expander speed and the by-pass are actively manipulated in order to ensure components safety and performance.
An important problem to be faced for the implementation of controllers is the limited computation power of the Electronic Control Unit (ECU) in the automobile; this strongly limits the complexity of the controllers to be used. In order to limit the utilization of the computational power, here different local linear models of first and second order have been studied; this flexible approach allows the usage of simple PID controllers in place of more complicated control algorithms as MPC.
Considering the level of maturity that the components have reached in terms of reliability and performance, the optimal control has to be considered a major step for the improvement of the system performance. In this thesis, a real-time optimization, based on a simplified model, reaches better results than the reference case in different road and ambient conditions. In the future, the increasing computation power of the ECU could open to the possibility of implementation of more complicated strategies and controllers, leading to better control performance and, possibly, system performance in terms of net power produced.

PhD thesis contributions

- Fan and condenser modeling to fully implement direct condensation configuration
- Design and implementation of an algorithm to select the representative operating points to linearize the system and implement controllers
- Model-based control of the subcooling, using the condensation pressure as manipulated variable
- Model-based real-time optimization of the net power output of the system, ensuring the tracking of the subcooling
- Usage of the artificial intelligence, replacing the weighting estimators in order to determine the adaptive representative model, used to design the controller

Manuscript contents

The manuscript is organized in three main parts.

1. The first part, composed of the Chap. 1, presents the legislation framework and the most important obstacles to the implementation of the ORC based waste heat recovery system in the vehicle. An overview and discussion about relevant scientific productions is given, introducing the topics treated in this thesis.

2. The second part is composed of the Chap. 2, 3 and 4, as they all deal with the modeling and simulation. Chap. 2 illustrates the modeling of components, as well as the validation according to experimental results or supplier data. Chap. 3 presents a global Rankine simulation model, composed of the single component models presented in the previous chapter; once a working fluid and a Rankine architecture are selected, the main dynamics of the system are studied and model-based controllers are developed. Simulation results are then presented on different road cycles. Chap. 4 investigates the engine coolant recovery, by means of a simulation work (with implementation of model-based controllers) and an experimental campaign.

3. The third part, composed of the Chap. 5, deals with optimal control of subcooling and superheat. In the first case, a model-based optimization is developed and run in order to ensure the control of the subcooling and maximize the net power of the system; in the latter case, a deep neural network, trained on-line, is used to replace the weighting estimators and determine an adaptive representative model to design the controller.

Chapter 1

Rankine based waste heat recovery for heavy duty trucks: state of the art and challenges

The aim of this chapter is to provide an overview of the state of the art of the waste heat recovery solutions that are considered in the long-haul heavy duty trucks and analyse the challenges to be faced to integrate a Rankine based waste hear recovery system in the vehicle. Working fluids and components selection, subsystem interaction, usage of the energy recovered and control are the main topics that are addressed and further developed in the following chapters of this thesis.

1.1 Energy consumption and emissions

The production of goods and services always requires an amount of energy to supply under different forms and quantity. The latest IEA report (IEA 2019) concluded that in 2018 the global energy consumption increased with a factor that is double the average rate of 2010. In the same time, the CO_2 emissions also grew to an historic peak (33.1 Gton), mainly because of the power sector that still uses coal in countries like India, China and United States, followed by the transportation sector (23%) whose buses and heavy-duty (HD) trucks (4x2, 6x2 for European application, weight from 16 tons) emissions account for one fourth (Marcilio et al. 2018). On May 2018, the European Union released a proposal for reducing the CO_2 emissions of long-haul HD trucks by 15% in 2025 with respect to the 2019 baseline; this percentage is going to be increased to 30% in 2030 with respect to the same 2019 baseline(Rodriguez, 2018) (Fig. 1.1). The reduction of the CO_2 emissions can be achieved via a correct use of the energy by improving the efficiency of the processes and therefore reducing waste.
In the automobile sector, the reduction of the CO_2 emission can be achieved in a effective way by introducing zero tailpipe emission via electric vehicles, that are charged by renewable energy (Muneer and García, 2017). Full electric cars and even buses and light and medium duty trucks are already a solid reality; on the other hand the use of electric heavy duty trucks involves freight transport operations that can differ for each country. A commodity-level analysis have been performed by Liimatainen et al. 2019; this analysis underlines the fact that electrification of trucks will strongly impact the electricity grids and the only solution for countries like Finland, with a massive use of long and heavy truck trailer combinations, is the electrification of the roads. However, without considering the limitation of the electric grid and the freight transport operations, a Pareto front optimization performed by Sen et al. 2019 in the US transportation panorama, shows the op-

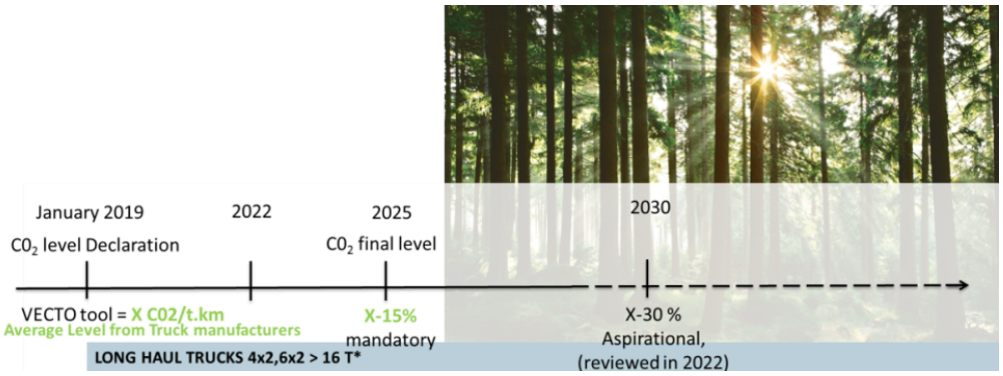

Figure 1.1 – CO_2 reduction steps for long haul heavy-duty trucks (Source: Volvo Internal).

timal fleet composition for different transport applications, with the goal to minimize the life-cycle costs (LCCs), life cycle greenhouse gases, GHG (LCGHGs) and life cycle air pollution externality costs (LCAPECs). Results show that for each applications, Diesel trucks class represents the non negligible percentage between 15% and 33% of the whole optimal fleet.
Therefore the improvement of the Diesel engine and classical drive-line is necessary to ensure sustainable costs and reduction of greenhouse gas emissions.

1.2 Heat recovery devices and technologies

The Ricardo company, in a final report written for the International Council on Clean Transportation, clearly showed the main losses that take place in a long-haul tractor (Norris and Escher, 2017); considering different trucks combinations, the total fuel consumption is divided in the different contributions (Fig. 1.3). The potential of fuel consumption reduction for 2030 is evaluated in the percentage of 33% and the fuel consumption due to the engine losses reduces from roughly 20% to 12%. In the same work, the authors highlight the distribution of the original fuel energy in a truck (Fig. 1.2); only 43% of the fuel energy, averagely speaking, represents the brake power, the remaining part is wasted. In particular, 22% of the original fuel energy is wasted in the exhaust gas flow, as well as in the cooling system (considering the EGR flow cooling); another important part of the wasted energy is attributed to the Charge Air Cooler (CaC), that reduces the temperature of the compressed air (and consequently increases the density of the air introduced in the engine.)
Many authors investigated the possibility to recover the waste energy in the truck and, somehow, re-convert it into useful energy. In this work, the main technologies that are briefly review are:

- Thermo-electrical generators (TEG), using the Seebeck effect
- Turbo-compound, commercially available, that recovers part of the energy in the exhaust gas by expanding the exhaust flow in the turbine
- Stirling engine, where the working medium recovers the heat of the hot source and convert it into power
- Organic Rankine Cycle (ORC), where the pressurized working medium, in liquid phase, recovers the heat of the hot source, it evaporates and it is expanded in the expansion machine

TEG convert heat into electricity through the Seebeck effect, exploiting a temperature difference between two surfaces. As highlighted in the works of Ahmadi Atouei et al. 2017, the heat

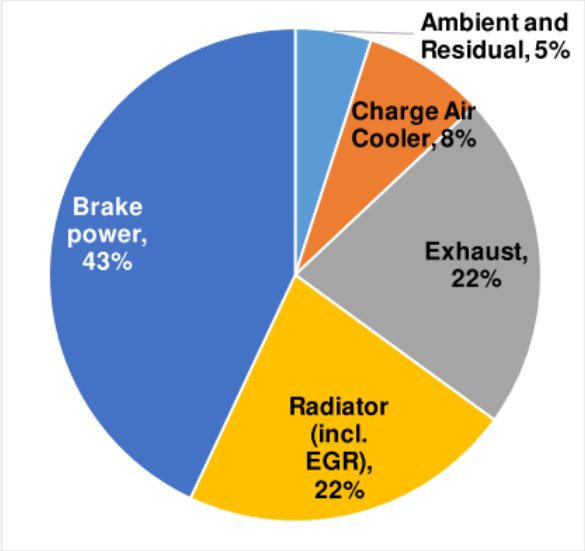

Figure 1.2 – Original fuel energy distribution in a truck (Norris and Escher, 2017)).

to electricity ratio of TEG is only about 2% and this solution is not the focus of any industrial development.

Turbo compound recovers part of the residual energy of the tailpipe exhaust gas, improving the overall fuel efficiency. This technology consists in a gas turbine that is installed in series in the exhaust gas tailpipe and, in the mechanical version of turbo-compound, it is directly connected to the engine crankshaft; the utilization of the mechanical turbo compounding leads to advantages mainly related to packaging. On the other hand, mechanical turbo-compounding can require the use of a variable or constant speed transmission between the turbocharger and the engine (Varnier 2012) and in the same time it increases the engine exhaust backpressure. Moreover the turbine power delivered increases with the engine speed and load, therefore it is particularly effective with highly rated or high engine speed and not in truck cruise conditions.

A more valuable alternative is the use of an electrical turbocompound system; a high speed generator is connected to the turbine and the energy is then injected in the crankshaft through a motor-generator. The advantage of this solution is the lack of any direct connection to the engine and therefore the possibility to control the turbine speed to maximize power and increase efficiency. On the other hand, this solution requires the installation of an electrical energy storage device and an electric machine, that generates additional costs and integration problems.

Thermodynamic cycles have also been studied; recently, Güven et al. 2019 proposed a Stirling engine recovering exhaust gas on a Euro VI heavy duty truck. The authors compared the Stirling engine with Organic Rankine cycle (ORC) and Inverted Brayton cycle (IBC) and claimed a fuel consumption reduction of 1% as a result of road cycle simulations.

Focusing on ORC, the performance of this technology is strongly dependent on the architecture, heat sources, working fluids, components efficiency and control.

Mahmoudi et al. 2018 describes a basic ORC as a system that is composed by four main components and four thermodynamic transformations, where isentropic compression, heat addition, isentropic expansion and heat rejection take place. Peris et al. 2013 considers also a regenerative or double regenerative ORC, that uses a working fluid stream from the expansion machine to pre heat the working fluid stream at the outlet of the pump. This solution increases the cycle efficiency as well as investment costs. Another valuable variant of the basic ORC is the use of the supercritical Rankine cycle, deeply investigated in concentrated solar power (Bauer et al., 2016) and nuclear (Abram and Ion, 2008).

A valuable analysis on the use of CO_2 supercritical Rankine cycle for waste heat recovery application from turbine exhaust is provided by (Kim et al., 2017); three different configurations of the system

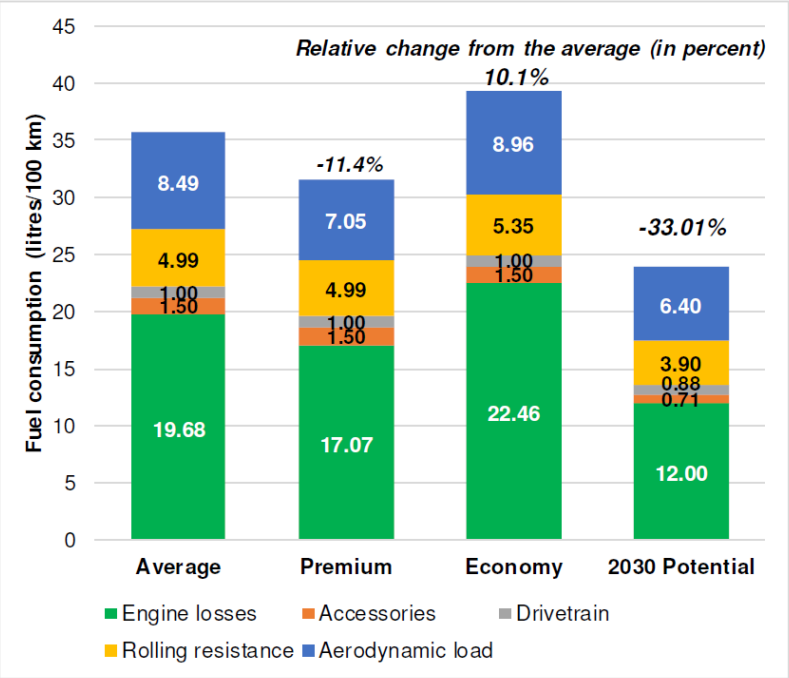

Figure 1.3 – Percentage of the single phenomena contribution in the total fuel consumption evaluation for log haul tractors (Norris and Escher, 2017)).

are investigated in order to match in the most suitable way the heat source. The use of a recuperator and low temperature (LT) and high temperature (HT) radiators leads to the best performance with respect to the simple and cascade CO_2 cycle. However research and commercial prototypes of supercritical Rankine cycle are limited. Hence it needs more experimental research and developments on transcritical Rankine cycles for detailed techno-economical comparison of CO_2 with other working fluids for both full load and part load conditions (Quoilin et al. 2013,Sarkar 2015).
In Eichler et al. 2015, a comparison between TEG technology, turbocoumpound and ORC has been performed by means of 0D simulations; authors claim a BTE improvement up to 5% using ORC, that is higher than the improvement that has been found using the remaining two technologies. Another meaningful comparison by means of steady state simulations of the main waste heat recovery solutions to adopt in internal combustion engine (ICE) vehicle was developed by Legros et al. 2014. Authors highlighted the advantages and drawbacks of different technologies (turbo-compound, thermoelectric generators, thermoacoustic generators, Stirling engine and Rankine cycle) considering efficiency, cost, packaging, maturity and weight to power ratio. Thermoelectricity shows very limited potential on power production, while ORC produces slightly less power than turbo-compound but with higher utilization. On the other hand, Rankine cycle needs to be cooled, therefore thermal power has to be rejected from the condenser. Authors in Jeihouni et al. 2017 also point out that the turbocompound system increases backpressure of the engine in non optimal engine points and therefore Rankine based waste heat recovery appears as the most suitable bottoming technology for vehicles.
Therefore, considering the mentioned waste energy recovery solutions, the focus of this work is on the ORC technology, as it is suitable to reduce the fuel consumption of the vehicle and, in the same time, offers valuable scientific topics to be investigated for future commercialization.

1.3 Rankine based waste heat recovery

1.3.1 Thermodynamic features

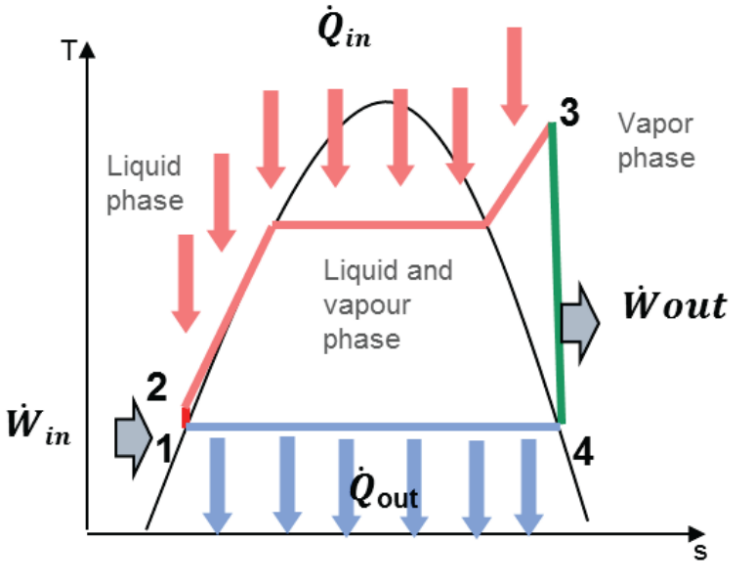

Figure 1.4 – Ideal Rankine Cycle Temperature-Entropy (T-S) diagram.

The Organic Rankine cycle is considered one of the best ways to recover heat from industrial processes (Daccord et al., 2014). However, the characteristics of the thermodynamic cycle should be chosen attentively by considering the nature of the heat source (steady state or transient) and its temperature.
Focusing on the waste heat recovery from internal combustion engines, the most common heat sources are represented by the exhaust gas, the Exhaust Gas Recirculation (EGR) flow and the cooling fluid of the cooling package of the vehicle. Each of the mentioned heat sources has its own characteristics in terms of variability over the road cycle of the mass flow and temperature.
The configuration of the Rankine cycle as well as the choice of the most suitable working fluid is a result of a thermodynamic analysis that involves performance, cost and safety. Vaja and Gambarotta 2010 pointed out that organic fluids are preferred to water when temperature of the heat source is limited, since such fluids are characterized by lower heat of vaporization and match in a better way the temperature profile of the heat sources, reducing irreversibilities and exergy destruction in the heat exchangers. In Panesar et al. 2013 a working fluid selection is performed and applied to a high exhaust gas recirculation engine. The evaluation is based on the second law efficiency, conversion efficiency, EGR efficiency and expansion volume ratio; the results highlight that using acetone, dichloromethane (R30) and trans-1,2-dichloroethylene (R1130), an improvement of 13.7, 12.2 and 12.7 % can be reached with respect to common working fluids like ethanol, R1233zd and water. Recently, Preißinger et al. 2017 performed a computational chemical and thermodynamic selection among 72 millions of chemical substances, to be used in an Organic Rankine cycle recovering energy from internal combustion engine heat rejection; two different configurations of the ORC and three different cooling concepts are investigated. The multi-criteria evaluation considers thermodynamic aspects and regulations and safety issues and a trade-off occurs. Among the fluids with highest score, ethanol is present.
The research about fluid selection for ORC-based waste heat recovery is also oriented towards the evaluation of the effectiveness of zeotropic mixtures as working fluids; Li et al. 2014 considered different zeotropic mixtures and compared them with pure fluids in terms of thermodynamic

performance and thermo-economics. The simple 0D thermodynamic model showed that when condensing dew point is kept fixed, zeotropic mixtures have a better performance than pure fluids, in the other cases pure fluids show better thermodynamic performance. Focusing on thermo-economic indicators, EPC (electricity production cost) and CRF (capital recovery cost) are always higher for zeotropic mixtures with respect to the pure fluids.
In its simplest configuration, the ideal Rankine cycle is constituted by two isobaric and two isentropic transformations (Fig. 1.4; in the isobaric transformations the working fluid absorbs and rejects heat, in the isentropic transformations the working fluid is pumped and expanded. Such thermodynamic cycle is similar to a Carnot cycle, but the main difference is that the isobaric transformations do not fully occur in the two-phase regime. In fact, for reasons that are linked to the reliability and availability of components, the pumping of the working fluid should take place in liquid phase and expansion transformation in vapor phase.
The real Rankine cycle differs from the ideal Rankine cycle because of the irreversibilities that take place in the components constituting the system:

- Thermal and friction losses in pumping and expansion phase, therefore the compression and expansion transformations are not isentropic
- Pressure losses in the evaporation and condensation transformations, therefore the absorption and rejection of the heat are not isobaric transformations

The four types of heat sources that have been mentioned at the beginning of the current paragraph (exhaust gas flow, EGR flow, cooling flow) are available at different temperature and mass flow; the engine regime impacts the nature of the hot source introducing variation in temperature and mass flow rate.
The available energy of each source can be easily calculated based on the first principle of the thermodynamics, but a fair comparison can be done considering the maximum work that is possible to retrieve from one source when it performs a transformation from its thermodynamic state (that differs from the ambient state because of a difference in temperature, pressure or chemical nature) to the ambient state, that is considered as the sink (Teng et al. 2007). The second law of thermodynamics and the concept of exergy are therefore more suitable to define the maximum work that is possible to retrieve from each heat source. Grelet 2016 concluded that the heat source represented by the coolant is more interesting than the exhaust gas considering the first principle of thermodynamics, but results of a second principle of thermodynamic analysis show that the exhaust gas is the heat source that is characterized by the highest amount of exergy. This can be explained by noticing that the exhaust gas source is at higher average temperature than the coolant, therefore the exhaust gas thermal level is further from the ambient.
Among the heat sources that have been previously listed, the exhaust gas flow represents the main focus, as it is characterized by high available thermal power and temperature. The recuperation of the engine coolant flow waste heat is also investigated in this thesis, as a cost-effective solution.

1.3.2 Components

A waste heat recovery system on heavy-duty truck should ideally meet requirements that are not only related to performance; important features of such a system are related to cost, weight, packaging and energy use. Latz et al. 2013 highlighted the most suitable applications of a positive displacement expander and a turbo-expander; the positive displacement expander is more suitable for a mechanical coupling of the Rankine with the drive-line of the vehicle, because its rotating speed is in the same ranges of the rotating speed of the vehicle crankshaft. On the other hand, positive displacement expanders are usually heavier than turbines, which is particularly interesting when

packaging is a main requirement. In the frame of the internal development of a piston expander in Exoes, Daccord et al. 2016 presented a compact machine suitable for truck integration. The piston expander is equipped by 6 pistons and a double swashplate technology with dedicated lubricant and integrated oil pump. The expander, rotating between 1500 and 4500 rpm, with nominal pressure ratio between 25 and 30, shows an effective isentropic efficiency up to 60%. Scroll expanders attract much interest recently, because of the reduced number of moving parts, reliability and wide power production. Quoilin et al. 2010 presented an experimental study and modeling of an organic Rankine cycle system using a scroll as expansion machine and HCFC-123 as working fluid; the scroll expander showed isentropic efficiency values ranging from 42 to 68 %, in the same ranges as the values measured by T. Yanagisawa, M. Fukuta, Y. Ogi 2001 and Ziviani et al. 2018.
Heat exchangers can be considered other key components of the system, to be chosen accurately. The nature of the heat source as well as the choice of the working fluid are factors that should also be considered. Current technologies of heat exchangers for ORC in heavy-duty trucks have been widely presented in Lopes et al. 2012. Additionally to the characteristics related to fluid phase, relative temperature, mass flow rate, density and flow direction, the author considers pressure drops, size and heat transfer efficiency. The density of the heat transfer surface area of the heat exchanger β (defined as the ratio between the surface area and the volume) is often considered to classify the heat exchangers based on their volume; higher density of heat transfer surface area leads to lower volume of the heat exchanger for the same heat transfer surface area. Shell and tube heat exchangers, particularly used in high load applications are characterized by β from 60 to 500 $\frac{m^2}{m^3}$, while plate and fin type, used for low and medium grade sources, are characterized by β values of about 110 to 600 $\frac{m^2}{m^3}$.
Ambros et al. 2011 showed the three types of heat exchangers that were under development by Thesys in 2011: bar and plate, twin round tube and twin flat tube heat exchangers have been designed in order to cope with different fluid density and velocities distribution and in the same time being suitable for packaging. Three years later, the same author (Ambros and Fezer, 2014) presented in detail the twin round tube evaporator: test results show an efficiency improvement up to 15% and a pressure drop reduction by 80% with respect to a conventional tube bundle heat exchanger.
In a recent study presenting a prototype of pump, Albergucci et al. 2019, from Exoes, claims a good volumetric efficiency, working with ethanol and an important reduction of the NPSH (net positive suction head) values, that influences the overall efficiency of the Rankine cycle and eventual cavitation phenomena of the pump. Results show that, reducing the NPSH, the pump relative performance increases towards the value of 100% with a theoretical value of NPSH equal to zero.
Complete modular systems are also designed and already tested in test bench and vehicles; one of the most recent examples is provided by Mahle in Marlok et al. 2019. The modular and compact solution has been designed in order to meet efficiency and packaging requirements, using cyclopentane as working fluid without any interface to the cooling system. The energy delivered by the Rankine unit is electrical and the operating voltage is 48V. The system has been integrated in a standard long haul truck, equipped with a mild-hybrid system, featuring a 13 kW electric motor mounted in the power takeoff (PTO) of the engine. Results in road cycles show an increase of the unit performance with decreasing the ambient temperature. The unit has been tested on a wide range of operating points, leading to different thermal power input values, showing electric net system efficiency up to 11.5% and fuel saving up to 3%. Future challenges lie in the optimization of the energy management, the reduction of weight and the component adaptation to cyclopentane.
Fouquet and Roussilhe 2018, in the frame of the development of a demonstrator (Renault Truck, Faurecia and Exoes cooperated to design, realize and test a Rankine cycle based waste heat recovery system) presented the selected architecture and its integration in the truck, focusing on the aspect that the fuel tank capacity is not impacted by the system. Tests in the roller bench facility of Renault Trucks showed a measured fuel economy up to 2.7% on steady state.
Considering the main components and complete systems that have been tested by the main academical and industrial actors in the context of the ORC based waste heat recovery technology, it can be

noticed that the component maturity has still to be reached, as most of the cases are prototypes, still far from a series production.
In this thesis, particular attention is dedicated to the development of the simulation models of components, as well as to their testing; particular attention is dedicated to compact (plate and fins are preferred to the shell and tube heat exchangers) components, while both positive displacement expander (piston) and turbine are tested experimentally.

1.3.3 Integration challenges and subsystem interactions

The Rankine system can be represented as a box, where fluid streams and other forms of energy can be considered as inputs and outputs. Depending on the heat sources and sinks that are used, the Rankine system imposes interactions and integration problems to be solved in order to assess in an effective way the potential of the system.
Karvountzis-Kontakiotis et al. 2017 investigated the effects of the ORC on fuel economy of a heavy duty vehicle; the main focus of the analysis is a trade-off between the heat transfer area of the evaporator and the pressure drop that it imposes to the exhaust gas used as main heat source; the author also identifies the weight of the system as one of the main limitations of the ORC systems in vehicles. The final results show an optimal value of the length of the heat exchanger among the exhaust backpressure, ORC required net power and weight. Di Battista et al. 2018 added to the analysis the effect of the weight of the system, comparing two different architectures, considering the recuperator or not. Reducing the pressure losses of the exhaust gas from 80 mbar to 20 mbar leads to an increase of weight of 15kg of the heat exchanger. Therefore the exhaust backpressure through the ORC evaporator is not negligible and should be taken into account to assess the fuel economy of the whole vehicle. However the authors did not investigate deeply the problem of the heat rejection, limiting their research to the sizing of a condenser placed in the front face of the truck.
Using an additional direct radiator placed in the front-face of the truck, Hountalas et al. 2012 studied the problem of the rejection of excess heat; authors used exhaust gas as main heat source and by adding a EGR and a CaC cooler, they proved a further improvement of the expander output power and in the same time a reduction of the thermal load in the cooling radiator, leading to the reduction of the fan power demand.
Yang et al. 2018 proposed the installation of additional indirect high temperature radiator in the front face of the truck; they highlighted that control and optimization of the system, involving exhaust gas by-pass, condensation pressure and engine fan are necessary to ensure complete condensation and achieve the best overall performance. Grelet 2016 presented a similar architecture, highlighting the fact that the higher load in the cooling module can lead to the limitation of the heat recovery and by consequence of the produced useful work.
An additional challenge for the implementation of the technology on the vehicle is the necessity of implementing robust controllers, that, in the same time, can be used on standard automotive control unit (ECU). Seitz et al. 2018 claim that advanced methods, as non-linear model predictive controllers (NMPC) are too complex for the implementation in a standard ECU, therefore they presented a model-based controller, that can be implemented in standard ECU.
As it can be noticed in the researches that have been cited, the installation of the Rankine system in the vehicle influences the normal and correct operation of other subsystems, already existing. Impacts on the vehicle cooling system, as well as the additional pressure drop due to the evaporator recovering the waste heat of the exhaust flow are the main aspects to take into account and that have been considered in the evaluation of the potential of this technology. Additionally, the usage of simpler control algorithm should be preferred to the more complex ones (in case of comparable performance), in order to make possible the implementation on standard ECU.
In this thesis, particular attention is dedicated to the integration challenges; the exhaust gas recuperation as well as the coolant flow waste heat recuperation are explored and the main advantages

and drawbacks are identified. Additionally, in both cases, the available cooling capacity is taken into account and the impacts of the heat removal from the Rankine to the cooling system of the vehicle are explored.

1.3.4 Energy recovered usage

In the previous paragraph the different heat sources and possibilities to reject heat from the Rankine system have been investigated.
On the other hand, the main ambition of the system is to produce energy and reduce the fuel consumption of the vehicle, therefore the investigation about the destination of the energy produced has to be performed.
The expansion machine transforms the thermal energy of the working fluid into mechanical energy that can be directly used as useful energy to be injected in the drive-line of the vehicle and therefore reduce the fuel consumption. This solutions leads to a mechanical connection between the expansion machine and the engine crankshaft via a gear and the instantaneous delivery of power to the vehicle drive-line. On the other hand, during the break and down-hill phases the production of power should be stopped, because the mechanical power cannot be provided to the user, because torque is not requested to the engine. Additionally the use of a kinetic machine can be tricky because of the much higher speed in which those machines operate with respect to the typical values of engine speed; therefore a gear ratio should be carefully designed in order to ensure the good operation of the machine and obtain good values of expander efficiency (Treutler et al. 2017, Grelet 2016).
Another option is to transform the mechanical energy produced by the expansion machine into electrical energy. This leads to an additional power loss and reduction of the overall efficiency, but on the other hand, it ensures more flexibility, since the power production can continue even in the phases characterized by null torque demand to the engine, thanks to the evaporator inertia (Fig.1.5). During a braking phase (between 1275 and 1325 seconds) the mechanical recovery architecture does not produce any power, however the electrical recovery architecture takes advantage of the inertia of the system to extend the power production that slowly decreases.
Another advantage of the electrical recovery architecture is the fact that the expansion machine is not directly connected to the engine crankshaft, but directly to the electrical machine. This leads to the fact that it is possible to vary the expansion machine speed in order to control the pressure at the inlet of the expander. In the mechanical recovery architecture the pressure at the inlet of the expander can not be controlled because the expander speed is fixed by the gear and the engine speed.
An interesting approach for the integration of an Organic Rankine Cycle in a Class 8 tractor is provided by Joshi et al. 2019; starting from a previous work (Joshi et al., 2018) the authors replaced the turbo-compound unit with a ORC. Depending on the operating region in the engine map, the ORC can be electrically integrated with a motor/generator unit or mechanically integrated in the crankshaft of the engine or secondary compressor (that provides power by the turbo-compound turbine and electric motor/generator depending on boost pressure demand), by means of clutches. The authors claimed an estimation of 4.8 % in fuel consumption reduction by means of simulations using GT power.

1.3.5 Control

Despite the operation of a heavy duty truck consists mainly in highway paths with rare variation of the engine working point, the phases of start up, shut down, and possibly sudden variations of the engine working point due to braking must be faced. Control is therefore an additional challenge

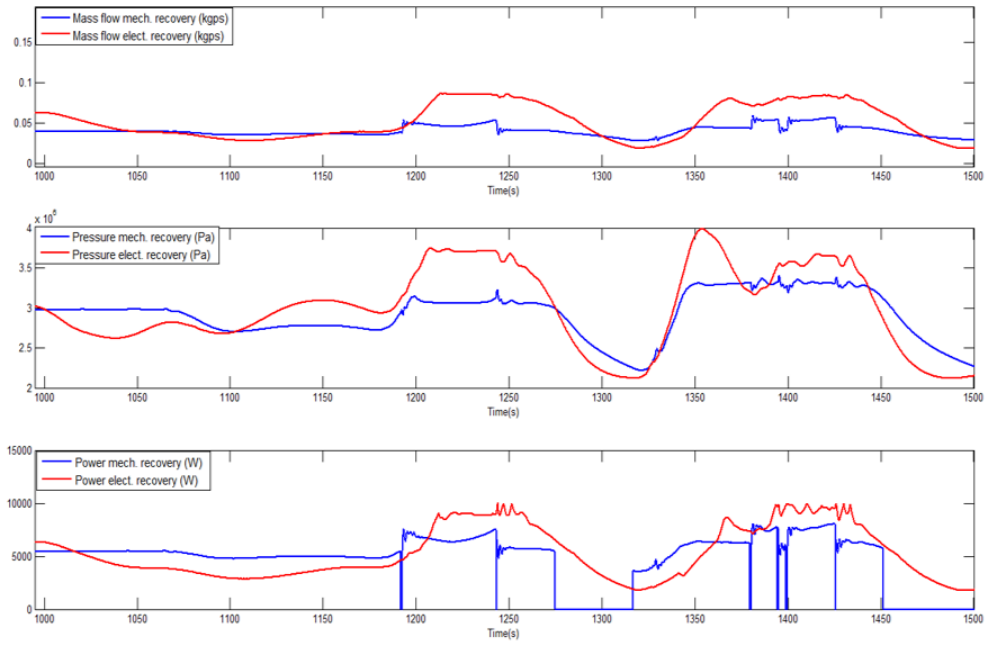

Figure 1.5 – Mechanical vs Electrical recovery: electrical recovery produces energy even during braking phases thanks to the inertia of the evaporator.

that has the goal to meet the requirements of safety of components and performance.
The main studies focus the effort on the control of the vapor superheat at the inlet of the expander in order to prevent the contact of liquid droplets of working fluid with the internal parts of the expander during the whole process of the expansion. Alshammari and Pesyridis 2019 investigated the effect of the superheat on the efficiency of a radial inflow turbine using a dry fluid (Novec649) in an experimental setup; the authors concluded that increasing the superheat has a negative effect on the efficiency of the turbine and its power produced. Additionally, a higher superheat using a dry fluid is not necessary. Guillaume and Lemort 2019 proposed a fluid selection based on thermodynamic and economical considerations; they pointed out the fact that the superheat, in itself, has limited influence on the efficiency of volumetric expanders, but indirectly affects its design, as a change of the superheat leads to a change of the working fluid mass flow rate in the system. Therefore, the control of the superheat is also necessary in order to let the system working in the right operating conditions once the design of the system is defined.
Grelet et al. 2015 compared the use of a non linear inverse model and a PI controller to track the set point of the temperature at the inlet of the expander; the inverse model leads to the best strategy, but the model has not been validated on test bench. Seitz et al. 2016 designed a feedforward controller, with online parameter adaptation, to control the temperature at the outlet of the evaporator; however according to the author the inverse model must be rechecked to increase the performance in highly transient situations.
Torregrosa et al. 2016 proposed an adaptive PID controller of the pump speed in a Rankine system fed by thermal power from a 2 L gasoline engine; the adaptive gains are evaluated based on the working fluid temperature at the outlet of the evaporator and the estimation of the power released by the exhaust gas. Map based controller of the volumetric expander speed is also included. The controller is validated in test bench and, according to the authors, allows the control of the ORC in real driving conditions. Another example of feedforward controller designed to control the superheat of the working fluid at the inlet of the expander is presented by Peralez et al. 2013; the author used an inverse reduced model in the feedforward path and a gain-scheduling PID controller in the

feedback path. Experimental results show a good performance of the controller, that allows to keep a superheat of 30 K.
Extensive literature about controllers oriented towards the maximization of the net power of the ORC is available; a model predictive controller was used by Koppauer et al. 2018 in order to maximize the net produced energy of the Rankine system; the controller uses a gain scheduling model based on quasi-linear local model approximation. Model plant mismatches are taken into account and the minimum vapor quantity at the inlet of the radial turbine is ensured. The controller tracks well the reference enthalpy at the inlet of the turbine, but validation on test bench has not been provided.
A non-linear model predictive controller has been developed by Esposito et al. 2015 and run in transient simulations; the authors compared the performance of this controller with a feed-forward PID controller and they pointed out that the non-linear model predictive controller is effective, allowing the system to operate within the acceptable conditions. Hernandez et al. 2014 developed a classical PID controller for regulating the SH and a multi-linear model predictive controller to maximize the electrical net power of the system, ensuring superheat control at the inlet of the expander. The authors conclude that the MPC strategy results in a better control than the PID and leads to a higher electrical net power especially when unstable thermal power source is experienced.
The above cited papers dealing with control of the Rankine system do not consider any control action on the low pressure loop of the system. The installation of a Rankine based waste heat recovery system in a heavy-duty truck requires a particular attention to the choice of the condenser and the heat sink to cool down the working fluid before it enters in the feed pump. However the temperature of the heat sink at the inlet of the condenser can be variable and influenced by the road cycle and other components that affects the external air temperature in the surroundings (for example the Exhaust Gas Treatment System, EATS). Therefore, the use of controllers involving the regulation of the condensation pressure or optimization algorithms performed on the low pressure loop of the Rankine cycle looks as an useful solution to ensure a sufficient subcooling to the feed pump.

1.4 Perspectives and challenges

The topics that have been treated in this chapter clearly identify the role of the ORC based waste heat recovery for long-haul heavy-duty trucks in the truck industry; this technology is unequivocally considered a potential and valuable solution to reduce the fuel consumption of the vehicles and, consequently, reduce emissions.
In the same time the current status of the technology suggests important scientific directions and non-negligible challenges to sustain the commercialization of the technology; considering that an higher amount of scientific works have been published about preliminary potential of different configurations of the system and modeling approaches, the integration challenges in the vehicle have not always been addressed with the same strength. The impact of cost and weight, as well as the complicated interactions between the Rankine and the cooling system introduce additional challenges for the manufacturer, that has to ensure high performance and availability and, in the same time, reduced total cost of ownership (TCO). These aspects involve the component maturity as well, considering that most of the components that are tested are still prototypes and are far from being considered optimized for the current application.
Many researchers also focused on the control, that is particularly important to ensure safety and high performance of the system; control challenges may change a lot depending on the boundary conditions (weather conditions, application), as well as the specific configuration of the Rankine system; tests on vehicle on real road cycles should be performed more intensively in order to identify issues and verify the correct operation of the controllers in any operating conditions and distur-

bance.
The aim of this thesis is to focus on most of the challenges that have been identified in this first chapter. The second chapter deals with modeling of every single component that is involved in. the high fidelity ORC simulator, that is used for the potential assessment of different Rankine configurations. The third chapter opens with an investigation of two different ORC configurations and the usage of different working fluids; performance, material compatibility and heat sink nature are the main aspects that have been taken into account for the current investigation. Afterwards, the dynamics, control issues and performance of the system under transient operating conditions are treated, in order to assess the potential of the ORC architecture that has been chosen for the development of a truck demonstrator. The third chapter deals with the recuperation of the waste heat from the engine coolant flow; an experimental campaign is described and the results are discussed, identifying the challenges and the issues to solve for a potential implementation in a vehicle. Transient simulations have also been performed, implementing different strategies for the control of the working fluid conditions at the inlet of the feed pump, to avoid cavitation and, in the same time, keeping high standard of performance. In the fifth and final chapter of the this work, two problems related to the optimization of the operating conditions of the Rankine systems are addressed. The optimal control of the low-pressure side of the system, intended for the control of the working fluid condition at the inlet of the feed pump and the improvement of the net power production with respect to the reference presented in the Chapter 3, is developed. Afterwords, the usage of the artificial intelligence (AI) is applied to the on-line determination of a combined model such that the output of the model best match with the output of the plant; such an approach is useful for the design of a controller for the conditions of the working fluid at the inlet of the expander in a wide range of operating conditions.

Conclusion. *In this chapter, the status of the Organic Rankine cycle based waste heat recovery technology is presented, highlighting the main obstacles to the integration of the system in a vehicle; the different topics, regarding working fluid and component selection, usage of the energy, interaction of the Rankine system with other subsystems of the vehicle and control are detailed, presenting and discussing the most important and recent contributions of the scientific community in the domain. These topics will therefore be deeply taken into account and analyzed in this thesis developing the components, the whole system model, as well as the control strategies.*

Chapter 2

Rankine system modeling

This chapter deals with the modeling of each component that is therefore integrated in the global Rankine simulation platform, assembled according to the specific Rankine architecture. Most of the 1D models are validated by means of comparison with the experimental results, gathered from experimental campaigns or suppliers data, depending on the specific component.
The model in Sec. 2.6 has been presented in the 5th International Seminar on ORC Power Systems in Athens, 2019 (Galuppo et al. 2019a).

2.1 Overview on the system and components

One of the main goals to develop a Rankine cycle based waste heat recovery model is to evaluate the potential of the technology in terms of benefit on fuel consumption. However, the complexity of the model usually depends on the available tools and the accuracy that has to be reached.
In this work, the use of 1D models is preferred to a 0D approach, in order to increase the accuracy of the results and evaluate, from a physical point of view, important phenomena that can impact, as an example, the choice of the best fluid or the use of an additional component in the system. These models are particularly useful to design controllers, in particular model based controllers, that would not be as accurate using 0D models.
The working fluid thermodynamic properties are communicated between two different models by means of a group of signals (lately called bus) that contains:

- Pressure, expressed in Pa
- Enthalpy, expressed in $\frac{J}{kg}$
- Quality (-)
- Density, expressed in $\frac{kg}{m^3}$
- Temperature, expressed in K

2.2 Feed pump

The feed pump model receives as input the pump speed from its controller and the pressure ratio and provides as outputs the working fluid mass flow rate and the pump power demand. The pressure

at the outlet of the pump is calculated in the expander model (Sec. 2.4), as a positive displacement expander imposes the high pressure of the Rankine cycle for given working fluid mass flow rate and expander swept volume flow rate; the pressure at the inlet of the pump is a function of the mass flow rate and the temperature of the coolant heat sink. As a function of the rotating speed N, pressure ratio and displacement of the pump C, the model calculates the mass flow rate of working fluid (2.1) and the pump power demand (2.2).

$$\dot{m}_{wf} = N_{pump} C_{pump} \rho \tag{2.1}$$

$$\dot{W}_{pump} = \frac{\dot{m}_{wf}(h_{ex,is} - h_{su})}{\eta_{gl,pump}} \tag{2.2}$$

2.3 Evaporator models

The evaporator model receives as input the working fluid bus and mass flow rate, the temperature and mass flow of the heat source and provides as output the working fluid bus at the outlet of the evaporator, the heat source temperature at the outlet of the evaporator and the evaporator wall temperature.
The evaporator that is modeled and tested is a plate-fin heat exchanger, widely used in small-scale waste heat recovery applications (Lopes et al., 2012). Fig. 2.1 shows a frontal and side view of the evaporator as well as the inlet and outlet sections of the working fluid and exhaust gas; plates, where the working fluid flows, are disposed in parallel with respect to the view from the top, therefore a counter-flow approach for modeling is fully justified.
The model of the evaporator is a 1D finite volume (FV) model, where N_{vol} volumes are identified by discretizing the component along the longer dimension. The number of volumes N_{vol} should be identified as a trade-off between the accuracy and the stability that is necessary to reach and the acceptable computational cost to perform the simulations. In this application, the heat exchanger model is, as first approach, simulated as a standalone component, afterwards it is integrated into a complete Organic Rankine Cycle model (see next chapter) and finally in a complete vehicle model, where cooling system, driver and all the mechanical components are modelled. Taking into account the general frame of this work, the number of volumes N_{vol} is set to 10, as an optimal trade-off between accuracy and stability of the model and computational cost.

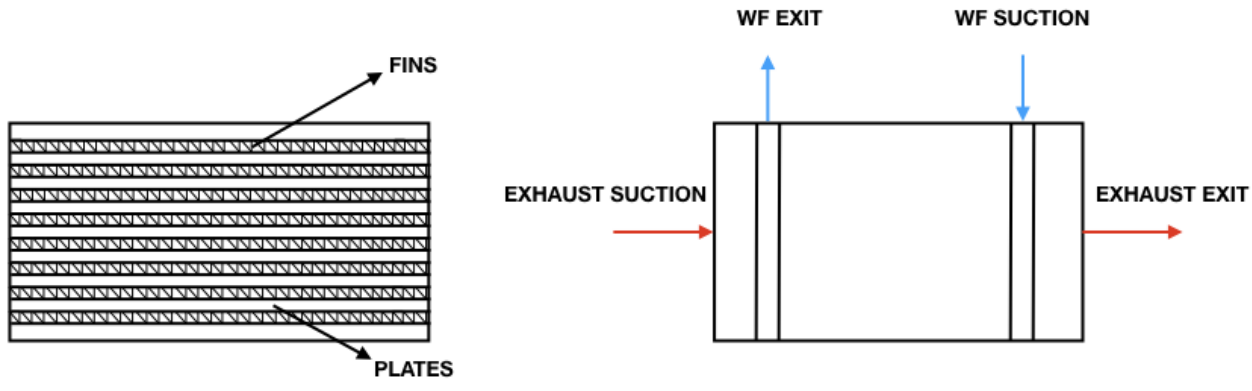

Figure 2.1 – Frontal and side evaporator views; inlet and outlet of working fluid and exhaust flow as well as fins and plates are highlighted.

Fig. 2.2 shows that each volume is divided into three zones: the fluid side, the separation wall and the gas side. On the fluid and gas sides, mass and energy balance equations are applied in order to calculate respectively the fluid state and the temperature of the exhaust gas at the outlet of each volume; in the separation wall the only energy balance equation is applied in order to calculate the average temperature of the wall in the specific volume. It can be noticed that the number of volumes is N_{vol} and the two nodes before and after the volume i are named $i-1$ and i respectively. In order to distinguish the volume variables from the node variables, the latter are denoted by a "'" subscript.

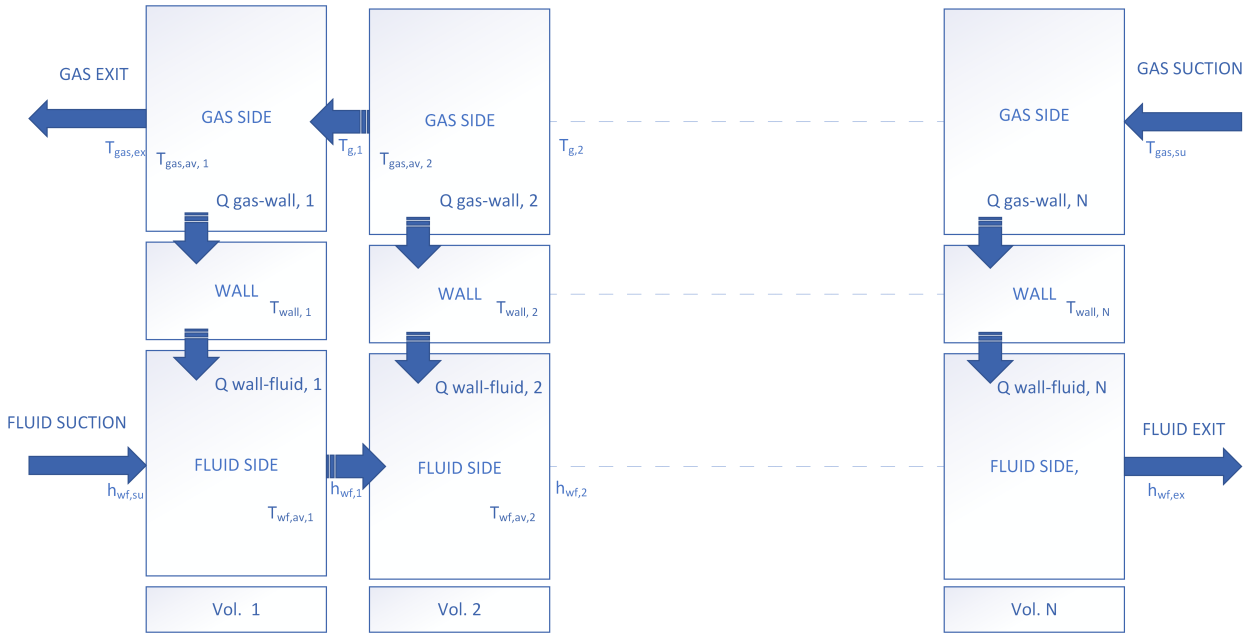

Figure 2.2 – Spatial discretization of the evaporator.

The mass variation in time in each volume can be expressed by means of the differential of the enthalpy and pressure, as follows:

$$\frac{dM_i}{dt} = V\frac{\partial \rho}{\partial t} = V\left(\frac{\partial \rho}{\partial h}\frac{\partial h}{\partial t} + \frac{\partial \rho}{\partial p}\frac{\partial p}{\partial t}\right) = \dot{m}'_i - \dot{m}'_{i-1}$$

(2.3)

The energy balance can be written as follows:

$$\frac{dU_i}{dt} = \dot{m}'_{i-1}h'_{i-1} - m'_i h'_i + \dot{Q}_i + \dot{W}_i - p\frac{dV_i}{dt} \tag{2.4}$$

Considering that no source of work is existing in the volumes, using the definition of the internal energy ($U = H - pV$) and the equation (2.3), the energy balance can be written as follow:

$$\rho_i V_i \frac{\partial h_i}{\partial t} = \dot{m}'_{i-1}(h'_{i-1} - h_i) - \dot{m}'_i(h'_i - h_i) + \dot{Q}_i + V\frac{dp}{dt} \tag{2.5}$$

The equation (2.5) can be also written for the gas side considering that the enthalpy can be replaced by the product between the gas specific heat c_p and temperature T. The power balance equation applied to the gas side is:

$$\rho_i V_i cp \frac{\partial T_i}{\partial t} = \dot{m}'_{i-1} cp(T'_{i-1} - T_i) - \dot{m}'_i cp(T'_i - T_i) + \dot{Q}_i \tag{2.6}$$

considering the specific heat *cp* constant and the gas as incompressible fluid.
The energy balance equation applied to the wall can be finally written as follows:

$$M_w cp_w \frac{\partial T_{w,i}}{\partial t} = \dot{Q}_{gas-wall,i} - \dot{Q}_{wall-fluid,i} \tag{2.7}$$

In order to evaluate the heat transfer occurring between the exhaust gas and the fluid flow (via the internal wall of the heat exchanger) external and internal dimensions of the component are measured or calculated. In particular, the following geometrical data are used in the evaluation of the heat transfer:

- Heat transfer area for fluid and gas sides
- Flow section for fluid and gas sides
- Volume for fluid and gas sides
- Separation wall volume

The thermal power that is exchanged between the exhaust gas and the fluid can be calculated by:

$$\dot{Q}_{th,exch} = A_{glob} U_{glob} \Delta T_{suit} \tag{2.8}$$

where ΔT_{suit} is a suitable temperature difference between exhaust gas and fluid (i.e. the mean logarithmic temperature difference) and the product $A_{glob}U_{glob}$ is the global heat transfer coefficient (Incropera et al., 1993). The equation (2.8) can be written for each side of the heat exchanger by introducing the wall properties. Consequently the thermal power exhanged between the exhaust gas and the separation wall and between the separation wall and the fluid can be written respectively as in (2.9) and (2.10).

$$\dot{Q}_{th,exch,gas-wall} = A_{exch,gas} U_{gas} \Delta T_{gas-wall} \tag{2.9}$$

$$\dot{Q}_{th,exch,wall-fluid} = A_{exch,fluid} U_{fluid} \Delta T_{wall-fluid} \tag{2.10}$$

The heat transfer coefficient U should be determined for the gas U_{gas} and fluid U_{fluid}. As reminded by Quoilin 2011 the gas heat transfer coefficient in single-phase flow is mainly dependent on the mass flow rate. Fixing a nominal heat transfer coefficient for a nominal mass flow rate of exhaust gas, the heat transfer coefficient is determined as follows:

$$U_{gas} = U_{gas,n} (\frac{\dot{m}}{\dot{m}_{nom}})^m \tag{2.11}$$

where the coefficient m is the Reynolds exponent.
In this work, the heat transfer coefficient of the fluid is calculated taking into account the flow regime as well as the nature of the fluid; for the single-phase flow and double-phase flow, the Dittus-Boelter and the Shah correlation are used respectively to calculate the Nusselt number, directly correlated to the heat transfer coefficient.
The Dittus-Boelter correlation, according to turbulent flow in ducts (Winterton 1998) is given by:

$$Nu_{sp} = 0.023 Re_{D_h}^{0.8} Pr^{0.3} \tag{2.12}$$

where Re_{D_h} is the Reynolds number calculated in the flow area fluid side and Pr is the Prandtl number.

The Shah correlation is expressed as (for evaporation and condensation phases respectively):

$$Nu = \begin{cases} \psi Nu_{sp} & (2.13) \\ Nu_{sp}\left[(1-q)^{0.8} + \dfrac{3.8q^{0.76}(1-q)^{0.04}}{P_{red}^{0.38}}\right] & (2.14) \end{cases}$$

where q is the quality of vapor and P_{red} is the reduced pressure defined as the ratio of the actual fluid pressure and the critical pressure of the fluid (Shah 1979).
Therefore, the calculation of the heat transfer coefficient in the working fluid takes into account the conditions of the working fluid and the transition between two phases; the use of the correlations (2.12) and (2.13) leads to discontinuities in the overall function of the heat transfer coefficient that have to be treated in order to ensure the stability of the model as well as the accuracy. Fig. 2.3 shows the evolution in time of the heat transfer coefficient calculated in each volume; the volume 10 (as well as the 9, not shown in this figures) are involved in the change phase of the working fluid, while the working fluid in the other volumes is in the liquid phase.

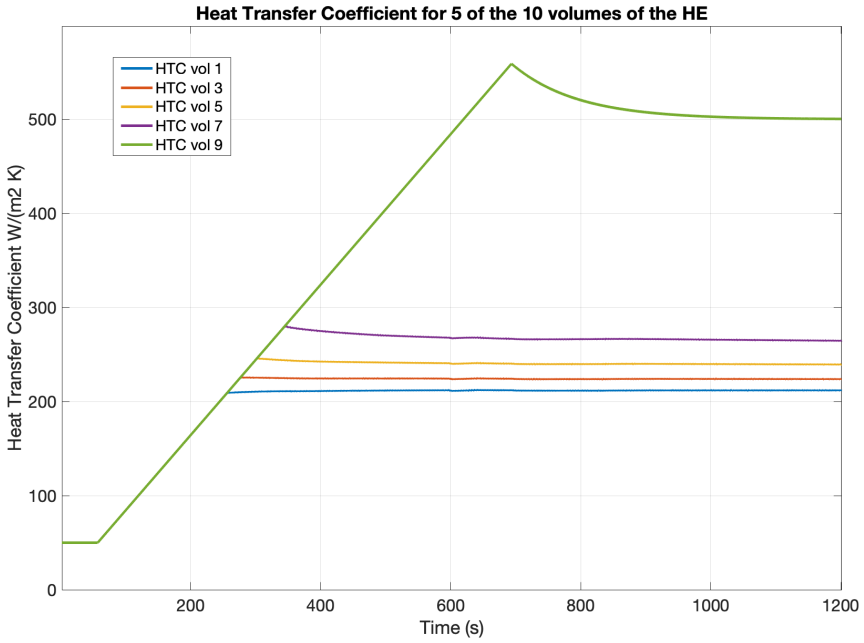

Figure 2.3 – Heat transfer coefficient (HTC) of the working fluid evolution in time for 5 of the 10 volumes modeled in the evaporator for an operating point characterized by $m_{exh} = 0.2kg/s$ and $T_{exh} = 350°C$ using cyclopentane as working fluid.

The evaporator has been tested in the Volvo facility in Saint Priest (France). The test bench is equipped with a 13-liter non-EGR engine that provides the exhaust gas flow to the Rankine system. The latter is composed by the feed pump, the evaporator, the expander and the condenser and the working fluid is ethanol.
Focusing on the evaporator, the experiments are realized in steady state conditions in different engine operating points and consequently thermal power ranking from 20 to 70 kW. In each experiment the working fluid mass flow is adjusted in order to obtain the same superheat conditions at the outlet of the evaporator.

Fig. 2.4 shows the Rankine experimental setup (right side of the figure) that has been used for test validation; the test bench is useful for testing different architectures (and number of heat sources), as well as components and is directly fed by the exhaust gas of a long haul heavy duty truck engine (left side of the figure).

Figure 2.4 – Test bench in the Volvo facility in Lyon, widely used for model validation and testing of system architectures.

Among the large number of signals that are measured in the test bench, the following variables can be mentioned:

- Mass flow rate of the working fluid by means of a Coriolis flow-meter at the outlet of the feed pump and mass flow rate of the exhaust gas by means of a Annubar flow-meter at the inlet of the evaporator.
- Pressure on the working fluid side by means of differential pressure sensors, at the suction and exit of the evaporator.
- Temperature on the working fluid side by means of thermocouples T, one at the suction and one at the exit of the evaporator and on the gas side, three thermocouples K at the suction of the evaporator and one at the exit of the evaporator.

The thermal power exchanged between exhaust gas and working fluid has been plotted in Fig. 2.5. The relative maximum error between the thermal power predicted by the model and measured from experiments, according to (2.15), is 1.82%.

$$e = \left\| \left(\frac{\dot{Q}_{expe} - \dot{Q}_{sim}}{\dot{Q}_{expe}} \right) \right\| \tag{2.15}$$

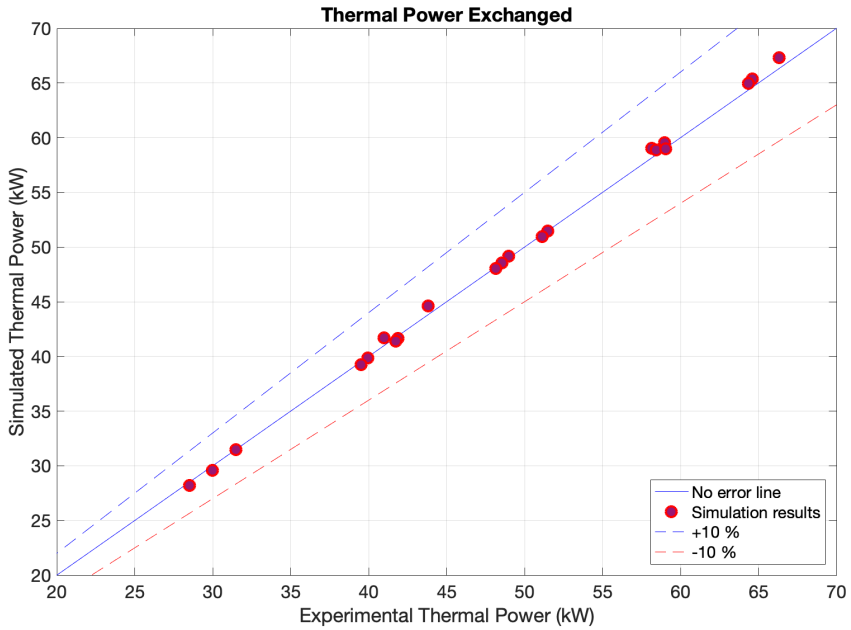

Figure 2.5 – The thermal power exchanged in the evaporator.

Fig. 2.6 shows the validation of the exhaust gas temperature at the outlet of the evaporator. In this case the maximum absolute error of the prediction is 3.29 K.

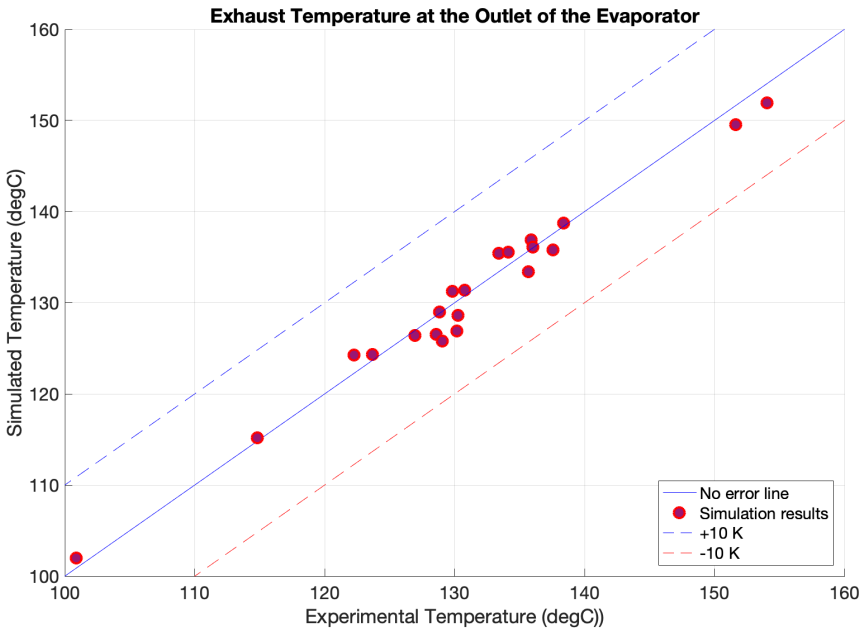

Figure 2.6 – The exhaust temperature at the outlet of the evaporator using ethanol.

The effectiveness of the evaporator is also evaluated and defined as follows:

$$\epsilon_{evap} = \frac{T_{exh,su} - T_{exh,ex}}{T_{exh,su} - T_{wf,su}} \tag{2.16}$$

The validation of the simulated evaporator efficiency according to experiments is shown in Fig. 2.7.

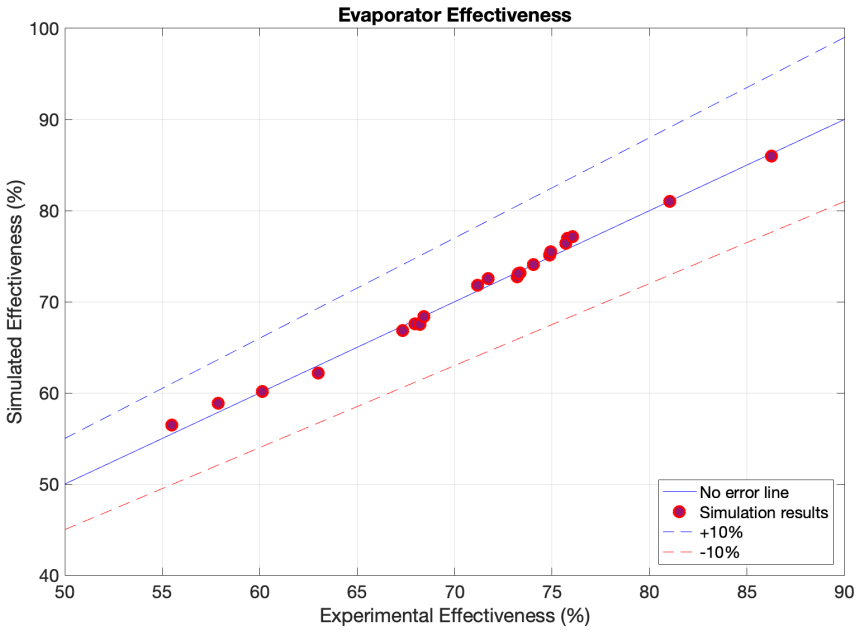

Figure 2.7 – Evaporator effectiveness validation vs experiments, according to (2.16).

2.4 Expander

The expander model receives as input the working fluid bus at the outlet of the evaporator and mass flow rate, the expander speed and the discharge pressure of the expander; it provides as output the working fluid bus at the outlet of the expander, the expander efficiency and power produced.
The considered expansion machine is a piston expander, belonging to the family of positive displacement expanders. The indicator diagram of the crossflow piston expander is represented in Fig. 2.8, considering that neither over-expansion, nor under-expansion take place.

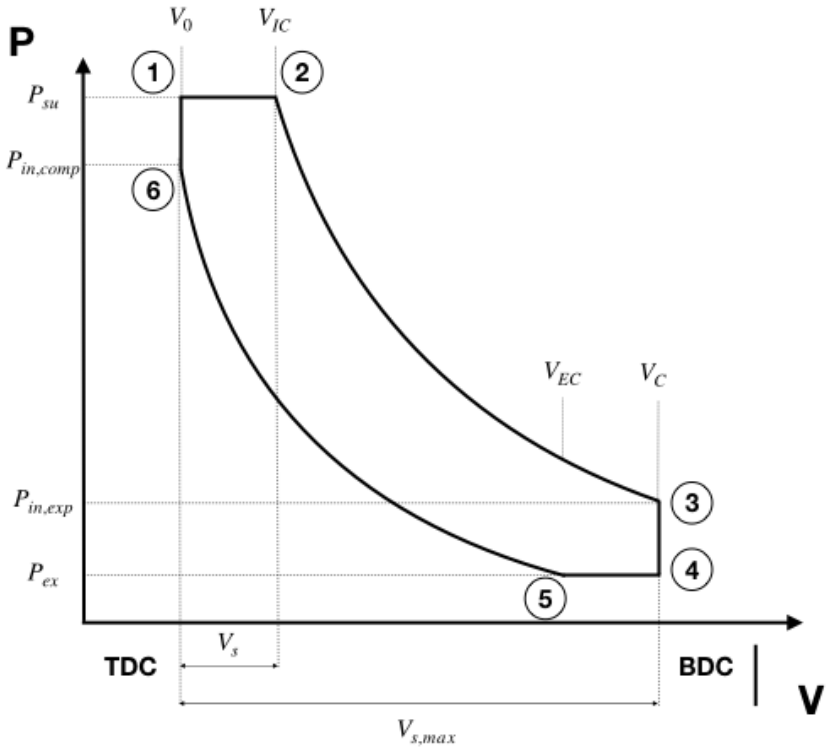

Figure 2.8 – Crossflow piston expander indicator diagram.

In such an expander, a certain number of pistons move inside the corresponding cylinder from the Top Dead Center (TDC), which corresponds to the clearance volume V_0 towards the Bottom Dead Center (BDC). During the suction process the cylinder moves from the position 1 to 2 and the working fluid enters in the cylinders at pressure p_{su} (pressure losses can take place); the suction process finishes until the admission valves close and the cylinder volume is equal to V_{IC}. The increase of the volume from position 1 to 2 is called expander displacement V_s; the ratio between the expander displacement and the volume corresponding to the full stroke ($V_{s,max}$) is called cut-off ratio CO. In the position 2, the expansion of the working fluid stored inside the cylinders start and reaches the pressure $p_{in,exp}$; at this point the exhaust valves open and the discharge process starts (Lemort and Legros 2016). The actual piston expander, rotating at variable speed ranging from 1000 to 3500 rpm, impacts the high pressure in the Rankine system; therefore, varying the expander speed, it is possible to optimize the evaporation process, achieving a better match between the heat source and the working fluid temperature profile, as well as the expander efficiency that is also dependent on the rotating speed (Teng et al. 2007). The speed range that has been already mentioned is suitable for a direct belt compounding coupling with the vehicle propulsion system, avoiding the use of gear that induces additional losses to the system.
The expander chambers accept in their volume a mass of working fluid that is function of the mass flow rate of the working fluid and its rotating speed. The model calculates the density as a function of the mass that is stored in the expander chambers for one revolution and the geometrical data of the machine.

$$\begin{cases} V_s = V_{s,max} CO \\ \rho_{su,exp} = \frac{\frac{\dot{m}_{wf}}{N_{exp}}}{V_{s,max} CO + V_0} \\ p_{su,exp} = f(\rho_{su,exp}, T_{su,exp}) \end{cases} \tag{2.17}$$

The denominator of the (2.17) represents the volume occupied by the working fluid at the end of the suction process, in other words when the supply valve closes.
From density $\rho_{su,exp}$, calculated in (2.17) and temperature calculated as the temperature at the outlet of the evaporator in the evaporator model, it is possible to obtain the pressure of the working fluid at the inlet of the expander. This information is also used by the pump model, (2.1)(2.2) to consider the pressure ratio between inlet and outlet of the pump.
Once the state of the working fluid at the inlet of the expander is completely defined, it is possible to calculate, assuming no heat transfer with the ambient, the gross power production of the expander, knowing the map of the total expander isentropic efficiency ($\eta_{tot,exp}$) and the pressure at the outlet of the expansion machine (Fig. 2.9).

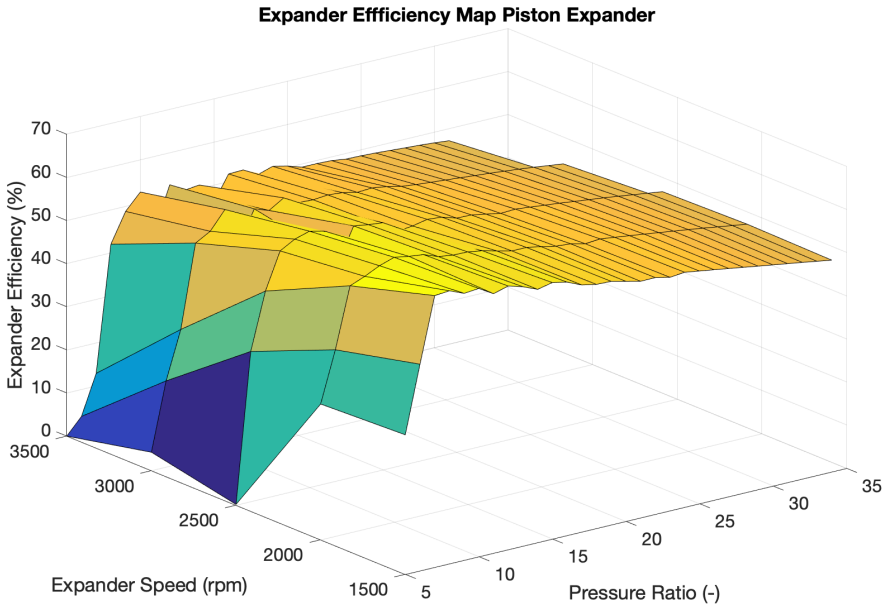

Figure 2.9 – Total expander efficiency as a function of the pressure ratio and the expander speed.

$$\dot{W}_{gross,exp} = \dot{m}_{wf}(h_{su,exp}(T_{wf,su,exp}, p_{wf,su,exp}) - h_{ex,exp}(T_{wf,ex,exp}, p_{wf,ex,exp})) \tag{2.18}$$

2.5 Turbo-expanders

The turbine model receives as input the working fluid bus at the outlet of the evaporator and mass flow rate, the turbine speed and the discharge pressure of the turbine; it provides as output the working fluid bus at the outlet of the turbine, the turbine efficiency and power produced.
Axial and radial inflow turbines belong to the category of turbo-expanders. They can be used in an effective way when packaging represents one of the main constraints and simplification is required (as they usually do not require any lubricant loop, Latz et al. 2013). The higher rotating speed, with respect to positive displacement expanders, makes complicated the direct belt compounding with the vehicle drive-line; therefore, turbines are more suitable for a direct connection to the electrical generator.

The turbine model can be implemented considering the characteristic constant of the turbine K_{eq}, called Stodola constant, that characterises the mass flow rate of the working fluid through the turbine. (2.19), also reported in Vaja and Gambarotta 2010, can be useful to determine the pressure p_{su} of the working fluid at the inlet of the turbine, once the design of the turbine is defined.

$$K_{eq} = \frac{\dot{m}_{wf}}{\sqrt{\rho_{su} p_{su} [1 - (\frac{1}{\epsilon})^2]}} \tag{2.19}$$

where ϵ is the ratio between the turbine inlet and outlet pressure.

Similarly as the positive displacement expander (2.18), the turbine power production $\dot{W}_{turb}$ is calculated by means of a table indicating the isentropic efficiency of the turbine, that, as a first approximation, is set to a constant value.

To conclude, it is important to note that, for the current application, the rotating speed of the turbine N_{turb} has no relevant influence on the pressure at its inlet, therefore the control of the turbine speed can have, as only goal, to maximize the efficiency of the machine itself or of the coupling between the machine and the electrical machine eventually coupled to the turbine.

2.6 Direct Condenser and fan

The direct condenser model receives as input the working fluid bus and mass flow rate, the ambient air temperature, the vehicle and fan speed; it provides as output the working fluid bus at the outlet of the condenser, the average temperature of the cooling air at the outlet of the condenser and the fan power demand.
The selected condenser is an aluminum heat exchanger made up of flat extruded tubes and of corrugated louvered fins. Assuming a perfect distribution of the cooling air on the surface of the condenser, it is possible to consider a cross-flow pattern; Fig. 2.10 shows the inlet and outlet section of the working fluid as well as the cooling fan.
The condenser model is obtained using a 1D finite volume (FV) discretization. Energy and mass balance conservation equations are applied to the gas side, fluid side and separation wall ((2.3), (2.5), (2.6), (2.7)). The overall mass flow of cooling air is divided by the number of volumes adopted for the discretization and its outlet temperature is computed as the average of the outlet temperature of the cooling air from each volume.

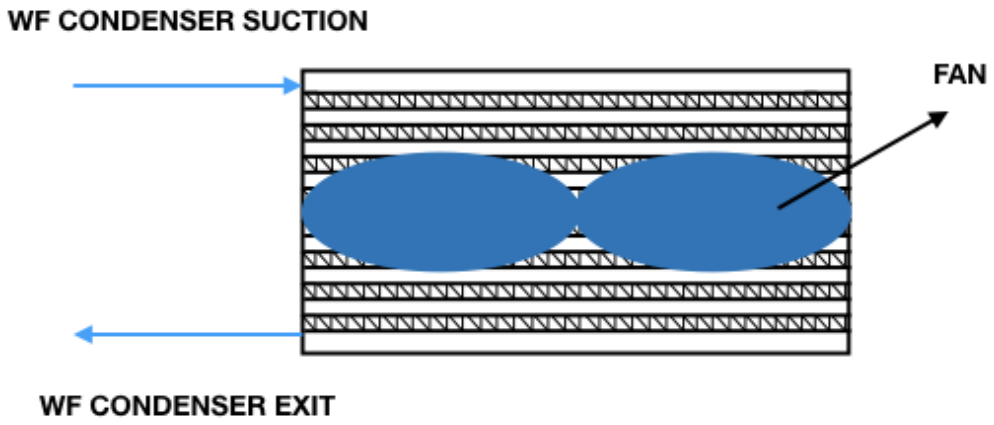

Figure 2.10 – Direct condenser, tube and fin heat exchanger, scheme.

In order to compute correctly the thermal power exchanged between the fluid and the wall, and between the wall and air flow, a geometrical analysis of the condenser is necessary. Geometrical data can be retrieved by calculations, once the fluid side and air side exchange areas are set (these data are available from the supplier). In particular, the following data are retrieved or calculated:

- Number of tubes
- Fin density (expressed $\frac{N_{fin}}{dm}$)
- Heat transfer area for fluid and gas side
- Flow section for fluid and gas
- Volume for fluid and gas side
- Separation wall volume

Considering the fluid side, the fluid flows in channels that are realized in the tubes; according to Chan Kang and Jun 2011 channels of the size that is between 0.2 and 3 mm are considered as mini-channels. Here the mini channels have a rectangular section. Using this data and knowing the fluid side heat exchange area, it is possible to compute the fluid flow area and the number of mini channels per tube. These data are particularly useful for the definition of the flow regime and calculation of the heat transfer coefficients in single phase and two-phase ((2.12), 2.13).

Regarding the air side, several other studies have been conducted in the last decades (Chang et al. 1997, Chan Kang and Jun 2011, El Hajal et al. 2003). For this work, the correlation proposed by Chan Kang and Jun 2011 has been chosen because of the large number of combinations of different geometries of louvers and fins that have been investigated and the range of validity of the correlations, as a function of the Reynolds number calculated in the louver pitch section, the ratio of the louver pitch and fin pitch and the louver angle.
The empirical correlations (2.20) allow to compute the Colburn number j and the friction factor f (Fig. 2.11.a), that are useful to find the heat transfer coefficient on air side h (Fig. 2.11.b) and the the pressure drop of the air through the condenser, respectively.

$$\begin{cases} j = \frac{\eta_{fin} h Pr^{2/3}}{\rho u_c c_p} \\ f = \frac{2 A_c \Delta P}{\rho A u_c^2} \end{cases} \tag{2.20}$$

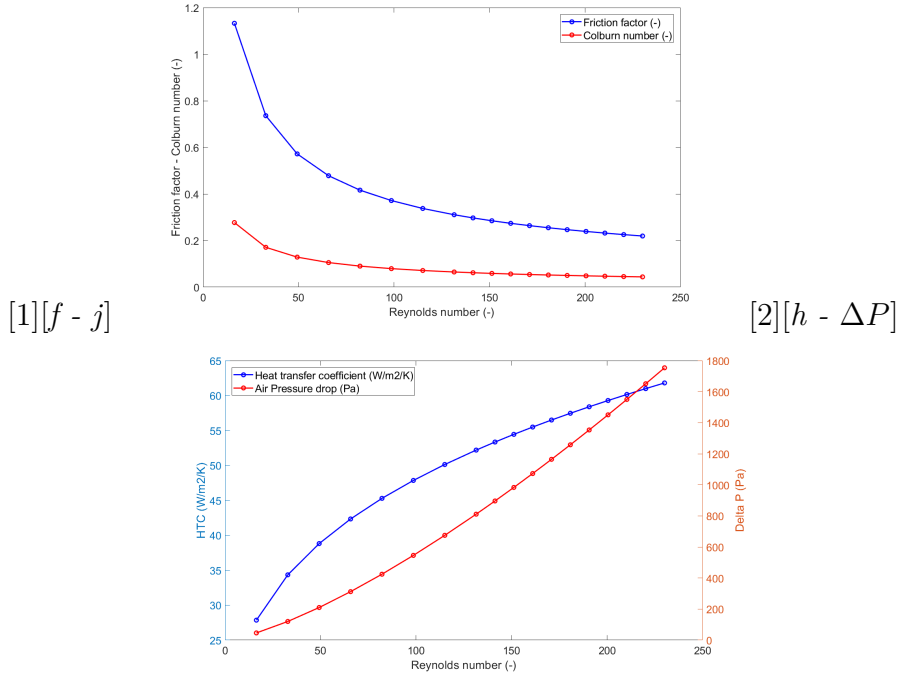

[1][f - j] [2][h - ΔP]

Figure 2.11 – (a) Friction factor and Colburn number as a function of the Reynolds number calculated in the minimum flow section (louver section) by simulation. (b) Heat transfer coefficient and pressure drop as a function of the Reynolds number calculated in the minimum flow section (louver section) by simulation.

where η_{fin} is the fin efficiency, c_p is the specific heat of the air at constant pressure, u_c is the velocity of the air in the louver section (minimum flow section), A is the air side are of the heat exchanger, A_c is the minimum flow area, ΔP is the pressure drop across the heat exchanger, Pr is the Prandtl number.

The heat transfer coefficient and the air pressure drop as a function of the Reynolds number calculated in the louver pitch L_p are shown in Fig. 2.11; the variation of f and j, as well as the variation of h and ΔP are coherent with the literature (Chang et al. 1997, Chan Kang and Jun 2011, El Hajal et al. 2003). Fan suppliers provide the fan curve, which expresses the static pressure (Δp) variation through the fan as a function of the volumetric flow rate (m^3/h) at nominal speed. Curves at other speeds can be found thanks to the Fan Laws (Kanefsky et al. 1999). Plotting in the same graph the fan curves at different fan speeds and the pressure drop curve characteristic of the condenser, it is possible to identify the intersections of these curves, hence the operating points of the system. The condenser model predicts the condenser pressure drop from data supplier with a relative error of 1% in the range of interest of volume flow rate (Fig. 2.12). In the same figure, it is possible to identify the curves related to the fan power demand; once the characteristics of the condenser is defined, for each value of cooling air volume flow rate, it is possible to identify the fan power required by the fan. This information is useful in order to validate the model of the condenser, as well as to perform dynamic simulations and quantify the fan power demand and the air flow rate to the condenser.

Regarding the steady-state performance of the direct condenser, results have been compared and validated according to steady-state measurement provided by the supplier, using cyclopentane as working fluid. The choice of using cyclopentane derives from the fact that material compatibility tests conducted by Modine (Kimmel 2017) and FVV (Reitz et al. 2018) on ethanol and aluminum

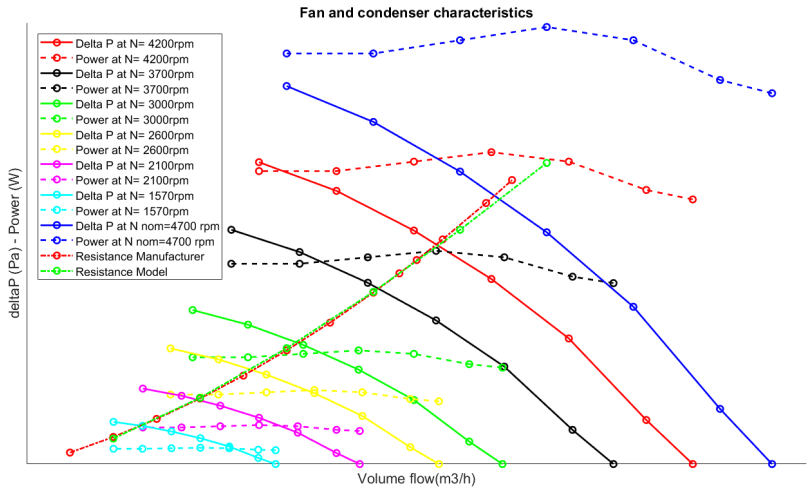

Figure 2.12 – Fan static pressures and power demands at different fan speeds and condenser pressure drops. The condenser pressure drop is predicted (green resistance line) with an error of 1% with respect to the supplier data (red resistance line).

showed corrosion products presence, later thicknesses and progressive selective material dissolution. Syvertsen 2017, from FVV, confirmed the ethanol corrosion and showed no significant material degradation and corrosion attack after 480 hours reactor immersion test using cyclopentane.
The pressure supply ranks from the atmospheric pressure to 2 bar as, in most of cases, it is necessary to pressurize the low pressure loop of the Rankine system in order to condensate the cyclopentane. The corresponding thermal power exchanged in the condenser between the coolant air and the working fluid ranks from roughly 15 kW to 60 kW.
Fig. 2.13 shows the validation according to supplier data of the air temperature at the outlet of the condenser; the temperature is computed as the average of the air temperature at the outlet of each volume of discretization. The absolute maximum error of the prediction is 3.79K.
Fig. 2.14 shows the validation according to the same supplier data of the thermal power exchanged between coolant air and working fluid in the direct condenser. The relative error of the prediction is 0.80%.

2.7 Indirect condenser

The indirect condenser model receives as input the working fluid bus at the outlet of the expander and mass flow rate and the coolant temperature and mass flow ratre at the inlet of the condenser; it provides as output the working fluid bus at the outlet of the condenser and the temperature of the coolant at the outlet of the condenser.
The indirect condenser is a plate heat exchanger that uses as heat sink cooling water. Such heat exchangers consist in a certain number of brazed plates stacked one above the other; in order to increase the heat exchange area and the turbulence of the flow, different corrugation patterns have been designed by manufacturers. The chevron corrugation, characterized by the inclination angle and a sinusoidal pattern relative to the main flow direction, is definitely the most common nowadays (Martin 1996). The use of this component, integrated in the Rankine system, leads to the necessity to have an additional glycol-water loop that has to be cooled down by means of the main radiator of the cooling system of the vehicle.

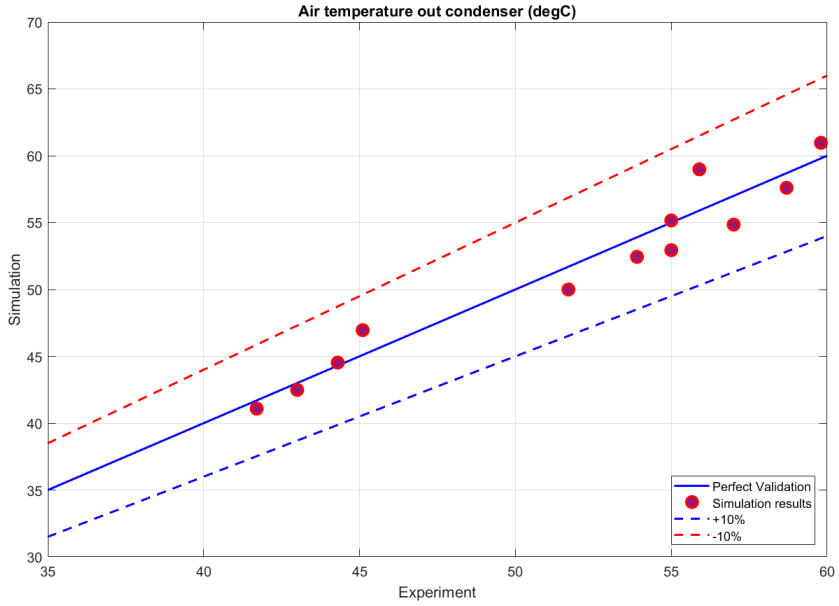

Figure 2.13 – Air temperature at the outlet of the direct condenser, computed as the average of the air temperature at the outlet of each volume.

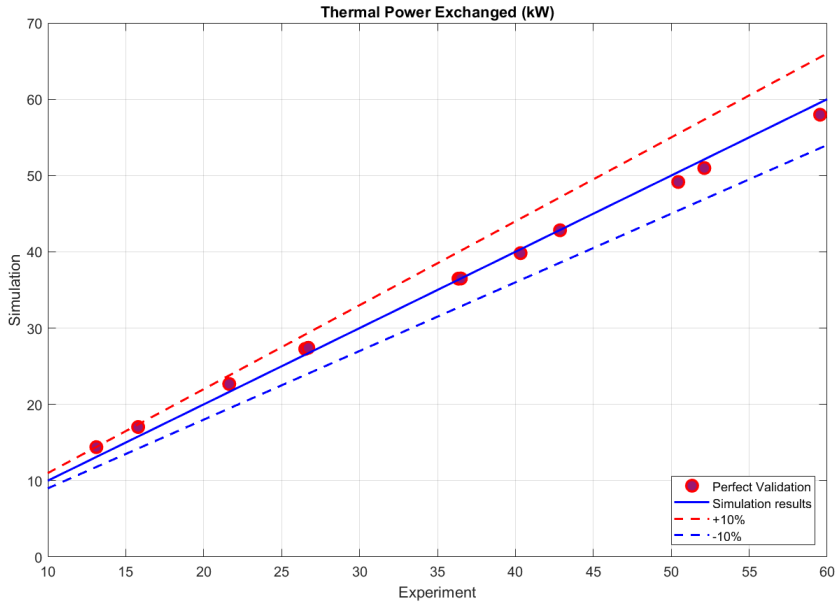

Figure 2.14 – Thermal power exchanged between coolant air and working fluid in the direct condenser.

Fig. 2.15 shows that, according to the position of the suction and the exit sections of the hot and cold fluid in such a condenser and the flow pattern, a counter-flow pattern approach is fully justified.

The presence of an additional cooling glycol-water loop and the dedicated circulation pump leads to unavoidable pressure losses that could heavily penalize the performance of the waste heat recovery system (Fig. 2.16), that includes the Rankine system and the cooling loop. In existing cooling systems of heavy-duty trucks, it is possible to quantify roughly a pressure drop of 1 bar for 1 kg/s

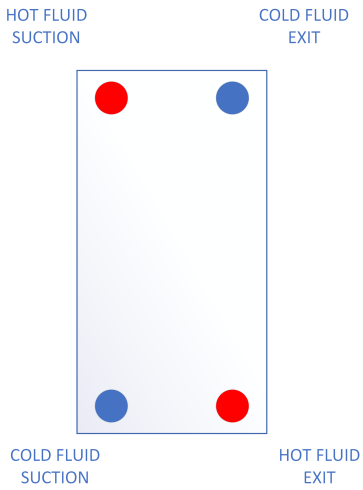

Figure 2.15 – Inlet and outlet sections of the indirect condenser (brazed plates heat exchanger).

of mass flow rate of coolant flow. This assumption is useful in order to compare the performance of different systems and take into account the cooling pump power demand in the energy balance of the system.

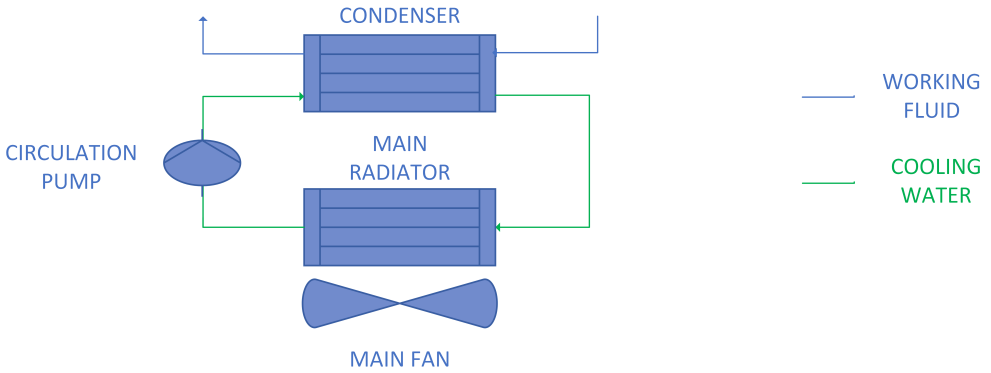

Figure 2.16 – Rankine system using the indirect condensation. The cooling water is cooled down in the main vehicle radiator and circulates by means of an additional pump.

The additional thermal load to reject from the main radiator of the vehicle can impact the correct operation of the whole cooling system of the truck, leading to main fan activation and, consequently, high power demand (Galuppo et al. 2018c). Therefore strategies are required to limit the fan activation and ensure the positive net power production of the Rankine in any road cycle operations: this will be discussed in Chapter 5.

2.8 Recuperator

The recuperator model receives as input the working fluid bus at the outlet of the pump (cold stream) and the expander (hot stream), as well as the working fluid mass flow rate; it provides as output the working fluid bus at the outlet of the recuperator of both cold and hot side.
The recuperator (also called regenerator) is a basic heat exchanger, often a plate heat exchanger, that is used in order to partially recover heat from a hot fluid flow and transfer it to a cold fluid

flow. The use of this component can lead to an increase of the thermal efficiency of the Rankine system, as a consequence of the reduced heat that is necessary to remove from the condenser (even though lower heat is recovered in the evaporator as a result of a higher temperature of the working fluid at the inlet of the evaporator). The beneficial that is possible to obtain is a function of the heat that is actually recovered, heavily changing with the nature of the working fluid.
The model of the recuperator is a 0D model, as a clear design and prototype of such component is not available today. The thermal power that is recovered by the working fluid flow in the cold side of the recuperator is defined as a fraction of the available thermal power of working fluid flow in the hot side, calculated as the thermal power that has to be removed from the working fluid to bring it to the condition of saturated vapour. By means of a thermal balance and fitting of supplier preliminary data, the enthalpy at the outlet of the recuperator (inlet of the evaporator) is found.

Conclusions. *This chapter deals with the modeling of each component that is used for further simulations; pump, evaporator, piston expander, turbine, direct and indirect condenser and recuperator models are available. Most of the 1D models are validated according to experimental results and are further integrated in the global simulation platform in order to perform road cycle simulations and assess the potential of the technology. The validation procedure always shows acceptable results in terms of relative error and maximum absolute difference between the measured and the simulated value. In the next chapter each model is therefore integrated in a complete Rankine model in a close-to real vehicle environment, in order to assess the potential of the technology and implement model based controllers.*

Chapter 3

Working fluid selection and model based control

This chapter faces the challenges related to the implementation of the models seen in Chap. 2 in a global simulation platform of the Rankine. Firstly, a working fluid selection is performed, therefore the optimal set-points of superheat and pressure at the inlet of the expander are determined by means of steady-state simulations. Furthermore the dynamics of the evaporator and condenser are studied in detail and model based controllers are implemented; finally the performance of the system in different road cycles is evaluated and presented.
The algorithm used for the selection of the most representative operating points and the dynamic model in Sec. 3.3.1 have been presented in the 3rd IFAC ECoSM in Changchun, 2018 (Galuppo et al. 2018b); the implementation of the controllers of the superheat has been presented in the 9th Symposium on Advances in Automotive Control in Orleans, 2019 (Galuppo et al. 2019b).

3.1 Rankine system architectures

In the frame of the development of the Rankine based waste heat recovery technology for heavy-duty trucks in Volvo Group, several architectures have been investigated in the previous years. Grelet 2016 studied 4 different architectures according to the waste heat sources that are used: recuperation from exhaust gas flow only, EGR flow only, combined use of exhaust flow and EGR flow in a parallel and serial patterns. This analysis shows that the combined use of these two heat sources in a parallel pattern has the highest performance criterion. Recently, the usage of the combined heat sources has not been the target anymore, especially because of packaging and cost; these aspects are universally considered among the main issues for the implementation of the Rankine system in the vehicle (Hountalas et al. 2012, Yang et al. 2018), as the use of an additional heat source implies the installation of an additional heat exchanger and pipes and, consequently, increasing costs. Therefore the focus of the present analysis is the usage of the only exhaust flow energy as single heat source, that will lead to lower performance, but, in the same time, limited packaging issues and costs.
The first architecture that is investigated (presented in Fig. 3.1) uses a direct aluminum condenser, cooled down by air provided by an electrically-driven fan (the model of the system represented by the direct condenser and the electrically-driven fan is presented in Sec. 2.6) and an additional heat exchanger, lately called recuperator. This additional component is used to pre-heat the working fluid flow at the outlet of the feed pump, exploiting the excessive thermal power of the working fluid flow at the outlet of the expansion machine. The use of the recuperator reduces the thermal power

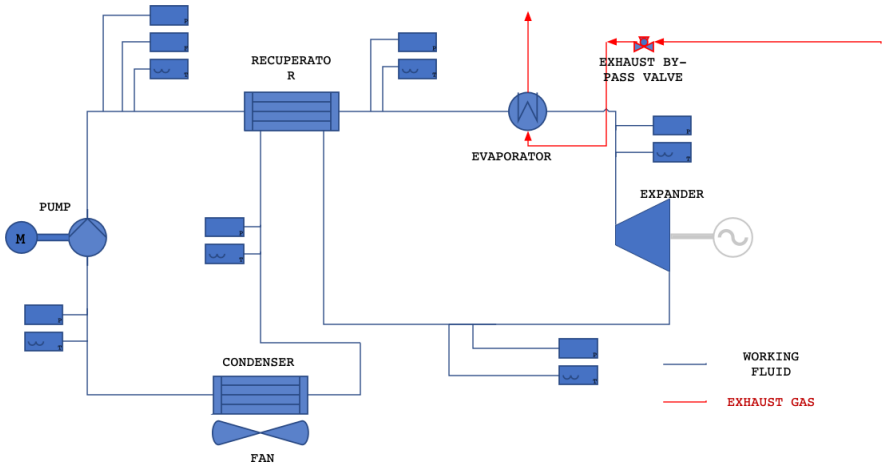

Figure 3.1 – Layout of the direct condenser Rankine architecture, characterized by a completely independent solution for the condensation phase; the condenser and dedicated fan are placed in one side of the vehicle.

that has to be removed from the condenser; one part of the excessive thermal power is therefore "recirculated" to the high-pressure side of the Rankine cycle and it is used to generate additional power. The remaining components are a feed pump, a plate and fin evaporator and a positive displacement expansion machine. This architecture is interesting for further development, as it does not impact in any way the correct operation of the cooling system and the expander shaft is directly connected to the electrical generator, avoiding any connection with the vehicle mechanical drive-line. It is important to notice that the condenser and the dedicated fan are not placed in the front-face of the vehicle, but one side of the vehicle; it is assumed that no RAM air-flow is admitted at the inlet of the condenser and the cooling of the system is fully demanded to the electrically-driven fans (Fig. 3.2).

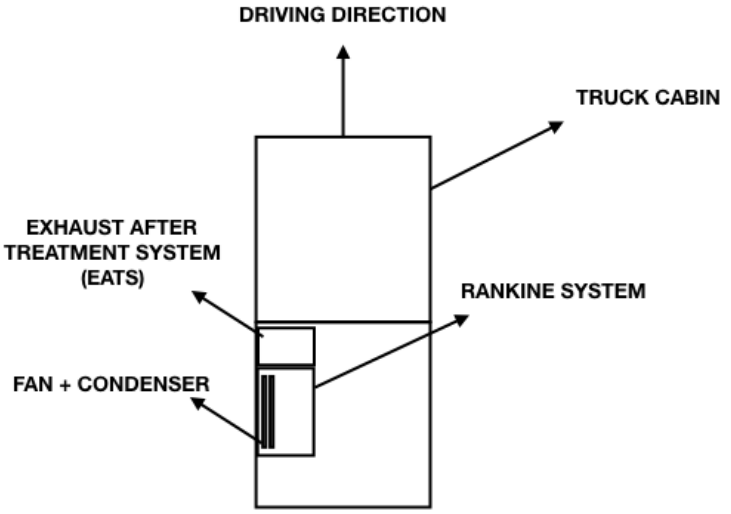

Figure 3.2 – Direct condenser position in the truck (view from the top, not to scale).

The second architecture (presented in Fig. 3.3) differs from the first one as it uses, in place of the direct condenser and dedicated fans, an indirect stainless steel condenser (model in Sec. 2.7), cooled down by water, circulating in an low-temperature loop by means of an additional Rankine

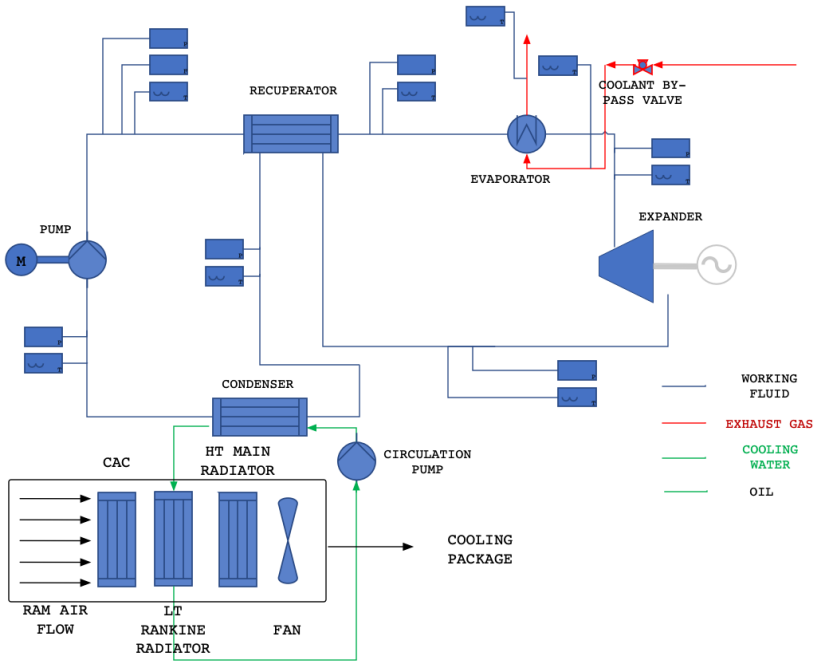

Figure 3.3 – Layout of the indirect condenser Rankine architecture, characterized by an additional cooling loop for the Rankine system and, consequently, an additional low temperature radiator in the cooling package.

coolant pump. As already mentioned, this configuration implies the use of an additional low-temperature (LT) radiator in the front-face of the truck that has the role to reduce the temperature of the Rankine water coolant, by means of the RAM intake air and, in the phases characterized by high thermal load, the cooling system fan. The LT radiator, in the indirect condenser Rankine architecture is positioned between the Charge Air Cooler (CaC) and the high-temperature (HT) radiator, defining the new cooling package of the cooling system (Fig. 3.4.
This configuration leads to a reduction of the energy needed for cooling down the Rankine system, as it uses the RAM intake air as heat sink for the removal of the excessive heat, without any additional energy consume in most of the operating points; on the other hand, it implies the modification of the usual cooling system of the vehicle as well as packaging related issues.

In order to assess the potential of both architectures, the expander power produced, as well as the pump power demand and the power that is necessary to supply in order to remove the excessive heat in the condenser are calculated. The expander gross power is the electrical power that is produced by the expander and takes into account the losses linked to the machine and the transformation from mechanical to electrical energy and the pump power. The cooling power demand is the electrical power that is needed to cool down the system:

- As for the direct condenser Rankine architecture, the cooling power demand is the electrical power demand of the fans that deliver the air flow to the condenser
- As for the indirect condenser Rankine architecture, the cooling power demand is the electrical power demand of the cooling circulation pump; according to the design of the cooling system and the type of road cycle, the main fan of the cooling system could be engaged to face high load transients, leading to higher power consumption to cool down the system

For both architectures, steady state simulations have been realized (simulations have a key role to assess the potential of different Rankine architectures and working fluid, as performing intensive and time-consuming experimental campaigns is often not possible in the industry) in the whole

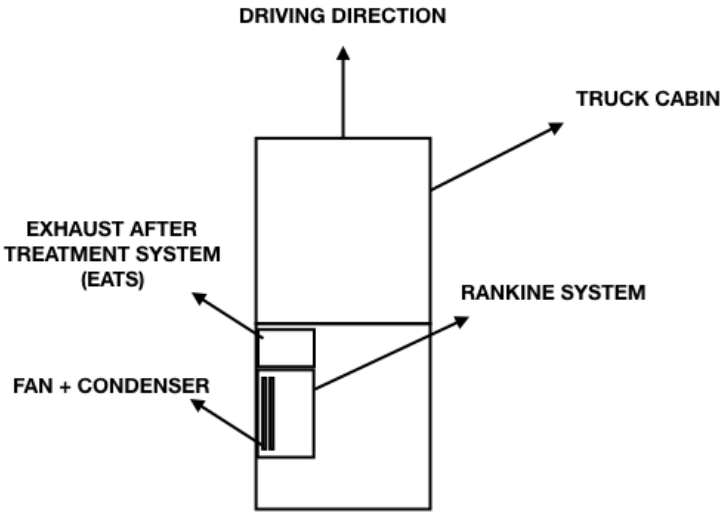

Figure 3.4 – Indirect condenser and LT radiator position in the truck (view from the top, not to scale).

engine map and the net power is calculated; the Diesel engine is a 13-liter, non-EGR engine and the vehicle weight is 35 tons . The components that are in common in both architectures, such as the pump, evaporator, expander and recuperator have the same size; additionally expander and pump have the same isentropic efficiency. The main difference between the models representing the two architectures is in the condenser and the heat sink (plate and fins heat exchanger and ambient air for the direct condenser architecture, the brazed plate heat exchanger and coolant glycol-water mixture for the indirect condenser architecture); the condensation pressure is chosen according to the heat sink temperature at the inlet of the condenser. Tab. 3.1 highlights the main differences between the direct and indirect condenser architecture; in the last column of the table, the condensation pressure is found as the saturation pressure at the coolant temperature at the inlet of the condenser, increased by 30 and 10 K for direct and indirect condensation respectively. This difference has been chosen as a result of the fact that a lower amount of air flow rate is available for direct condensation, with respect to the glycol-water for the indirect condensation and as a consequence of the fact that the convective heat exchange is less performing using air as secondary fluid; therefore higher temperature difference between the coolant and the working fluid flow has to be ensured in the direct condensation with respect to the indirect condensation.

Arch	Condenser	Coolant	Cool Temp(°C)	Cool max $\dot{m}$(kg/s)	Cond Press(bar)
Direct	Plate and fins	Air	40	1.5	$\mathrm{p}_{sat}(T_{cool,su,cond}+30)$
Indirect	Brazed plates	Glycol-Water	60	5	$\mathrm{p}_{sat}(T_{cool,su,cond}+10)$

Table 3.1 – Main characteristics of the different fluids.

$$\dot{W}_{net} = \dot{W}_{gross} - \dot{W}_{pump} - \dot{W}_{cooling} \tag{3.1}$$

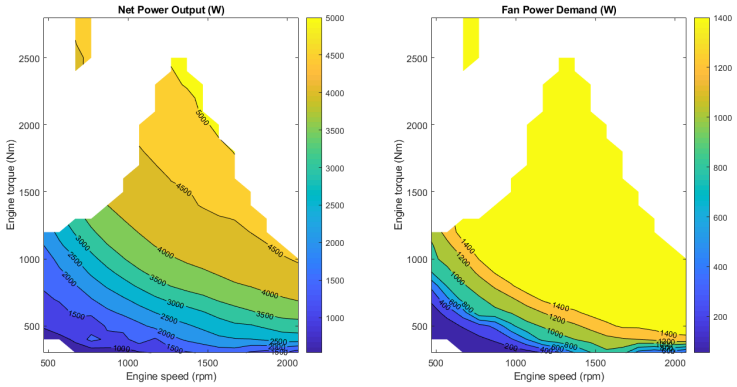

Figure 3.5 – Direct condensation: net power produced and fan power demand using cyclopentane as working fluid.

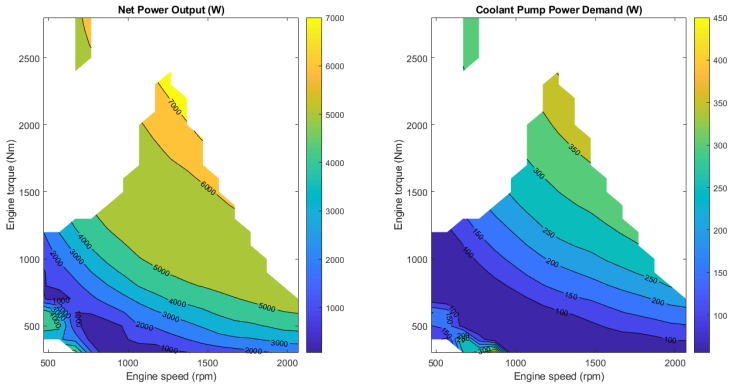

Figure 3.6 – Indirect condensation: net power produced and coolant pump power demand using cyclopentane as working fluid.

The results in Fig. 3.5 and 3.6 for direct and indirect condensation respectively show the fact that the direct condensation configuration leads to a lower performance than the indirect condensation using cyclopentane as working fluid (tendency is confirmed using ethanol); the comparison between the fan power demand for the direct condensation architecture and the cooling pump power demand for indirect condensation shows that the fan power demand impacts in a more significant way, reducing the net power production of the system. This result is a consequence of the sizing of the system and the components that are used, as well as the hypothesis on the pressure drop of the coolant flow in the indirect condensation configuration.
The two architectures under investigations provide different results in terms of performance; in particular, our previous results show that the indirect condensation architecture provides higher overall performance than the direct condensation. On the other hand, the indirect condensation impacts heavily on the cooling system of the vehicle, inducing modifications and additional installation of longer pipes.
Considering advantages and drawbacks of both architecture, related to the performance of the specific Rankine system and the challenges to be faced in order to integrate the system in the vehicle, the direct condensation architecture has been chosen; therefore all the further investigations in this thesis are performed on the direct condensation architecture, that has the advantage to impact as little as possible the normal operation of the cooling system.

3.2 Working fluid selection

One of the major topics that has involved the researchers in the Organic Rankine Cycle scientific community is the working fluid selection. As already mentioned in Sec.1.3, the selection of the working fluid is specific for each application and an universal optimal working fluid for every Rankine configurations has not been identified yet (Stijepovic et al., 2012). This implies that for every system configuration and performance goal, the fluid selection procedure provides different results. For the two Rankine architectures in Sec. 3.1, a first screening on the available working fluids for the current application is performed from literature, leading to ethanol, R1233ZD, Novec649 and cyclopentane as the four working fluids to be investigated. The results of the analysis in Preißinger et al. 2017 shows that ethanol is the overall best ranked fluid as it is applicable to all the investigated operating points and, in the same time, it is not toxic and has no-significant Global Warmin Potential (GWP). R1233ZD and Novec649 have similar thermodynamic performance and lower GWP with respect to R245fa, which is considered a common benchmark, but it is characterized by a GWP of 1030. Marlok et al. 2019 shows the benefit of using cyclopentane in place of ethanol in a direct condenser Rankine system, therefore it has been added in the current analysis. The four working fluids, as well as their main characteristics, are listed in Tab.3.2.

Fluid	Type	Boiling point (°C)	$\Delta H_{vap}(\frac{kJ}{kg})$	$P_{crit}(bar)$
Cyclopentane	Dry	49	389	45.15
Ethanol	Wet	78	850	61.48
*Novec*649	Dry	49	88	18.69
*R*1233*ZD*	Dry-Isentropic	14	195	36.23

Table 3.2 – Main characteristics of the different fluids.

As it is possible to notice from the Tab. 3.2, the working fluids can be preliminary compared according to the slope of the saturated vapor curve (type), boiling point, latent heat of vaporization and critical point:

- The working fluids are commonly classified in three categories: wet, dry and isentropic. A working fluid is named wet if the slope of the saturated vapor curve is negative (water, ethanol); fluids that are characterized by a positive and infinite slope of the saturated vapor curve are named dry (cyclopentane, Novec649) and isentropic (R11,R12), respectively. R1233zd shows a slight positive slope and can be regarded as dry-isentropic fluids (Ziviani et al. 2016). The nature of the fluids based on the type leads to practical considerations that are useful to ensure performance and the safe mode operation of components; this implies that a wet fluid should be superheated more than a dry fluid in order to ensure that the expansion fully takes place in the superheated vapor zone of the T-S diagram. A dry fluid normally needs to be less superheated, as once the expansion process starts with a vapor quality of 1, it is ensured the expansion is fully in the superheated vapor zone. Therefore, the use of a dry fluid leads to the possibility to limit the superheat and increase the mass flow rate of the working fluid. An example of the saturated vapor curves for the three different types of working fluids is provided in Fig. 3.7.
- The normal boiling point is defined as the temperature at which the saturated vapor pressure of a liquid is equal to the surrounding atmospheric pressure; as for water, the boiling point is 100°C, while Tab. 3.2 shows in the third column the normal boiling point for the fluids that are investigated. This property has to be taken into account because it has a central role in the match between the working fluid temperature profile in the condenser and the temperature

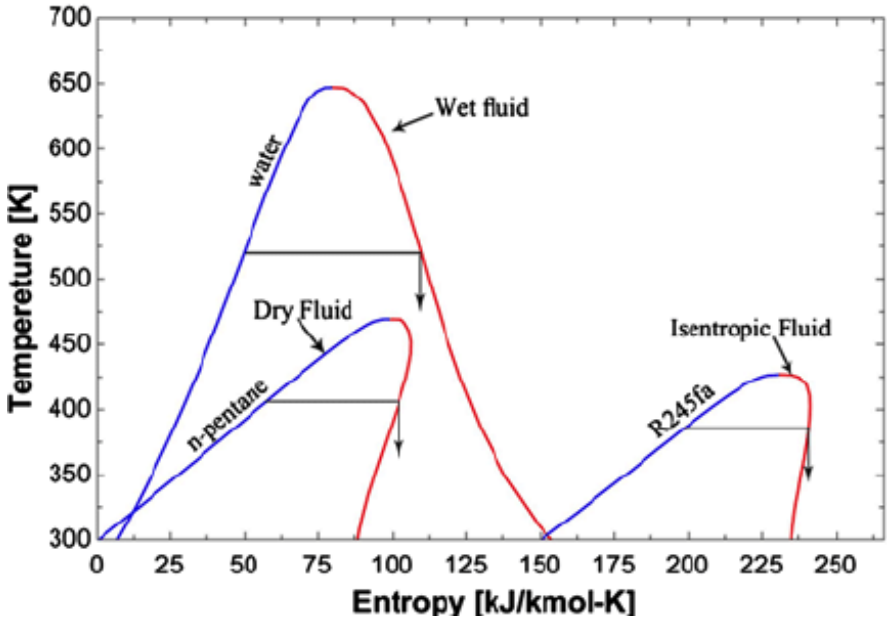

Figure 3.7 – T-S (temperature-entropy) diagram for different types of working fluid (Bahrami et al. 2013).

of the heat sink. R1233ZD has the lowest boiling point among the selected working fluids, consequently, in order to operate at the atmospheric pressure in the condensing loop, the heat sink should operate at lower temperature than its boiling point, otherwise the condensing loop has to be pressurized in order to ensure the full condensation.

- The latent heat of vaporization ΔH_{vap} is defined as the heat that is required in order to vaporize 1 kg of fluid at the atmospheric pressure. Ethanol is characterized by the highest latent heat of vaporization among the working fluids listed in Tab. 3.2; this leads to the fact that, transferring the same amount of heat to the fluid, the mass flow rate of ethanol in the system is lower than using any other working fluids listed in the table.
- The critical point (critical temperature and pressure p_{crit}) is defined as the point at which the phase boundaries liquid-vapor vanishes. The actual investigation regards sub-critical transformations, therefore no working fluid operates beyond its critical pressure and the maximum operating pressure for each fluid is the critical pressure.

3.2.1 Comparison of working fluids in terms of net power

The comparative analysis of the working fluids in terms of performance is conducted on one specific operating point, characterized by the temperature and the mass flow rate of the exhaust has at the inlet of the evaporator, $T_{exh,su,ev}$=350 °C and $\dot{m}_{exh,su,ev}$=0.2 kg/s, found as the average of the exhaust temperature and mass flow rate provided by the 13-liter non-EGR engine driving common European road cycles; the heat sink nature and temperature have already been presented in Tab. 3.1 and are confirmed for the current study.
In this analysis, the "high-level" design of the components is set beforehand; however, in order to take into account the different nature of the working fluids, in particular the different volume flow rate in the system, modifications are applied to the heat exchangers, expander and feed pump. The flow sections, volumes and heat exchange surface in the working fluid side of the heat exchangers are increased using Novec649 and R1233ZD, as their volume flow rate is sensibly higher than using the cyclopentane and ethanol. The cut-off ratio of the expander is also modified, in order to adapt

the evaporating pressure of the working fluids in the system, because of the different volume flow rate at the inlet of the expander; the cut-off ratio of the piston expander (Sec. 2.4) is increased using Novec649 and R1233ZD as working fluids and the global expander efficiency is set to 60 % for each working fluid. The feed pump displacement is also increased when using Novec649 and R1233ZD with respect to cyclopentane and ethanol, but its isentropic efficiency is set to 55% for each working fluid.
The set-point of the evaporation pressure is 25 bar for ethanol, R1233ZD and cyclopentane and 16 bar for Novec649, because of its lower critical pressure with respect to the other fluids. The superheat, defined in 3.2, at inlet of the expander is set at 30 K for cyclopentane and to 10 K for Novec649 and R1233ZD. The subcooling, defined in 3.9, is set to 9 K for all the working fluids.
The main results, specifically for the direct condensation (first architecture), are listed in Tab. 3.3. As already mentioned in Sec. 2.6 the use of ethanol on aluminum components leads to corrosion, under operating conditions that are comparable with the pressure and temperature values that is possible to encounter in the condensation of the ethanol. For this reason, the working fluid selection, in the case of direct condensation architecture, is limited to cyclopentane, Novec649 and R1233ZD. The fluid R1233ZD is penalized because of the high condensation pressure that has been set in order to ensure a complete condensation of the working fluid, impacting in a dramatic way the power production of the expansion machine. The fluid Novec649 is also penalized because of its low critical pressure (16 bar). An important remark on the usage of the Novec649 is that it looks more suitable with low-grade thermal heat sources; this statement will be verified in Chap. 4, where the performance of Novec649 and R1233ZD are compared in a Rankine system that recovers energy from the coolant flow. Fig. 3.8 shows that cyclopentane is the best fluids, in terms of performance, for this specific architecture; despite the high fan power demand, the net power is higher than using the remaining fluids, because of the higher pressure ratio at the inlet and outlet of the expander that is possible to reach. Novec649 and R1233zd also lead to higher pump power demand with respect to the cyclopentane, impacting the energy balance of the Rankine system.
The same study can be performed on the Rankine architecture characterized by the indirect condensation; in this case, the ethanol is considered in the analysis, as no material compatibility issues are reported between ethanol and stainless steel. Tab. 3.4 shows a comparison among the four different working fluids, operating in an indirect condensed Rankine system. The use of ethanol leads the lowest condensation pressure among the working fluids analysed as a consequence of the highest boiling point; R1233ZD, because of its lowest normal boiling point, leads to the highest condensation pressure, impacting on the expander power production and, consequently, on the net power production. Fig. 3.9 shows that the contribution of the coolant pump power demand, feed pump power demand and gross expander power for each working fluid; cyclopentane is again the best fluid in terms of net power production, on the other hand, ethanol presents the possibility to not pressurize (or weakly pressurize) the cold side of the Rankine, with performance that are comparable with the cyclopentane; this aspect has to be taken into account, as the adoption of the atmospheric pressure on the cold side of the Rankine system is a strong simplification in terms of control (the condensation pressure control is not needed) and equipment (the valve that regulates the pressure of the pressurized air that is used to pressurize the cold side of the Rankine system is not needed).

Fluid	$\rho_{su,exp}(\frac{kg}{m^3})$	$\dot{V}_{su,exp}(\frac{dm^3}{s})$	$P_{ev}(bar)$	$P_{cond}(bar)$	$NetPower(kW)$
Cyclopentane	61.2	1.410	25	2.46	3.76
*Novec*649	235.1	1.895	16	3.85	2.26
*R*1233*ZD*	111.2	2.114	25	8.42	2.11

Table 3.3 – Main results of the simulation study based on the different fluids, direct condensation in the operating point characterized by $T_{exh,su,ev}$=350 °C and $\dot{m}_{exh,su,ev}$=0.2 kg/s. Ethanol is not considered because of material compatibility issues with the direct aluminum condenser.

Fluid	$\rho_{su,exp}(\frac{kg}{m^3})$	$\dot{V}_{su,exp}(\frac{dm^3}{s})$	$P_{ev}(bar)$	$P_{cond}(bar)$	$NetPower(kW)$
Cyclopentane	61.2	1.410	25	2.13	4.82
Ethanol	28.92	1.520	25	1.08	4.58
*Novec*649	235.1	1.895	16	2.64	2.58
*R*1233*ZD*	111.2	2.114	25	6.6	2.69

Table 3.4 – Main results of the simulation study based on the different fluids, indirect condensation in the operating point characterized by $T_{exh,su,ev}$=350 °C and $\dot{m}_{exh,su,ev}$=0.2 kg/s. Ethanol is considered in this case, as no material compatibility issues are reported between ethanol and stainless steel.

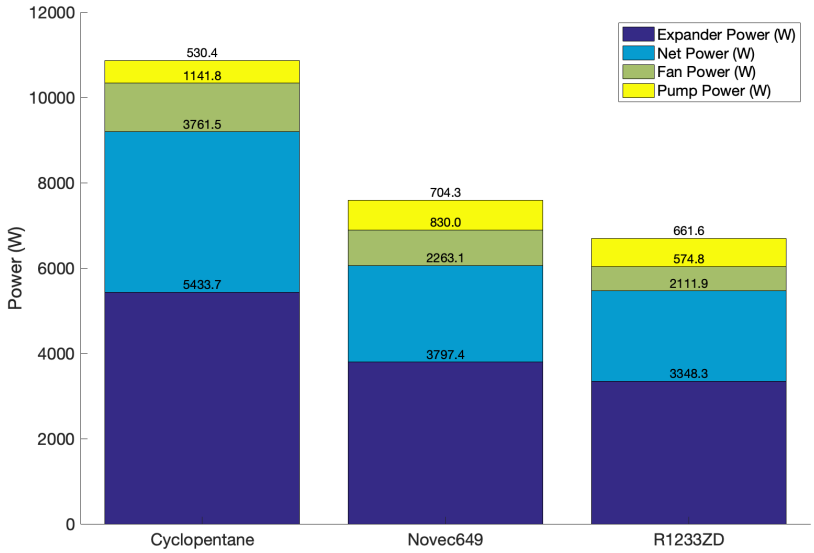

Figure 3.8 – Power demands and production of the Rankine system using the three fluids in direct condensation in the operating point characterized by $T_{exh,su,ev}$=350 °C and $\dot{m}_{exh,su,ev}$=0.2 kg/s: the net performance of the Rankine system is evaluated subtracting the pump and fan power demand to the expander power produced.

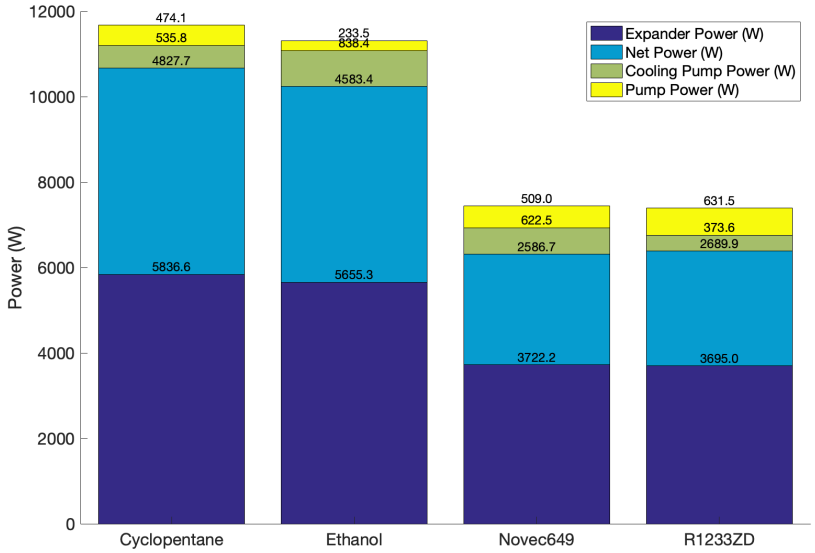

Figure 3.9 – Power demands and production of the Rankine system using the four fluids in indirect condensation in the operating point characterized by $T_{exh,su,ev}$=350 °C and $\dot{m}_{exh,su,ev}$=0.2 kg/s: the net performance of the Rankine system is evaluated subtracting the pump and fan power demand to the expander power produced.

3.2.2 Selection of the most suitable working fluid

The analysis that is performed on both the direct and indirect condensation architecture highlights that cyclopentane is the most suitable working fluid in terms of performance; on the other hand, the use of cyclopentane leads to issues relative to safety (as cyclopentane is strongly flammable) and integration (as it is necessary, in this application, to pressurize the cold side of the Rankine system in order to obtain the highest performance). Ethanol, analysed for the indirect condensation architecture only, present comparable performance with cyclopentane, with the possibility of not pressurizing the cold side of the Rankine system to obtain the highest performance. Novec649 and R1233ZD lead to a net power production that is clearly lower than cyclopentane and ethanol; R1233ZD, characterized by a low boiling point, leads to the necessity to strongly pressurize the cold side of the Rankine system in both the direct and indirect condensation architecture, Novec649 is penalized as well because of the low critical pressure that limits the pressure ratio between the inlet and outlet of the expander and, consequently, the expander power production.
The conclusion of the analysis, leads to the choice of cyclopentane in the case of the direct condensation architecture (because of a gain in performance of 66% and 78% with respect to Novec649 and R1233ZD respectively) and the ethanol in the case of the indirect condensation architecture because of the possibility to use atmospheric pressure in the cold side of the Rankine system and comparable performance with cyclopentane (net power output using ethanol is 5% lower than cyclopentane).

3.3 Establishment of a dynamic model

The models that have been presented in Chapter 2 have been validated according to experimental results in steady-state conditions. However, considering the highly-transient nature of the system inputs and perturbations, the dynamic study of the models is necessary, as well as the dynamic

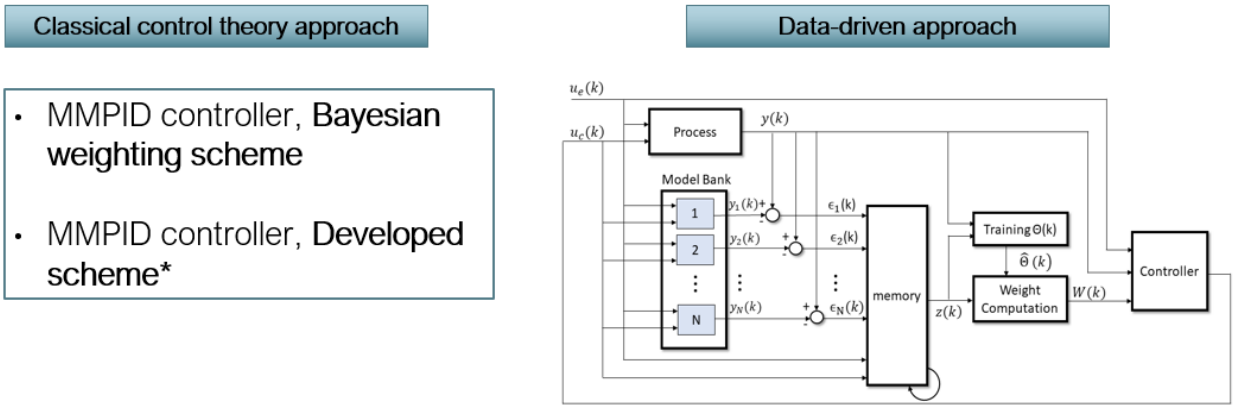

Figure 3.10 – Presentation of the two different options for controller design adopted in the manuscript.

validation of the results according to experimental results.
In the Rankine system, a large number of dynamics takes place; in this application, the most relevant dynamics is related to the heat exchangers, while the pressure dynamics is neglected since they are faster. Considering the two heat exchangers of the system, the condenser and the evaporator:

- The latter is characterized by higher mass and dimension that make favorable the introduction of the most relevant dynamics in the system.
- The direct condenser is a 4 kg radiator, characterized by a separation-wall thickness of the order of hundreds of microns; although the dynamics in the condenser are expected to be faster than the evaporator, in the following paragraphs (Sec. 3.7)the dynamics in the condenser are studied as the accumulation of the working fluid in the condenser can lead to the introduction of further dynamics.

Focusing on the evaporator, different operating conditions can induce different behaviors of the evaporator and its dynamics. Due to the complexity of the system, as it involves non-linearity, couplings and phase change, the use of one single model, with fixed parameters, can be not effective enough to describe the behavior of the evaporator in all the operating range of interest. For further control design, it has been chosen to linearize the model in specific operating points that are selected according to criteria that are presented in the Sec. 3.3.1; once the operating points have been selected, an unique controller can be implemented based on a single model that is found as linear combination of the operating points selected (the linear combination is operated by dedicated weighting schemes, as the Bayesian weighting scheme). Another option that has been adopted in this thesis is the usage of a deep neural network (Sec. 5.2) that leads to the definition of the unique model that is used to design the controller (Fig. 3.10).

3.3.1 Evaporator dynamics

In this work, a linear model based approach, identified from experimental results in the engine test bench, is proposed. As for practical reasons, linked to cost and availability of the test cell, it is not possible to handle and test all the engine operating points, a methodology for the selection of the engine operating points is also proposed in order to perform the experiments that are necessary to retrieve the linear models used for further control design. For any chosen ORC configuration, the methodology is able to reduce the size of the set of the experiments to perform; the operating points

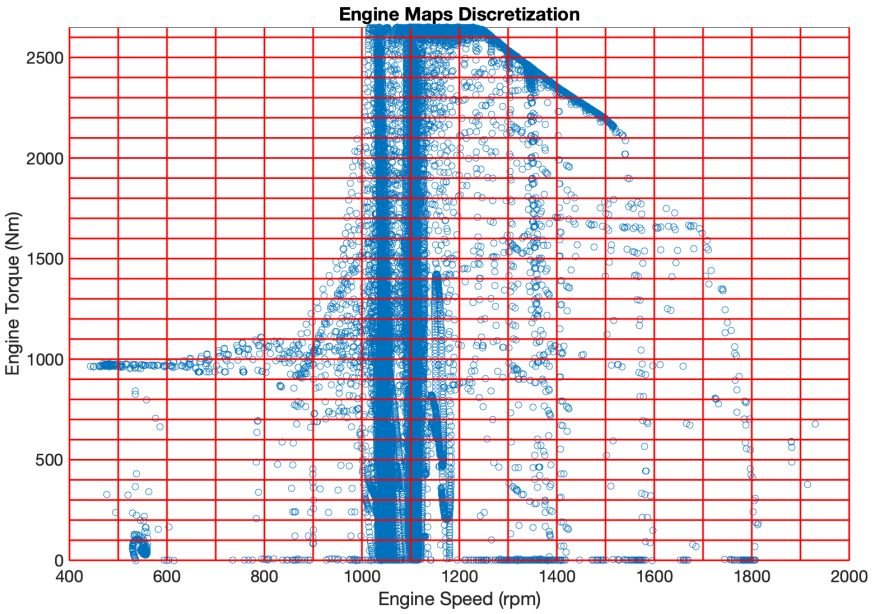

Figure 3.11 – The engine map is discretized in order to obtain squares where the operating points lie.

of the engine can be represented in the engine map, depending on the engine speed and torque. Depending on the chosen road cycle, the engine map usually contains a few tens of thousand points, each of them characterized by a value of engine speed and torque value.
The methodology that is here presented sorts the importance of the engine operating points in a given road cycle depending on two criteria:

- Likelihood of the operating point during the road cycle. The typical mission of a long haul heavy-duty truck is performed in the highway, at constant speed and obviously the operating points that correspond to these situations are more likely than others
- Available thermal power of the exhaust gas for the corresponding operating point. Operating points characterized by low torque values are characterized by lower available thermal power, that is not enough to guarantee the normal operation mode of the Rankine system, therefore these points are excluded from the analysis

The engine map, that gathers all the operating points that are experienced by the vehicle in the French highway road cycle LCG (Lyon-Chambery-Goncelin), are shown in Fig. 3.11; the map is discretized into several squares characterized by edges of 100 rpm and 100 Nm, in order to group narrow operating points that supply the same (or mostly the same) temperature and mass flow of the exhaust gas flow. The most representative squares are determined counting the number of operating points that occupy every single square; once all the operating points have been identified and assigned to each square, the squares are listed by number of operating points in decreasing order.

The algorithm that is used to select the squares that are more representative of the road cycle requires, as input, the number of squares to select. This number is a result of a compromise between the accuracy of the identification of the models to identify and the tests that is possible to perform in the test cell; Fig. 3.12 shows the percentage of the operating points in the specific road cycle that are represented by the number of squares. The analysis of the figure leads to the fact that, according to the discretization adopted in the engine map ($\Delta\Omega$=100 rpm and ΔT=100 Nm), the

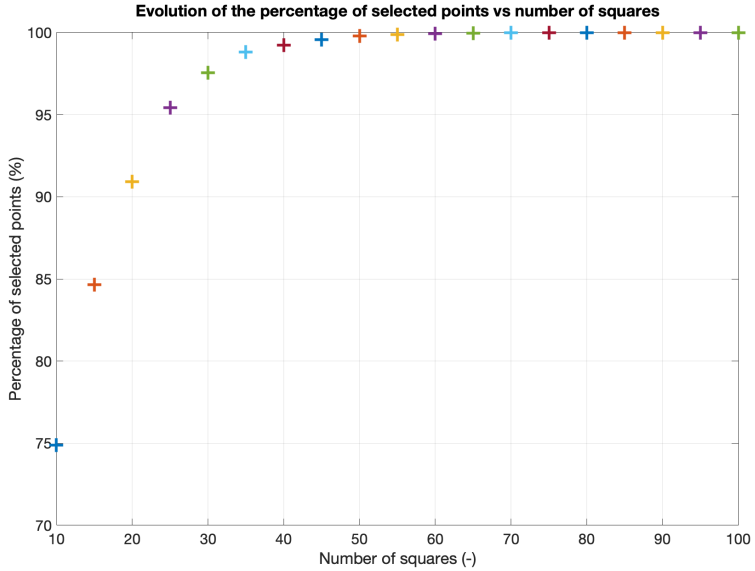

Figure 3.12 – Percentage of the operating point that are represented by the square numbers.

first 10 squares allow to represent 75% of the total number of operating points. This percentage can be increased, in a substantial way, increasing the number of squares to 40, corresponding to roughly 98% of the total operating points. Furthermore increasing the number of squares does not impact significantly the percentage of the represented operating point, as the remaining squares contain less and less operating points; moreover it generates additional complexity and effort in term of number of experiments to perform. In conclusion, 40 is the number of squares that has been chosen, among 98000 at the departure of the analysis, as a good compromise to ensure a good representation of the whole set of operating points. The Algorithm 1 shows the determination of the most representative squares in terms of number of operating points that lie in each of them; the discretization and separation of the engine map in several squares of the edges $\Delta\Omega$xΔT is visualized and the vectors Ω_d and T_d are created. Afterwards all the operating points of the road cycle are extracted and assigned to the square each of them belongs to; $p(i,j)$ is a counter that increases its value by 1 every time an operating point is assigned to the (i,j) square. In the same time, the thermal power associated to every single square is calculated. Afterwards, the probability $P(i,j)$ associated to each square is calculated.

Algorithm 1: Operating points selection.

N_{OP}=98000;
$\Delta\Omega = 100rpm; \Delta T = 100Nm$;
$\Omega_d = min(\Omega) : \Delta\Omega : max(\Omega)$;
$T_d = min(T) : \Delta T : max(T)$;
set: $N_{\Omega_d} = length(\Omega_d), N_{T_d} = length(T_d), T_0 = 293K$;
for *k=1→N_{OP}; i=1→N_{Ω_d}; j=1→N_{T_d}* **do**
  Q(i,j)=$cp_{exh} m_{exh,su,ev}(i,j)(T_{exh,su,ev}(i,j) - T_0)$;
  if $\Omega_d(i) \leq \Omega(k) \leq \Omega_d(i+1) and T_d(j) \leq T(k) \leq T_d(j+1)$ **then**
    p(i,j)=p(i,j)+1;
  else
    p(i,j)=p(i,j);
  end
  P(i,j)=p(i,j)/N_{T_d}
end

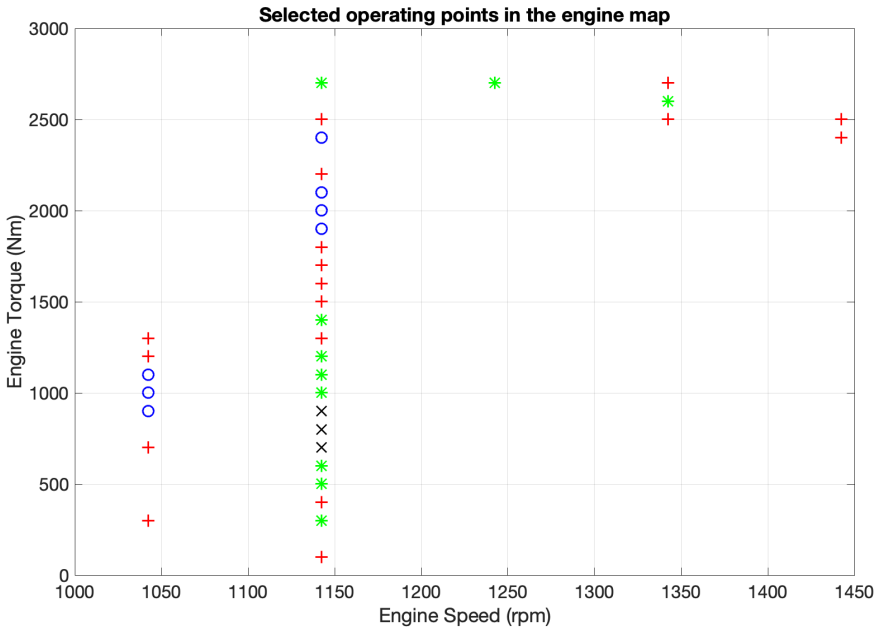

Figure 3.13 – Selected squares in the engine map as a result of the selection method: **x** is for $6.86\% < P(i,j) < 9.38\%$; * is for $2.58\% < P(i,j) < 4.33\%$; + is for $0.70\% < P(i,j) < 2.49\%$; **o** is for $0.47\% < P(i,j) < 0.56\%$.

The squares characterized by the first 40 largest p values are listed in a decreasing order of p, with the corresponding thermal power; the squares that are characterized by thermal power that is lower than 25 kW are excluded from the analysis, as for such weak thermal input the cyclopentane cannot reach the nominal operating conditions at the outlet of the evaporator; therefore the number of operating points that have to be tested is limited to 37.
In Fig. 3.13 the 37 selected points are presented and divided according to the $P(i,j)$ values calculated in the algorithm; the sum of all $P(i,j)$ values is roughly 90%, lower than the announced 98% as some squares have been excluded because of low exhaust power. In particular, three point among the 37 selected are characterized by high P value, up to 9.38%; ten points are characterized by a P value up to 4.33 %, seventeen points up to 2.5 % and seven points up to 0.56 %. All the other operating points are characterized by lower P value and are not selected by the current methodology.

Once the operating points to be tested have been found, an experimental campaign based on step and response is performed in the test cell in Renault Trucks site, Saint Priest, France. The manipulated variable (MV) in the experiments is the pump speed N_{pump}, that leads to a change in the mass flow rate delivered; the measured variable is an important property in our study: the superheat at the outlet of the evaporator. The superheat $SH_{ex,ev}$ is defined as the difference of the working fluid temperature and the saturation temperature corresponding to its pressure at the outlet of the evaporator (3.2).

$$SH_{ex,ev} = T_{ex,ev} - T_{sat}(p_{ex,ev}) \tag{3.2}$$

It is important to highlight that the expansion machine has been changed during the experimental campaign, because of test bench preparation for following experiments on the new component; the second expander, characterized by an integrated by-pass valve and installed since the experiment 12, induces higher evaporating pressure in the circuit high pressure side of the Rankine system.
The model responses have been identified by means of a local optimizer (fmincon optimization

algorithm), using three different model structures, a First Order model (FO), a First Order Plus Time Delay model (FOPTD) and a model which is the sum of a First Order and a First Order Plus Time Delay model (FOFOPTD). The experimental responses of the steps, applied to each operating point, are shown in Fig. 3.14 for the FO model, depending on the working fluid pressure, working fluid and exhaust gas mass flow rate. It is possible to notice the different pressure that is imposed by the two different expanders; although the operating points tested with the second expander are characterized by comparable values of mass and exhaust mass flow rate with the first expander, the working fluid pressure is generally higher. It is observed that for higher values of pressure, the time constant is higher and on the other hand, the gain is not impacted. Moreover the increase of the working fluid and exhaust mass flow rate does not impact the gain and the time constant either, but the subplots are reported in order to verify that the high pressure of the working fluid is not related to higher working fluid mass flow rate or an operating point characterized by high engine regime.

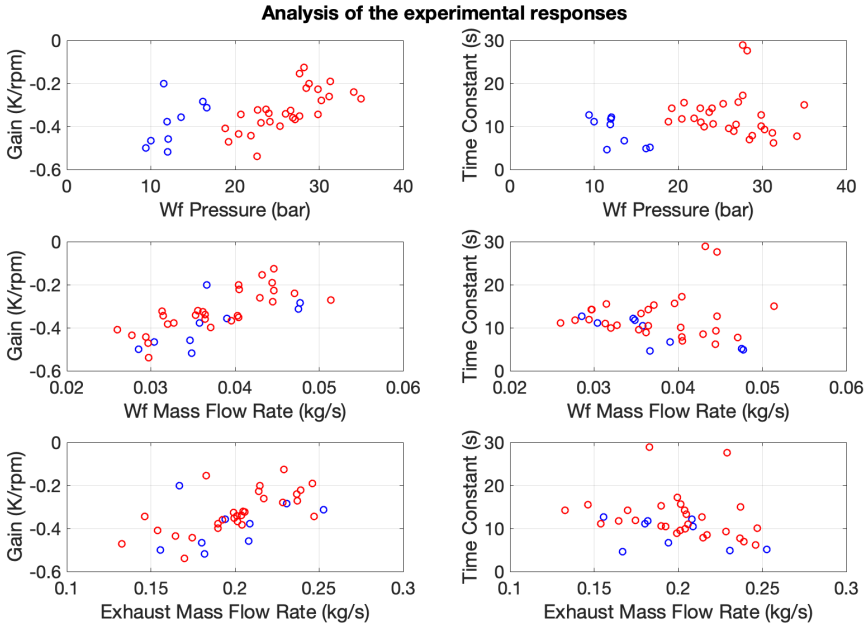

Figure 3.14 – Static gain and time constant of the experimental responses, modeled as a FO model; it is possible to notice the different pressure imposed by the two different expanders (o: Expander 1, o: Expander 2).

During the identification, the model parameters are therefore optimized to reduce the modeling error (3.3)

$$e = \frac{1}{N}\sum_{i=1}^{N}\sqrt{(SH_{exp}(i) - SH_{model}(i))^2} \tag{3.3}$$

where N is the number of samples, and achieve the best match with the experimental response. The normalized modeling errors in Fig. 3.15 are generally higher when the experimental response is modeled as a FO model; FOPTD and FOFOPTD modeling gives the lowest errors in roughly 90% of the total number of experiments. Fig. 3.16 shows, for three different experiment, the step on the pump speed and the experimental and modeling responses for three different models.

Focusing on the FOPTD model structure (3.4):

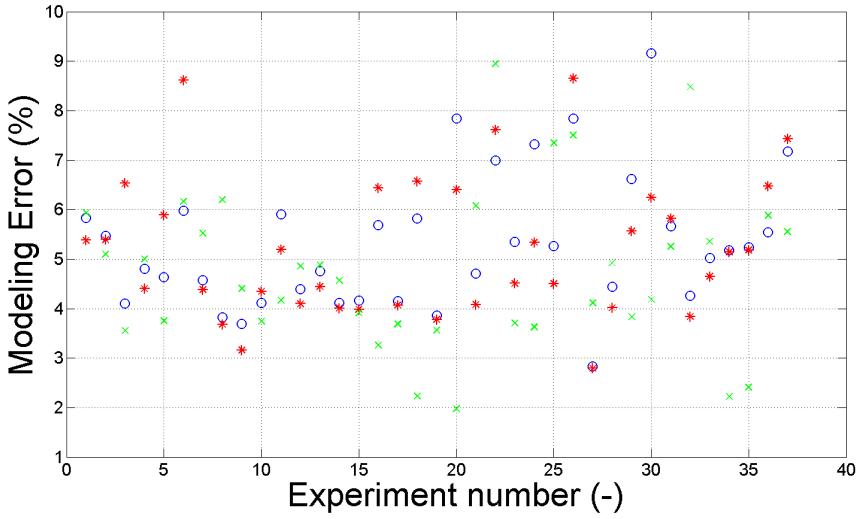

Figure 3.15 – Modeling error (o: FO model, *: FOPTD model, x: FOFOPTD model).

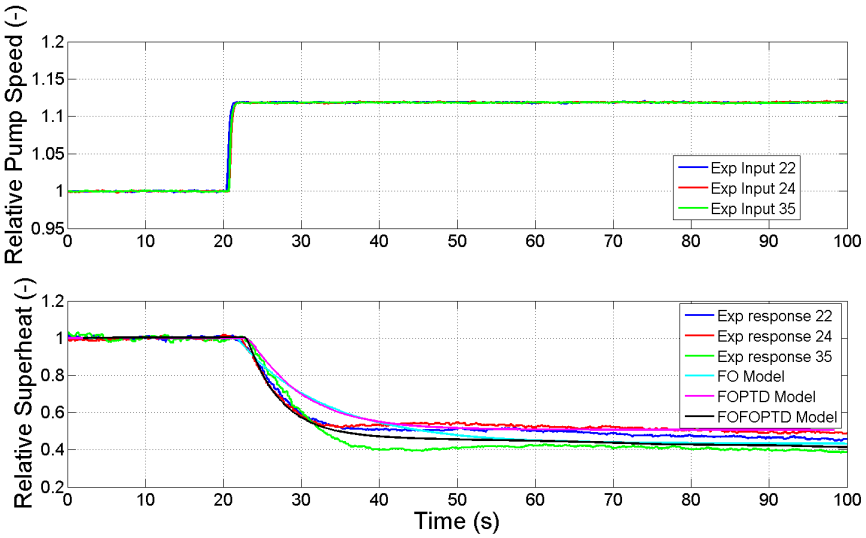

Figure 3.16 – Normalized experimental inputs and responses with respect to the experiments 22, 24 and 35.

$$F(s) = \frac{G.e^{-\theta s}}{1 + \tau s} \tag{3.4}$$

the analysis of the identification (see Fig. 3.17 for all experiments) shows the strong non-linearities of the model (see Table 3.5) since the variation of the parameters covered for all experiments is large. The static gain G changes in a ratio of one to six, while the time constant τ and the lag θ change in a ratio of one to five and one to two, respectively. Moreover the gain and the lag look quite similar for both expanders, while the time constant related to the second expander is higher: according to the fact that the second expander imposes lower pressure in the high pressure side of the Rankine system, the time constant reduces at lower pressure. This can lead to different behavior of the response as SH is a function of the evaporating pressure.

The statistical analysis, showing the high variations of the model parameters along the experimental campaign, suggests that the use of a single model for further control design of the superheat at the outlet of the evaporator could not be appropriate; the use of different linear models, that are

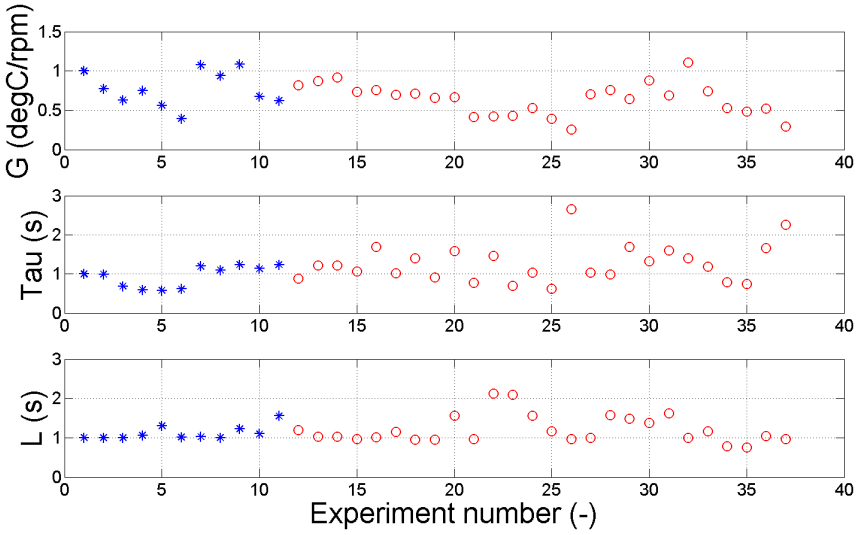

Figure 3.17 – Normalized parameters for the FOPTD model for all experiments (* is for expender 1, o is for expender 2). The first experiment gives the reference values.

Experiments	$\bar{G}$	G_σ	$\bar{\tau}$	τ_σ	$\bar{\theta}$	θ_σ
1-11	0.77	0.23	0.94	0.27	1.12	0.36
12-37	0.64	0.20	1.26	0.48	1.21	0.18

Table 3.5 – Statistic analysis of the normalized FOPTD parameters for the two expanders ($\bar{.}$: mean value, $.-_\sigma$: standard deviation).

afterwards mixed to determine an adaptive model depending on the current operating point could be a successful way to reach good performance of the controller of the superheat at the outlet of the evaporator.

3.4 Set-point determination for further control development

In this section, a set of steady state simulations is performed in order to identify the optimal operating conditions of the system and set-point of controlled variables that are studied in the following section. Four different operating points P_i are considered in order to take into account, in the current analysis, different conditions of the exhaust gas flow at the inlet of the evaporator; these operating points are chosen considering the mean values of exhaust mass flow rate and temperature, that are listed in Tab. 3.10. In Tab. 3.6 the four operating points are presented in terms of exhaust temperature and mass flow rate.

Input	P1	P2	P3	P4
$T_{exh,su,ev}$ (°C)	300	320	350	380
$\dot{m}_{exh,su,ev}(kg/s)$	0.16	0.18	0.20	0.22
$\dot{Q}_{exh,su,ev}(kW)$ 25	35	45	55	

Table 3.6 – Chosen operating points for the steady-state investigation on high pressure and superheat, with corresponding exhaust temperature, mass flow rate and thermal power transferred to the working fluid.

In equation (3.5) additional inputs are provided as different set-points of working fluid superheat at the inlet of the expander $SH_{su,exp}$ and pressure at the inlet of the expander $p_{su,exp}$, as well as parameters as the condensation pressure $p_{su,pump}$, working fluid subcooling at the inlet of the pump $SC_{su,pump}$ and the temperature of the cooling air at the inlet of the condenser $T_{air,su,cond}$. Overall, the number of steady-state simulations for the current analysis is 60.

$$\begin{aligned} &SH_{su,exp}(K) = [20\ 30\ 40] \\ &p_{su,exp}(bar) = [21\ 24\ 27\ 30\ 33] \\ &p_{su,pump}(bar) = 3.5 \\ &SC_{su,pump}(K) = 9 \\ &T_{air,su,cond}(°C) = 35. \end{aligned} \tag{3.5}$$

The different sensitivity of the results to superheat and pressure is presented in Fig. 3.18 and is discussed in the following sections. A conclusion on the determination of the set-points of the superheat and pressure is finally provided.

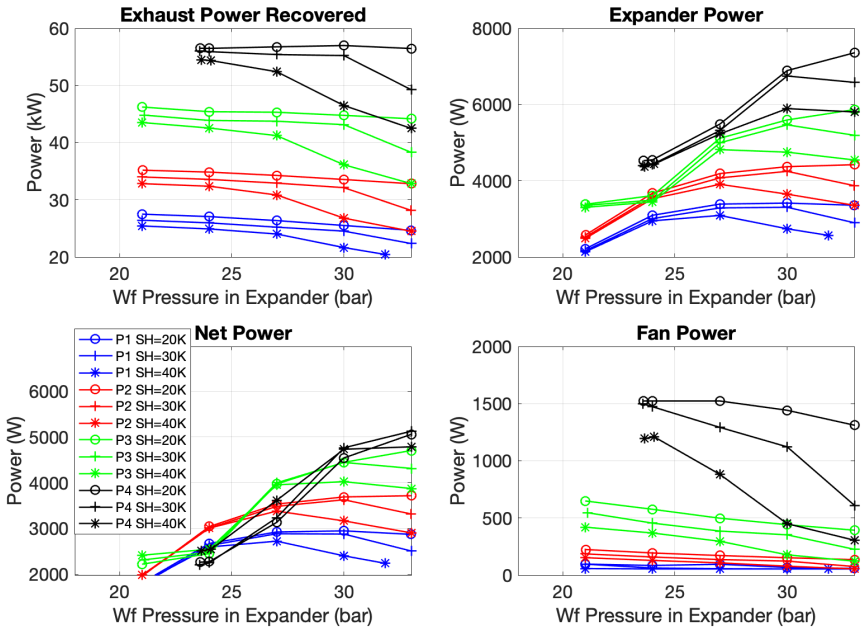

Figure 3.18 – Steady state simulation results on four operating points, with different set-point of superheat and pressure at the inlet of the expander.

3.4.1 Superheat effect

The thermal power recovered in the evaporator is slightly influenced by the superheat for each operating point. In the simulations characterized by high superheat (40 K), the Rankine system recovers less thermal power, because of the partial opening of the exhaust by-pass, that intervenes as soon as the temperature of the working fluid reaches 240 °C. Looking at the expander power, for each operating point and any pressure set-point, 40 K superheat never returns the best result. Considering the net power of the system, 40 K superheat gives the best result just when the pressure is not optimized; as an example, the operating point P4, at 23 bar gives the best net power setting higher superheat, but the result is still much lower than the simulation at higher pressure in the same operating point. Therefore, all the operating points, in appropriate ranges of pressure, never return the best performance at high superheat (40 K); for the operating points P1 and P2 the best performance is found at 20 K superheat, for P3 and P4 is found at 30 K superheat.

3.4.2 Pressure effect

Evaporating pressure can indirectly reduce the exhaust power recovered, as the working fluid maximum temperature is reached and the exhaust by-pass opens. Considering that the highest possible pressure in the system is 35 bar, the optimal pressure that is attributed to the P4 is 33 bar, as the optimal pressure for P1, P2 and P3 is respectively 24, 27 and 30 bar, using a 30 K as superheat. The fan power demand strongly decreases for P4 at high pressure (30 and 33 bar), as the working fluid mass flow rate reduces consistently because of the opening of the by-pass; for P1 and P2 a slight reduction of the fan power demand is also observed.

3.4.3 Conclusion of the analysis

From the analysis of the Fig. 3.18, it is possible to retrieve useful information about the optimal set-point of variables as the working fluid superheat and pressure at the inlet of the expander. As for the set-point of the superheat, the value of 30 K seems to be the best compromise that covers all the cases at different operating points in the pressure ranges of interest.
In order to generate an on-line set-point of the working fluid pressure at the inlet of the expander, it is necessary to correlate the results with a variable that is easily measurable or calculated from other measures. The results in Fig. 3.19 show that an optimal working fluid pressure at the inlet of the expander can be found; in this case the working fluid mass flow is correlated to the set-point of pressure, making possible the on-line generation of the pressure set-point: It shows the correlation between working fluid mass flow rate and optimal pressure at the inlet of the expander to be used as set-point of the expander speed controller in the following sections.

3.5 Control of the superheat

The superheat at the outlet of the evaporator (inlet of the expander) has been considered a critical and crucial point for the effective control of the Rankine system; this variable is a key for the correct operation of the system, because it is an indicator of the aggregation state of the fluid. Additionally, the superheat set-point is indirectly a parameter that intervenes in the mass and volume flow rate of the working fluid in the system, therefore it imposes the design of the components.
As mentioned in Sec. 1.3.3, the implementation of too complicated and advanced controllers in

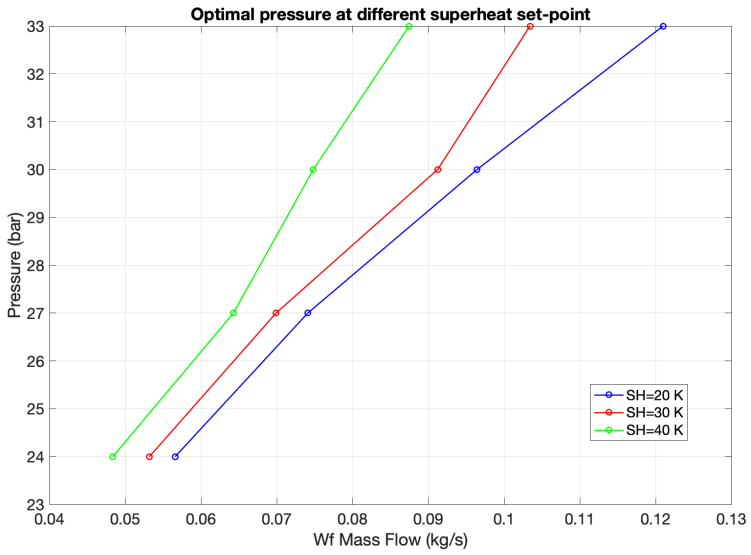

Figure 3.19 – Optimal working fluid pressure at the inlet of the expander, for different set-point of superheat.

the usual automotive ECU is not compatible. In the same time, such a system, working in highly transient conditions, has to be controlled in a robust and effective way in order to ensure the high performance and prevent the failure of the components.
In this section, three different controllers for the superheat are used and compared; the goal of the controller is to track a set-point of the superheat at the inlet of the expander and ensure a smooth variation of the actuator (pump speed) that can indirectly influence the control of other variable in the system (as an example the evaporation pressure set-point is directly linked to the working fluid mass flow rate). The three strategies compared in this section are:

- A PID controller, based on the single FOPTD model corresponding to the most recurrent operating point (Fig. 3.13), tuned by means of the Internal Model Control (IMC) technics.
- A Multi Model PID (MMPID) controller, that has been tuned using the 37 FOPTD models retrieved in Sec. 3.3 and a weighting scheme that calculates a unique set of model parameters (static gain, time constant and time delay) at each time step to be used in the controller (Bayesian weighting scheme, Aufderheide and Bequette 2003)
- A Multi Model PID (MMPID) controller, that has been tuned using the 37 FOPTD models retrieved in Sec. 3.3 and a weighting scheme that has been introduced in Grelet et al. 2016 to reduce the number of setting parameters (Developed weighting scheme).

The sets of parameters (static gain, time constant and time delay) that have been found applying the two algorithms to the superheat problem are presented in Fig. 3.20. The Bayesian and developed algorithm identify a single set of FOPTD parameters that is calculated on-line, by means of the weight $w_{i,k}$, specific for each weighting estimator; in (3.6) the equivalent set of parameters G_{eq}, τ_{eq} and θ_{eq} is found.

$$\begin{cases} G_{eq} = \sum_{i=1}^{N} w_{i,k} G_i \\ \tau_{eq} = \sum_{i=1}^{N} w_{i,k} \tau_i \\ \theta_{eq} = \sum_{i=1}^{N} w_{i,k} \theta_i \end{cases} \tag{3.6}$$

where N is the total number of models (37 in the current application). As it is shown in Tab. 3.7, using the developed scheme, the static gain experiences a lower dispersion with respect to the time constant.

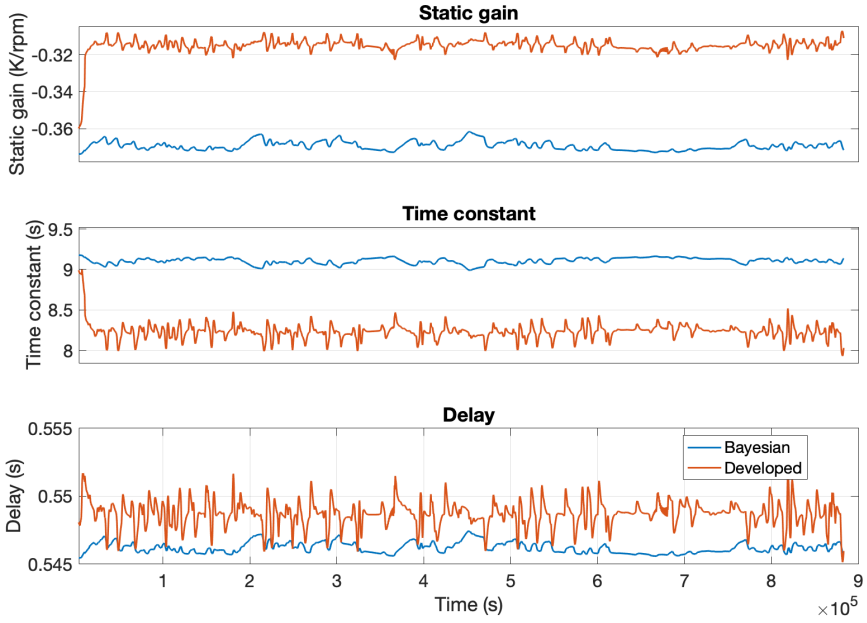

Figure 3.20 – FOPTD parameters identified using the Bayesian and Developed scheme.

Table 3.7 – FOPTD parameters, statistical analysis.

Weighting scheme	$\overline{G}$	τ	θ	$\sigma(G)$	$\sigma(\tau)$	$\sigma(\theta)$
Bayesian	-0.37	9.10	0.54	2.3e-3	3.6e-2	3.9e-4
Developed	-0.31	8.23	0.55	0.0051	0.1108	9.31e-4

Once the specific weighting estimator has been applied to the whole set of 37 models and one single resulting model is found, the SIMC approach proposed by Skogestad 2006 has been used to tune the deriving controller (3.7).

$$\begin{cases} K_p = \frac{1}{G_{eq}} \frac{\tau_{eq}}{\tau_c \theta_{eq}} \\ T_I = min(\tau_{eq}, 4(\tau_c + \theta_{eq})) \\ T_d = 0 \end{cases} \tag{3.7}$$

Once the τ_c parameter is tuned in order to get a good compromise between rapidity and good stability of the controller, the simulation model is run over common highway road cycle (lately called FK), fixing the set-point of the superheat at 30K (as a result of Sec. 3.4). The results, over a portion of the road cycle, are shown in Fig. 3.21.

The control algorithms are compared according to four criteria (3.8): the relative error η of the actual superheat value with respect to the superheat set-point, the standard deviation σ, the integrated absolute error IAE and the total variation of the manipulated variable TV.

$$\begin{cases} \eta = \frac{1}{N} \sum_{1=1}^{N} \left| \frac{SH_{SP} - SH_{actual}(i)}{SH_{SP}} \right| \\ \sigma = \sqrt{\frac{1}{N} \sum_{i=1}^{N} (SH_{actual}(i) - SH_{mean})^2} \\ IAE = \int_0^\infty |SH_{actual}(t) - SH_{SP}| \, dt \\ TV = \int_0^\infty \left| \dot{N}_{pump}(t) \right| dt \end{cases} \tag{3.8}$$

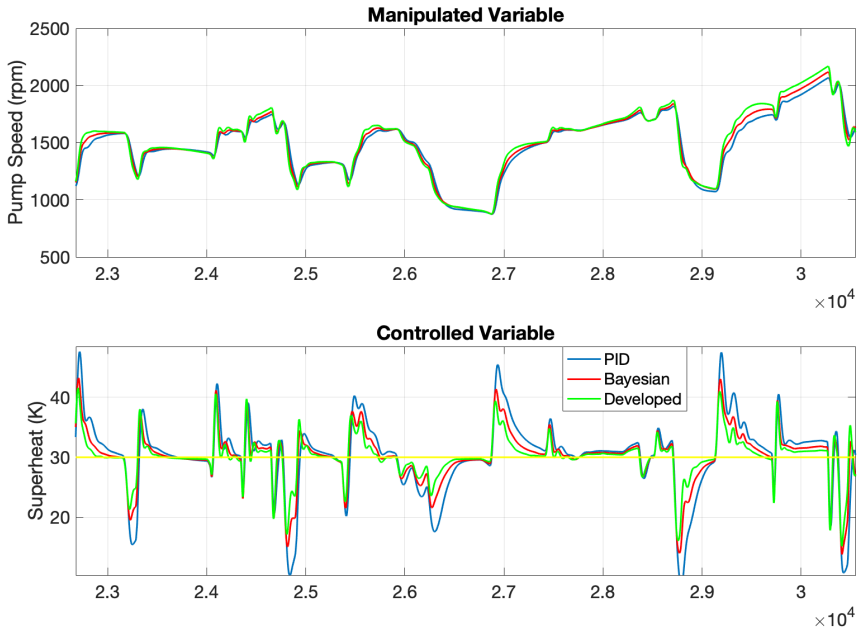

Figure 3.21 – Closed-loop results for the superheat control, using the three different strategies.

Tab. 3.8 shows that the use of the multi-model controllers results into better relative error η and standard deviation σ than the use of a single PID, as for the relative error as for the standard deviation. The integrated absolute error over the road cycle confirms that the multi-model PID controllers track the set-point of the controller variable in a better way and in particular the developed weighting scheme ensures a more accurate tracking. The total variation of the manipulated variable is comparable for the three controllers, confirming that better results are reached with respect to the simple PID controller, with a comparable computational effort. Therefore the statistical results, shown in Tab.3.8, confirm that the two multi model controllers are suitable to control the superheat at the outlet of the condenser in the current road cycle.

Table 3.8 – Statistic analysis of performance of PID and MMPID controllers.

Controller	η (%)	σ (K)	IAE (K s)	TV (rpm)
PID	10.8	5.14	3029	1092
MMPID - Bayesian	7.2	3.5	2085	1094
MMPID - Developed	5.5	2.8	1636	1099

3.6 Expander speed and exhaust by-pass control

The exhaust by-pass valve is a safety component that reduces the thermal power input to the Rankine system in case of over-temperature or over-pressure detected in the working fluid. The control of the exhaust by-pass valve is map-based and by-pass opens as soon as the maximum temperature of the working fluid reaches 240°C. Fig. 3.23 shows how the exhaust by-pass is fully closed in the phases that are characterized by the working fluid maximum temperature below 240 °C and the progressive opening of the by-pass as soon as the working fluid temperature is larger than 240 °C

The expander speed influences the high pressure loop of the Rankine system (2.17) and the track

of an optimal set-point leads to the operation of the expansion machine within the points that are characterized by highest efficiency values (3.4). The efficiency values of the expansion machine are stored in a map as a function of the pressure ratio and the expander speed (Fig. 2.9) and the set-point of the evaporation pressure is discussed and determined in Sec. 3.4 (the expander speed varies between 1000 and 3500 rpm, the exhaust by-pass value varies from 0, by-pass completely opened, to 100, by-pass completely closed). The controller is a PI (Proportional-Integral controller) that varies the expander speed to track the evaporation pressure set-point. The controller is tuned using the IMC technique and the computation of the gain and time constant is based on step and response campaign on the expander model. The results are shown in Fig 3.22; the evaporation pressure set-point varies according to the working fluid mass flow and the expander speed regulation ensures the tracking of the set-point.

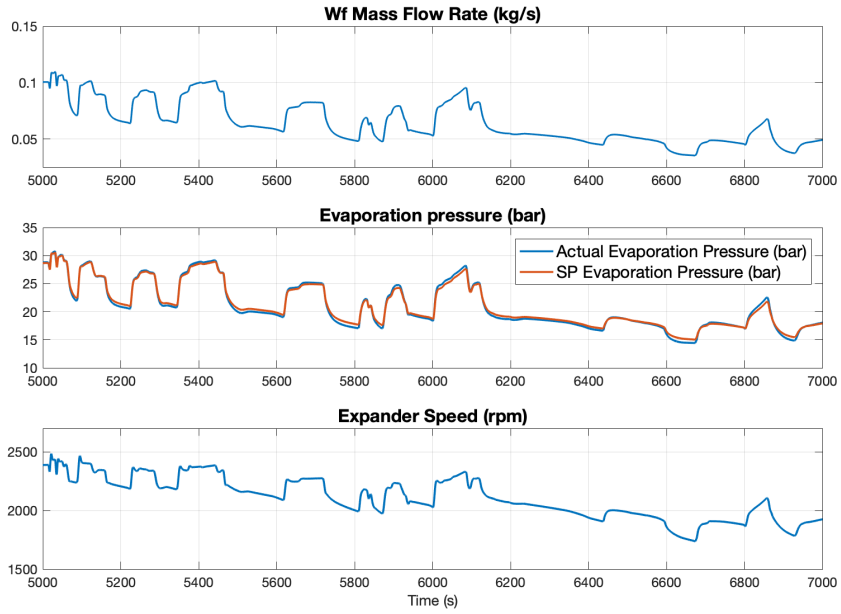

Figure 3.22 – Evaporation pressure control; the evaporator pressure set-point is computed for each time step as a function of the working fluid mass flow rate.

3.7 Subcooling control

The heat removal in the Organic Rankine cycle is one of the limiting factors that affects efficiency, cost and packaging. Despite the numerous publications (Hountalas et al. 2012, Di Battista et al. 2015, Zhao et al. 2018), it is not common to find in the literature any work addressed to the control and optimization of the condensing phase in an Organic Rankine cycle based waste heat recovery for heavy-duty trucks. Peralez 2015 proposed an optimal control strategy in order to maximize the net power produced by an Organic Rankine cycle system characterized by direct condensation, installed in a Diesel powered train; the dynamic optimization, based on predictive control, shows an improvement of the net power produced that is higher with respect to static optimization strategies. The architecture that is characterized by direct condensation, presented in Sec. 3.1, requires the installation of a tube and fin radiator (acting as condenser) and one or more electrically-driven fans to provide the air flow to cool down the working fluid. Manufacturer tests and simulation results show that this architecture presents considerable limitations of heat rejection and keeping

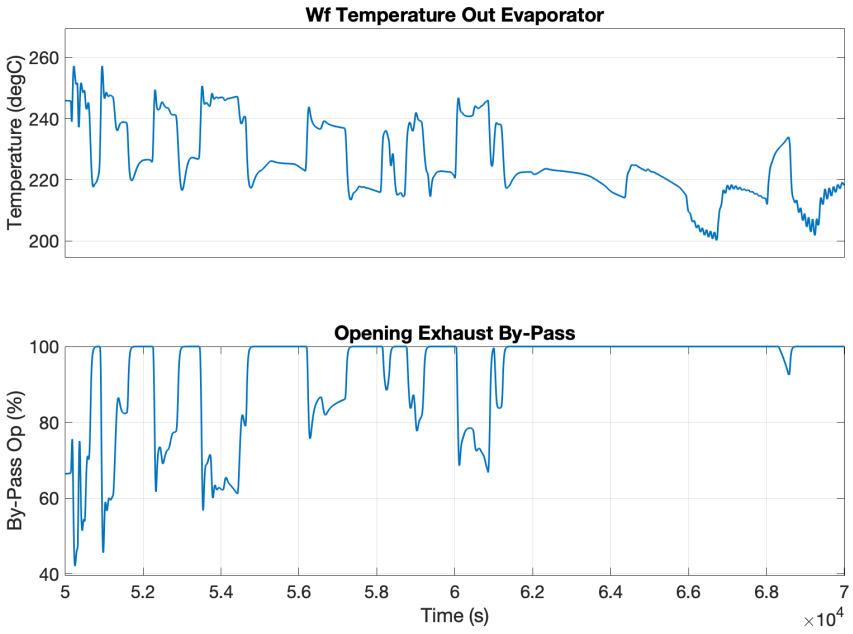

Figure 3.23 – Exhaust by-pass control depending on the maximum working fluid temperature admitted in the Rankine system.

the atmospheric pressure in the low-pressure loop of the system, using cyclopentane, is not possible, despite the installation of the recuperator that partially by-passes the excessive heat to the high pressure loop, reducing the thermal load in the condenser.
The electrically-driven fan delivers a maximum air mass flow rate of 1.5 kg/s and in high thermal loaded conditions, this air flow rate is not enough to achieve the complete condensation of the working fluid at low condensation pressure. For this reason, the low-pressure loop is pressurized, using 7 bar air that is stored on-board in the vehicle, by means of a membrane reservoir and a valve. This system keeps a pressure up to 5 bar in the condensing loop and can also regulate the condensation pressure on-line with a dedicated controller.
The variable that is controlled and imposed at the outlet of the condenser is the subcooling of the working fluid, defined as

$$SC = T_{sat}(p_{wf}) - T_{wf} \tag{3.9}$$

The choice of set-point of the subcooling at the outlet of the condenser is, at a first sight, straightforward. It is clear that, a higher subcooling value leads to higher energy demand of the cooling actuators, with a negative impact on the energy balance of the whole Rankine system. In the same time, a higher subcooling strongly impacts on the efficiency of the thermodynamic cycle, by reducing it.
Therefore, the main interest is to keep the subcooling particularly low, in order to reduce the impact on the energy balance and efficiency. Unfortunately, in the real life, two main problems arise when reducing the subcooling at the outlet of the condenser (inlet of the pump):

- When the subcooling is particularly low and the working fluid is very close to the saturation conditions, local phenomena of condensation, with formations of bubbles can appear. This situation is particularly dangerous for the correct operation of the pump, that requires a liquid fluid at the inlet section.

- As already mentioned in 1.3.5, the use of complicated controllers is forbidden in automotive applications. Therefore, the actual value of the subcooling deviates from the set-point in

highly transient conditions and choosing a too low value of subcooling would increase the risk of having a two-phase fluid at the inlet of the pump.

Considering these reasons and the definition of the subcooling, the condensation pressure can be used as an additional variable to manipulate in order to control the subcooling at the outlet of the condenser. Consequently, the system that is composed by the condenser and the fan is a MISO system (Multiple Input Single Output), where the inputs are the air flow (or the fans speed) and the condensation pressure and the output is the subcooling.
The nature of the system sets the problem of handling the two actuators to ensure the control of the subcooling and, in the same time, reach the best performance of the system, in terms of net power (3.1). The fans speed is directly proportional to the fans power demands (Fig. 2.12), therefore increasing the fan speed leads to the reduction of the net power production of the system. The condensation pressure sets the thermodynamic conditions of the working fluid at the outlet of the expander; increasing the condensation pressure leads to a reduction of the net power production of the system.
The fan speed is controlled to track a given set-point of the subcooling at the inlet of the pump, by means of a PI controller; this controller is tuned taking into account the analysis of a step and response simulation campaign on the direct condenser model.

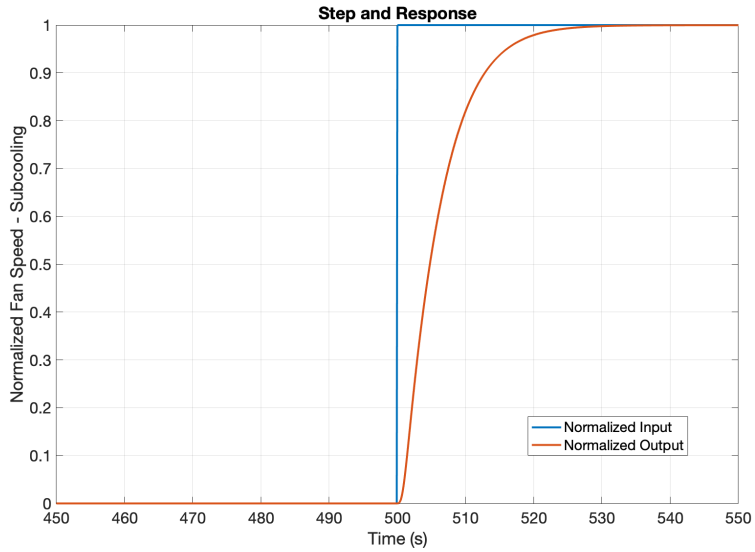

Figure 3.24 – Step on fan speed and response on the subcooling at outlet of the condenser.

In Fig. 3.24, with an example of the result of the step and response campaign, the response can be identified with a first order model, however each identified model is characterized by parameters that can vary a lot depending on the condensation pressure and working fluid mass flow rate, as it is shown in Fig. 3.25. Static gain and time constant values vary a lot; the first up to 5 times, the latter have a variation in the order of 2 or 3 times. Additionally, the time constant is significantly impacted by the condensation pressure, as lower time constant values correspond to higher condensation pressure values; the same trend of the variation is observed as a function of working fluid mass flow rate. The impact of the condensation pressure and working fluid mass flow rate on the gain looks weaker, but a decreasing trend of the gain values can be observed as well, as a consequence of the raise of the condensation pressure and working fluid mass flow rate.
Considering the non-negligible variation of the parameters in the simulation campaign, that analyzes operating points involved in common road cycles, a gain scheduling algorithm may be useful in order to control in an efficient way the subcooling at the inlet of the pump.

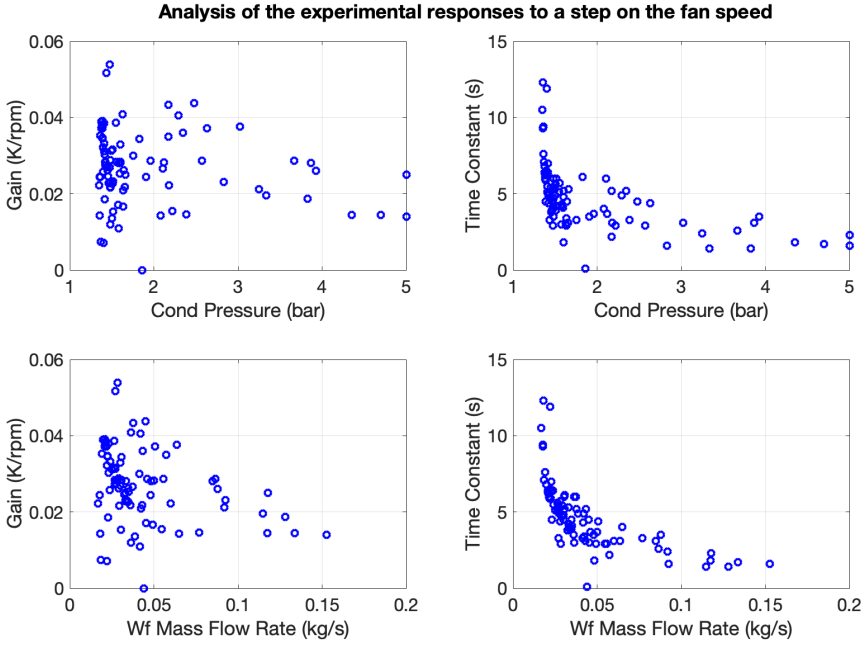

Figure 3.25 – The variation of the condenser FO model parameters as a function of the condensation pressure and working fluid mass flow rate.

As a first approach, the condensation pressure is kept constant to a value that matches with the heat sink temperature. The goal of this solution is to allow the correct operation of the system in any condition, ensuring the tracking of the set-point of the subcooling via fan speed regulation; setting the condensation pressure to 3.25 bar, the performance of a PI controller, with single set of parameters identifying a FO model is compared with the performance of a gain scheduling MMPI, where the model parameters are calculated online by means of the Bayesian and Developed scheme already used for the control of the superheat in Sec. 3.5. Fig. 3.26 shows a portion of a common road cycle; it is possible to notice how the set-point of the subcooling, 9 K, is tracked much better using the two MMPI algorithms (3.9), as the dispersion of the actual values of the controlled variable is extremely reduced with respect to results using a simple PI controller. The manipulated variable control is more aggressive, as the control effort TV, using the MMPI controllers, is higher than the simple PI, but still acceptable; additionally, the use of the developed algorithm leads to lower relative error and integrated absolute error over the whole road cycle. Considering all the aspects that have been mentioned, the developed scheme is used again as favourite controller for the control of the subcooling at the inlet of the pump and, considering the lower standard deviation, a lower set-point of the subcooling could be evoked, guaranteeing a higher net power production of the system.

Controller	Rel err (%)	St dev (K)	IAE (K s)	TV (rpm)
PI	5.16	0.75	494	2383
MMPI - Bayesian	2.96	0.44	336	2402
MMPI - Developed	1.42	0.27	204	2392

Table 3.9 – Statistic analysis of performance of PI and MMPI controllers.

A second approach is based on the determination of an imposed value of pressure ratio at the inlet-outlet of the expansion machine; this value is chosen according to the total efficiency chart of the expansion machine and allows the calculation of the condensation pressure to adopt; the control

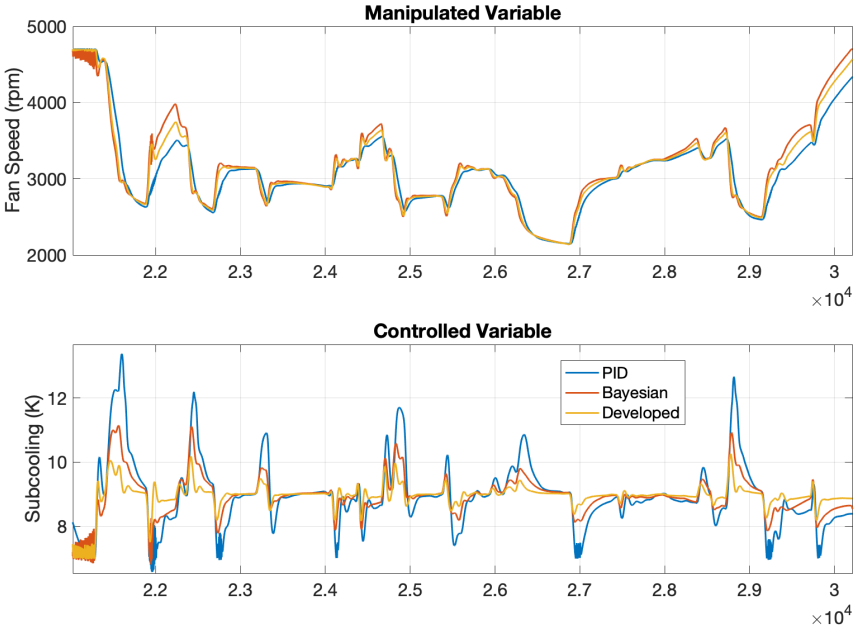

Figure 3.26 – Comparison between a PI and MMPI used to control the subcooling at the inlet of the pump. Condensation pressure is constant and set to 3.25 bar.

block scheme is presented in Fig. 3.27. In the last chapter of this thesis, an optimization algorithm will be used in order to determine the optimal condensation pressure that ensures, in the same time, the tracking of the subcooling set-point and the maximum net power production of the system.

The two different control strategies, as well as the use of the MMPI, with the Developed scheme, with reduced subcooling set-point are compared in Fig. 3.28, highlighting the good performance of the MMPI as controller and the higher net power produced by the system, by reducing the set-point. In particular, reducing the set-point of the subcooling to 7 and 5 K, using the MMPI, leads to an increase of the net power produced of roughly 1 and 1.7%.

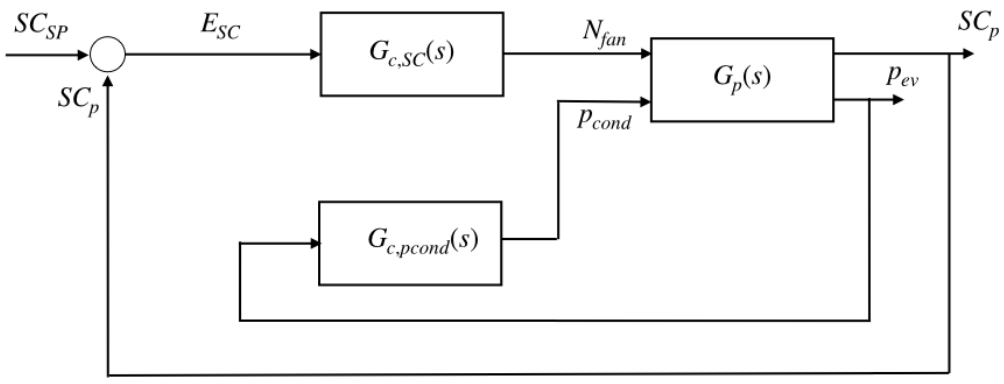

Figure 3.27 – Subcooling control via fan speed and variable condensation pressure (second strategy) according to the evaporation pressure and optimal pressure ratio (second strategy).

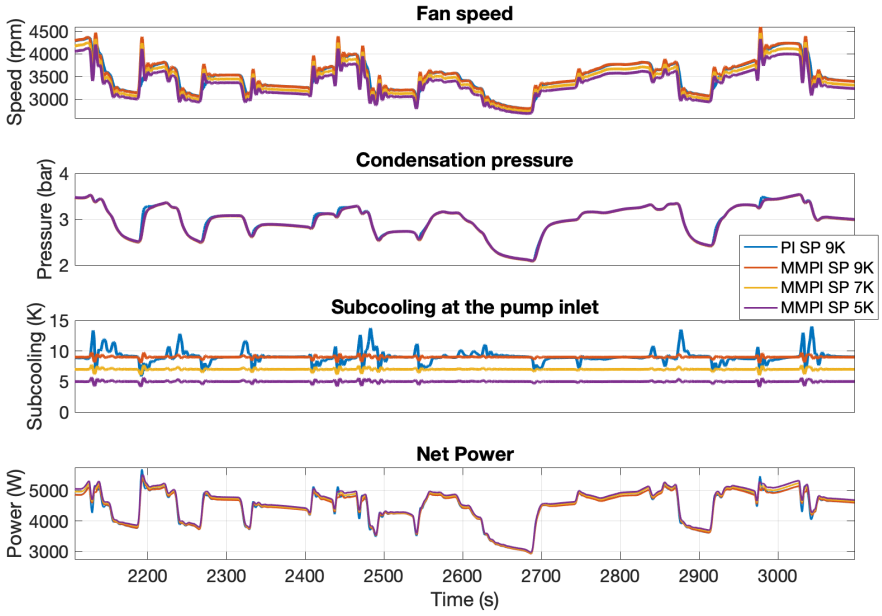

Figure 3.28 – Subcooling control using a constant condensation pressure (first strategy) and a condensation pressure level according to the constant pressure ratio (second strategy).

3.8 Integration in complete vehicle

The models presented in the Chap. 2 and the control strategies presented in Sec. 3.5, 3.6 and 3.7 are integrated in a complete vehicle environment, in order to assess the potential of the Rankine in a real road cycle mission.
In this phase, the focus of the analysis is on the first architecture, that is presented in Fig. 3.1; this configuration is preferred because of the compactness, easier integration and independence on the cooling system. Therefore, the expected net power output of the system is between 3-4 kW, that corresponds to 2.5-3% of fuel saving, with respect to the base vehicle fuel consumption.

LH08	FK	German	CC	Sweden	SX
Eng speed (rpm)	1260	1225	1048	1112	1191
Eng torque (Nm)	882	806	679	667	777
Veh speed (Km/h)	86	83	51	75	83
Exh Temperature (°C)	349	340	320	320	332
Exh Mass Flow (kg/s)	0.204	0.192	0.163	0.172	0.190
Air Temperature in cond (°C)	34	35	41	36	35
Weight Factor (-)	0.105	0.273	0.056	0.278	0.286

Table 3.10 – Average values over each road cycle composing the aggregate LH08.

The road cycle strongly impacts the performance of the Rankine system as it influences the inputs and perturbations. The assessment of the Rankine potential has to take into account many possible road cycle profiles, characterized by the different nature of the missions; for this reason the LH08, a set of five road cycles, has been chosen in order to assess the potential of the Rankine and taking into account the different missions. The five road cycles have different characteristics, that are representative of different driving conditions that is possible to encounter in European roads. Tab.3.10 shows the average values of the main variables of the engine and perturbations that affect

Ambient temperature (°C)	Vehicle speed (Km/h)	Air temperature at condenser inlet (°C)
0	90	23
	30	27
	0	30
20	90	34
	30	45
	0	50
40	90	50
	30	63
	0	70

Table 3.11 – Air temperature at the inlet of the condenser as a function of the ambient temperature and vehicle speed.

the performance of the Rankine system over each road cycle; as a first sight, it is possible to notice that the FK road cycle is characterized by higher average load, that leads to higher average mass flow and inlet temperature of the exhaust gas flow in the evaporator. CC road cycle is characterized by lowest vehicle speed, that results in the lowest amount of the average exhaust gas, as well as the highest air temperature at the inlet of the condenser. A weight factor is used in order to determine the importance of the single road cycle in the evaluation of the results in the whole LH08.
The air at the inlet of the condenser is found dependently on the ambient temperature and the vehicle speed. In fact, considering the design of the actual Rankine system, the condenser is placed nearby the Exhaust After Treatment System (EATS), that works at high temperature affecting the surrounding air flow temperature field (Wassén et al. 2019). CFD simulations, performed internally, correlate the vehicle speed and the air temperature at the inlet of the condenser at fixed ambient temperature; a linear trend is found for three different ambient temperature (0, 20, 40 °C) and the corresponding air temperature at the inlet of the condenser for different vehicle speed values are represented in Tab. 3.11.

The air temperature at the inlet of the condenser impacts a lot on the operation of the Rankine system in a negative way for two reasons:

- The higher the air temperature at the inlet of the condenser is, the higher the condensation pressure of the working fluid is set in order to ensure the heat removal from the condenser (limited by the size of the condenser and the maximum air flow rate supplied by the fans), reducing the power production of the expansion machine
- Higher air temperature leads to the needs of higher air flow rate in order to remove the heat from the condenser with smaller difference of temperature, consequently the fan power demand becomes higher and impacts in a negative way on the overall energy balance of the system

The evaluation of the Rankine potential, as well as the control strategies, are intended to describe the behavior of the system once fully operational. On the other hand, the system is initially at ambient temperature and pressure and the model reproduces the start-up phase, characterized by the raise of pressure and temperature in the system. The complete model presents a state machine developed by the Simulink Toolbox Stateflow, that switches to different control structures depending on the fluid properties. In particular, three different modes are identified:

- Start-up phase: in this phase the system is at ambient temperature. The working fluid is locally heated up in the evaporator and the pump speed and expander speed are running at

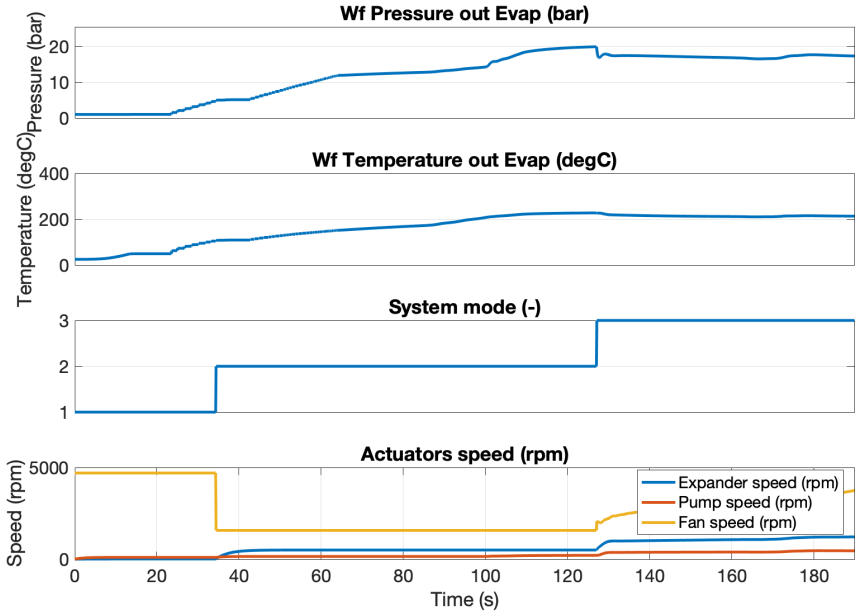

Figure 3.29 – Switch of the three phases, according to working fluid pressure and temperature at the inlet of the expander and actuators speed.

lowest speed. In this way, incoming fluid and heat in the evaporator contribute to raise the pressure and temperature. The whole start-up phase lasts, on average, 1% of the whole road cycle duration

- Pre-power generation phase: in this phase the system is already heated-up and the working fluid is in vapor state at the outlet of the expander. The system already produces power, but the temperature and pressure values do not lie in the full operation ranges yet

- Power generation phase: in this phase the internal states of the system lie in the full operation range and the controller algorithms operate to fulfill safety and performance requirements

As it is possible to notice in Fig. 3.29, the system is initialized at ambient temperature (20°C) and current mode is the first (mode 1); after 40 seconds the system is heated-up and expander and pump speed increase, increasing pressure and temperature until the conditions to switch to mode 3 are realized (after roughly 130 seconds). The controllers, in mode 3, operate in order to guarantee the correct operation of the system.
The start-up procedure, that is described, is not validated in the truck demonstrator as, nowadays, no tests have been performed in a real road cycle. Therefore this procedure should be reviewed and calibrated according to tests on real drive conditions. As a result of this consideration, the evaluation on the performance of the Rankine is calculated once the system is fully operational and the mode control is the one corresponding to the power generation phase.

The chosen architecture for the assessment of the Rankine potential is the configuration that is characterized by the direct condensation, using cyclopentane as working fluid. From Fig. 3.30, as expected the FK road cycle is characterized by the highest expander power as well as net power production, as a result of the higher mass flow and temperature at the inlet of the evaporator of the exhaust flow. CC road cycle, on the other hand is characterized by the lowest production, as a result of the lowest values of mass flow and temperature of the exhaust flow. In the same time, CC is characterized by the higher average fan power demand, because of the lowest average speed of the vehicle that implies the higher temperature of the air flow at the inlet of the condenser.

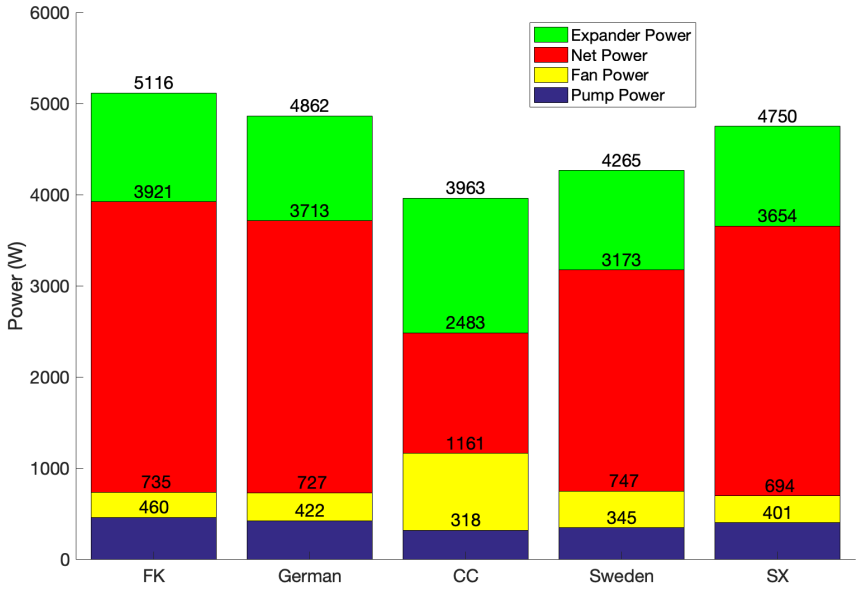

Figure 3.30 – Simulated average power on the different cycle composing the LH08.

The different nature of the road cycles, involving the vehicle speed and, consequently, the temperature of the air at the inlet of the condenser, impacts heavily the performance of the system, as well as the different control strategies to adopt; it might be possible that, depending on the nature of the road cycle, the control strategy changes, in order to ensure high standards of performance.
Therefore, aggregating the single road cycles and performing a weight average of the net power produced based on the weight factor in Tab. 3.10, the final result leads to almost 3.5 kW, that represents roughly 4% of the power supplied by the engine (as announced as goal) in the aggregate road cycle (3.10)

$$\dot{W}_{eng} = \frac{T\Omega}{60} \tag{3.10}$$

where T is the engine torque in Nm and Ω is the engine speed in rpm.
Although the final results meet the expectations in terms of fuel savings, the potential for further improvements has not been explored yet; in particular, the variation of the fan speed and condensation pressure, in order to ensure the tracking of the desired subcooling, may not represent the best trade-off; further investigation could provide meaningful gain in terms of net power produced and, consequently, fuel savings.

Conclusion. *In this chapter, the main dynamics of a Rankine based waste heat recovery from the exhaust gas flow are introduced. Initially, the target architecture and working fluid are chosen, taking into account the criteria of performance, material compatibility and safety; once the set-points of variables as superheat and pressure at the inlet of the expander have been set by means of simulations, a procedure for the selection of the most representative operating points of the engine map is exposed. The dynamics of the evaporator and condenser are studied in the operating points that are selected and the controllers of the superheat and subcooling have been implemented; in both cases, the importance of a weighting estimator, that determines a single resulting model used to design the controller, is highlighted, considering the non-linearity of the system and simulation results. Regarding to the control of the subcooling, it can be noticed that using the condensation pressure as manipulated variable is necessary for the current direct condensation architecture, using cyclopen-*

tane as working fluids. The results in terms of performance of the system are presented in real road cycles with different features (highway and urban road cycles), highlighting the impact of the nature of the mission on the Rankine performance. In the next chapter, new control strategies are adopted for a Rankine based waste heat recovery from the engine coolant flow and potentially critical issues of this application are identified by means of an experimental campaign. Furthermore a model based optimization on the cold side of the system is presented to improve the results shown in the current chapter, as the current combination of the actions of the two manipulated variables, fan speed and condensation pressure, may not result into the best strategy to ensure the highest standards of power production.

Chapter 4

Coolant recovery: modeling, control and experimental campaign

This chapter deals with the recuperation of the thermal energy that is available in the engine coolant flow. A simulation study on a Rankine system architecture, that has been integrated in a global vehicle model, is carried out, identifying the variables to control and manipulate in order to obtain high standard of performance in road cycle simulations. Therefore an experimental campaign is performed, testing components and analyzing potential issues that is possible to encounter with such Rankine architecture, using Novec649 as working fluid. The simulation and experimental results present a discrepancy that is explained because of the excessive pressure losses in the heat exchangers and partial admission of the working fluid in the turbine.

4.1 State of the art

The waste heat recovery available in the coolant flow in the cooling system of the vehicle represents a non-negligible portion of the energy that is not converted into useful energy in the vehicle and therefore is wasted. As already mentioned in Sec. 1.2, 22% of the energy in the heavy-duty truck is wasted via the cooling system (considering the EGR cooler as well). Although this percentage is roughly equivalent to the percentage of the losses attributed to the exhaust gas, the thermal energy in the cooling system is available at lower temperature than the exhaust flow, therefore recovering this energy by means of an Organic Rankine Cycle results in a low-grade waste heat recovery application.
The heat source is the coolant flow that removes heat from the engine and possibly the EGR flow; the excessive heat that in the coolant is removed in a radiator placed in the front-face of the truck, by means of the RAM air flow. According to the vehicle and the design of the cooling system and the radiator itself, in case of high load, the fan of the cooling system is activated and provides additional air flow to the radiator (in Sec. 4.3 the details of the cooling system as well as the associated Rankine system are provided).
The use of the coolant flow as main heat source has significant advantages with respect to the exhaust gas flow, despite the thermal energy is available at low temperature; in fact, in a heavy-duty long haul truck, the thermal inertia of the large coolant mass flow rate (up to 6 $\frac{kg}{s}$) leads the temperature of the coolant flow in the cooling system to be stable around 85 and 90°C, while the temperature of the exhaust gas changes between 150 and 400°C and it is characterized by variations in the road cycle, depending on the engine operating point (Furukawa et al. 2014). The modest variation of the cooling flow temperature leads to important simplification in terms of control of

the system in real road cycle operations, reducing computational efforts and cost.
However, the Rankine cycle efficiency is strongly influenced by the temperature of the hot source; the total efficiency of the Organic Rankine Cycle based waste heat recovery from the exhaust flow, that has been presented in Chap. 3, is characterized by values ranging from 8 to 12%, according to the operating point. This values are further decreased in a low-grade Organic Rankine Cycle, recovering thermal energy from the coolant flow of a heavy-duty long-haul vehicle, to roughly 5% (the efficiency of the Rankine cycle resulting from simulation and experiments is discussed and compared in Sec. 4.3 and 4.4). The net power target for such architecture is between 1.5 and 2 kW, less than the net power that is possible to produce by a waste heat recovery system with exhaust gas recuperation.
Considering the beneficial limits of the recuperation of the coolant flow thermal energy and, in the same time, the simplifications that are linked to the reduced thermal constraints of the system and the simpler controllers, the waste heat recovery from coolant flow is considered as a lightweight, compact and low-cost solution (Leduc et al. 2017). The advantages of the recuperation of the coolant flow thermal energy that have been presented drive to a deeper investigation, that is performed in this chapter by means of the implementation of simulation models and experiments.

4.2 Working fluids

The choice of the working fluid for the application of coolant waste heat recovery follows the same criteria already mentioned and described in Sec. 1.3 and Sec. 3.2. Clearly, the main difference with respect to the exhaust recuperation is linked to the low-grade temperature of the heat source. Therefore, the most appropriate working fluids should be the ones that match better with the temperature profile of the heat source.
Considering the limited temperature of the heat source, the most important requirement of the working fluid is the pressure at which it evaporates at the temperature of the heat source. Mansour et al. 2018 investigated the potential of an Organic Rankine cycle based waste heat recovery system using engine-coolant waste heat recuperation; the chosen working fluid, R1234yf, has a null ozone depletion potential (ODP) and a low Global Warming potential (GWP is 4). Moreover, this working fluid, at the temperature of the heat source, evaporates at higher pressure with respect to other candidates (the maximum pressure admitted in the system by the author is 30 bar, considering that the critical pressure of the R1234yf is 32 bar).
A high-level analysis of the working fluids, that have already been investigated in Sec. 3.2, highlights that ethanol is not suitable to such application, as at the temperature of 90°C, it evaporates at 1.58 bar, dramatically reducing the available pressure ratio measured between the inlet and the outlet of the expander. Novec649 and cyclopentane evaporates at similar pressure (3.47 and 3.24 bar respectively), while R123ZD evaporates at the highest pressure among those candidates, 8.33 bar. In the same time, R1233ZD is characterized by the lowest normal boiling point; this leads to the increase of the pressure at the outlet of the expander, limiting the pressure ratio.
Smague et al. 2019 presented a work with IFPEN, in partnership with ENOGIA related to the implementation of a waste heat recovery system from engine-coolant flow of a passenger car. Two working fluids have been selected: R122ZD and Novec649. Differences between the two fluids are highlighted, as the latent heat of vaporization that influences the mass flow rate of the working fluid in the system, and afterwards Novec649 is selected because it operates with larger mass flow rate, ensuring an easier design of the turbine by ENOGIA. In this thesis, both fluids are investigated by simulation, while experiments are conducted with Novec649, that has been chosen by the consortium of the partners in the frame of the Falcon Project (Green Car Congress 2017).

4.3 Case study - Modeling

In order to deeply investigate the Rankine-based waste heat recovery technology on engine-coolant flow, various simulation models have been implemented. The models are implemented in a complete vehicle environment, where the cooling system is modeled and modified according to the proposed architecture (Fig. 4.1).
The engine coolant removes the excessive heat in the engine. In a vehicle that is not equipped with a waste heat recovery system on the engine coolant, the cooling fluid temperature is controlled by means of a thermostat, a wax pellet valve that lets a portion of the coolant flow to the main radiator, in order to keep the desired temperature (Kanefsky et al. 1999); the coolant flow that is not recirculated and is sent to the main radiator is cooled down by the RAM air flow and, possibly, the fan of the cooling system. In the system that is here proposed, the coolant flow is sent to the evaporator, the main heat exchanger of the Rankine system, it cedes part of its thermal energy to the working fluid and its residual excessive heat is removed in the main radiator of the cooling system.

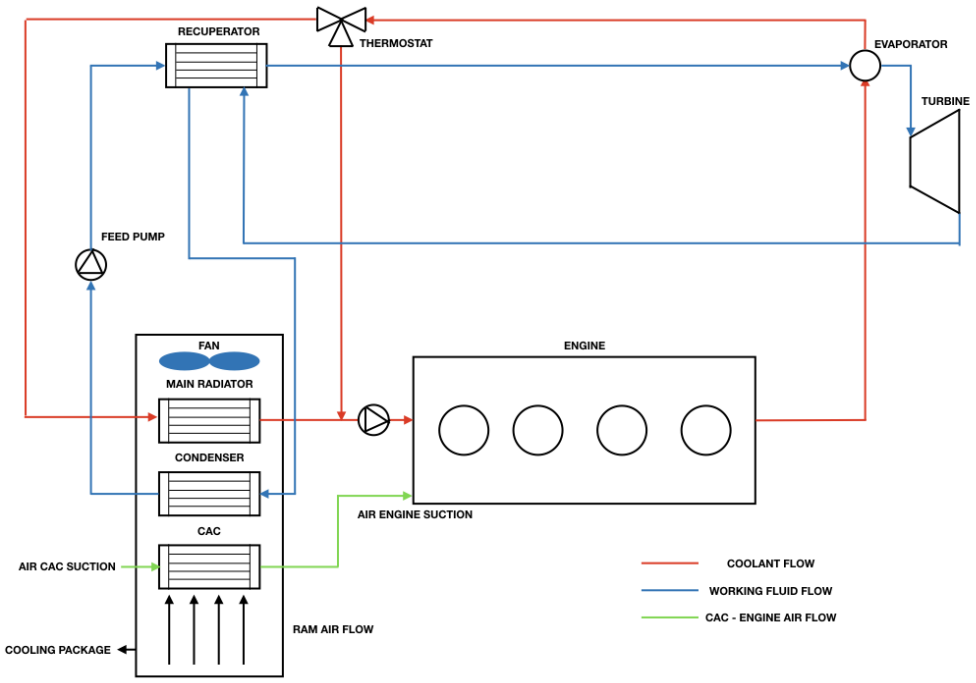

Figure 4.1 – Simplified layout of the cooling and Rankine system investigated in the simulation activities.

In Fig. 4.1, the simplified scheme of the cooling package is presented; the RAM air flow invests, firstly, the Charge Air Cooler (CaC), as this component strongly influences the performance and the efficiency of the engine. In parallel, the condenser of the Rankine system is placed, between the CaC and the main radiator of the cooling system. During normal operation, without any particularly high load operations, the RAM air flow rate is enough in order to cool down the CaC and the engine-coolant; the add of a new radiator (the Rankine condenser), in front of the main radiator of the cooling system, implies the fact that the RAM air flow that invests the main radiator has higher temperature than the air flow temperature in a vehicle that is not equipped with such type of waste heat recovery system. In the same time, the thermal power to remove from the main radiator is lower in a vehicle that is equipped with a coolant recovery Rankine system, as

part of the thermal power contained in the engine coolant is transferred to the Rankine working fluid; therefore part of the thermal power to remove is transferred from the main radiator to the Rankine condenser. The fan of the cooling system, mechanically coupled to the engine, is activated when the RAM air flow cannot evacuate all the excessive thermal energy of the cooling system. It consumes additional energy and strongly impacts the fuel consumption of the vehicle; a controller regulates the engagement of the fan and its speed, based on the coolant temperature at the outlet of the radiator, therefore high temperature of the coolant flow at the outlet of the main radiator can result in the activation of the fan, leading to higher fan power demand and reduction (or even complete waste) of the benefit provided by the Rankine system. The engagement of the fan can occur even in the case of a vehicle equipped with such a waste heat recovery system and, therefore, control strategies have to be implemented in order to reduce as much as possible the activation of the fan of the cooling system.
The working fluids that are selected for modeling are Novec649 and R1233ZD; the use of two different fluids implies, obviously, differences in the sizing of the components. As previously mentioned and noticed in Smague et al. 2019, the different latent heat of the two fluids, operating with the same heat source, leads to mass and volume flow rate values (at the inlet of the turbine) that are particularly different in the case of the two fluids; consequently, the sizing of the turbine is impacted. Tab. 4.1 shows the variables that are needed in order to calculate the equivalent throat diameter of the turbine K_{eq} (defined in (2.19)) for a design operating point ($m_{cool,su,ev} = 5.2$kg/s, $T_{cool,su,ev} = 90$°C, $T_{air,su,cond} = 30$°C); as it is possible to notice the equivalent throat diameter K_{eq} varies considerably for the two working fluids, consequently, the design of the turbine is strongly impacted.

Variable	Novec649	R1233ZD
Mass flow rate (kg/s)	0.41	0.25
Density at turb inl ($\frac{kg}{m^3}$)	34.7	36.48
Volume flow rate at turb inl ($\frac{m^3}{s}$)	0.0118	0.0069
Pressure at turbine inlet (bar)	2.88	7.07
Pressure at turbine outlet (bar)	1.1	3.0
Equivalent throat diameter (m^2)	**1.41e-4**	**5.39e-4**

Table 4.1 – Main characteristics of the fluids to size the turbine equivalent throat diameter K_{eq}.

4.3.1 0D model: steady state results

In order to preliminary analyze the architecture presented in Sec. 4.3, the 0D steady state model (4.1) has been used. This model is not suitable for a deep evaluation of the potential of the Rankine system in the vehicle, as it does not reproduce the driving conditions that heavily affect the operation of the system; on the other hand the 0D model is useful for a preliminary evaluation of the system performance and comparison between different working fluids.
The expected result from the usage of such a model is a comparison between the working fluids Novec649 and R1233ZD, in terms of net power production of the system, evaluated as $\dot{W}_{net} = \dot{W}_{turb} - \dot{W}_{pump}$; the inputs of the model are the mass flow rate and the temperature of the coolant and the condensation pressure of the fluids.
The thermodynamic variables of the working fluids at the inlet and outlet of each component are calculated by means of the REFPROP database (Lemmon et al. 2018). Additional parameters are also provided to the model, as the isentropic efficiency of the pump and turbine, the pinch point in the heat exchangers, the maximum evaporating pressure and the minimum condensing pressure

and the subcooling at the inlet of the pump.

$$\begin{cases} p_{wf,su,pump} = p_{cond} \\ T_{wf,su,pump} = T_{sat}(p_{wf,su,pump}) - SC \\ h_{wf,su,pump} = h(T_{wf,su,pump}, p_{wf,su,pump}) \\ s_{wf,su,pump} = s(h_{wf,su,pump}, p_{wf,su,pump}) \\ p_{wf,ex,pump} = p_{ev} \\ h_{wf,ex,pump,is} = h(s_{wf,su,pump}, p_{wf,ex,pump}) \\ h_{wf,ex,pump} = h_{wf,su,pump} + \frac{h_{wf,ex,pump,is} - h_{wf,su,pump}}{\eta_{is,pump}} \\ T_{wf,ex,pump} = T(h_{wf,ex,pump}, p_{wf,ex,pump}) \\ s_{wf,ex,pump} = s(h_{wf,ex,pump}, p_{wf,ex,pump}) \\ p_{wf,ex,ev} = p_{wf,ex,pump} \\ h_{wf,ex,ev} = h_{wf,su,ev} + \frac{\dot{m}_{cool} c_{p,cool} \left(T_{cool,su,ev} - T_{ex,coo,ev}\right)}{\dot{m}_{wf}} \\ T_{wf,ex,ev} = T(h_{wf,ex,ev}, p_{wf,ex,ev}) \\ s_{wf,ex,ev} = s(h_{wf,ex,ev}, p_{wf,ex,ev}) \\ p_{wf,ex,turb} = p_{cond} \\ h_{wf,ex,turb} = h_{wf,ex,ev} + \left(h_{wf,ex,ev} - h_{wf,ex,turb,is}\right) \eta_{is,exp} \\ s_{wf,ex,turb} = s(h_{wf,ex,turb}, p_{wf,ex,turb}) \\ p_{wf,ex,cond} = p_{wf,ex,turb} \\ T_{wf,ex,cond} = T_{sat}(p_{wf,ex,cond}) - SC \\ h_{wf,ex,cond} = h(T_{wf,ex,cond}, p_{wf,ex,cond}) \\ s_{wf,ex,cond} = s(h_{wf,ex,cond}, p_{wf,ex,cond}) \end{cases} \tag{4.1}$$

Variable	Novec649	R1233ZD
Mass flow rate (kg/s)	0.41	0.25
High pressure (bar)	2.88	7.07
Low pressure (bar)	1.1	3.0
Cycle efficiency (%)	5.3	6.2
Expander power (kW)	2.72	3.33
Pump Power (kW)	0.024	0.042
Fan power (kW)	0	0.041
Net power (kW)	2.69	3.24

Table 4.2 – Results of the 0D model in the operating point $m_{cool,su,ev} = 5.2$kg/s, $T_{cool,su,ev} = 90$°C, $T_{air,su,cond} = 30$°C).

The results in Tab. 4.2 show that the fluid R1233ZD has better performance than the Novec649, as the expander power production as well as the net power production is higher. This is due to the fact that the R1233ZD temperature profile matches much better with the hot source and the recovered power in the evaporator is higher than using Novec649 (51.9 kW using R1233ZD, 50.8 using Novec649).
However, this analysis is based on a preliminary result, that cannot be considered as a definitive analysis, because in the steady-state 0D simulation model real factors that occur in the mission over a real road cycle are not taken into account.

4.3.2 1D model: control strategies and results

A 1D Rankine model in a vehicle environment, resulting from the assembly of single models presented in Chap. 2, is used in order to assess the potential of the technology and identify the critical aspects

that can be visible when the vehicle performs its mission over a real road cycle. The variability of the hot source as well as of the cooling capacity, influenced by the vehicle speed and cooling fan engagement (Fig. 4.2) leads to the necessity of studying strategies in order to improve the performance of the system. All the results that are provided refer to the specific road cycle Lyon-Chambery-Goncelin (LCG) that has been used extensively as the reference road cycle in the Falcon project.
The goal of the Fig. 4.2 is to link the road cycle and driving condition features (vehicle speed), the cooling fan engagement and the cooling package air temperature profile (referring to the cooling package version presenting the Rankine condenser between the CaC and the main radiator, Fig. 4.1); the air mass flow rate in the cooling package is defined as the RAM air flow rate (depending on the vehicle speed) and, possibly, the cooling fan speed. Between 2000 and 2500 seconds, the cooling fan is engaged and adds air mass flow rate in the cooling package, increasing the cooling capacity. In the following phase, between roughly 2500 to roughly 2900 seconds, the cooling fan is not engaged (default minimum speed of the fan is 200 rpm) and the vehicle speed is constant, 90 km/h; consequently the air mass flow rate is constant as well at the maximum value of air mass flow rate in the cooling package, without fan engagement. Just before 3000 seconds, the vehicle speed drops; the air mass flow rate starts dropping as well and the cooling fan speed increases, re-increasing the air mass flow rate in the cooling package. It is possible to notice that, corresponding to the reduction of the vehicle speed, the temperature of the air at the outlet of the Rankine condenser increases (as a result of the temporary reduction of the air mass flow rate in the cooling package); the increase is stopped by the increase of the air mass flow rate operated by the cooling fan action.

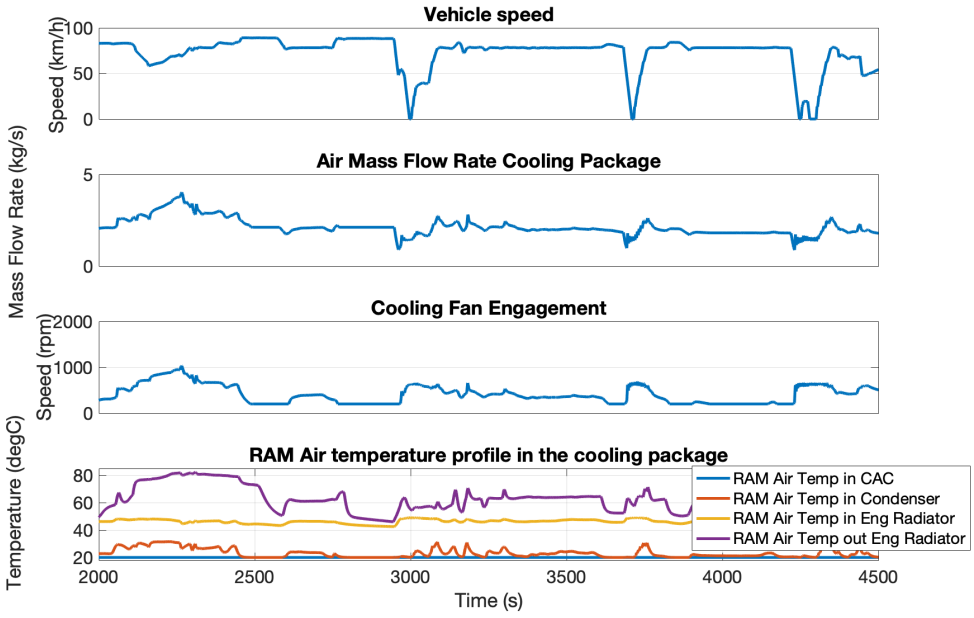

Figure 4.2 – Air temperature profile in the cooling package over a complete road cycle, in the fourth subplot. - refers to the RAM air temperature at the CaC inlet, - at condenser inlet, - at main radiator inlet, - at main radiator outlet. The temperature profiles can change according to the engagement of the cooling fan.

Because of the high mass flow rate of the heat source and, consequently, the thermal inertia of the engine-coolant flow, the superheat control is not the major control issue; a basic PID algorithm can be used as controller for the superheat of the working fluid at the inlet of the turbine. In all the road cycles the controller reacts quickly to the disturbances and tracks the set-point of the superheat, that for this application, using dry fluids and a turbine as expansion machine, is set to

5K.
The main issue is therefore identified in the control of the subcooling at the outlet of the condenser (inlet of the feed pump); three different strategies are implemented in order to control successfully the subcooling and track the set-point of 10 K and are then compared. Although most of the discussion about the control of the subcooling is dedicated to the use of the R1233ZD, as it is characterized by the lowest normal boiling point that induces more difficulties in the control of the subcooling, the extensive comparison of the strategies, in terms of relative error, standard deviation, integrated absolute error (IAE) and total variation (TV) is provided at the end of the chapter for both working fluids, R1233ZD and Novec649.

- Strategy 1: activation of a feedforward action on the cooling fan controller, that operates as soon as the working fluid subcooling at the outlet of the condenser drops below 5 K, keeping the condensation pressure at a constant value, by means of the compressed air loop, according to the working fluid boiling point (3.5 bar using R1233ZD, 1.2 bar using Novec649)
- Strategy 2: control by means of the condensation pressure, activating the feedforward action on the fan speed as soon as the working fluid subcooling at the outlet of the condenser drops below 5 K
- Strategy 3: control by means of the condensation pressure (regulated from the minimum value to 5 bar, higher values are not admitted in order to keep a gap between the condensation pressure and the compressed air loop at 7 bar), limiting the feed pump speed (and consequently the working fluid mass flow rate) in order to prevent fan activation (overshoot of the superheat at the inlet of the turbine with respect to the set-point is accepted); the controller of the superheat by means of the pump speed is deactivated as a consequence of a reduction of the cooling capacity and the pump speed is reduced according to the vehicle speed.

Cooling fan speed and condensation pressure are the manipulated variables of the controllers of the coolant temperature at the outlet of the engine and the subcooling respectively. The controller of the coolant temperature is not the object of this section, therefore details are not provided. In order to use the cooling fan as a manipulated variable to control the subcooling as well, the original controller of the coolant temperature at the outlet of the engine is modified, adding a feedforward term, in order to increase the fan speed in case of the subcooling is reducing below 5 K. Both controllers, the feedforward term on the fan speed and the condensation pressure as manipulated variables, are based on FOPTD models (First Order plus Time Delay), as shown in (4.2), identified in simulation; the parameters G ($\frac{K}{rpm}$ for the cooling fan, $\frac{K}{bar}$ for the condensation pressure), τ (s) and θ (s) of the two transfer functions are shown in Tab. 4.3.

$$\begin{cases} \frac{y_{FanSpeed}(s)}{u_{FanSpeed}(s)} = \frac{SC(s)}{N_{fan}(s)} = \frac{G}{1+\tau s} \cdot e^{-(\theta s)} \\ \frac{y_{CondPres}(s)}{u_{CondPres}(s)} = \frac{SC(s)}{p_{cond}(s)} = \frac{G}{1+\tau s} \cdot e^{-(\theta s)} \end{cases} \tag{4.2}$$

Model	G	τ	θ
Cooling Fan Feedforward	50,3	18	10
Condensation Pressure	-0.004	0.5	5

Table 4.3 – Parameters of the FOPTD models used for the controllers.

The PID controllers based on the models in Tab. 4.3 are tuned using the technique already introduced in (3.7). It is possible to notice how the cooling fan model is characterized by large delay and time constant; this can suggest that using the cooling fan as main actuator for the control of the working fluid subcooling at the inlet of the pump can be a non-optimal choice, as it can induce

extremely large amplitude of the speed variation and non-effective tracking of the subcooling because of its large dynamics.

- The first strategy, that consists in the activation of the feedforward action on the fan speed as soon as the subcooling drops below 5 K, is initially adopted; as shown in Fig. 4.3, the actual value of the subcooling is always positive. Between 2500 and 3000 s the subcooling is much higher than the set-point; this leads, as already explained in Chap. 3 to a loss of power production of the Rankine system. As announced the condensation pressure is set to 3.5 bar and the fan speed varies. The fan power is divided in two parts: the total fan power, that is actually requested by the cooling system and the fan power that is related to the presence of the Rankine condenser in the cooling package (calculated subtracting a reference fan power, from simulation results on a vehicle that is not equipped with a Rankine system, to the total fan power). Between 2000 and 2500 s the Rankine fan power is null and the total fan power reaches roughly 4kW; this situation is very specific of the road cycle and does not depend on the Rankine system, as it happens in the simulation on the vehicle that is not equipped with the Rankine system as well. Although this strategy ensures a positive value of the actual value of the subcooling along the whole road cycle, but it does not provide a tight control on the subcooling, that often presents higher actual values than its set-point; between roughly 2400 and 300 seconds, the subcooling is higher than the set-point, the fan speed is equal to the minimum value and no regulation to furtherly reduce the subcooling is available. The same situation occurs using Novec649 as working fluid. To conclude, this strategy does not allow the exploitation of the full potential of the system.

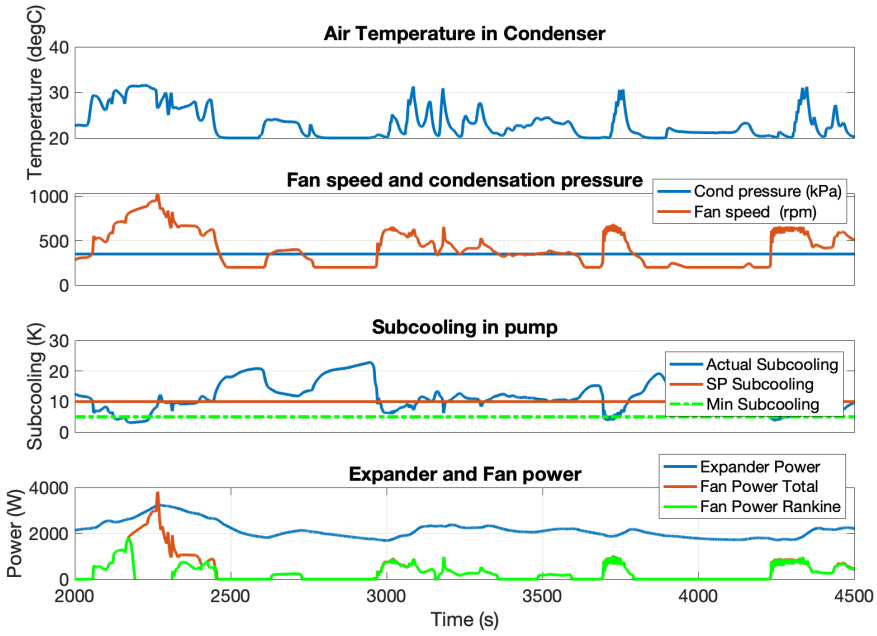

Figure 4.3 – First strategy using R1233ZD: subcooling control by means of the only action of the fan.

- In the second strategy, the subcooling is controlled, by adding the regulation of the condensation pressure with respect to the first strategy, in order to avoid the overshoot of the subcooling actual value with respect to the set-point. As it is shown in Fig. 4.4, using R1233ZD as working fluid, the condensation pressure saturates at 5 bar and its average value over the whole road cycle is roughly 4 bar. The set-point of the subcooling is well tracked

with respect to the first strategy, as the actual value rarely overshoots with respect to the set-point. The fan power that is related to the presence of the Rankine condenser in the cooling package is much reduced with respect to the first strategy; the expander power is roughly 2 kW and drops as soon as the condensation pressure raises. This strategy represents an important improvement with respect to the first strategy as it ensures a control of the subcooling and a limitation of the engagement of the cooling fan; the necessity of the regulation of the condensation pressure is confirmed in the current architecture, using the engine coolant as heat source.

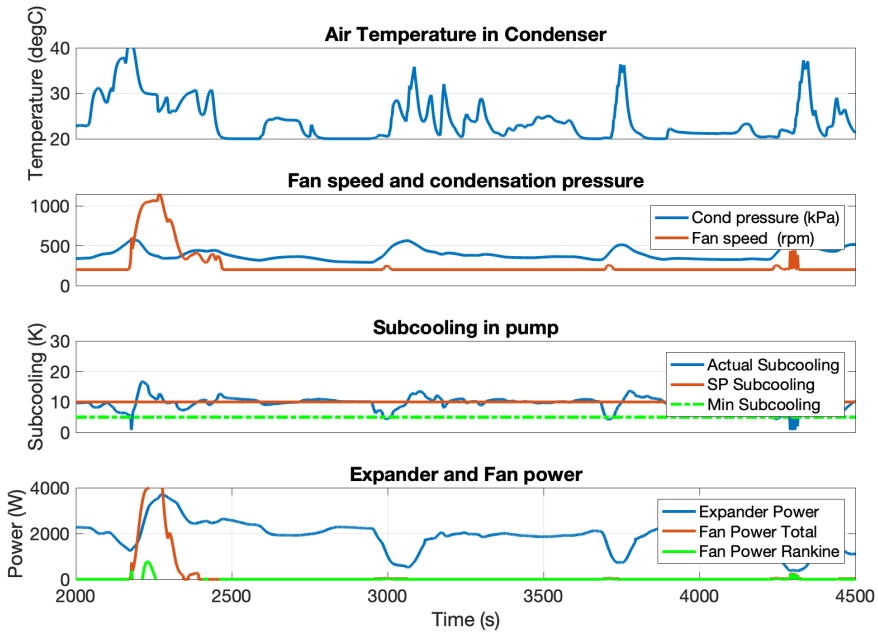

Figure 4.4 – Second strategy using R1233ZD: subcooling control by means of the fan speed and condensation pressure control.

The same analysis is repeated for the Novec649, based on Fig. 4.5; the main difference using Novec649, with respect of applying the strategy to R1233ZD, is the fact that the actual value of the subcooling is never below 5 K and the tracking of the subcooling set-point is largely acceptable. Therefore the strategy 2 is considered as the suitable strategy for the current application using Novec649 as working fluid. The larger effectiveness of the second strategy using Novec649, with respect to R1233ZD, is a result of the higher normal boiling point of the Novec649, that leads to higher difference of the coolant air and working fluid temperature profiles in the condenser, allowing higher thermal power removal than using R1233ZD, with the same amount of mass flow rate.

- The first two strategies reveal that the cooling system fan is not appropriate for an efficient control of the subcooling, because its power demand is too high at low regimes and its operation is characterized by long dynamics. Therefore the third strategy is applied, acting on the condensation pressure and limiting the pump speed in order to control the subcooling and prevent the fan activation. The pump speed is regulated in order to ensure the superheat set-point in normal operating conditions that are here characterized by a vehicle speed higher that 70 km/h; lower vehicle speed implies lower air mass flow in the cooling package and consequently a rise of the temperature profile of the RAM air at the outlet of the CaC (inlet of the condenser), affecting (reducing) the cooling capacity and increasing the engagement of the cooling fan. Therefore the strategy is to reduce the working fluid mass flow provided by

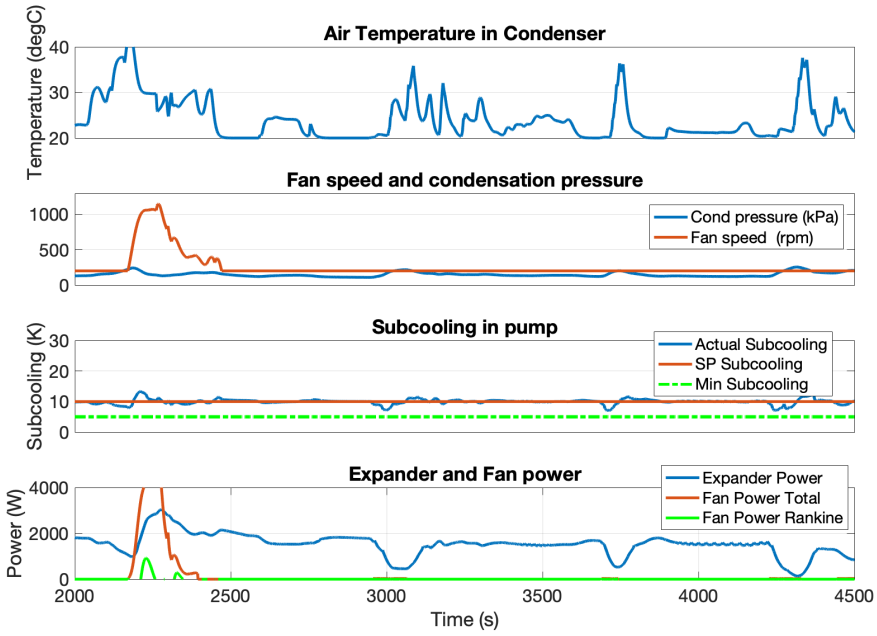

Figure 4.5 – Second strategy using Novec649: subcooling control by means of the condensation pressure and pump speed control. The actual value of the subcooling is never below 5K.

the feed pump, in order to reduce the thermal load in the condenser during the phases characterized by low cooling capacity. In order to do that, the controller of the superheat, acting on the feed pump speed, is deactivated during the phases of the road cycle characterized by vehicle speed that is lower than 70 km/h and the actual pump speed is reduced by means of a factor ϕ that depends on the vehicle speed, as it is specified in (4.3). Consequently, the real pump speed is written as (4.4) and the control scheme is shown in Fig. 4.6; $G_{c,SH}(s)$ is the transfer function of the controller of the superheat at the inlet of the expansion machine by means of the pump speed (Sec. 3.5) and $G_{c,SC}(s)$ is the transfer function of the controller of the subcooling at the inlet of the pump by means of the condensation pressure.
Fig. 4.8 shows the effect of the deactivation of the controller of the superheat; the feed pump speed is reduced as a result of the reduction of the vehicle speed and the superheat correspondingly increases.

$$\phi(v_{veh}) = \begin{cases} 0.4 & \text{if } v_{veh} < 40km/h \\ 0.02v_{veh} - 0.4 & \text{if } 40km/h < v_{veh} < 70km/h \\ 1 & \text{if } v_{veh} > 70km/h \end{cases} \tag{4.3}$$

$$N_{pump,y} = N_{pump,c}\phi(v_{veh}). \tag{4.4}$$

As it is shown in Fig. 4.7, the reduction of the pump speed in the phases characterized by low vehicle speed leads to an increase of the superheat at the inlet of the turbine. It shows as well that the tracking of the subcooling is tight and the actual value never drops below 5 K. The fan power that can be related to the Rankine system is reduced with respect to the first strategy and comparable with the second, while the expander power is roughly similar to the second strategy, but it drops (as expected) correspondingly to the reduction of the feed pump speed. This strategy ensure the best tracking of the subcooling among the three strategies

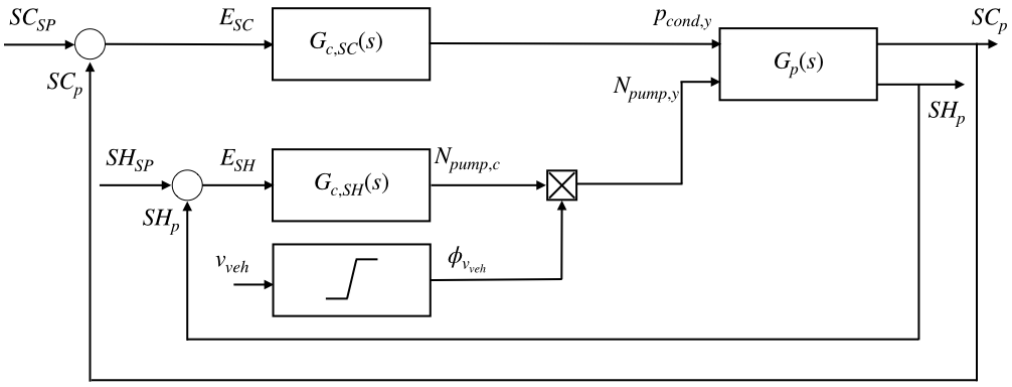

Figure 4.6 – Control scheme of the third strategy; $G_{c,SC}(s)$ and $G_{c,SH}(s)$ are defined above in the current section, v_{veh} is the vehicle speed, $G_p(s)$ is the transfer function of the plant related to the SC_p and $SH_p(s)$ with respect to $p_{cond,y}$ and $N_{pump,y}$ respectively.

that have been implemented using R1233ZD and ensure a good standard of power produced by the Rankine system.

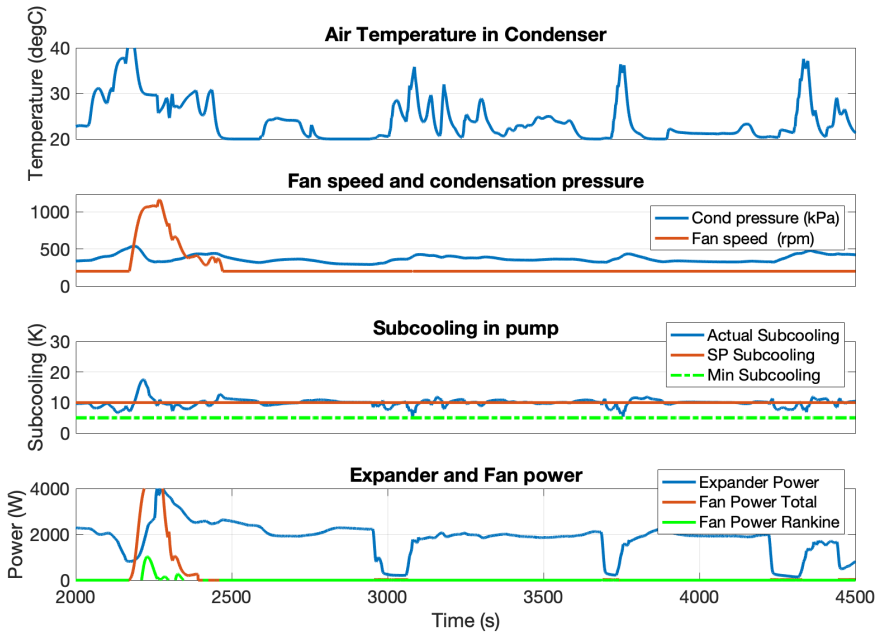

Figure 4.7 – Third strategy using R1233ZD: subcooling control by means of the condensation pressure and pump speed control.

The three strategies are compared, using both R1233ZD and Novec649, over the LCG road cycle, in terms of the four criteria already presented in (3.8). The results, presented in Tab. 4.4 show that; strategy 1, characterized by the control of the subcooling at the inlet of the pump by means of the fan speed only, presents, for both the working fluids, a very high error Err and integrated absolute error IAE; as already remarked, the performance of the controller is not acceptable. Strategy 2 (control by means of the fan speed and condensation pressure) and 3 (control by means of the fan speed and condensation pressure, with reduction of the pump speed) present a clear reduction of Err and IAE. Using R1233ZD, strategy 3 shows the lowest Err and IAE and comparable manipulated variable effort TV with respect to the strategy 2. Strategy 3 is therefore the more

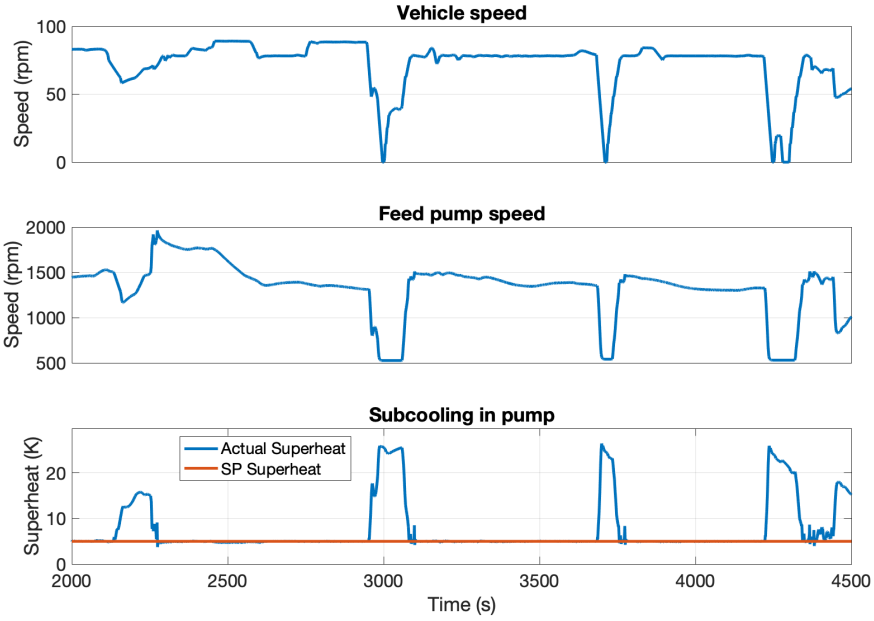

Figure 4.8 – Pump speed reduction as a consequence of the vehicle speed reduction using R1233ZD: the superheat increases as the main controller is deactivated as the vehicle speed is lower than 70 km/h.

appropriate to ensure a good tracking of the subcooling at the inlet of the pump. Using Novec649, strategy 2, as already discussed, leads to the best results in terms of Err, Std and IAE.

	R12233ZD			Novec649	
Variable	Str 1	Str 2	Str 3	Str 1	Str 2
Err	0.442	0.131	0.0872	0.242	0.058
Std	5.0	2.21	1.4	2.97	1.10
IAE	4422.0	1322.0	894.0	2430.0	590.0
TV	$3.68{\cdot}10^5$	$2.47{\cdot}10^5$	$2.46{\cdot}10^5$	$4.64{\cdot}10^5$	$2.45{\cdot}10^5$

Table 4.4 – Comparison of the strategies in terms of controller performance and working fluid.

The three strategies are also compared over the whole LCG road cycle in terms of mean value of the main variables that characterize the operation of the Rankine system. In the case of the R1233ZD the strategies 2 and 3 always reduce the expander power as a result of the raise of the condensation pressure, but on the other hand they provide a very similar result in terms of net power produced with respect to strategy 1, as a result of a reduced fan power demand. The strategy 3 is still the preferable one, because it provides comparable net power production with respect to the strategies 1 and 2, but it ensures better tracking of the subcooling. In the case of the Novec649, the strategy 2 is more reliable for control purposes as well as for the net power produced. Comparing the two working fluids, it is possible to notice that the working fluid R1233ZD performs better than the Novec649, producing average net power that is 20% higher.
To conclude, the low normal boiling point of the R1233ZD makes necessary the use of the third strategy in order to track the subcooling set-point, deactivating the superheat controller as soon as the cooling capacity reduces (accordingly to a reduction of the vehicle speed); Novec649 presents limited issues as it is characterized by higher normal boiling point than R1233ZD, therefore the control of the subcooling is ensured by means of the condensation pressure manipulation.

	R12233ZD			Novec649	
Variable	Str 1	Str 2	Str 3	Str 1	Str 2
Mass flow rate (kg/s)	0.240	0.243	0.23	0.40	0.40
Cond pressure (bar)	3.5	3.87	3.70	1.2	1.53
Expander power (kW)	2.10	2.00	1.94	1.88	1.58
Pump Power (W)	133	133	126	80	76
Fan power (W)	148	38	15	353	12
Net power (kW)	1.82	1.83	1.80	1.45	1.49

Table 4.5 – Analysis of the simulation mean results using the selected strategies for the two fluids, R1233ZD and Novec649.

4.4 Test bench and experimental results

The target application of the engine-coolant waste heat recovery is the long-haul heavy-duty, 13-liter non-EGR, 35 tons; the architecture that has been studied for such a system is shown in Fig. 4.9 and experiments are performed in the Thermodynamics Laboratory of the University of Liège. The test bench has been sized according to the design point (Tab. 4.6) that has been identified by IFPEN, based on the data supplied by Volvo.

Coolant Mass Flow Rate (kg/s)	Coolant Temperature (°C)	Inlet Condenser Air Temp (°C)
5.2	90	30

Table 4.6 – Design point for the sizing of the test bench.

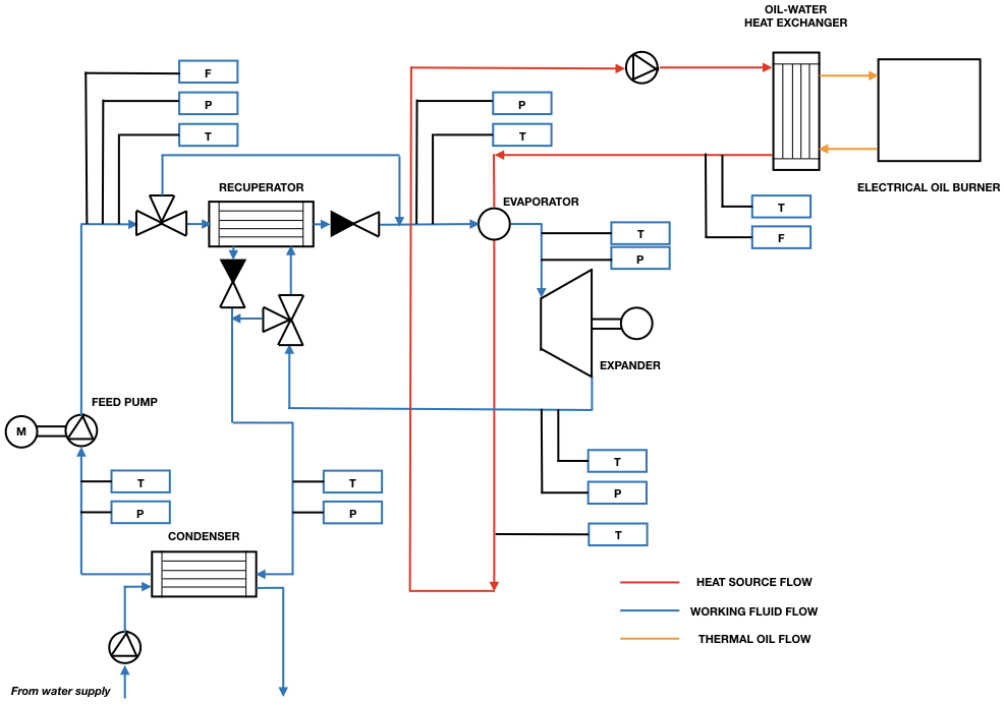

Figure 4.9 – Waste heat recovery from coolant, test bench architecture.

As a heavy-duty truck engine is not available during the experimental campaign, an electrical oil

burner is used to make available the heat source characterized by mass flow rate and temperature values that are encountered in the cooling system of the vehicle of the current application. The mass flow rate and the temperature of the heat source can be adjusted manually and measured via a flow-meter and a thermocouple T. Sensors as thermocouples T and pressure sensors, as well as a flow-meters are used to measure temperature, pressure and mass flow rate of the working fluid at the inlet and outlet of each component. The coolant water circulating in the condenser is tap running water, that is available in a temperature range between 7 and 10 °C, depending on the weather conditions.
The present architecture uses a centrifugal feed pump, a plate and fin heat exchanger as evaporator, condenser and recuperator and a radial inflow turbine as expansion machine. The recuperator is by-passed, as it has been noticed experimentally, that it imposes too high pressure drops. A LabView code has been developed in order to ensure the control of actuators like the feed pump speed and visualize in real time the measured values in the system; the pump speed is adjusted in order to ensure a working fluid superheat at the inlet of the turbine of 5 K. The turbine speed is controlled manually via the skid supplied by ENOGIA and the incorporated screen shows the actual electrical power produced.
According to the usage conditions and the application and the limited available time for performing the experiments, 11 operating points have been tested; the experiments, in terms of mass flow rate and temperature of the heat source are listed in Tab. 4.7; as it is possible to notice, the injection of the turbine is varied along the experimental campaign. For a given volumetric flow rate of the working fluid, the variation of the injection section influences the pressure at the inlet of the turbine. It has been found experimentally that the full injection is not suitable for this application, as, even for very high loads (first experiment listed in the Tab. 4.7) Considering the poor pressure ratio that has been realized in the experiments characterized by a full injection, a partial admission has been adopted for the following experiments, by reducing the number of active nozzles in the stator; Fig. 4.10 shows a basic scheme of the stator, in which nozzles can be plugged in order to realize a partial admission. Although the adoption of the partial admission in this specific situation is expected to improve the power production of the turbine (expectations are fulfilled by the experimental results) as a consequence of higher pressure ratio, additional losses take place and can degrade the efficiency of the turbine. As noticed in Cho et al. 2007, a turbine that operates in partial admission encounters losses that are related to the windage loss, due to the force that the rotor applies on the stagnant fluid in the inactive regions, the expansion loss, due to the expansion of a portion of fluid in the inactive regions and the mixing loss, due to the carrying by the rotor blades of the stagnant fluid from inactive regions to the active regions.

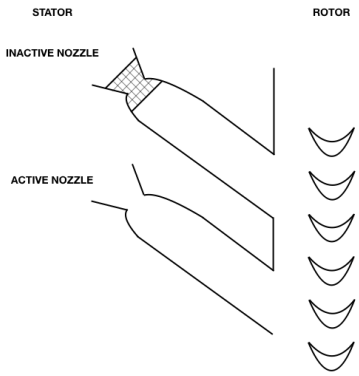

Figure 4.10 – Active and inactive nozzle in the stator of the turbine influencing pressure and flow rate of the working fluid sent to the blades of the rotor.

Based on the different injection conditions that have been tested, the equivalent throat diameter of the turbine has been calculated according to (2.19); analyzing Fig. 4.11, it is possible to get the confirmation that the full injection imposes pressure ratio values that are too modest to ensure an

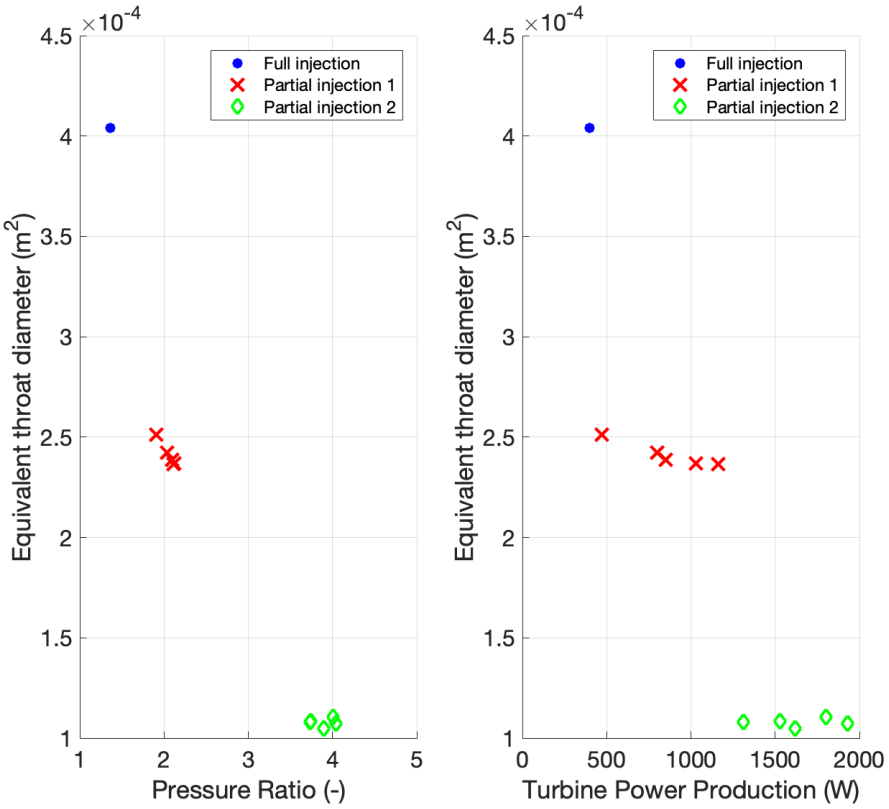

Figure 4.11 – Calculated equivalent throat diameter of the turbine, based on the characteristics of the fluid measured in the test bench.

interesting power production. Reducing the number of active nozzles of the turbine, it is possible to obtain higher pressure ratio and, consequently, higher turbine power production, even using a lower thermal quality heat source. The equivalent throat diameter of the turbine, during the experimental campaign, is reduced from roughly 4 cm^2 to 2.5 cm^2 and 1 cm^2; consequently the pressure ratio increases from roughly 1.2 to 2 and 4 and the turbine power production increases from roughly 300 W to 1.20 kW and 1.90 kW.

Fig. 4.12 shows the results in terms of pump power demand and turbine power production as a function of the working fluid mass flow rate and the different injection conditions; the only point with full injection is characterized by working fluid mass flow rate of roughly 0.62 $\frac{kg}{s}$ and modest turbine power production; this value of mass flow rate is too low to reach the required superheat at the inlet of the turbine (5 K as already announced) and it could be increased, considering that it is the point characterized by highest thermal power transferred to the working fluid in the evaporator (more details in Tab. 4.7). But in the test bench it has been noticed that the feed pump could not keep a constant mass flow rate in these conditions and cavitation phenomena occurred. The experiments characterized by the first condition of partial injection experience higher turbine power production, as a result of an increased pressure ratio; this increasing trend can be noticed in the operating points characterized by the second partial injection conditions, with the lowest number of active nozzles in the stator of the turbine.

Fig. 4.13 shows the increased pressure at the inlet of the turbine, by reducing the admission to the turbine, as well as the increase of the pressure drops at the inlet/outlet of the evaporator and condenser by increasing the working fluid mass flow rate. Although the pressure drops that take

Injection	$\dot{m}_{cool,su,ev}(kg/s)$	$T_{cool,su,ev}(°C)$	$\dot{Q}_{ev}(W)$	$\dot{m}_{wf}(kg/s)$	$p_{wf,su,turb}(bar)$	$K_{eq}(m2)$	$\dot{W}_{pump}(W)$	$\dot{W}_{turb}(W)$	$\dot{W}_{net}(W)$
Full	3.83	111.0	$1.06 \cdot 10^5$	0.61	2.13	$4.04 \cdot 10^{-4}$	126.0	400.0	273.8
Partial 1	3.67	92.0	$5.56 \cdot 10^4$	0.373	1.64	$2.51 \cdot 10^{-4}$	62.8	470.0	407.2
Partial 1	4.15	86.6	$6.57 \cdot 10^4$	0.463	2.02	$2.42 \cdot 10^{-4}$	188.0	800.0	611.7
Partial 1	4.53	82.0	$7.28 \cdot 10^4$	0.544	2.34	$2.39 \cdot 10^{-4}$	155.0	850.0	694.6
Partial 1	4.41	86.2	$8.19 \cdot 10^4$	0.601	2.6	$2.37 \cdot 10^{-4}$	164.0	1033.0	866.2
Partial 1	4.29	90.9	$9.59 \cdot 10^4$	0.659	2.87	$2.37 \cdot 10^{-4}$	421.0	1166.0	739.4
Partial 2	5.4	86.6	$4.56 \cdot 10^4$	0.321	2.78	$1.08 \cdot 10^{-4}$	64.3	1311.0	1245.7
Partial 2	5.35	92.1	$5.17 \cdot 10^4$	0.358	3.09	$1.08 \cdot 10^{-4}$	269.0	1533.0	1260.5
Partial 2	4.82	97.1	$6.19 \cdot 10^4$	0.418	3.61	$1.07 \cdot 10^{-4}$	489.0	1933.0	1440.7
Partial 2	4.93	93.5	$5.8 \cdot 10^4$	0.396	3.42	$1.11 \cdot 10^{-4}$	285.0	1800.0	1514.6
Partial 2	4.93	93.5	$5.8 \cdot 10^4$	0.396	3.42	$1.11 \cdot 10^{-4}$	285.0	1800.0	1514.6
Partial 2	5.04	90.3	$5.23 \cdot 10^4$	0.359	3.14	$1.05 \cdot 10^{-4}$	227.0	1622.0	1393.

Table 4.7 – List of the experiments performed in the test bench.

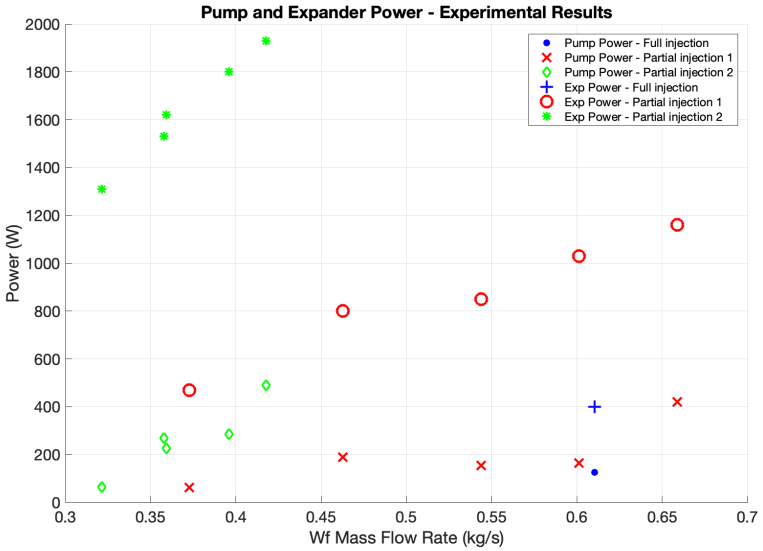

Figure 4.12 – Experimental turbine power production and pump power demand as a function of the working fluid mass flow for the three different turbine admission conditions: the reduction of the active nozzles in the stator of the turbine leads to higher turbine power production.

place in the condenser are usually higher than the evaporator, the pressure drops that are attributed to the condenser looks too high, because of a non-optimal sizing of the condenser.
Fig. 4.14 shows, in the first subplot, the turbine isentropic efficiency (calculated as $\eta_{is} = \frac{\dot{W}_{meas}}{\dot{W}_{is}}$); the low value related to the full injection is due to the low pressure ratio and, consequently, the low power produced. On the other hand, the low values related to the two partial injections are due to the additional losses that the turbine is subjected in case of partial injection. In the second and third subplot, the isentropic and measured power are shown; the difference between the two series of values is related to the mentioned isentropic efficiency and the efficiency of the synchronous electric machine, that is installed downstream the turbine.

The analysis of the experimental results can be concluded observing that the efficiency of the cycle (calculated as $\eta_{cycle} = \frac{\dot{W}_{meas}}{\dot{Q}_{evap}}$) is lower than the values that have been announced in Sec. 4.1; this difference is mainly related to the high pressure losses that are experienced in the evaporator and, in particular, in the condenser and the low efficiency of the turbine, due to the partial injection that induces additional losses.

Although the experimental campaign on the coolant recovery Rankine system leads to results that are lower than the expected, in terms of efficiency and power produced, the potential of this technology is confirmed. As a first remark, the pressure losses dramatically influence the turbine power production, considering the limited pressure ratio due to the heat source and the nature of the working fluid. The problem related to the limited resulting pressure ratio has been partially solved realizing a partial injection of the working fluid in the turbine, by progressively reducing the number of active nozzles in the stator of the turbine; this leads to an increase of the turbine power production, despite the low isentropic efficiency, due to the fact that the turbine encounters additional losses because of the partial injection.
To conclude, the experimental campaign has been useful, as it gives key suggestions in order to identify critical aspects of the architecture and improve performance.
Chap. 3 and 4 presented the implementation of the single models of the components into a close-to-real vehicle environment and different control strategies have been compared in order to improve

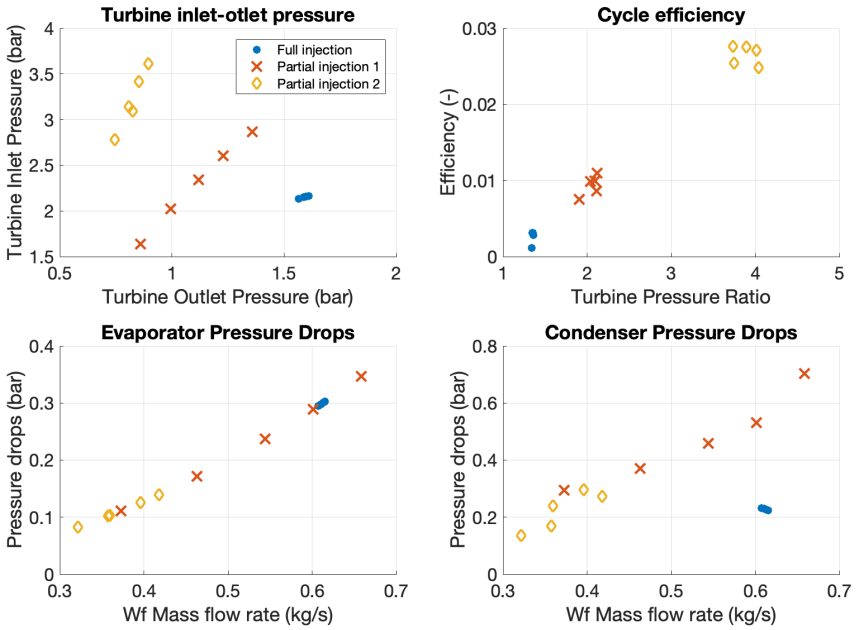

Figure 4.13 – Additional experimental results showing the limited pressure ratio in the full injection condition, the limited cycle efficiency and the values of the pressure losses in the evaporator and condenser that affect the net power production of the Rankine system.

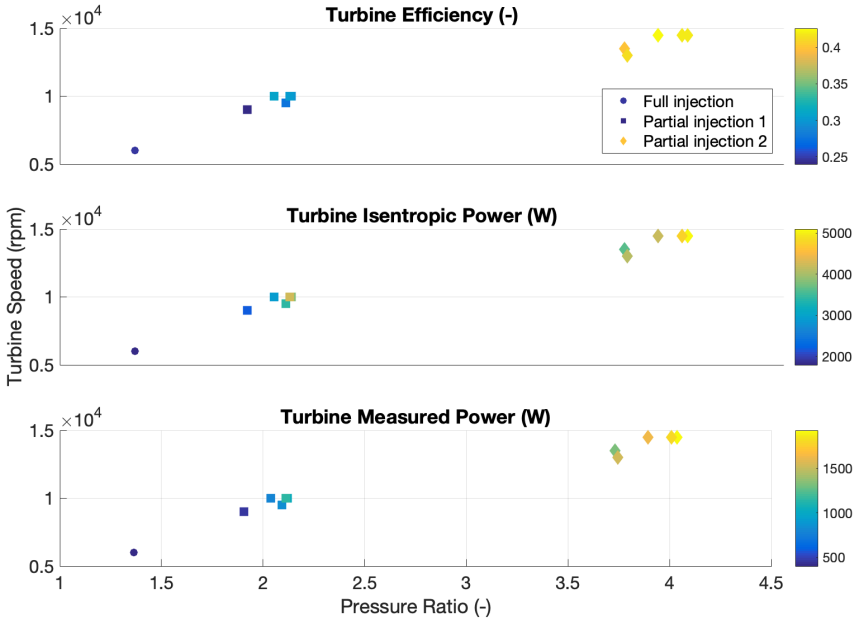

Figure 4.14 – The isentropic efficiency of the turbine is lower than expected, because of the additional losses that are encountered, as the turbine works in partial injection. The isentropic power and the measured power differ as a result of the low isentropic efficiency of the turbine, as well as of the poor efficiency of the synchronous electrical machine.

the tracking of variables as the superheat at the inlet of the expander and the subcooling at the inlet of the pump and, in the same time, ensure that the Rankine system power production fulfills the expected goals; the main remark that is possible to set out is that the control of condensation pressure, using cyclopentane, R1233ZD and Novec649 as working fluids, is necessary to improve control and performance.

Conclusion. *This chapter deals with the coolant flow waste heat recovery, showing a simulation work based on different control strategies to improve control performance as well as the power output and an experimental campaign, to assess the potential of the technology and identify critical issues. The simulation work, using two different working fluids, R1233ZD and Novec649, highlights the impact of the cooling architecture on the Rankine performance; three different control strategies have been developed and compared, taking into account the integration of the system in the vehicle, leading to the conclusion that the fan of the vehicle cooling system is not suitable to control the subcooling of the Rankine and that the mass flow rate of the working fluid has to be reduced as soon as the cooling capacity drops (because of a reduction of the vehicle speed). The consequent main remark of the simulation results is that using the condensation pressure as manipulated variable, for the current architecture and R1233ZD and Novec649 as working fluids, is not only recommended, but rather necessary to improve the control of the subcooling; this aspect is further considered in the last chapter of this thesis. The experimental campaign highlighted the technical aspects to be considered in order to meet the expectation in terms of net power production of the architecture. The pressure loss and well as the design of the turbine are the factors that limited the performance of the system that has been tested.*

Chapter 5

Subcooling and superheat control optimization

The focus of this chapter is to present specific strategies that are addressed to the optimal control of the Rankine system. This chapter presents two main contributions that are oriented towards the improvement of the previous results:

- As for the superheat control, in the Chap. 3, 37 multi-linear controllers (chosen based on the most representative operating points for a specific road cycle) have been combined and weighted using two different weighting schemes algorithms, in order to identify at single controller for each time step. In this chapter, artificial intelligence (AI) is used in order to predict the weights of the selected multi-linear controllers, to identify a unique controller for each time step. The methods and results have been presented in the 59th IEEE Conference on Decision and Control, 2020 (Peralez et al. 2020).
- As for the subcooling control, in the Chap. 3 the condensation pressure set-point has been computed fixing the pressure ratio between upstream and downstream the expander. In this chapter an optimal control strategy that leads to a compromise between the engagement of the fan and the pressure of the low-pressure side of the system is presented. Based on a simplified analytical Rankine model, a local optimization is performed to improve the net power of the system in two different road cycles with different environmental conditions. The results have been published in the Energy Journal in 2021 (Galuppo et al. 2021).

5.1 Low pressure side optimization

5.1.1 State of the art

Under definite constraints and for specific processes, process conditions can be manipulated in order to maximize the productivity of the plant. For such a goal, a real-time optimization (RTO) can be performed in order to maximize the performance of the process in real time, using the plant measurements as inputs to the optimization model (Taha and Khan 2011). RTO encompasses a family of optimization methods that incorporate process measurements in the optimization framework to drive a real process (or plant) to optimal performance, while guaranteeing constraint satisfaction (Bonvin 2017). As specified in Ahmad et al. 2018, the feasibility and optimality of the proposed strategies rely on the accuracy of the plant model, therefore it is necessary to verify that the model is

coherent with the plant measurements in different operating conditions; the unavoidable mismatches between the model and the plant can be corrected via modifier adaptation for RTO (Marchetti et al. 2010).
In Di Cairano and Kolmanovsky 2018, the authors indicated that in the recent years, MPC has been one of the most investigated RTO techniques in the aerospace and automobile applications. However the authors underline the fact that many challenges should still be faced, as the computational cost of the algorithms and the reliability of the approximated model, to ensure the MPC application to more practical problems.
Referring to ORC, depending on the application and architecture of the system, different objective functions can be considered. Braimakis and Karellas 2018, in a regenerative ORC, focused on the energetic efficiency of the cycle, acting on the evaporation pressure and the bleed pressure that impacts the pressure ratios of the low and high pressure expanders and the consumption of the low and high pressure pumps. Quoilin et al. 2011 studied the optimal control of a small-scale ORC system subjected to variable flow rate and temperature waste heat source; three strategies have been compared, but the best result on the overall cycle efficiency is achieved by the determination of the optimal evaporating temperature based on the condensing temperature, heat source temperature and working fluid mass flow rate (measured or either calculated by means of the pump speed). Sun and Li 2011 investigated the optimization of a heat recovery power plant using geothermal or industry process waste heat. The system is characterized by an air cooled condenser and the air flow is provided by fan; the goal of the optimization is to maximize the net power output or the overall efficiency of the process, using as controlled variables the pressure at the inlet of the expander, the air cooling mass flow rate and the working fluid mass low rate. The optimization, using the ROSENB algorithm (Vassiliadis and Conejeros 2009) is run for a set of steady-state points and the authors identified the optimal behavior of each controlled variable, depending on the heat source mass flow rate and temperature value.
In this thesis, the plant model developed in Chapter 2 and 3 is considered as physical system reference (the plant model is validated and can replace expensive and time-consuming road tests) and a reduced model is implemented in order to express the objective function of the optimization as a quadratic function, with quadratic constraints. As first step, the reduced model is validated according to the complete model and a local model based optimization problem is developed to generate the appropriate condensation pressure value and the optimal subcooling set-point.

5.1.2 Case study

The choice of the direct condenser architecture, characterized by the direct condensation, defines the system and the challenges related to control and optimization. As already investigated in Chapter 3, this architecture is characterized by lower performance than the indirect condensation architecture, but, on the other hand, the margin to improve the overall performance of the architecture is considerable, because of the high fan power demand and the ambient conditions that impact the temperature of the heat sink.
The control problem of the subcooling has been defined in Sec. 3.7 and two manipulated variables have been identified; this leads to a MISO system (5.1), where the inputs $u = [u_1; u_2]$ are the fan speed and the condensation pressure and the output is the net power production of the system.

$$\begin{cases} u_1 = N_{fan}(rpm) \\ u_2 = p_{cond}(bar) \\ y = \dot{W}_{net}(W). \end{cases} \tag{5.1}$$

The usage of a controller involving the condensation pressure instead of a constant value high-

lighted an important advantage; the possibility to vary the condensation pressure depending on the operating point allows to increase the net power output in case of low load, reducing the average condensation pressure in any road cycle. In Sec. 3.7, the condensation pressure has been varied according to a fixed pressure ratio value.
However, this combination of the actions of the two actuators may not represent the best strategy to improve the overall performance of the system, as the two actuators have a different impact in (3.1) (N_{fan} on $\dot{W}_{fan}$ and p_{cond} on $\dot{W}_{exp}$ and $\dot{W}_{pump}$). In this chapter, the challenge is to ensure the tracking of the subcooling set-point and in the same time provide the conditions to maximize the net power output of the system, defined as (3.1).
In Fig. 5.1, the selected architecture is highlighted as well as the sensors that are places in the system.

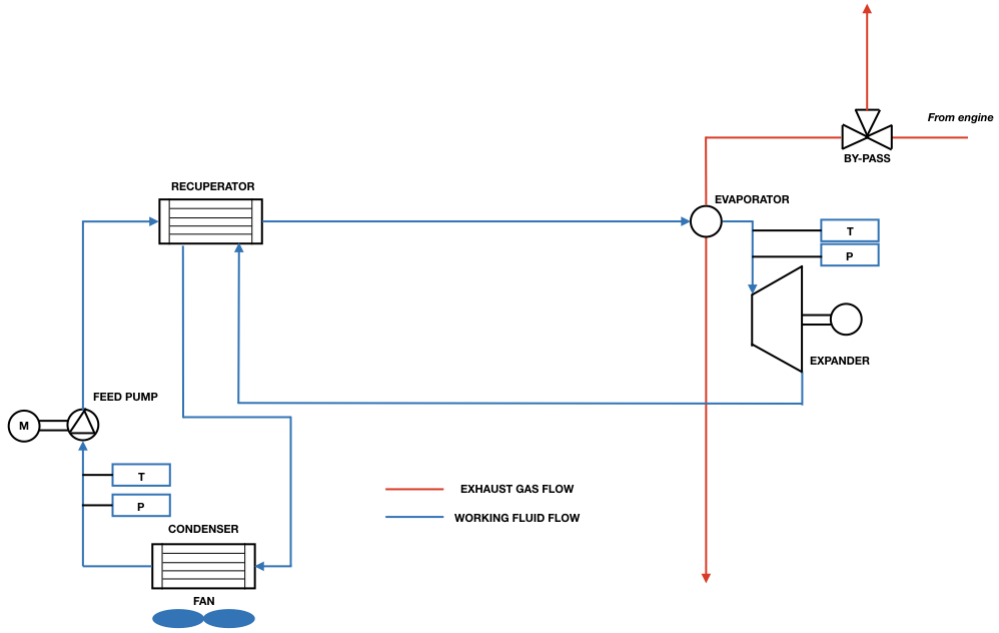

Figure 5.1 – Layout of the case study and signals used in the study.

The only measurements that are available for monitoring and that can be used to perform an RTO are the following:

- Pressure and temperature at the inlet of the feed pump
- Pressure and temperature at the inlet of the expander
- Feed Pump speed
- Fan speed
- Expander speed.

In Tab. 5.1, the controllable signals are listed, with the corresponding upper and lower bounds and type of the controller used for every actuators. The feed pump and expander speed are controlled by means of the controller presented in Chap. 3, while the condensation pressure and fan speed control are the object of the real-time optimization that is implemented in this chapter and is addressed to the optimal control of the low pressure loop. The objective function of the optimization is given by (3.1) and reformulated as follow:

$$\dot{W}_{net} = \dot{W}_{exp} - \dot{W}_{pump} - \dot{W}_{fan}. \tag{5.2}$$

Signal	Upper bound	Lower bound	Control
Feed pump speed (rpm)	2500	150	MMPID
Fan Speed (rpm)	4700	1570	MMPID
Expander speed (rpm)	3000	1000	PID
Condensation pressure (bar)	5	1.5	Opt

Table 5.1 – Available signals, upper and lower bounds and control.

The general idea of the optimal control strategy that is implemented is shown in Fig. 5.2, based on the control structure presented in Sec. 3.7: the controller represented by $G_{c,SC}(s)$ is a developed scheme MMPI controller, while the condensation pressure p_{cond} is now the output of a new optimization block. The second output of this optimization algorithm is the optimal subcooling, in other words the set-point of the subcooling that has to be tracked by the controller $G_{c,SC}(s)$; this value, during all the simulations that have been performed, is the minimum possible value defined in the constraints, as the lower the subcooling value is, the more the system produces in terms of net power. The optimization block input is constituted by the vector x_p, that represents the states that are needed to run the model contained in the optimization function.

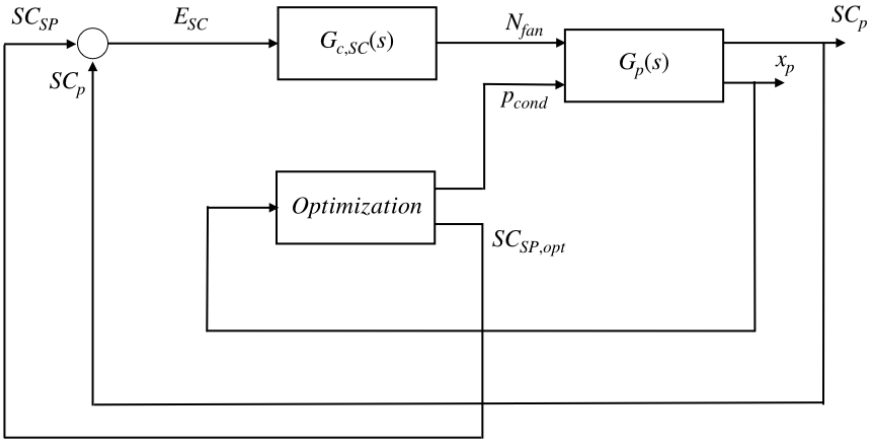

Figure 5.2 – Optimal control strategy of the subcooling.

The plant state vector x_p, presented in (5.3), contains variables that are involved in the optimization algorithms and that are outputs of the plants. The variables $x_{p,1}$ and $x_{p,2}$ are measured and their values are available in real-time, $x_{p,3}$ and $x_{p,4}$ varies according the controllers presented in Chap.3 and are not sensibly impacted by the optimization algorithm. To conclude, the optimization algorithm that is proposed in this chapter aims at the development of a strategy that involved the only cold side of the Rankine system, with very little impact on the hot side of the system.

$$x_p = [x_{p,1}\ x_{p,2}\ x_{p,3}\ x_{p,4}], \quad \text{where} \begin{cases} x_{p,1} = p_{su,exp}(bar) \\ x_{p,2} = T_{su,exp}(°C) \\ x_{p,3} = N_{pump}(rpm) \\ x_{p,4} = N_{exp}(rpm) \end{cases}. \tag{5.3}$$

5.1.3 Optimization problem formulation

The simple analytical model that has to be developed should be suitable for improving the net power output of the system, with respect to a defined base set of results, consuming low memory

and running in real-time. In order to ensure this task, the model has been developed via fitting functions and energy balance equations; the coefficients that are used in the fitting functions are constant and presented in Appendix B. The approach that is proposed is to calculate each term of the objective function (5.2) and then to gather the equations. The pressure drops in the working fluid loop are neglected, therefore the pressure measured at the inlet of the expander and pump are considered as the pressure for the whole high pressure and low pressure side respectively.
Once the condenser and the electrically-driven fan have been defined, the fan power $\dot{W}_{fan}$ demand can be directly related to the fan speed N_{fan}, neglecting the variation of the air density with the temperature. The quadratic relation between these two variables is easily defined as follows (5.4) and has been found by data fitting of simulation results on two different road cycles, a highway (FK) and a urban road cycles (CC), reaching R^2=99.7% :

$$\dot{W}_{fan} = a_1 N_{fan}^2 + b_1 N_{fan} + c_1, \tag{5.4}$$

where $a_1 > 0$, b_1 and c_1 are constant coefficients.

The pump power demand is a function of the flow rate and the pressure difference between outlet and inlet section (5.5)

$$\dot{W}_{pump} = \frac{\dot{V}\Delta P}{\eta_{gl,pump}} = \frac{\dot{m}_{wf}\Delta P}{\rho\eta_{gl,pump}}. \tag{5.5}$$

The working fluid mass flow rate $\dot{m}_{wf}$ involved her is not measured, but it is calculated from the pump speed signal; (5.6) show the relationship between the pump speed and the working fluid mass flow, once the displacement of the pump and the density of the working fluid at the inlet of the pump are fixed.

$$\dot{m}_{wf} = C\rho N_{pump}. \tag{5.6}$$

The density of the working fluid, in reality, is not perfectly constant at the inlet of the pump speed, but it is slightly variable. In order to reduce the complexity of the model, the density is considered constant as a first approach.
Therefore the pump power demand can be written as as a function of the pump speed as:

$$\dot{W}_{pump} = \frac{CN_{pump}\Delta P}{\eta_{gl,pump}} = \frac{CN_{pump}(p_{ev} - p_{cond})}{\eta_{gl,pump}}. \tag{5.7}$$

The expander power $\dot{W}_{exp}$ is calculated knowing the mass flow rate $\dot{m}_{wf}$ and the condition of the working fluid at the inlet and outlet section of the expansion machine, represented by the enthalpy at the inlet and outlet of the expander ($h_{su,exp}$ and $h_{ex,exp}$ respectively), as in (5.8). The mass flow rate is calculated according to (5.6); the enthalpy at the inlet of the expander can be easily calculated from the measurement of pressure and temperature at the inlet of the expander, by fitting function. The isentropic enthalpy at the outlet of the expander is found by fitting function of entropy at the inlet of the expander and the condensation pressure. The efficiency of the expander $\eta_{gl,exp}$ is found by fitting function of the expander speed and the inverse of the pressure ratio.

$$\dot{W}_{exp} = \dot{m}_{wf}(h_{su,exp} - h_{ex,exp}) = \dot{m}_{wf}(h_{su,exp} - h_{is,ex,exp})\eta_{gl,exp}. \tag{5.8}$$

The formulation (5.8) can be rewritten as in (5.9) using the fitting, by means of constant coefficients, for the enthalpies ($h_{su,exp}$ and $h_{is,ex,exp}$) and the expander efficiency ($\eta_{gl,exp}$), highlighting

the condensation pressure p_{cond} that is one of the inputs of the MISO system (5.1):

$$\begin{aligned} \dot{W}_{exp} &= \dot{m}_{wf}(h_{su,exp} - h_{is,ex,exp})\eta_{gl,exp} \\ &= C\rho N_{pump}\left((a_2 + b_2 p_{ev} + c_2 T_{su,exp}) - (a_4 + b_4 s_{su,exp} + c_4 p_{cond})\right)\left(a_5 + b_5 N_{exp} + c_5 \frac{p_{cond}}{p_{ev}}\right). \end{aligned} \tag{5.9}$$

where the coefficients a_2, b_2, c_2, a_4, b_4, c_4, a_5, b_5, c_5 are constant and presented in Appendix B. Gathering the equations (5.4), (5.7) and (5.9), it is possible to retrieve the complete equation of the net power (5.2) as a quadratic form with respect to the expander speed N_{fan} and condensation pressure p_{cond}:

$$\dot{W}_{net} = A_1 N_{fan}^2 + A_2 p_{cond}^2 + B_1 N_{fan} + B_2 p_{cond} + C. \tag{5.10}$$

where the coefficients A_i, B_i and C are depending on the plant state vector, consequently they are variable in time.

The quadratic problem (5.10) that has been exposed is subjected to constraints that refer to physical limits of the actuators and the necessity of keeping in a defined range other important variables of the Rankine system. The inequality constraints that are applied are listed.

- Fan speed constraint: 1570 $rpm \leq N_{fan} \leq 4700$ rpm
- Condensation pressure constraint: 1.5 $bar \leq p_{cond} \leq 5$ bar
- Subcooling at the outlet of the condenser: $SC_{ex,cond} \geq 9$ K.

The subcooling at the inlet of the pump (outlet of the condenser) is also subjected to constraint as it is the controlled variable of the fan speed controller and the goal of the optimization is to maximize the net power production of the system, ensuring the tracking of the subcooling set-point.

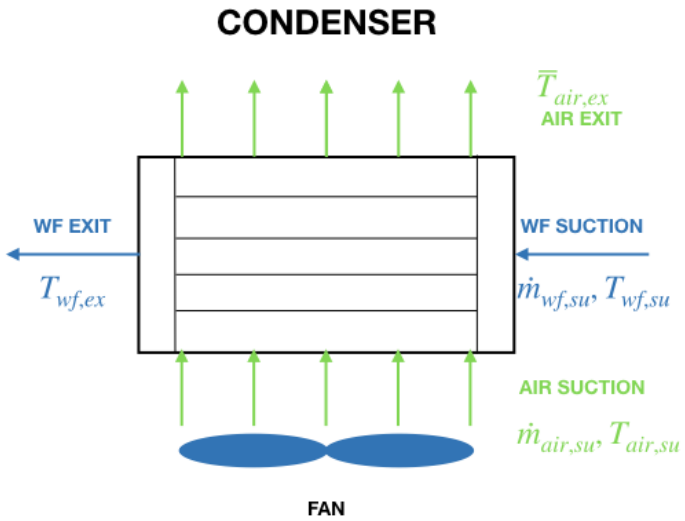

Figure 5.3 – Condenser model, inputs and outputs.

Fig. 5.3 shows the inputs and the outputs of the direct condenser; the calculation of the working fluid temperature using a simplified model can be hard considering all the variables that influence the energy balance of the considered system. Working fluid and air mass flow rate, working fluid

pressure at the inlet of the condenser as well as the air flow temperature at the inlet of the condenser intervene in the determination of the working fluid temperature at the outlet of the condenser. In order to maintain the simplified nature of the proposed approach, the temperature of the working fluid at the outlet of the condenser is fitted by a function of the working fluid and the air mass flow rate and the condensation pressure, taking the air flow temperature at the inlet of the condenser apart; using different temperature of the air flow at the inlet of the condenser it is possible to find different functions of the working fluid temperature at the outlet of the condenser. Consequently, the temperature of the air flow at the inlet of the condenser is another input of the optimization algorithm, as it influences the shape of the function of the working fluid temperature at the outlet of the condenser. The temperature at the outlet of the condenser is observed and showed in Fig. 5.4; the model predicts well the conditions of the working fluid at the outlet of the condenser according to the complete model results, with a relative error of less than 3%. Considering that the saturation temperature of the working fluid is a quadratic function of the condensation pressure, the subcooling can be written as in (5.11)

$$SC_{ex,cond} = T_{sat}(p_{cond}) - T_{wf,ex,cond} = A'_2 p^2_{cond} + B'_1 N_{fan} + B'_2 p_{cond} + C', \tag{5.11}$$

where $A'_2 < 0$, $B'_1 > 0$, $B'_2 > 0$ and $C' < 0$ are time varying coefficients depending on the state of the plant and on the air flow temperature at the inlet of the condenser.

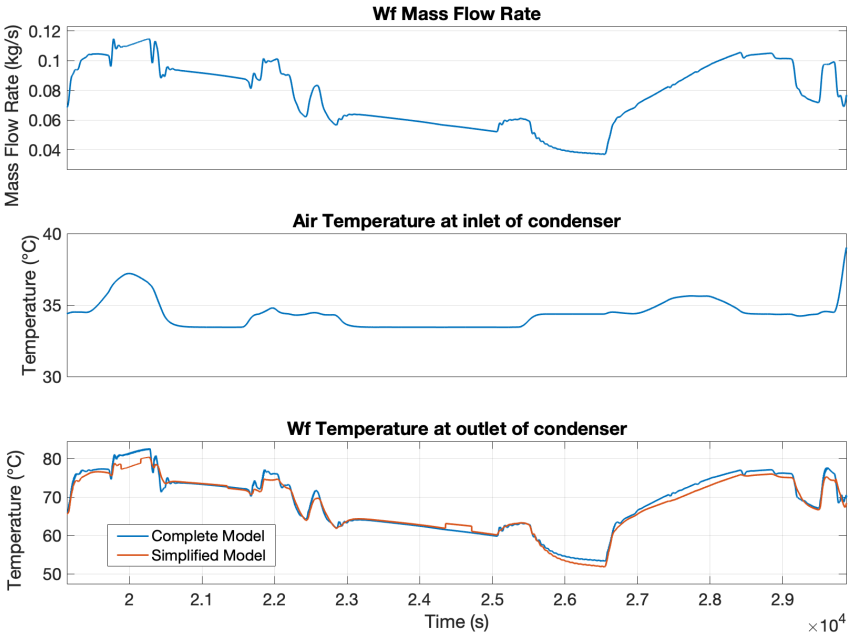

Figure 5.4 – Working fluid temperature at the outlet of the condenser: analytical model validation versus the complete model.

Since the model equations and the constraints are all defined, it is possible to define that the optimization problem with a quadratic function J subject to quadratic inequality constraints:

$$J = \min_u (\frac{1}{2} u^T Q u + f^T u + c), \tag{5.12}$$

subjected to

$$\frac{1}{2} u^T H_i u + k_i^T u + D_i \leq 0. \tag{5.13}$$

where i is the dimension of constraints and Q, H_i, k_i, c and d_i are given by

$$Q = -2\begin{bmatrix} A_1 & 0 \\ 0 & A_2 \end{bmatrix}; f = -\begin{bmatrix} B_1 \\ B_2 \end{bmatrix}; c = -C \tag{5.14}$$

$$H_i = -2\begin{bmatrix} h_{11_i} & 0 \\ 0 & h22_i \end{bmatrix}; K_i = -\begin{bmatrix} k_{1_i} \\ k_{2_i} \end{bmatrix}; D = -d_i \tag{5.15}$$

where $A_1 < 0$, $A_2 > 0$, $B_1 > 0$, $B_2 > 0$ and $C > 0$.
The coefficients of H_i, K_i and D_i are specific for each constraints; as an example, the coefficients related to the constraint of the subcooling (i=3) (5.11) are reported in (5.16)

$$\begin{cases} h_{11_3} = 0 \\ h_{22_3} = A_2' \\ k_{1_3} = B_1' \\ k_{2_3} = B_2' \\ d_3 = C'. \end{cases} . \tag{5.16}$$

where $A_2' < 0$, $B_1' > 0$, $B_2' > 0$, $B' > 0$, $B' > 0$, $C' < 0$.
The remaining constraints are related to the limits of the actuators of the fan speed and condensation pressure; indicating $i = 1$ the constraint related to the fan speed and $i = 2$ the constraint related to the condensation pressure, in both cases the quadratic term does not appear, therefore the matrices H_1 and H_2 are null. As for the other terms: k_{1_1}, k_{2_2}, d_1 and d_2 are positive, k_{1_2} and k_{2_1} are null.
As previously explained, the coefficients appearing in the formulation of the problem and constraints are time varying. This does not represent an issue since the optimization algorithm is executed at each time step, independently of an explicit dynamic model.

5.1.4 Results and discussion

The investigation on the improvement of the net power production of the system is performed considering two road cycles, corresponding two different kinds of missions. Tab. 3.10 highlights that the FK and CC road cycles represent two very different types of missions. As the temperature of the air at the inlet of the condenser depends on the vehicle speed (for details Tab. 3.11), it is necessary to apply the optimization algorithm and provide an interpretation of the results of both road cycles.
Different ambient temperature have been considered for both road cycles in order to cover a large spectrum of conditions and air temperature at the inlet of the condenser. For both road cycles, the constant ambient temperature of 0, 20, 40 °C has been considered and the optimization algorithm is run for the whole road cycles; the results are compared with the simulation results characterized by constant condensation pressure and condensation pressure calculated imposing an optimal pressure ratio. The sampling time of the computation involving the optimization algorithm is 0.3 seconds, in other words, every three samples; this choice reduced the computational time without affecting the accuracy of the solution. The optimization problem is solved, on average, in 0.12 seconds using a MacBook Air, processor 1.6 GHz Intel Core i5, RAM memory 8 GB.

Fig. 5.5 shows the behavior of the two actuators involved in the optimization algorithm over the FK road cycle, for each ambient temperature, considering the reference (condensation pressure calculated imposing an optimal constant pressure ratio) and the optimized strategy; analyzing the figure it is possible to notice that the compromise between the usage of the two actuators differs according to the ambient temperature. As for the ambient temperature of 0 and 20 °C, the optimized strategy imposes a stronger usage of the fan over the pressurization of the condensing side of the system with respect to the reference; as for ambient temperature of 40 °C, the optimized strategy

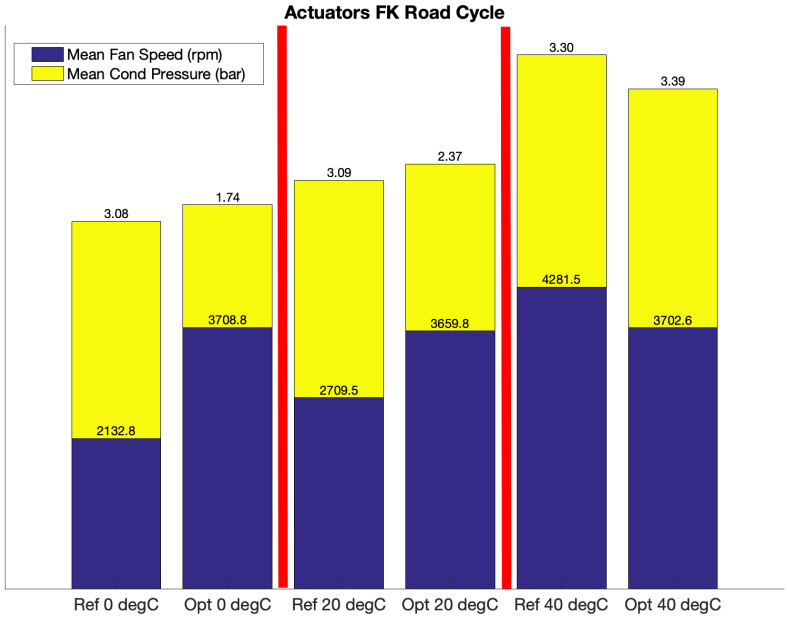

Figure 5.5 – Fan Speed and Condensation Pressure in FK road cycle for each different temperature using the two strategies; according to the ambient temperature, the optimized strategy favorites one actuator over the other one.

imposes a stronger pressurization of the condensing side of the system with respect to the reference. This result is physically logical, as for higher temperature of the air at the inlet of the condenser, the thermal exchange in the condenser is less performing and it is more convenient to pressurize the condensing side of the system. The results are confirmed using the CC road cycle, but, considering the nature of the road cycle, that imposes low vehicle speed, the temperature of the air flow at the inlet of the condenser is always higher than the values experienced in the FK road cycle, therefore the optimized strategy always imposes a rise of the condensation pressure and a reduction of the fan speed with respect to the reference.

Fig. 5.6 shows the results of the optimization analysis using the FK road cycle, for different ambient temperatures that has been announced. Fig. 5.6 (Top) shows the comparison with respect to the reference characterized by constant condensation pressure, that is fixed to 2.5 bar, while Fig. 5.6 (Bottom) shows the comparison with respect to the reference characterized by the condensation pressure calculated with respect to an optimal pressure ratio. The optimized strategy always improves the net power output; in the case of T_{amb}=20 °C, compared with the condensation pressure calculated imposing an optimal pressure ratio, the improvement is very little; in all the other cases the improvement is meaningful. The constant condensation pressure strategy is far from being optimized as the condensation pressure could be reduced in the phases of the road cycle characterized by low regimes and therefore improve the net power production. The results further confirm that the current direct condensation architecture, using cyclopentane as working fluid, has to include the control of the condensation pressure to reach higher performance level.

Fig. 5.7, additionally, shows the overall results running the optimized strategy in the CC road cycle, highlighting the fact that the percentage of the net power improvement in the road cycle CC are higher with respect to the FK. In fact, considering the same optimal pressure ratio used in the FK road cycle, the condensation pressure that is obtained in the CC road cycle is lower, because of the lower evaporation pressure as a result that the road cycle is characterized by lower thermal power recovered. This implies that the condensation is achieved via fan action, that provide hotter air

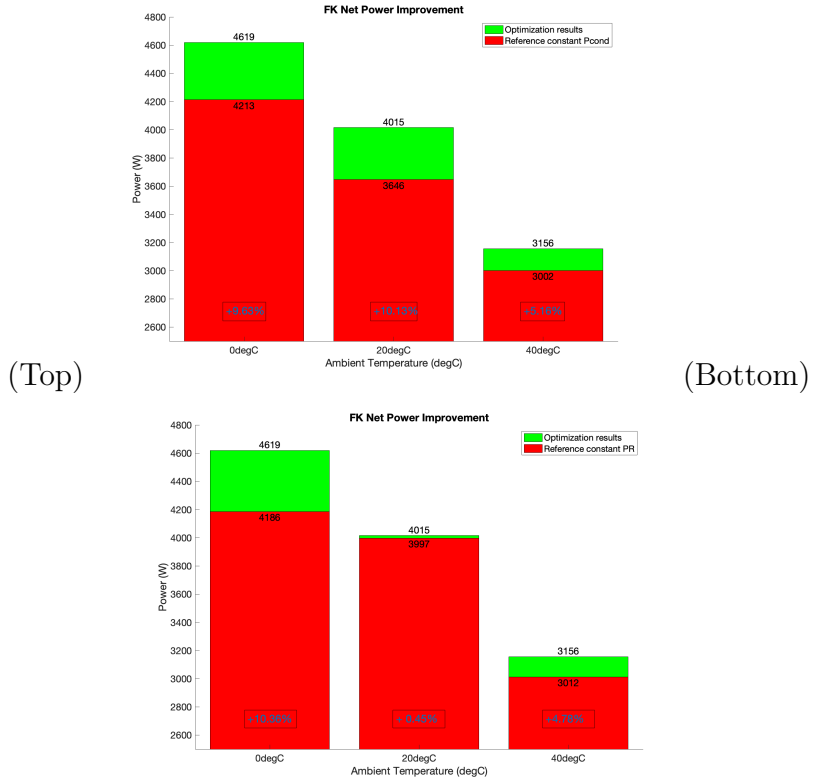

Figure 5.6 – (Top) Improvement vs reference consisting in constant condensation pressure. (Bottom) Improvement vs reference consisting in variable condensation pressure having set a constant pressure ratio PR.

with respect to the FK road cycle, as a consequence of the fact that the vehicle speed in the CC road cycle is reduced.

The proposed methodology improves the net power produced by the Rankine system. Indeed the percentage of the net improvement in power is 13.4 % using the CC road cycle and T_{amb}=20 °C however, it is of 0.5 % using the FK road cycle and T_{amb} = 20 ° C. Considering the sensible improvement that is possible to obtain using this methodology, especially in case of driving conditions that move away from the usual mission of a long-haul heavy-duty truck (urban in place of a highway road cycle) and more extreme ambient temperature (0 deg C or 40 deg C in place of 20 deg C), the usage of the strategies that have been presented is highly recommended. In addition, the algorithm can operate in real time and can be easily implemented in the embedded controller. On the other hand, a particular effort must be devoted to the calibration of the simplified analytical model, to take account of the temperature of the air at the inlet of the condenser.
In the past sections of this thesis, it has been noticed that the performance of the direct condensation architecture, using cyclopentane as working fluid, is strongly impacted by the cold side of the system. The current section shows that a better trade-off can be found between the action of the two actuators involved in the subcooling control, the fan speed N_{fan} and condensation pressure p_{cond}; in particular, the trade-off is influenced by the ambient air temperature and, consequently, the temperature of the cooling air at the inlet of the condenser. The lower the temperature of the cooling air, the higher the fan speed and, consequently the lower the condensation pressure, has to be set. The solution of the optimization problem provides an improvement of the net power output, with respect to the results found using a variable condensation pressure according to a fixed pressure ratio PR, in all the ambient conditions considered and in both road cycles that have been taken into account (FK highway and CC urban road cycle), therefore the results fulfill the expectations

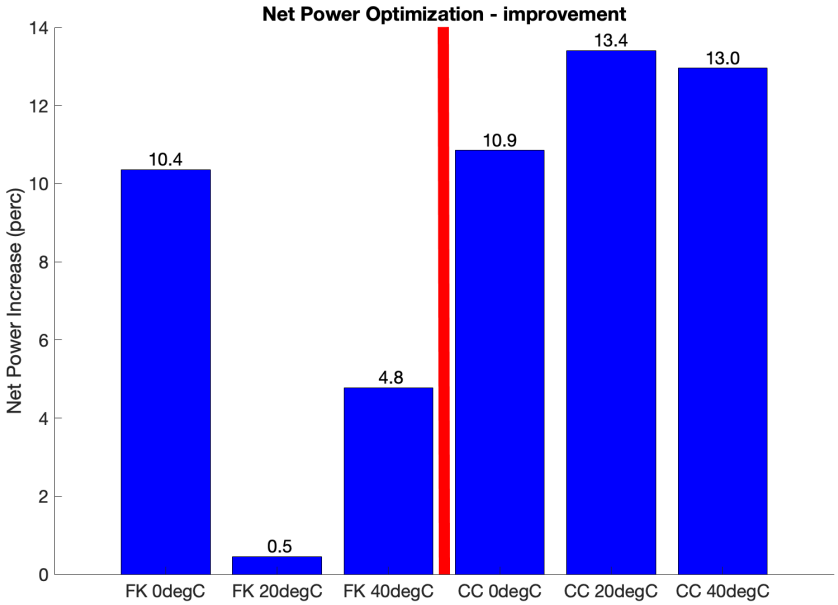

Figure 5.7 – Net power improvement over the FK and CC road cycle and all the ambient temperature values investigated with respect to the reference consisting in variable condensation pressure having set a constant pressure ratio PR.

announced at the beginning of this chapter.

5.2 Data-driven multi-model control for a waste heat recovery

5.2.1 Motivation and related work

The ORC based waste heat recovery system that is proposed in this work, as already discussed, is fundamentally a non-linear system; in Sec. 3.3, the approach that has been proposed to deal with the control of such a non-linear system is the use of multiple linear control, used to track the working fluid superheat and subcooling at the expander inlet and the feed pump inlet respectively. In this control, a weighting scheme uses a Bayesian estimator as in Aufderheide and Bequette 2003, or other algorithm (so-called developed algorithm) proposed in Grelet et al. 2015; the control performance, measured via different indicators, as the relative error, standard deviation, TV and IAE, has increased with respect to the use of a single linear controller for all the operating points.
Recently, with the growing interest in the Artificial Intelligence (AI), authors study the possibility to use artificial neural networks for the self-tuning of PID controllers. In Rossomando et al. 2011, the authors use a multilayer perceptron-neural network combined with a support vector machine for adaptive tuning of a PID controller. Reinforcement learning has also been used in the literature to design an adaptive PID based method, as in Neftci 2018. Compared to this work, the goal of the current research is to learn the dynamic weighting of an ensemble of PID controllers, instead of adapting the parameters of a single PID, which is less adapted to nonlinear systems.
The modification compared to the previous sections is in the weight computation that are predicted by a deep neural network trained online in a supervised way. The neural network takes as input

the process and model outputs as well as the errors over a short horizon, allowing it to learn their temporal evolution. Although the resulting PID is used to control the working fluid superheat at the outlet of the evaporator, the methodology can be used for the control of the working fluid subcooling at the outlet of the condenser as well.

5.2.2 Local multi-model controller

We consider the nonlinear discrete model in the form

$$\begin{cases} x(k+1) = f\big(x(k), u(k)\big) \\ y(k) = g\big(x(k), u(k)\big), \end{cases} \tag{5.17}$$

with $y \in \mathcal{R}^{n_y}$ the measured outputs, $u \in \mathcal{R}^{n_u}$ the measured inputs. A set of N local linear simplified models can be written as in (5.18)

$$\begin{cases} x_i(k+1) = Ax_i(k) + Bu(k) \\ y_i(k) = Cx_i(k) + Du(k). \end{cases} \tag{5.18}$$

Each tuned to approximate (5.17) around an operating point. To obtain a global model, these local models have to be combined. The chosen approach is to construct a global model by linearly interpolating between the local models:

$$\hat{y}(k) = \sum_{i=1}^{N} w_i(k) y_i(k). \tag{5.19}$$

Here, the weights w_i are provided in a time-varying adaptation. They need to be identified on-line so that the outputs of the global model $\hat{y}$ best match those of the plant. The considered problem is then to find an on-line estimation of the weights $w_i(k)$ such that the multi-model (5.18)-(5.19) approximates the initial system (5.17) on a wide range of operating conditions.
In Fig. 5.8, it is proposed a multi-model controller, where the weights w_i of each linear model are predicted by a deep neural network trained on-line; the inputs of the network are at each time step t_k, not only the last model errors $\epsilon(k)$ but the error sequences z_k (5.20), that is the flattened representation of the local modeling errors on the previous d sampling times concatenated with the process inputs. In the controller block the single resulting PID is used in order to regulate the pump speed u_c and control the superheat at the outlet of the evaporator.

$$z(k) = (\epsilon_1(k), ..., \epsilon_1(k-d), ..., \epsilon_N(k), ..., \epsilon_N(k-d), u(k), ..., u(k-d)). \tag{5.20}$$

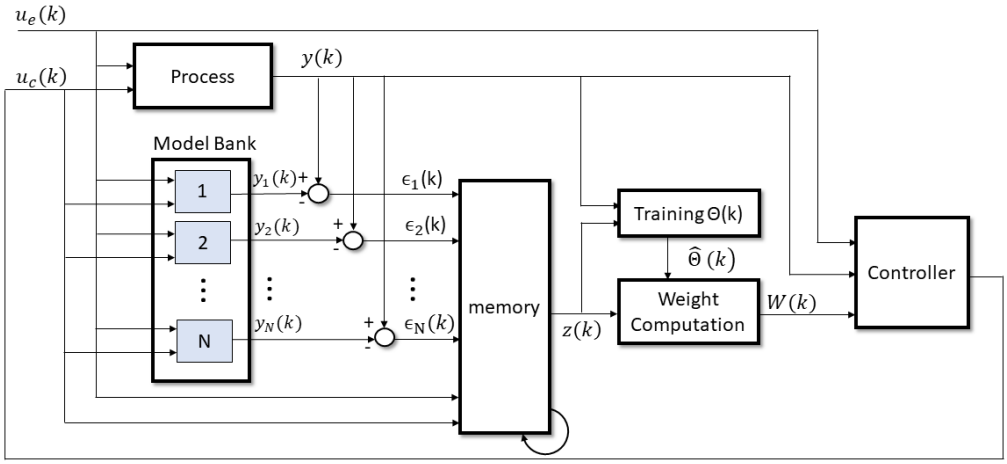

Figure 5.8 – A block diagram of the proposed multi-model controller: a bank of linear models are combined with weights predicted by a deep neural network trained online. In the case of the ORC application, the controlled input u_c correspond to the pump speed, the exogenous input u_e is the exhaust gas and y the superheat at evaporator outlet.

5.2.3 Controller based on an online neural network estimator

Real engine measurements, stored in a dataset $D = \{x_j{=}(T_{exh,j}, \dot{m}_{exh,j})\}$, have been collected from the french highway LCG road cycle (extensively used in the Sec. 4.3.2) to define the operating conditions for the identification of local models, with the aim of covering a wide range of operating conditions with a limited number of local models. A subset $\hat{D}$ of N representative points is selected with respect to the criterion (5.21).

$$\hat{D} = \arg\min_{D'} \sum_{x_j \in D} \min_{x'_j \in D'} ||x_j - x'_j||^2. \tag{5.21}$$

A genetic algorithm is used to perform the outer minimization in (5.21). The result of this procedure is illustrated in Fig. 5.9 for $N = 5$.

As seen previously, the relationship between the pump actuator and the superheat at the evaporator outlet can be modeled by a low order linear system around an equilibrium point (first order models in Sec. 3.3.1). Here, based on the selected operating conditions, a second order model (SO) is identified as the most suitable structure, as, with respect to a first order model with time delay (FOPTD), it does not contain delay and a FOPTD can be scaled to a SO using the half-rule presented in Skogestad 2004. For each selected operating point, which can be written with the following transfer function:

$$\frac{y_u(s)}{u(s)} = \frac{K_u}{(1+\tau_{u,1}s)(1+\tau_{u,2}s)}, \tag{5.22}$$

where u is the pump speed and y_u the effect of the pump speed on the superheat the evaporator outlet.

Hereafter the model that represents the relationship between the (non-controlled) exhaust gas flow and superheat at evaporator outlet is found as first order transfer function:

$$\frac{y_{exh}(s)}{\dot{m}_{exh}(s)} = \frac{K_{exh}}{1+\tau_{exh}s}, \tag{5.23}$$

where $\dot{m}_{exh}$ is the exhaust mass flow rate and y_{exh} is the effect of the exhaust mass flow rate on superheat.

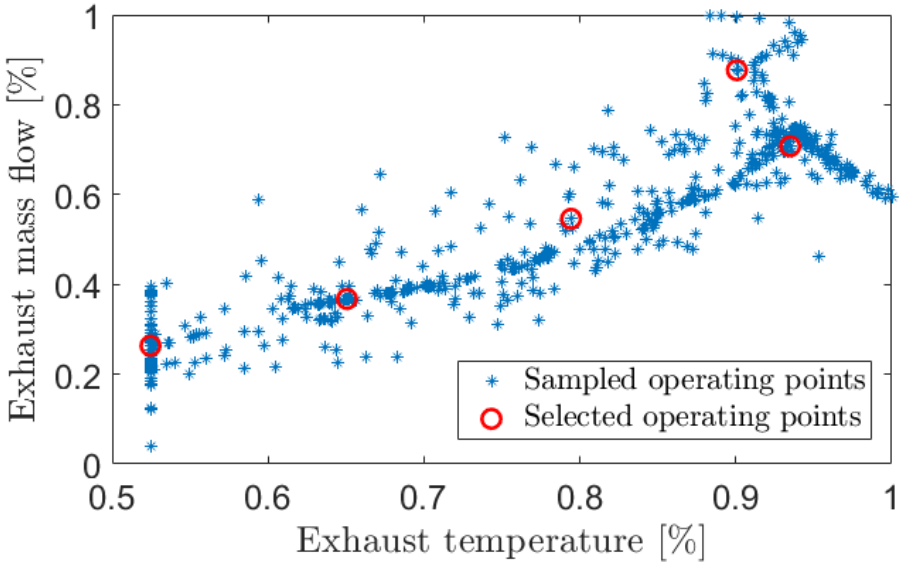

Figure 5.9 – Selection of operating points of the different linear models.

Effective superheat at evaporator outlet y is then assumed to be the linear combination of these two effects:

$$y = y_{exh} + y_u. \tag{5.24}$$

The neural network, fed with 10 previous samples (d=10) while 5 local linear models are used (N=5), and its training are implemented in Python and using the Pytorch library (Paszke et al. 2019). A separate network for the weight computation, calculates and send the weight to the controller (implemented in MatLab) with a sampling time set to 0.5 s; it has been noticed that a lower sampling time does not provide sensibly different results than the current sampling time and higher values than d=10 and N=5 do not lead to any additional benefit. In consequence, neural network inputs $z(k)$ — defined by (5.20) — are of dimension 70. The neural network (dense) structure is completed with two hidden layers of 64 neurons (tuning obtained by trial error procedure).

As already shown in (3.6), a single equivalent linear model is weighted using the neural network estimator developed, in order to find the equivalent parameters $G_{u,eq}$, $\tau_{u,1,eq}$ and $\tau_{u,2,eq}$. The resulting PID from the equivalent parameters is characterized by the Proportional, Integral and Derivative parameters, respectively denoted $K_{P,eq}$, $K_{I,eq}$, $K_{D,eq}$, obtained using the IMC formulas (5.25):

$$\begin{cases} K_{P,eq} = \frac{\tau_{u,1,eq}+\tau_{u,2,eq}}{\tau_m G_{u,eq}} \\ K_{I,eq} = K_{P,eq} \times \frac{1}{\tau_{u,1,eq}+\tau_{u,2,eq}} \\ K_{D,eq} = K_{P,eq} \times \frac{\tau_{u,1,eq}\tau_{u,2,eq}}{\tau_{u,1,eq}+\tau_{u,2,eq}}. \end{cases} \tag{5.25}$$

$$u_{fb}(t) = K_{p,eq}e(t) + K_{I,eq}\int_0^t e(t)dt + K_{D,eq}\frac{de(t)}{dt}, \tag{5.26}$$

where $e(t) = y(t) - y^{SP}(t)$ is the error in tracking the setpoint $y^{SP}(t)$.
Hereafter a feedforward term is computed for each local model detailed. As already proposed in Peralez et al. 2013 a two-time-scale dynamic behavior is assumed where (5.23) capture the slow dynamics. Neglecting $\tau_{u,1}$ and $\tau_{u,2}$, relation (5.22) is rewritten $u(s) = \frac{y_u(s)}{K_u}$. With (5.23), this yields

$$\begin{cases} \frac{y_{exh}(s)}{\dot{m}_{exh}(s)} = \frac{K_{exh}}{1+\tau_{exh}s} \\ u(s) = \frac{y_u(s)}{G_u}. \end{cases} \tag{5.27}$$

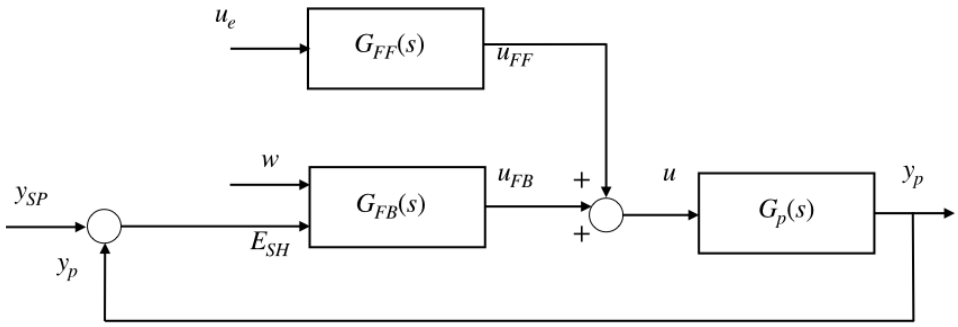

Figure 5.10 – Scheme of the controller that highlights the feedback and feedforward actions; u is the pump speed requested (sum of the feedback u_{FB} and feedforward u_{FF} parts), u_e is the exogenous input (exhaust mass flow rate), y_p is the superheat at the outlet of the evaporator.

The feedforward part of the controller u_{ff} is computed as the value of u vanishing the effect of exhaust flow on superheating, i.e such that $y_u = -y_{exh}$. With (5.27), this gives

$$u_{ff}(s) = \frac{-K_{exh}}{G_u(1+\tau_{exh})s}\dot{m}_{exh}(s). \tag{5.28}$$

Hence, each local model feedforward signal $u_{ff,i}(t)$ is computed from the exhaust gas signal $\dot{m}_{exh}$ filtered by the i^{th} first order of static gain $\frac{-K_{exh}}{K_u}$ and of constant time τ_{exh}. Notice that while the measurement $\dot{m}_{exh}$ is usually not directly available, a real-time estimation is provided by the engine control unit.
The neural network estimator is then used to weight the local feedforwards:

$$u_{ff}(k) = \sum_{i=1}^{N} w_i u_{ff,i}(k). \tag{5.29}$$

Finally feedback and feedforward signals defined in (5.26) and (5.29) are summed to give the control value sent to the pump actuator: $u(k) = u_{fb}(k) + u_{ff}(k)$, as seen in Fig. 5.10.

5.2.4 Results and discussion

In order to assess the performance of the controller, the set-point of the superheat is changed during the simulation time. Fig. 5.11 shows the variation of the 5 weights during the simulation time; during most of the time of the simulation, the value of the weights lies between 0 and 0.5. Between roughly 1250 and 1500 seconds, the weight w_2 increases reaching the value 1; during this phase of the time simulation, one model among the 5 initial models coincides with the single resulting model, used to design the PID controller. This situation occurs in one phase of the road cycle characterized by low exhaust mass flow rate, roughly 0.1 kg/s and temperature, roughly 260 °C, followed by a sudden increase of this value to roughly 0.3 kg/s; correspondingly the absolute value of controller gain K_c reaches the highest value (integral K_t and derivative gain K_d reach the highest absolute value as well). Overall, considering the whole time simulation, the distribution of the weights further justifies the multi-linear approach for this application.

Results in Tab. 5.2 show good improvement in performances with both criterion ISE and IAE (improved by 35 to 40%.). However and despite the large inputs disturbances of the representative long haul truck driving cycle used, the superheating is kept close to the set-point in the three experiments. The same analysis is performed using the proposed estimator with only the feedback part of the controller ($u_(k) = u_{fb}(k)$); a value of 0.2328 was obtained for ISE criterion (vs 0.0734

Weight estimator	**mean(ISE)**	**mean(IAE)**
Constant weights	0.2750	0.3025
Bayesian	0.1362	0.2101
Distance-based	0.1254	0.1898
Proposed neural network	**0.0734**	**0.1376**

Table 5.2 – Controller performance comparison with the state of the art in terms of $ISE = \sum_k (y(k) - y^{SP}(k))^2$ and $IAE = \sum_k |y(k) - y^{SP}(k)|$.

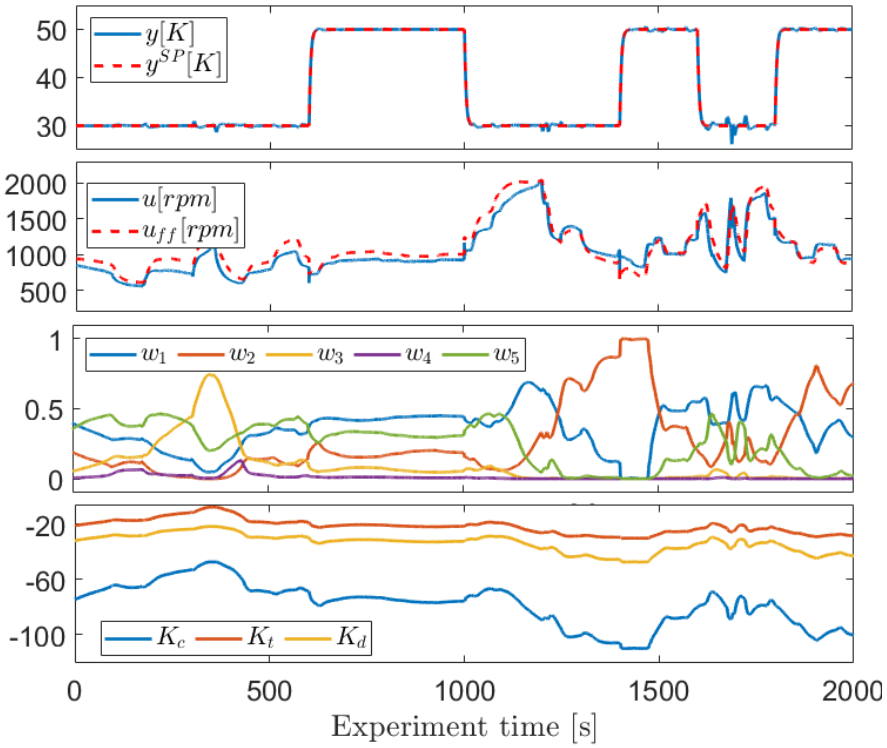

Figure 5.11 – Simulation results: superheating y (with setpoint y^{SP}), pump speed u (with feeforward part u_{ff}), weigths w_i and resulting PID parameters K_c, K_i and K_d.

with feedforward) and 0.2416 for IAE criterion (vs 0.1376). The results suggest that the use of the feedforward is beneficial in order to improve the performance of the controller.
To conclude, the AI application to the current problem reveal promising potential in the improvement of the performance of a Rankine system controller. The results, considering the limited available set of data, show an improvement of the performance of the controller with respect to other well-known weighting estimators as the Bayesian and the Distance-based. The margin for a further improvement lies into the possibility to access to a larger set of data, that can improve the training of the neural network.

Conclusion. *In this chapter, two different methodologies, intended to the improvement of the results in the Chap. 3, are presented. In the first application, regarding the control of the subcooling at the outlet of the condenser (inlet of the pump), a real-time optimization, based on a simplified analytical model is implemented and applied; the results showed an improvement of the net power output of the Rankine system, in two different road cycles (a highway and a urban road cycle) and for different ambient temperatures. In the second application, the weighting estimators that are used in the chapter 3, in order to determine the single representative model at each time step, are replaced by a deep neural network trained on-line that predicts the weights of each linear model previously selected. The resulting representative model and, consequently, the resulting controller shows a better performance than other weighting estimators in terms of ISE and IAE.*

Conclusion

The Organic Rankine cycle based waste heat recovery technology has attracted many researchers in the last decade, followed by the growing industrial interest in the technology. The new strict European legislation regarding the CO_2 emissions of the long haul heavy duty trucks accelerated the need of implementation of suitable solutions to reduce the fuel consumption and, consequently, meet the new limit of emission in 2025.
Nowadays, more than the past, the integration of the system in the vehicle, as well as its cost and weight, is crucial for a future commercialization of the technology, therefore most of the manufactures are looking at a compact solution that involves the usage of a single heat source and independence from the cooling system.
The exhaust gas recuperation is still considered the favorite heat source for a waste heat recovery system in the heavy-duty trucks, as it contains 22% of the original fuel energy at temperature between roughly 250 and 450 °C (except for the Turbo-Compound engines that usually release, on average, the exhaust gas at lower temperature, reducing the efficiency of the bottoming Rankine cycle), that can provide between 3 and 4 kW of mean net power production in highway road cycle. However, the usage of other heat sources, as the EGR flow and the coolant flow, is still explored: the recuperation of the waste energy in the coolant flow, in particular, can result into a low-cost solution, light-weight, that can bring between 1 and 1.5 kW of mean net power production in highway road cycle.
The contributions presented in this thesis are devoted to the use of exhaust gas flow and coolant flow as single heat source of a Rankine based waste heat recovery system, in a long-haul heavy-duty vehicle, non-EGR engine.
As for the recuperation of the exhaust gas flow waste heat, two different architectures have been investigated; a direct condensation architecture characterized by an independent solution for the heat removal in the condenser, using electrically-driven fans that provide the requested amount of cooling air in order to condense the working fluid and an indirect solution, that uses an additional water pump and radiator in a separated water loop, in order to cool down the Rankine condenser. For both architectures, a working fluid selection has been performed, based on performance and material compatibility; cyclopentane and ethanol have been selected for the direct and indirect condensation architecture respectively.
The thesis focuses on the control and integration issues that are encountered in the direct condensation architecture, that is chosen as the architecture to investigate for further development, because of the absence of impact of the heat rejection in the cooling system of the vehicle. This features, recently, have gained high importance, as it allows the integration of the Rankine system without any modification of the cooling system of the vehicle, therefore it is suitable for a easier installation in the vehicle. Particular importance is given to the control of the superheat and the subcooling; in both cases, the use of a single controller, tuned with a single set of parameters, has not been considered sufficient, because of the wide variability of the model parameters of superheat and subcooling, with respect to pump and fan speed respectively. Additionally, it has been highlighted that the manipulation of the condensation pressure is necessary for the usage of the cyclopentane in the

direct condensation architecture, because of the limited temperature difference between the heat sink and the working fluid temperature profiles.
The possibility to manipulate the condensation pressure and use it as an additional variable to control the subcooling is crucial to better exploit the potential of the heat source and limit the opening of the by-pass valve because of a reduced cooling capacity; additionally, operating without the possibility of manipulating the condensation pressure leads to extremely high values of subcooling in weak load phases (in these phases the condensation pressure should be reduced) and, consequently, to a lower expander power production. In the exhaust recuperation, the fan speed and the condensation pressure are the two manipulated variables that are used in order to control the subcooling. The fan speed is the manipulated variable of a MMPID controller, the condensation pressure, as a first approach, is manipulated by imposing a constant pressure ratio between the inlet and the outlet of the expander. This solution ensures the tracking of the set-point of the subcooling, but, in terms of net power produced, it may not represent the best solution. As a second approach, an optimization problem, based on a simplified analytical Rankine model, is solved, in order to find the optimal condensation pressure in real time. The results show that, as for ambient temperature of 0 and 20 °C, the optimal strategy suggests to increase the fan speed and reduce the condensation pressure with respect to the results of the first approach; as for ambient temperature of 40 °C, the optimal strategy suggests to reduce the fan speed and increase the condensation pressure with respect to the results of the first approach.
In the engine cooling flow recuperation as well, the manipulation of the condensation pressure is necessary as it reduces the utilization of the cooling system fan, that is characterized by large inertia and high power consumption even at low rotating speed. The usage of the condensation pressure as manipulated variable ensures the appropriate tracking of the subcooling set-point, reduces the engagement of the cooling system fan and keeps high the power system production.

Taking into account the level of maturity that the technology has gained during the recent years and the imminent need of solutions that can contribute in meeting the new European legislation on trucks emissions, tests on vehicle and real road cycle should be increased. The control strategies that have been implemented should be verified in all the possible roads and traffic situations, in order to ensure the suitable operating conditions of the ORC and, in the same time, guarantee the highest possible energy production during the missions. Additionally, the introduction of more powerful ECU could open to more complicated controllers that are expected to perform well with the high disturbances that are encountered during the vehicle missions.
Moreover, the reliability and durability of the components, as well as possible material compatibility issues should be attentively verified, as the components that are tested, nowadays, are prototypes and possibly need further development in order to be brought to series production status. Additionally, particular attention should be paid to safety, as organic working fluids (as cyclopentane and ethanol) are highly flammable; different scenarios of accidents should be studied in order to set efficient safety measures to avoid fire, explosion and, in general, uncontrolled release of the working fluid at high pressure and temperature.

Compactness, weight and development time are other aspects that are particularly important in the industrial context; therefore, besides the evaluation of the performance, additional indicators should be introduced in order to take into account the possible drawbacks that the Rankine system could produce on the vehicle fuel consumption. Considering the necessity of finding effective solutions to meet the new limits of CO_2 emissions rapidly, a simple, compact and independent Rankine system looks the most appropriate choice.

To conclude, the main challenge of the manufacturers is to develop an ORC system that is safe, with a high utilization ratio, with no-impact on the up-time, reducing the total cost of ownership

(TCO) of the vehicle, in order to be a valuable solution, not only for the reduced CO_2 emitted, but also as a solution that decreases the expenses related to the fuel filling by the owner of the vehicle.

Bibliography

Abram, T. and Ion, S. (2008). Generation-IV nuclear power: A review of the state of the science. *Energy Policy*, 36(12):4323–4330.

Ahmad, A., Gao, W., and Engell, S. (2018). *Modifier Adaptation with Model Adaptation in Iterative Real-Time Optimization*, volume 44. Elsevier Masson SAS.

Ahmadi Atouei, S., Ranjbar, A. A., and Rezania, A. (2017). Experimental investigation of two-stage thermoelectric generator system integrated with phase change materials. *Applied Energy*, 208(September):332–343.

Albergucci, F., Watts, S., Pouponnot, J., Darmedru, A., and Daccord, R. (2019). Pump Development for an Exhaust Heat Recovery Box on Heavy Duty Trucks. pages 1–10. 5th International Seminar on ORC Power Systems, September 9 - 11, 2019, Athens, Greece.

Alshammari, F. and Pesyridis, A. (2019). Experimental study of organic Rankine cycle system and expander performance for heavy-duty diesel engine. *Energy Conversion and Management*, 199(June):111998.

Ambros, P. and Fezer, A. (2014). Twin-Round Tube Evaporator for Waste Heat Recovery. *MTZ*, 75:36–39.

Ambros, P., Orso, J., Fezer, A., and Necker, A. (2011). Evaporators for Mobile Waste Heat Recovery Systems. *MTZ*, pages 34–37.

Aufderheide, B. and Bequette, B. W. (2003). Extension of dynamic matrix control to multiple models. *Computers and Chemical Engineering*, 27(8-9):1079–1096.

Bahrami, M., Hamidi, A. A., and Porkhial, S. (2013). Investigation of the effect of organic working fluids on thermodynamic performance of combined cycle stirling-ORC. *International Journal of Energy and Environmental Engineering*, 4(1):1–9.

Bauer, M. L., Vijaykumar, R., Lausten, M., and Stekli, J. (2016). Pathways to Cost Competitive Concentrated Solar Power Incorporating Supercritical Carbon Dioxide Power Cycles. *The 5th International Supercritical CO2 Power Cycles Symposium*, pages 1–22.

Bonvin, D. (2017). *Real-Time Optimization Edited by Real - Time Optimization*.

Braimakis, K. and Karellas, S. (2018). Energetic optimization of regenerative Organic Rankine Cycle (ORC) con fi gurations. *Energy Conversion and Management*, 159(September 2017):353–370.

Chan Kang, H. and Jun, G. W. (2011). Heat Transfer and Flow Resistance Characteristics of Louver Fin Geometry for Automobile Applications. *Journal of Heat Transfer*, 133(10):101802.

Chang, Y., Juei, W., and Chi, C. (1997). A generalized heat transfer correlation for louver fin geometry. *International Journal of Heat and Mass Transfer*, 40(3):533–544.

Cho, S. Y., Cho, C. H., and Kim, C. (2007). Performance prediction on a partially admitted small axial-type turbine. *JSME International Journal, Series B: Fluids and Thermal Engineering*, 49(4):1290–1297.

Daccord, R., Darmedru, A., and Melis, J. (2014). Oil-Free Axial Piston Expander for Waste Heat Recovery. *SAE Technical Paper Series*, 1.

Daccord, R., Mélis, J., Darmedru, A., Debaise, A., Kientz, T., and Davin, E. (2016). A piston expander for exhaust heat recovery on heavy commercial vehicles. *FISITA 2016 World Automotive Congress - Proceedings, Busan*, (November 2015).

Di Battista, D., Di Bartolomeo, M., Villante, C., and Cipollone, R. (2018). On the limiting factors of the waste heat recovery via ORC-based power units for on-the-road transportation sector. *Energy Conversion and Management*, 155(July 2017):68–77.

Di Battista, D., Mauriello, M., and Cipollone, R. (2015). Waste heat recovery of an ORC-based power unit in a turbocharged diesel engine propelling a light duty vehicle. *Applied Energy*, 152:109–120.

Di Cairano, S. and Kolmanovsky, I. V. (2018). Real-time optimization and model predictive control for aerospace and automotive applications. *Proceedings of the American Control Conference, Milwaukee*, 2018-June:2392–2409.

Eichler, K., Jeihouni, Y., and Ritterskamp, C. (2015). Fuel Economy Benefits for Commercial Diesel Engines with Waste Heat Recovery. *SAE International Journal of Commercial Vehicles*, 8(2):491–505.

El Hajal, J., Thome, J. R., and Cavallini, A. (2003). Condensation in horizontal tubes, part 1: two-phase flow pattern map. *International Journal of Heat and Mass Transfer*, 46(18):3349–3363.

Esposito, M. C., Pompini, N., Gambarotta, A., Chandrasekaran, V., Zhou, J., and Canova, M. (2015). Nonlinear model predictive control of an Organic Rankine Cycle for exhaust waste heat recovery in automotive engines. *IFAC-PapersOnLine*, 28(15):411–418.

Fouquet, T. and Roussilhe, J. (2018). Rankine cycle – from thermodynamic equation to road test. *12th International MTZ Conference on Heavy-Duty Engines, Augsburg*, pages 259–276.

Furukawa, T., Nakamura, M., Machida, K., and Shimokawa, K. (2014). A Study of the Rankine Cycle Generating System for Heavy Duty HV Trucks. *SAE Technical Paper Series*, 1.

Galuppo, F., Dufour, P., Nadri, M., Reiche, T., and Lemort, V. (2018a). Experiment Design for Waste Heat Recovery Modeling in Heavy Duty Trucks. *IFAC-PapersOnLine*, 51(31).

Galuppo, F., Dufour, P., Nadri, M., Reiche, T., and Lemort, V. (2018b). Experiment Design for Waste Heat Recovery Modeling in Heavy Duty Trucks. *IFAC-PapersOnLine*, 51(31):726–731.

Galuppo, F., Lemort, V., Nadri, M., Dufour, P., and Reiche, T. (2019a). Assessment of Rankine Waste Heat Recovery Potential on Heavy Duty Trucks Using Direct Condensation. *Proceedings of the 5th International Seminar on ORC Power Systems, Athens*, 1(36):1–10.

Galuppo, F., Nadri, M., Dufour, P., Reiche, T., and Lemort, V. (2019b). Evaluation of a Coupled Organic Rankine Cycle Mild Hybrid Architecture for Long-Haul Heavy-Duty Truck. *IFAC-PapersOnLine*, 52(5):478–483.

Galuppo, F., Reiche, T., Lemort, V., Dufour, P., and Nadri, M. (2021). Organic Rankine Cycle based waste heat recovery modeling and control of the low pressure side using direct condensation and dedicated fans. *Energy*, 216:119074.

Galuppo, F., Reiche, T., Lemort, V., Dufour, P., Nadri, M., Galuppo, F., Reiche, T., Lemort, V., Dufour, P., Nadri, M., Galuppo, F., Reiche, T., Lemort, V., Dufour, P., Nadri, M., and Huin, X. (2018c). Waste heat recovery (WHR) assessment in complete truck simulation environment. *Proceedings SIA Powertrain, 2018, Rouen*.

Green Car Congress (2017). Renault Trucks leading FALCON project to cut heavy-duty tractor-trailer fuel consumption 13%.

Grelet, V. (2016). Rankine cycle based waste heat recovery system applied to heavy duty vehicles: topological optimization and model based control.

Grelet, V., Dufour, P., Nadri, M., Reiche, T., and Lemort, V. (2015). Modeling and control of Rankine based waste heat recovery systems for heavy duty trucks. In *IFAC-PapersOnLine, Brussels*.

Grelet, V., Reiche, T., Lemort, V., Nadri, M., and Dufour, P. (2016). Transient performance evaluation of waste heat recovery rankine cycle based system for heavy duty trucks. *Applied Energy*, 165:878–892.

Guillaume, L. and Lemort, V. (2019). Comparison of different ORC typologies for heavy-duty trucks by means of a thermo-economic optimization. *Energy*, 182:706–728.

Güven, M., Bedir, H., and Anla\cs, G. (2019). Optimization and application of Stirling engine for waste heat recovery from a heavy-duty truck engine. *Energy Conversion and Management*, 180(November 2018):411–424.

Hernandez, A., Desideri, A., Ionescu, C., Quoilin, S., Lemort, V., and De Keyser, R. (2014). Increasing the efficiency of Organic Rankine Cycle technology by means of multivariable Predictive Control. *IFAC Proceedings Volumes (IFAC-PapersOnline), Cape Town*, 19:2195–2200.

Hountalas, D. T., Mavropoulos, G. C., Katsanos, C., and Knecht, W. (2012). Improvement of bottoming cycle efficiency and heat rejection for HD truck applications by utilization of EGR and CAC heat. *Energy Conversion and Management*, 53(1):19–32.

IEA (2019). Global Energy & CO2 Status Report: Emissions. *Iea.org*, page 14.

Incropera, F., Dewitt, D., Bergman, T., and Lavine, A. (1993). *Fundamentals of Heat and Mass Hransfer*. Number 1986.

Jeihouni, Y., Eichler, K., and Franke, M. (2017). Lower Emissions in Commercial Diesel Engines through Waste Heat Recovery Engine Strategy for California ' s Low NOx.

Joshi, S., Dahodwala, M., Koehler, E., Dhanraj, F. N. U., Franke, M., Tomazic, D., and Naber, J. (2019). Integration of an orc waste heat recovery with electrification and supercharging through use of a planetary gear system for a class 8 tractor application. *SAE Technical Papers*, -(April):1–10.

Joshi, S., Dahodwala, M., Koehler, E. W., Franke, M., Tomazic, D., and Naber, J. (2018). Novel Approach to Integration of Turbocompounding, Electrification and Supercharging Through Use of Planetary Gear System. *SAE Technical Papers*, 2018-April:1–12.

Kanefsky, P., Nelson, V., and Ranger, M. (1999). A Systems Engineering Approach to Engine Cooling Design. Technical report.

Karvountzis-Kontakiotis, A., Pesiridis, A., Zhao, H., Alshammari, F., Franchetti, B., Pesmazoglou, I., and Tocci, L. (2017). Effect of an ORC Waste Heat Recovery System on Diesel Engine Fuel Economy for Off-Highway Vehicles. *SAE Technical Papers*, 2017-March(March).

Kim, Y. M., Sohn, J. L., and Yoon, E. S. (2017). Supercritical CO 2 Rankine cycles for waste heat recovery from gas turbine. *Energy*, 118:893–905.

Kimmel, A. S. (2017). Material Choice for Liquid-Cooled Condensers Using an Ethanol / Water Mixture as a Working Fluid. Objective : Experimentally assess aluminum.

Koppauer, H., Kemmetmüller, W., and Kugi, A. (2018). Model predictive control of an automotive waste heat recovery system. *Control Engineering Practice*, 81(2018):28–42.

Latz, G., Andersson, S., and Munch, K. (2013). Selecting an expansion machine for vehicle waste-heat recovery systems based on the rankine cycle. *SAE Technical Papers*, 2.

Leduc, P., Smague, P., Leroux, A., and Henry, G. (2017). Low temperature heat recovery in engine coolant for stationary and road transport applications. *Energy Procedia*, 129:834–842.

Legros, A., Guillaume, L., Diny, M., Zai¨di, H., and Lemort, V. (2014). Comparison and impact of waste heat recovery technologies on passenger car fuel Zconsumption in a normalized driving cycle. *Energies*, 7(8):5273–5290.

Lemmon, E. W., Bell, I. H., Huber, M. L., and McLinden, M. O. (2018). NIST Standard Reference Database 23: Reference Fluid Thermodynamic and Transport Properties-REFPROP, Version 10.0, National Institute of Standards and Technology.

Lemort, V. and Legros, A. (2016). *Positive displacement expanders for Organic Rankine Cycle systems*.

Li, Y. R., Du, M. T., Wu, C. M., Wu, S. Y., Liu, C., and Xu, J. L. (2014). Economical evaluation and optimization of subcritical organic Rankine cycle based on temperature matching analysis. *Energy*, 68:238–247.

Liimatainen, H., van Vliet, O., and Aplyn, D. (2019). The potential of electric trucks – An international commodity-level analysis. *Applied Energy*, 236(November 2018):804–814.

Lopes, J., Douglas, R., McCullough, G., O'Shaughnessy, R., Hanna, A., Rouaud, C., and Seaman, R. (2012). Review of Rankine Cycle Systems Components for Hybrid Engines Waste Heat Recovery. *SAE Technical Paper Series*, 1.

Mahmoudi, A., Fazli, M., and Morad, M. R. (2018). A recent review of waste heat recovery by Organic Rankine Cycle. *Applied Thermal Engineering*, 143(January):660–675.

Mansour, C., Bou Nader, W., Dumand, C., and Nemer, M. (2018). Waste heat recovery from engine coolant on mild hybrid vehicle using organic Rankine cycle. *Proceedings of the Institution of Mechanical Engineers, Part D: Journal of Automobile Engineering*, (September).

Marchetti, A., Chachuat, B., and Bonvin, D. (2010). A dual modifier-adaptation approach for real-time optimization. *Journal of Process Control*, 20(9):1027–1037.

Marcilio, G. P., Rangel, J. J. d. A., de Souza, C. L. M., Shimoda, E., da Silva, F. F., and Peixoto, T. A. (2018). Analysis of greenhouse gas emissions in the road freight transportation using simulation. *Journal of Cleaner Production*, 170:298–309.

Marlok, H., Pfeifer, A., Hötger, M., and Bucher, M. (2019). Modular Waste Heat Recovery System with Electric Power Output. *ATZ heavy duty worldwide*, 12(2):30–35.

Martin, H. (1996). A theoretical approach to predict the performance of chevron-type plate heat exchangers. *Chemical Engineering and Processing: Process Intensification*, 35(4):301–310.

Muneer, T. and García, I. I. (2017). *The automobile*.

Neftci, E. O. (2018). Data and Power Efficient Intelligence with Neuromorphic Learning Machines. *iScience*, 5:52–68.

Norris, J. and Escher, G. (2017). Heavy Duty Vehicles Technology Potential and Cost Study. (5):96p.

Panesar, A. S., Morgan, R. E., Miché, N. D. D., and Heikal, M. R. (2013). Working fluid selection for a subcritical bottoming cycle applied to a high exhaust gas recirculation engine. *Energy*, (60):388–400.

Paszke, A., Gross, S., Massa, F., Lerer, A., Bradbury, J., Chanan, G., Killeen, T., Lin, Z., Gimelshein, N., Antiga, L., Desmaison, A., Köpf, A., Yang, E., DeVito, Z., Raison, M., Tejani, A., Chilamkurthy, S., Steiner, B., Fang, L., Bai, J., and Chintala, S. (2019). PyTorch: An Imperative Style, High-Performance Deep Learning Library. (NeurIPS).

Peralez, J. (2015). Recuperation d ' energie par cycle de Rankine à bord d 'un véhicule : commande et gestion d'énergie.

Peralez, J., Galuppo, F., Dufour, P., Wolf, C., and Nadri, M. (2020). Data-driven multi-model control for a waste heat recovery system. *2020 59th IEEE Conference on Decision and Control (CDC)*, Jeju Island, Korea (South):5501–5506.

Peralez, J., Tona, P., Lepreux, O., Sciarretta, A., Voise, L., Dufour, P., and Nadri, M. (2013). Improving the control performance of an organic rankine cycle system for waste heat recovery from a heavy-duty diesel engine using a model-based approach. *Proceedings of the IEEE Conference on Decision and Control, Florence*, pages 6830–6836.

Peris, B., Navarro-Esbrí, J., and Molés, F. (2013). Bottoming organic Rankine cycle configurations to increase Internal Combustion Engines power output from cooling water waste heat recovery. *Applied Thermal Engineering*, 61(2):364–371.

Preißinger, M., Schwöbel, J. A. H., Klamt, A., and Brüggemann, D. (2017). Multi-criteria evaluation of several million working fluids for waste heat recovery by means of Organic Rankine Cycle in passenger cars and heavy-duty trucks. *Applied Energy*, 206(August):887–899.

Quoilin, S. (2011). Sustainable energy conversion through the use of organic rankine cycles for waste heat recovery and solar applications. *Doctoral Thesis, University of Liège, Belgium*, (October).

Quoilin, S., Aumann, R., Grill, A., Schuster, A., Lemort, V., and Spliethoff, H. (2011). Dynamic modeling and optimal control strategy of waste heat recovery Organic Rankine Cycles. *Applied Energy*, 88(6):2183–2190.

Quoilin, S., Broek, M. V. D., Declaye, S., Dewallef, P., and Lemort, V. (2013). Techno-economic survey of organic rankine cycle (ORC) systems.

Quoilin, S., Lemort, V., and Lebrun, J. (2010). Experimental study and modeling of an Organic Rankine Cycle using scroll expander. *Applied Energy*, 87(4):1260–1268.

Reitz, R., Andersohn, G., and Oechsner, M. (2018). Evaluation of Materials and Media Resistance in Waste Heat Recovery Systems. *ATZ worldwide*, 120(4):68–73.

Rodriguez, F. (2018). The European Commission's Proposed CO2 Standards For Heavy-Duty Vehicles. *Icct*, (June 2018).

Rossomando, F. G., Soria, C., and Carelli, R. (2011). Autonomous mobile robots navigation using RBF neural compensator. *Control Engineering Practice*, 19(3):215–222.

Sarkar, J. (2015). Review and future trends of supercritical CO<inf>2</inf> Rankine cycle for low-grade heat conversion.

Seitz, D., Gehring, O., Bunz, C., Brunschier, M., and Sawodny, O. (2016). Design of a Nonlinear, Dynamic Feedforward Part for the Evaporator Control of an Organic Rankine Cycle in Heavy Duty Vehicles. *IFAC-PapersOnLine*.

Seitz, D., Gehring, O., Bunz, C., Brunschier, M., and Sawodny, O. (2018). Model-based control of exhaust heat recovery in a heavy-duty vehicle. *Control Engineering Practice*, 70(2018):15–28.

Sen, B., Ercan, T., Tatari, O., and Zheng, Q. P. (2019). Robust Pareto optimal approach to sustainable heavy-duty truck fleet composition. *Resources, Conservation and Recycling*, 146(146):502–513.

Shah, M. M. (1979). A general correlation for heat transfer during film condensation inside pipes. *International Journal of Heat and Mass Transfer*, 22(4):547–556.

Skogestad, S. (2004). Simple analytic rules for model reduction and PID controller tuning. *Modeling, Identification and Control*, 25(2):85–120.

Skogestad, S. (2006). Tuning for Smooth PID Control with Acceptable Disturbance Rejection. *Industrial & Engineering Chemistry Research*, 45(23):7817–7822.

Smague, P., Leduc, P., Pagnier, P., Leveque, G., Holaind, N., Henry, G., and Leroux, A. (2019). Development of an ORC turbo pump for waste heat recovery from the coolant of an HD truck. pages 411–433.

Stijepovic, M. Z., Linke, P., Papadopoulos, A. I., and Grujic, A. S. (2012). On the role of working fluid properties in Organic Rankine Cycle performance. *Applied Thermal Engineering*, 36(1):406–413.

Sun, J. and Li, W. (2011). Operation optimization of an organic rankine cycle (ORC) heat recovery power plant. *Applied Thermal Engineering*, 31(11-12):2032–2041.

Syvertsen, T. (2017). Media Resistance. *Media Resistance*.

T. Yanagisawa, M. Fukuta, Y. Ogi, T. H. (2001). Performance of an oilfree scroll-type air expander. *International Conference on Compressors and their Systems*, (March):167–174.

Taha, O. and Khan, M. R. (2011). *Advanced process control for clean fuel production: smart plant of the future*. Woodhead Publishing Limited.

Teng, H., Regner, G., and Cowland, C. (2007). Waste Heat Recovery of Heavy-Duty Diesel Engines by Organic Rankine Cycle Part II: Working Fluids for WHR-ORC. *SAE Technical Paper Series*, 1(724).

Torregrosa, A., Galindo, J., Dolz, V., Royo-Pascual, L., Haller, R., and Melis, J. (2016). Dynamic tests and adaptive control of a bottoming organic Rankine cycle of IC engine using swash-plate expander. *Energy Conversion and Management*, (126):168–176.

Treutler, J., Toepfer, T., and Dingel, O. (2017). Combination of ORC system and electrified auxiliaries on a long haul truck equipped with 48-Volt board net. *Energy Procedia*, 129:778–785.

Vaja, I. and Gambarotta, A. (2010). Internal Combustion Engine (ICE) bottoming with Organic Rankine Cycles (ORCs). *Energy*, 35(2):1084–1093.

Varnier, O. (2012). DOCTORAL THESIS : Trends and Limits of Two-Stage Boosting Systems for Automotive Diesel Engines by. (July 2012).

Vassiliadis, V. S. and Conejeros, R. (2009). *Rosenbrock method*, pages 3343–3345. Springer US, Boston, MA.

Wassén, H., Dahl, J., and Idelchi, A. (2019). Holistic Diesel Engine and Exhaust After-Treatment Model Predictive Control. *IFAC-PapersOnLine, 9th IFAC Symposium on Advances in Automotive Control AAC 2019, Orléans*, 52(5):347–352.

Winterton, R. H. S. (1998). Where did the Dittus and Boelter equation come from? *International Journal of Heat and Mass Transfer*, 41(4-5):809–810.

Yang, K., Bargende, M., and Grill, M. (2018). Evaluation of Engine-Related Restrictions for the Global Efficiency by Using a Rankine Cycle-Based Waste Heat Recovery System on Heavy Duty Truck by Means of 1D-Simulation. *SAE Technical Papers*, 2018-April:1–15.

Zhao, R., Zhang, H., Song, S., Tian, Y., Yang, Y., and Liu, Y. (2018). Integrated simulation and control strategy of the diesel engine–organic Rankine cycle (ORC) combined system. *Energy Conversion and Management*, 156(100):639–654.

Ziviani, D., Dickes, R., Quoilin, S., Lemort, V., de Paepe, M., and van den Broek, M. (2016). Organic Rankine cycle modelling and the ORCmKit library: Analysis of R1234ze(Z) as drop-in replacement of R245fa for low-grade waste heat recovery. *ECOS 2016 - Proceedings of the 29th International Conference on Efficiency, Cost, Optimisation, Simulation and Environmental Impact of Energy Systems, Portorož*.

Ziviani, D., James, N. A., Accorsi, F. A., Braun, J. E., and Groll, E. A. (2018). Experimental and numerical analyses of a 5 kWe oil-free open-drive scroll expander for small-scale organic Rankine cycle (ORC) applications. *Applied Energy*, 230(July):1140–1156.

Appendix

Appendix A

Test rig

The experiments conducted in the University of Liege and presented in the Chap. 4 have been performed in the test bench in Fig. A.1. The experimental setup has been built and assembled together with the personnel of the University of Liege; it is possible to notice the evaporator (thermally isolated) and the condenser on the top (green ellipse), the turbine and the skid equipped with the synchronous electrical machine on the right (red ellipse) and the centrifugal pump and the electrical cabinet on the left (blue ellipse).
The experimental setup is not equipped with a HD truck engine, therefore the coolant flow (heat source of the current ORC system) is produced by means of an electrical oil burner (not visible in the photo); the arrival of the coolant flow is on the top, as well as the departure from the condenser back to the electrical oil burner.
Pressure sensors and thermocouples are installed at the inlet and outlet of each component and the real time measurements are visible by means of a LabView code; sample time of the recordings is 0.5 seconds. The turbine itself presents pressure and temperature measurements at its inlet and outlet and real time values are visible directly in the screen of the skid.

Figure A.1 – Coolant recovery test bench

Appendix B

Simplified analytical model

The optimization problem that has been presented Sec. 5.1.3 is based on a simplified analytical model that expresses the net power production of the system (3.1) as a function of the states x_p and the inputs u. This model is a result of linear data fitting, resulting from the complete model in the FK and CC road cycles; the variable (Y) is found as a function of one (U) or two variables (U_1, U_2) and the uniformity of the subscripts, as in (B.1), is conserved.

$$\begin{cases} Y = a_i U^2 + b_i U + c_i \\ Y = a_i + b_i U_1 + c_i U_2 \end{cases} \tag{B.1}$$

- Fan power $\dot{W}_{fan}(W)$ fitting as a function of the fan speed $N_{fan}(rpm)$

$$\begin{cases} a_1 = 0.0001325 \frac{W}{rpm^2} \\ b_1 = -0.3646 \frac{W}{rpm} \\ c_1 = 310.6W \\ \dot{W}_{fan} = a_1 N_{fan}^2 + b_1 N_{fan} + c_1. \end{cases} \tag{B.2}$$

- Enthalpy at the inlet of the expander $h_{su,exp}(\frac{J}{kg})$ as a function of the pressure $p_{su,exp}(bar)$ and temperature $T_{su,exp}(°C)$

$$\begin{cases} a_2 = 1.737 \cdot 10^5 \frac{J}{kg} \\ b_2 = -2632 \frac{J}{kgbar} \\ c_2 = 2384 \frac{J}{kgK} \\ h_{su,exp} = a_2 + b_2 p_{su,exp} + c_2 T_{su,exp}. \end{cases} \tag{B.3}$$

- Entropy at the inlet of the expander $s_{su,exp}(\frac{J}{kgK})$ as a function of the pressure $p_{su,exp}(bar)$ and temperature $T_{su,exp}(°C)$

$$\begin{cases} a_3 = 681.7 \frac{J}{kgK} \\ b_3 = -8.197 \frac{J}{kgKbar} \\ c_3 = 4.57 \frac{J}{kgK^2} \\ s_{su,exp} = a_3 + b_3 p_{su,exp} + c_3 T_{su,exp}. \end{cases} \tag{B.4}$$

- Isentropic enthalpy at the outlet of the expander $h_{ex,exp,is}(\frac{J}{kg})$ as a function of the entropy

$s_{sun,exp}$ at the inlet of the expander and the pressure at the outlet of the expander $p_{ex,exp}(bar)$

$$\begin{cases} a_4 = -1.807 \cdot 10^5 \frac{J}{kg} \\ b_4 = 440.5kg \\ c_4 = 2.147 \cdot 10^5 \frac{J}{kgbar} \\ h_{ex,exp,is} = a_4 + b_4 s_{sun,exp} + c_4 p_{ex,exp}. \end{cases} \tag{B.5}$$

- Expander efficiency $\eta_{exp}(-)$ as a function of the expander speed $N_{exp}(rpm)$ and the inverse of the pressure ratio $PR^{-1} = \frac{p_{ex,exp}}{p_{su,exp}}(-)$

$$\begin{cases} a_5 = 0.6418 \\ b_5 = 0.0000319 \frac{1}{rpm} \\ c_5 = 0.2075 \\ \eta_{exp} = a_5 + b_5 N_{exp} + c_5 \frac{p_{ex,exp}}{p_{su,exp}}. \end{cases} \tag{B.6}$$

- Saturation temperature $T_{sat}(K)$ as a function of the pressure at the outlet of the expander $p_{ex,exp}(bar)$

$$\begin{cases} a_7 = -2.122 \frac{K}{bar^2} \\ b_7 = 26.82 \frac{K}{bar^2} \\ c_7 = 298.8K \\ T_{sat} = a_7 p_{ex,exp}^2 + b_7 p_{ex,exp} + c_7 \end{cases} \tag{B.7}$$

- As for the working fluid temperature at the outlet of the condenser $T_{wf,ex,cond}(°C)$ as a function of the ratio between the fan and pump speed $N_{fan}(rpm)$, $N_{pump}(rpm)$ and the pressure at the outlet of the condenser $p_{ex,exp}(bar)$ (B.8), the coefficients $a_6(K)$, $b_6(K)$, $c_6(K/bar)$ are not constant and vary as a function of the temperature of the air at the inlet of the condenser, as explained in Sec. 5.1.3. The variation of the three coefficients are shown in Fig. B.1.

$$T_{sat} = a_6 + b_6 \frac{N_{fan}}{N_{pump}} + c_6 p_{ex,exp} \tag{B.8}$$

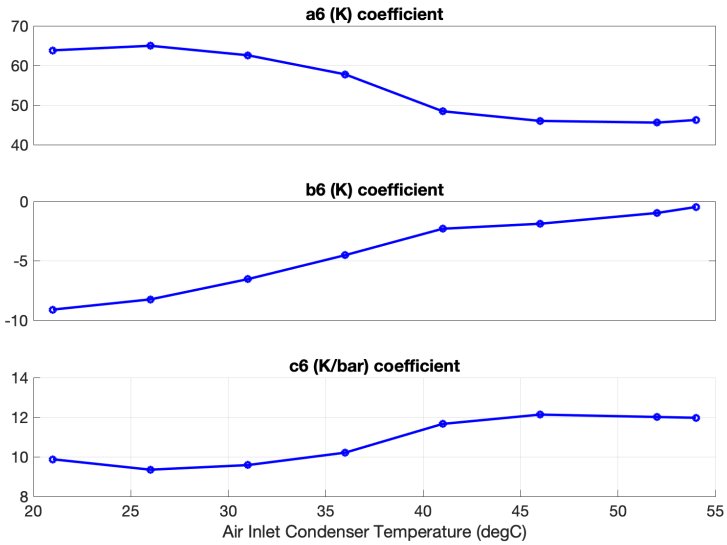

Figure B.1 – Variation of the coefficients a_6, b_6, c_6 as a function of the temperature of the air at the inlet of the condenser.

Appendix C

Résumé étendu en langue française

C.1 Introduction générale

De nos jours, les problématiques environnementales ont un impact primordial sur notre société. L'intérêt croissant pour le réchauffement climatique et la pollution conduisent à approfondir les recherches sur les économies d'énergie, les énergies renouvelables, l'amélioration de l'efficacité des procédés. L'Union Européenne a établi une nouvelle législation sur les émissions des poids lourds long-courriers, fixant la réduction attendue pour 2025 à 15% par rapport à la référence de 2019. Ce nouvel objectif ambitieux a poussé les constructeurs à accélérer la mise en œuvre de nouvelles solutions qui peuvent réduire les émissions de CO_2 directement, en réduisant la consommation de carburant.
Au cours des dernières années, l'évolution du secteur des transports vers l'électrification s'est fortement accélérée et l'électrification des voitures particulières est une réalité solide. Quant au domaine des camions, ce processus est plus lent, mais les villes utilisent déjà des camions à ordures électriques et des camions légers pour les livraisons urbaines. Dans le même temps, malgré des inconvénients connus liés au coût et au poids, l'industrie des camions lourds a étudié massivement l'hybridation. En particulier, l'hybridation "mild-hybrid" et, par conséquent, l'électrification du compresseur de climatisation, de la pompe EGR, du ventilateur de refroidissement par exemple, ont gagné un intérêt important, en raison d'une réduction du poids et du coût, de l'amélioration du rendement de la machine électrique et du stockage dans la batterie. D'autres raisons, qui pourraient contribuer à la réduction de la consommation de carburant et, en d'autres termes, à l'augmentation de l'efficacité thermique (Break Thermal Efficiency, BTE), sont liées à la combustion (surface isolée des pistons, température du liquide de refroidissement plus élevée) et au système de carburant (injecteurs à haut débit).
De la même manière, et c'est ce qui nous intéresse dans cette thèse, la récupération de l'énergie résiduelle est généralement considérée parmi les technologies susceptibles de contribuer au respect des nouvelles limites d'émission de CO_2. Les fabricants estiment que la récupération de la chaleur résiduelle des gaz d'échappement et du fluide de refroidissement peut permettre d'atteindre une économie de carburant de 4 à 5%. La technologie consiste en un système de cycle organique de Rankine, qui récupère la chaleur perdue d'une source de chaleur spécifique (dans la plupart des cas, le flux de gaz d'échappement), et la transfère à un fluide de travail mis sous pression par une pompe; puis le fluide transfère une partie de la chaleur résiduelle à un fluide à basse température dans le condenseur. Le fluide de travail s'évapore dans l'échangeur de chaleur et est donc détendu dans une machine de détente (un expanseur à déplacement positif ou une turbine), qui convertit la différence d'enthalpie en puissance mécanique ou électrique (dans le dernier cas une machine électrique est intégrée dans la machine de détente). L'exploration de cette technologie était, au départ,

basée sur la fourniture et les essais des composants; ensuite, les principaux sujets de recherche et de développement ont évolué vers le contrôle, l'optimisation du système et l'intégration du système dans le véhicule. De plus, la taille et le poids du système sont également considérés comme extrêmement importants dans la conception, car ils peuvent avoir un impact négatif sur la consommation de carburant du véhicule, malgré la récupération de l'énergie perdue.
Il est donc nécessaire d'estimer les performances de ce système dans un environnement réel de véhicule, en tenant en compte des interactions du système avec les autres sous-systèmes. Pour cette raison, la modélisation du système Rankine, ainsi que la modélisation des conditions environnementales et des principaux sous-systèmes du véhicule est extrêmement importante. Dans la plupart des cas, la définition de l'architecture Rankine (architecture et taille des composants) est nécessaire afin de prendre en compte les avantages et / ou les inconvénients que l'on ne rencontre pas avec d'autres architectures. A titre d'exemple, l'architecture de condensation directe a l'avantage de ne pas impacter le fonctionnement du système de refroidissement du véhicule, mais d'autre part, nécessite d'une modélisation du condenseur et du ventilateur dédié, afin d'évaluer le débit d'air de refroidissement au condenseur à une vitesse de rotation du ventilateur spécifique. Dans cette thèse, une fois la modélisation validée dans différentes conditions de fonctionnement avec des résultats expérimentaux, elle peut être utilisée efficacement pour évaluer le potentiel de la technologie, en comparant d'autres fluides de travail, les architectures Rankine ou d'autres technologies.
Le système de récupération de la chaleur basé sur cycle de Rankine doit fonctionner dans des conditions garantissant le temps d'utilisation maximal possible. La source de chaleur, ainsi que le fluide qui retire la chaleur dans le condenseur, sont des fluides qui changent continuellement de débit massique et de température : par conséquence, afin d'assurer de bonnes performances aussi longtemps que possible, le contrôle a un rôle important. Dans la plupart des travaux publiés, l'état du fluide de travail à l'entrée de la machine d'expansion est contrôlé avec précision afin d'assurer la production d'énergie dans toutes les phases de la mission. Dans cette thèse, de plus, une attention particulière doit est accordée à l'évacuation de la chaleur du Rankine, en particulier dans l'architecture de condensation directe, caractérisée par une faible capacité de refroidissement. Par conséquent, le contrôle des conditions du fluide de travail à la sortie du condenseur doit être contrôlé, ainsi que d'autres actionneurs comme la vitesse de la machine de détente et le by-pass sont activement manipulés afin d'assurer la sécurité et les performances des composants.
Un problème important à résoudre pour la mise en œuvre de ces contrôleurs est la puissance de calcul limitée de l'unité de contrôle électronique (ECU) utilisée dans ce milieu automobile; qui limite fortement la complexité des contrôleurs à utiliser. Afin de limiter l'utilisation d'une forte puissance de calcul, ici, différents modèles linéaires locaux de premier et second ordre ont été étudiés; cette approche flexible permet l'utilisation de contrôleurs PID simples à la place d'algorithmes de contrôle plus lourds comme la commande prédictive.
Compte tenu du niveau de maturité atteint par les composants en termes de fiabilité et de performances, le contrôle optimal a été considéré ici comme une étape majeure pour l'amélioration des performances du système. Dans cette thèse, une optimisation en temps réel, basée sur un modèle simplifié, a permis d'atteindre de meilleurs résultats que la référence dans différentes conditions routières et ambiantes. À l'avenir, la puissance de calcul croissante de l'ECU pourrait ouvrir la possibilité de mettre en œuvre des stratégies et des contrôleurs plus complexes, par exemple à base d'intelligence artificielle, comme nous les verrons ici.

C.2 Modélisation du système et sélection des fluides de travail

Le modèle de la pompe du fluide de travail reçoit comme entrée la vitesse de la pompe de son contrôleur et donne comme sortie le débit de fluide de travail et la demande de puissance de la

pompe. La pression à la sortie de la pompe est calculée dans le modèle de la machine de détente, qui impose la haute pression dans le cycle de Rankine pour un débit massique spécifique de fluide de travail et cylindrée de la machine de détente; la pression à l'entrée de la pompe est une fonction du débit et de la température du fluide de travail. En fonction de la vitesse de rotation N, du rapport de pression et du déplacement de la pompe C, le modèle calcule le débit de fluide de travail (C.1) et la demande de puissance de la pompe (C.2) :

$$\dot{m}_{wf} = N_{pump} C_{pump} \rho \tag{C.1}$$

$$\dot{W}_{pump} = \frac{\dot{m}_{wf}(h_{ex,is} - h_{su})}{\eta_{gl,pump}} \tag{C.2}$$

Le modèle de l'évaporateur reçoit comme entrée le fluide de travail via le débit massique, la température et le débit de gaz d'échappement et donne comme sortie le débit du fluide de travail à la sortie de l'évaporateur, la température de gaz d'échappement à la sortie de l'évaporateur et la température de la parois de l'évaporateur.
L'évaporateur modélisé et testé est un échangeur à plaques et ailettes, qui est largement utilisé dans les applications de récupération de la chaleur perdue à basse température (Lopes et al., 2012). La Fig. C.1 montre la vue frontale et latérale de l'évaporateur et même les sections d'entrée et sortie du fluide de travail et de gaz d'échappement; les plaques, où le fluide circule, sont disposées en parallèle par rapport à la vue d'en haut, c'est pour cela que l'approche contre-courant pour la modélisation semble tout à fait justifiée.
Le modèle de l'évaporateur est un modèle 1D à volumes finis, où les N_{vol} volumes sont identifiés avec une discrétisation du composant au long la dimension la plus longue. Le nombre de volumes N_{vol} doit être identifié comme un compromis entre l'exactitude de la solution et sa stabilité et le coût calculatoire. Dans cette application le modèle de l'échangeur est, dans un premier temps, simulé comme un composant distinct, puis il est intégré dans le modèle complet du cycle Rankine Organique et finalement dans le modèle complet du véhicule, où le système de refroidissement, le cycle de conduite et d'autres composants mécaniques sont modélisés. Pour cette application spécifique, le nombre de volumes N_{vol} a été fixé à 10, valeur identifiée comme un compromis entre l'exactitude de la solution et la stabilité du modèle et le coût calculatoire.

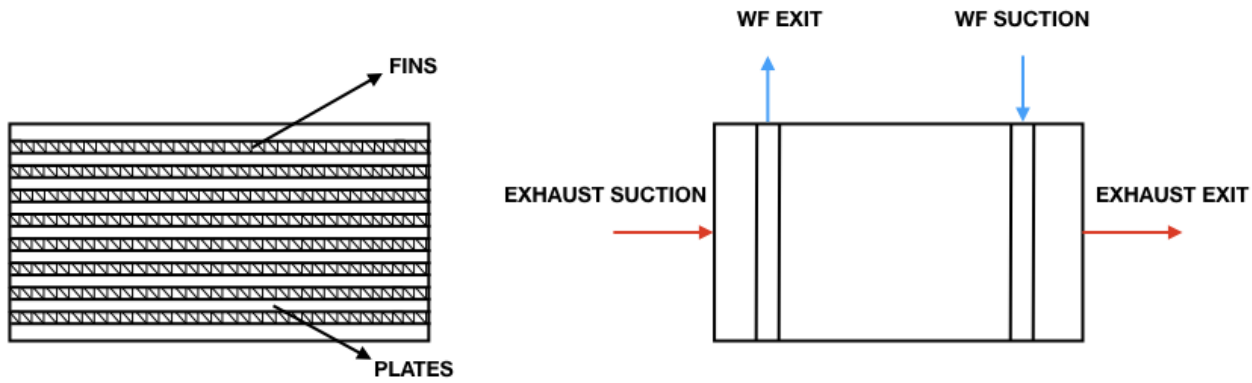

Figure C.1 – Vues frontale et latérale; l'entrée et sortie du fluide de travail et gaz d'échappement, néanmoins les ailettes et les plaques sont identifiées.

La Fig. C.2 montre que chaque volume est divisé en trois zones : le fluide de travail, la parois de séparation et le coté gaz. Du coté du fluide et du gaz, les équations de bilan de la masse et de l'énergie sont appliquées pour calculer respectivement l'état du fluide et la température de gaz

d'échappement à la sortie de chaque volume; dans la parois de séparation la seule équation de bilan d'énergie est appliquée pour calculer la température moyenne de la parois.

Il est peut être remarqué que le nombre de volumes est N_{vol} et les deux nœud avant et après le volume i sont appelés $i-1$ et i respectivement. Pour distinguer entre variables de volume et variables de nœuds, les variables de nœuds sont notées avec l'indice "'".

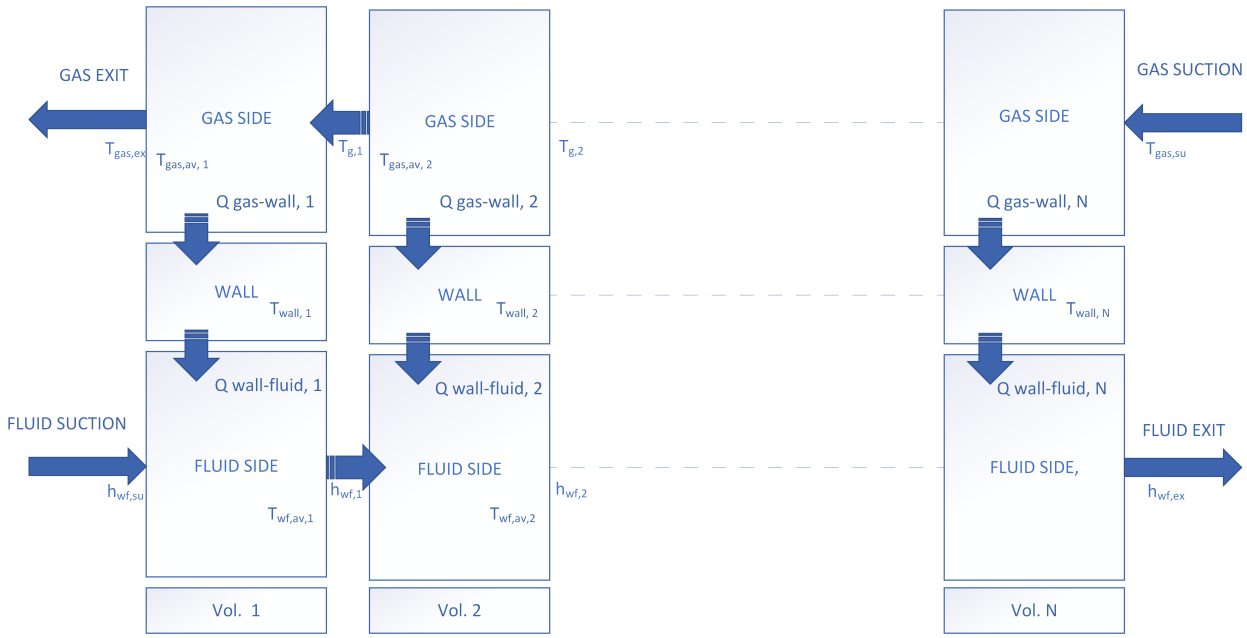

Figure C.2 – Discrétisation spatiale de l'évaporateur.

La variation de masse dans le temps dans chaque volume peut être écrite en fonction de la variation de l'enthalpie et de la pression :

$$\frac{dM_i}{dt} = V\frac{\partial \rho}{\partial t} = V\left(\frac{\partial \rho}{\partial h}\frac{\partial h}{\partial t} + \frac{\partial \rho}{\partial p}\frac{\partial p}{\partial t}\right) = \dot{m}'_i - \dot{m}'_{i-1} \tag{C.3}$$

Le bilan de masse peut être écrit :

$$\frac{dU_i}{dt} = \dot{m}'_{i-1}h'_{i-1} - m'_i h'_i + \dot{Q}_i + \dot{W}_i - p\frac{dV_i}{dt} \tag{C.4}$$

En absence de source de travail existante dans les volumes, en utilisant la définition de l'énergie interne ($U = H - pV$) et de l'équation (C.2), le bilan de l'énergie devient :

$$\rho_i V_i \frac{\partial h_i}{\partial t} = \dot{m}'_{i-1}(h'_{i-1} - h_i) - \dot{m}'_i(h'_i - h_i) + \dot{Q}_i + V\frac{dp}{dt} \tag{C.5}$$

L'équation (C.5) peut être aussi écrite pour le coté gaz, où l'enthalpie est remplacée par le produit entre la chaleur spécifique du gaz c_p et la température T. Le bilan d'énergie appliqué au coté gaz devient :

$$\rho_i V_i cp \frac{\partial T_i}{\partial t} = \dot{m}'_{i-1} cp(T'_{i-1} - T_i) - \dot{m}'_i cp(T'_i - T_i) + \dot{Q}_i \tag{C.6}$$

si le chaleur spécifique *cp* est constante et le gaz est incompressible.

Le bilan d'énergie appliqué à la parois peut finalement être écrit comme :

$$M_w cp_w \frac{\partial T_{w,i}}{\partial t} = \dot{Q}_{gas-wall,i} - \dot{Q}_{wall-fluid,i} \tag{C.7}$$

L'évaporateur a été testé dans l'établissement de Volvo à Saint Priest (France). Le banc d'essais est équipé d'un moteur 13 litres sans boucle EGR qui fournit le débit de gaz d'échappement au système de Rankine; Le système est aussi composé par une pompe, une machine de détente, un condenseur et l'éthanol comme fluide de travail.
L'évaporateur est testé dans des conditions stationnaires réalisées dans différents points opératoires et par conséquence puissance thermique entre 20 et 70 kW. Dans chaque expérience, le débit massique du fluide de travail est varié pour obtenir la même surchauffe à la sortie de l'évaporateur.
Dans le banc d'essais les variables suivantes peuvent être mesurées :

- Le débit massique de fluide travail mesuré avec un débitmètre Coriolis à la sortie de la pompe et le débit massique du gaz d'échappement avec une sonde Annubar à l'entrée de l'évaporateur.

- La pression du fluide de travail mesurée avec des capteurs différentiels à l'entrée et à la sortie de l'évaporateur.

- La température du fluide de travail avec des thermocouples T (un à l'entrée et un à la sortie de l'évaporateur) et la température du gaz d'échappement avec trois thermocouples K à l'entrée de l'évaporateur et un thermocouple K à la sortie de l'évaporateur.

La puissance thermique échangée entre le gaz d'échappement et le fluide de travail a été tracée dans la Fig. C.3. Le maximum erreur relatif entre la puissance thermique prédite par le modèle et celle mesurée par l'expérience, définie dans (C.8), est de 1.82 %.

$$e = \left\| \left(\frac{\dot{Q}_{expe} - \dot{Q}_{sim}}{\dot{Q}_{expe}} \right) \right\| \tag{C.8}$$

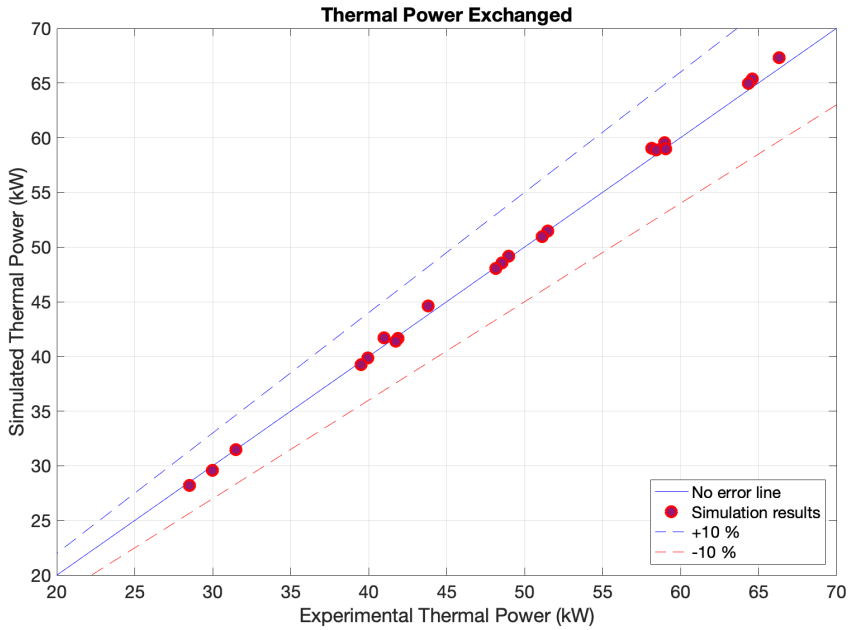

Figure C.3 – Puissance thermique échangée dans l'évaporateur.

La Fig. C.4 montre la validation de la température du gaz d'échappement à la sortie de l'évaporateur. Dans ce cas le maximum erreur absolu du modèle par rapport aux résultats expérimentaux est de 3.29 K.

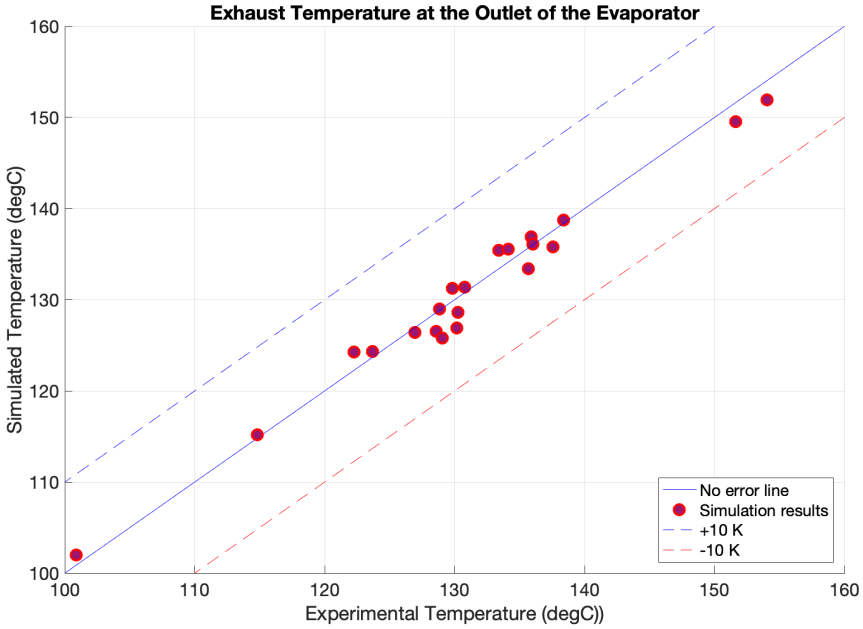

Figure C.4 – Température du gaz d'échappement à la sortie de l'évaporateur.

L'efficacité de l'évaporateur est aussi évaluée et définie comme :

$$\epsilon_{evap} = \frac{T_{exh,su} - T_{exh,ex}}{T_{exh,su} - T_{wf,su}} \tag{C.9}$$

La validation de l'efficacité de l'évaporateur calculée par le modèle par rapport aux résultats expérimentaux est montrée en Fig. C.5.

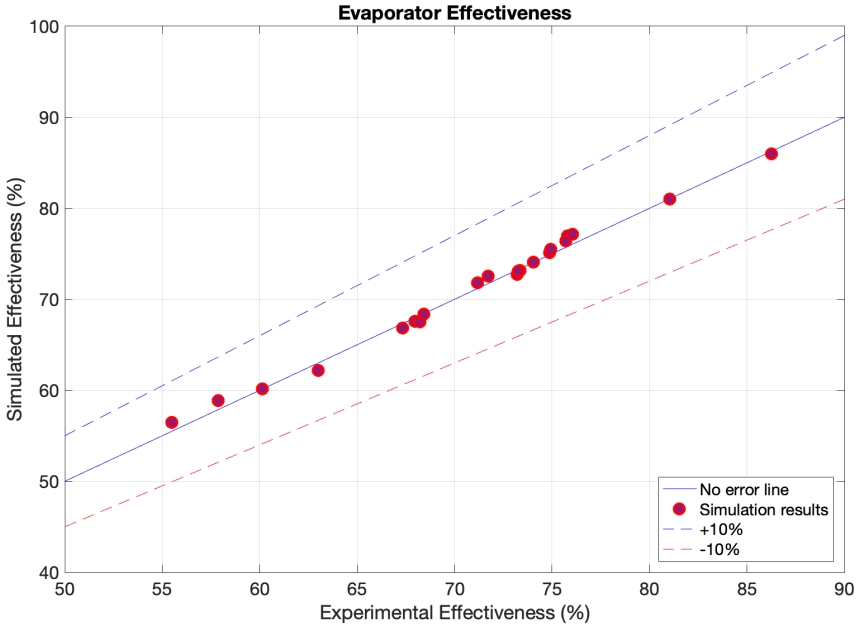

Figure C.5 – Validation de l'efficacité de l'évaporateur par rapport aux résultats expérimentaux. (C.9).

Le modèle de la machine de détente, ainsi dit expanseur, reçoit comme entrée le fluide de travail à la sortie de l'évaporateur et le débit massique, la vitesse de l'expanseur et la pression de sortie du fluide de l'expanseur; le modèle a comme sortie le fluide de travail à la sortie de l'expanseur, l'efficacité et la puissance produite.
La machine de détente qui a été considérée est un expanseur à pistons, qui fait partie de la famille des expanseurs à déplacement positif. Le diagramme indiqué d'un expanseur à pistons contre-courant est montré en figure Fig. C.6.

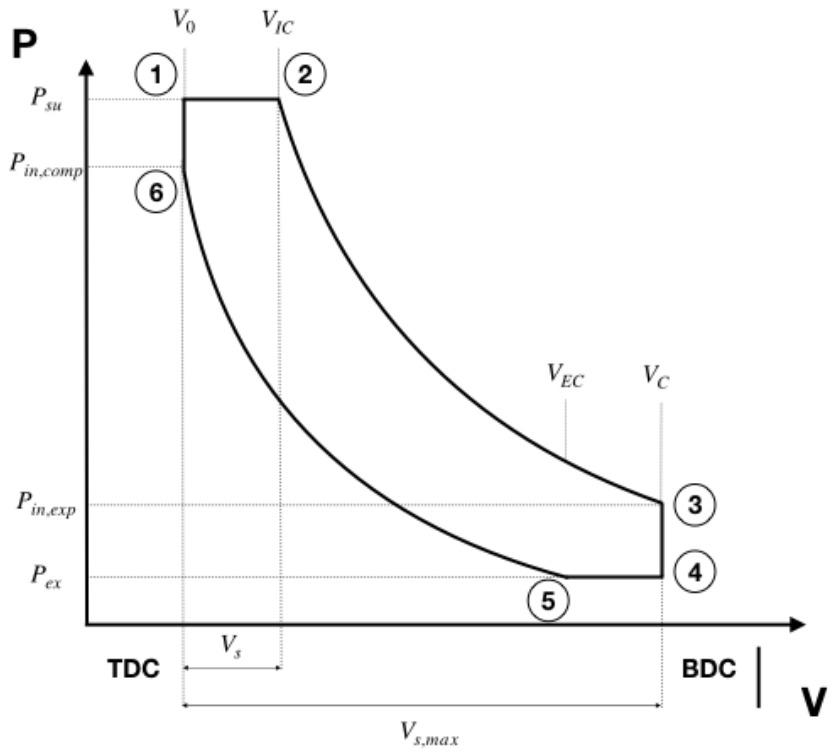

Figure C.6 – Diagramme de l'indicateur du expanseur à piston transversal.

Dans une telle machine de détente, un certain nombre de pistons se déplacent à l'intérieur du cylindre correspondant à partir du point mort haut (TDC), ce qui correspond au volume de jeu V_0 vers le point mort bas (BDC). Pendant le processus d'aspiration, le cylindre passe de la position 1 à la position 2 et le fluide de travail entre dans les cylindres à la pression p_{su} (des pertes de pression peuvent avoir lieu); le processus d'aspiration se termine jusqu'à ce que les vannes d'admission se ferment et que le volume du cylindre soit égal à V_{IC}. L'augmentation du volume de la position 1 à la position 2 est appelée déplacement de l'expanseur V_s; le rapport entre le déplacement de l'expanseur et le volume correspondant à la course complète ($V_{s,max}$) est appelé rapport de cut off CO. En position 2, la détente du fluide moteur stockée à l'intérieur des cylindres démarre et atteint la pression $p_{in,exp}$; à ce stade, les soupapes d'échappement s'ouvrent et le processus de décharge démarre (Lemort and Legros 2016).

La machine de détente à pistons, tournant à une vitesse variable allant de 1000 à 3500 rpm, a un impact sur la haute pression dans le système Rankine; par conséquent, en faisant varier la vitesse de l'expanseur, il est possible d'optimiser le processus d'évaporation, en obtenant une meilleure correspondance entre la source de chaleur et le profil de température du fluide de travail, ainsi que l'efficacité de l'expanseur qui dépend également de la vitesse de rotation (Teng et al. 2007). La plage de vitesse qui a déjà été mentionnée convient pour un couplage direct par courroie avec le système de propulsion du véhicule, en évitant l'utilisation de vitesse qui induit des pertes supplémentaires au système. Les chambres de détente acceptent dans leur volume une masse de fluide moteur qui est fonction du débit massique du fluide moteur et de sa vitesse de rotation. Le modèle calcule la densité en fonction de la masse stockée dans les chambres d'expansion pendant un tour et des données géométriques de la machine.

$$\begin{cases} V_s = V_{s,max} CO \\ \rho_{su,exp} = \frac{\frac{\dot{m}_{wf}}{N_{exp}}}{V_{s,max} CO + V_0} \\ p_{su,exp} = f(\rho_{su,exp}, T_{su,exp}) \end{cases} \tag{C.10}$$

Le dénominateur de (C.10) représente le volume occupé par le fluide de travail à la fin du processus d'aspiration, c'est-à-dire lorsque la vanne d'alimentation se ferme.
A partir de la densité $\rho_{su,exp}$, calculée dans (C.10) et de la température calculée comme la température à la sortie de l'évaporateur dans le modèle d'évaporateur, il est possible d'obtenir la pression du fluide de travail à l'entrée de l'expandeur. Cette information est également utilisée par le modèle de pompe, (2.1) (2.2) pour considérer le rapport de pression entre l'entrée et la sortie de la pompe. Une fois que l'état du fluide de travail à l'entrée du expanseur est complètement défini, il est possible de calculer, en supposant qu'il n'y a pas de transfert de chaleur avec l'ambiance, la production d'énergie brute de l'expanseur, connaissant la carte du rendement isentropique total de l'expanseur ($\eta_{tot,exp}$) et la pression à la sortie de la machine d'expansion (Fig. C.7).

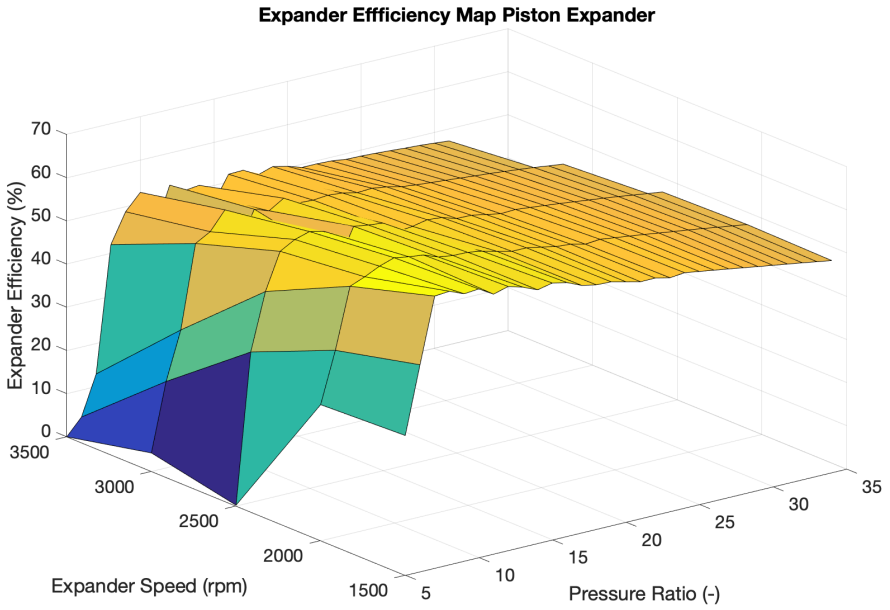

Figure C.7 – Efficacité totale du expanseur en fonction du rapport de pression et de la vitesse du expanseur.

$$\dot{W}_{gross,exp} = \dot{m}_{wf}(h_{su,exp}(T_{wf,su,exp}, p_{wf,su,exp}) - h_{ex,exp}(T_{wf,ex,exp}, p_{wf,ex,exp})) \tag{C.11}$$

Le modèle de turbine reçoit en entrée le bus de fluide de travail en sortie de l'évaporateur et le débit massique, la vitesse de la turbine et la pression de refoulement de la turbine; il fournit en sortie le fluide moteur à la sortie de la turbine, le rendement de la turbine et la puissance produite. Les turbines à flux axial et radial appartiennent à la catégorie des turbo-expanseurs. Ils peuvent être utilisés de manière efficace lorsque le conditionnement représente l'une des principales contraintes et qu'une simplification est nécessaire (car ils ne nécessitent généralement pas de boucle de lubrifiant,

Latz et al. 2013). La vitesse de rotation plus élevée, par rapport aux expanseurs à déplacement positif, complique la composition directe de la courroie avec la transmission du véhicule; par conséquent, les turbines sont plus appropriées pour une connexion directe au générateur électrique.
Le modèle de turbine peut être implémenté en considérant la constante caractéristique de la turbine K_{eq}, appelée constante de Stodola, qui caractérise le débit massique du fluide moteur à travers la turbine. (C.12), également reporté dans Vaja and Gambarotta 2010, peut être utile pour déterminer la pression p_{su} du fluide de travail à l'entrée de la turbine, une fois la conception de la turbine définie.

$$K_{eq} = \frac{\dot{m}_{wf}}{\sqrt{\rho_{su} p_{su} [1 - (\frac{1}{\epsilon})^2]}} \tag{C.12}$$

où ϵ est le rapport entre la pression d'entrée et de sortie de la turbine.

De même que l'expandeur à déplacement positif (2.18), la production d'énergie de la turbine $\dot{W}_{turb}$ est calculée au moyen d'un tableau indiquant le rendement isentropique de la turbine, qui, en première approximation, est défini sur une valeur constante.
Pour conclure, il est important de noter que, pour l'application actuelle, la vitesse de rotation de la turbine N_{turb} n'a pas d'influence pertinente sur la pression à son entrée, donc le contrôle de la vitesse de la turbine peut avoir, comme seulement objectif, maximiser le rendement de la machine elle-même ou du couplage entre la machine et la machine électrique éventuellement couplée à la turbine.

Le modèle de condenseur indirect reçoit en entrée le bus de fluide de travail à la sortie du expanseur et le débit massique ainsi que la température du liquide de refroidissement et le débit massique à l'entrée du condenseur; il fournit en sortie le bus de fluide de travail à la sortie du condenseur et la température du liquide de refroidissement à la sortie du condenseur.
Le condenseur indirect est un échangeur de chaleur à plaques qui utilise l'eau de refroidissement du dissipateur thermique. De tels échangeurs de chaleur consistent en un certain nombre de plaques brasées empilées les unes sur les autres; afin d'augmenter la surface d'échange thermique et la turbulence de l'écoulement, différents modèles d'ondulations ont été conçus par les fabricants. L'ondulation en chevron, caractérisée par l'angle d'inclinaison et un motif sinusoïdal par rapport au sens d'écoulement principal, est certainement la plus courante de nos jours (Martin 1996). L'utilisation de ce composant, intégré au système Rankine, conduit à la nécessité de disposer d'une boucle glycol-eau supplémentaire qui doit être refroidie au moyen du radiateur principal du système de refroidissement du véhicule.
Le modèle de récupérateur reçoit en entrée le bus de fluide de travail à la sortie de la pompe (flux froid) et du expanseur (flux chaud), ainsi que le débit massique du fluide de travail; il fournit en sortie le bus de fluide de travail à la sortie du récupérateur du côté froid et du côté chaud.
Le récupérateur (également appelé régénérateur) est un échangeur de chaleur de base, souvent un échangeur de chaleur à plaques, utilisé pour récupérer partiellement la chaleur d'un flux de fluide chaud et la transférer vers un flux de fluide froid. L'utilisation de ce composant peut conduire à une augmentation de l'efficacité thermique du système Rankine, en conséquence de la chaleur réduite qu'il est nécessaire d'évacuer du condenseur (même si une chaleur plus faible est récupérée dans l'évaporateur en raison d'un température du fluide de travail à l'entrée de l'évaporateur). L'intérêt qu'il est possible d'obtenir est fonction de la chaleur effectivement récupérée, qui change fortement avec la nature du fluide de travail.
Le modèle du récupérateur est un modèle 0D, car une conception claire et un prototype d'un tel composant ne sont pas disponibles aujourd'hui. La puissance thermique récupérée par le flux de fluide de travail dans le côté froid du récupérateur est définie comme une fraction de la puissance thermique disponible du flux de fluide de travail dans le côté chaud, calculée comme la puissance

thermique qui doit être retirée du fluide pour l'amener à l'état de vapeur saturée. Au moyen d'un bilan thermique et de l'ajustement des données préliminaires du fournisseur, l'enthalpie à la sortie du récupérateur (entrée de l'évaporateur) est trouvée.

C.3 Sélection du fluide de travail et contrôle basé sur modèles dynamiques

Dans le cadre du développement de la technologie de récupération de chaleur résiduelle basée sur Rankine pour les poids lourds du groupe Volvo, plusieurs architectures ont été étudiées au cours des années précédentes. Grelet 2016 a étudié 4 architectures différentes en fonction des sources de chaleur résiduelle utilisées : récupération à partir du flux de gaz d'échappement uniquement, flux EGR uniquement, utilisation combinée du flux d'échappement et du flux EGR dans un schéma parallèle et série. Cette analyse montre que l'utilisation combinée de ces deux sources de chaleur dans un modèle parallèle a le critère de performance le plus élevé. Récemment, l'utilisation des sources de chaleur combinées n'a plus été la cible, notamment en raison de l'emballage et du coût; ces aspects sont universellement considérés parmi les principaux problèmes pour la mise en œuvre du système Rankine dans le véhicule (Hountalas et al. 2012, Yang et al. 2018), car l'utilisation d'une source de chaleur supplémentaire implique l'installation d'un échangeur de chaleur supplémentaire et tuyaux et, par conséquent, des coûts croissants. Par conséquent, la présente analyse se concentre sur l'utilisation de la seule énergie de flux d'échappement comme source de chaleur unique, ce qui entraînera une baisse des performances, mais, dans le même temps, des problèmes d'emballage et des coûts limités.

La première architecture étudiée (présentée sur la Fig. C.8) utilise un condenseur direct en aluminium, refroidi par l'air fourni par un ventilateur à entraînement électrique (le modèle du système représenté par le condenseur direct et le ventilateur entraîné est présenté dans la Sec. 2.6) et un échangeur de chaleur supplémentaire, récemment appelé récupérateur. Ce composant supplémentaire est utilisé pour préchauffer le flux de fluide de travail en sortie de la pompe d'alimentation, en exploitant la puissance thermique excessive du flux de fluide de travail en sortie de la machine d'expansion. L'utilisation du récupérateur réduit la puissance thermique qui doit être évacuée du condenseur; une partie de la puissance thermique excessive est donc «recirculée» vers le côté haute pression du cycle de Rankine et elle est utilisée pour générer une puissance supplémentaire. Les autres composants sont une pompe d'alimentation, un évaporateur à plaques et ailettes et une machine à expansion volumétrique. Cette architecture est intéressante pour un développement ultérieur, car elle n'a aucun impact sur le bon fonctionnement du système de refroidissement et l'arbre de détente est directement connecté au générateur électrique, évitant toute connexion avec la transmission mécanique du véhicule. Il est important de noter que le condenseur et le ventilateur dédié ne sont pas placés sur la face avant du véhicule, mais sur un côté du véhicule; on suppose qu'aucun flux d'air RAM n'est admis à l'entrée du condenseur et que le refroidissement du système est entièrement demandé aux ventilateurs à entraînement électrique.

La seconde architecture (présentée sur la Fig. C.9) diffère de la première car elle utilise, à la place du condenseur direct et des ventilateurs dédiés, un condenseur indirect en acier inoxydable (modèle en Sec. 2.7), refroidi par eau, circulant dans une boucle basse température au moyen d'une pompe à liquide de refroidissement Rankine supplémentaire. Comme déjà mentionné, cette configuration implique l'utilisation d'un radiateur basse température (LT) supplémentaire dans la face avant du camion qui a pour rôle de réduire la température de l'eau de refroidissement Rankine, au moyen de l'air d'admission RAM et, dans les phases caractérisées par une charge thermique élevée, le ventilateur du système de refroidissement. Le radiateur LT, dans l'architecture Rankine à condensateur indirect, est positionné entre le refroidisseur d'air de suralimentation (CaC) et le radiateur haute

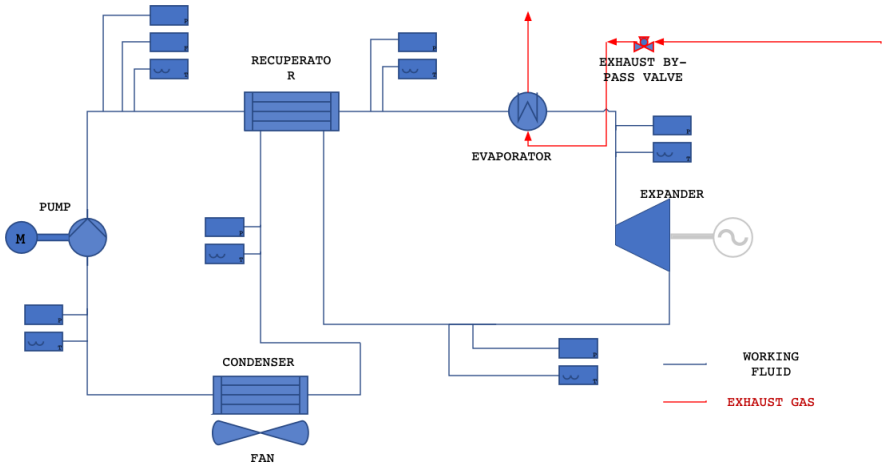

Figure C.8 – Disposition de l'architecture Rankine à condensateur direct, caractérisée par une solution totalement indépendante pour la phase de condensation; le condenseur et le ventilateur dédié sont placés d'un côté du véhicule.

température (HT), définissant le nouveau pack de refroidissement du système de refroidissement. Cette configuration conduit à une réduction de l'énergie nécessaire au refroidissement du système Rankine, car il utilise l'air d'admission de la RAM comme dissipateur thermique pour l'élimination de la chaleur excessive, sans aucune consommation d'énergie supplémentaire dans la plupart des points de fonctionnement; d'autre part, cela implique la modification du système de refroidissement habituel du véhicule ainsi que des problèmes liés à l'emballage.

Afin d'évaluer le potentiel des deux architectures, la puissance de l'expanseur produite, ainsi que la demande de puissance de la pompe et la puissance nécessaire à fournir pour éliminer la chaleur excessive dans le condenseur sont calculées. La puissance brute du expanseur est la puissance électrique produite par le expanseur et prend en compte les pertes liées à la machine et la transformation de l'énergie mécanique en énergie électrique et de la puissance de la pompe. La demande de puissance de refroidissement est la puissance électrique nécessaire pour refroidir le système :

- Pour l'architecture Rankine du condenseur direct, la demande de puissance de refroidissement est la demande de puissance électrique des ventilateurs qui fournissent le flux d'air au condenseur
- Pour l'architecture Rankine du condenseur indirect, la demande de puissance de refroidissement est la demande de puissance électrique de la pompe de circulation de refroidissement; selon la conception du système de refroidissement et le type de cycle routier, le ventilateur principal du système de refroidissement pourrait être engagé pour faire face aux transitoires de charge élevée, entraînant une consommation d'énergie plus élevée pour refroidir le système

Pour les deux architectures, des simulations en régime permanent ont été réalisées (les simulations ont un rôle clé pour évaluer le potentiel des différentes architectures Rankine et du fluide de travail, car la réalisation de campagnes expérimentales intensives n'est souvent pas possible dans l'industrie) dans l'ensemble de la carte moteur.

L'un des sujets majeurs qui a impliqué les chercheurs de la communauté scientifique du cycle de Rankine organique est la sélection des fluides de travail. Comme déjà mentionné dans la Sec. 1.3, la sélection du fluide de travail est spécifique pour chaque application et un fluide de travail optimal universel pour chaque configuration de Rankine n'a pas encore été identifié (Stijepovic et al., 2012).

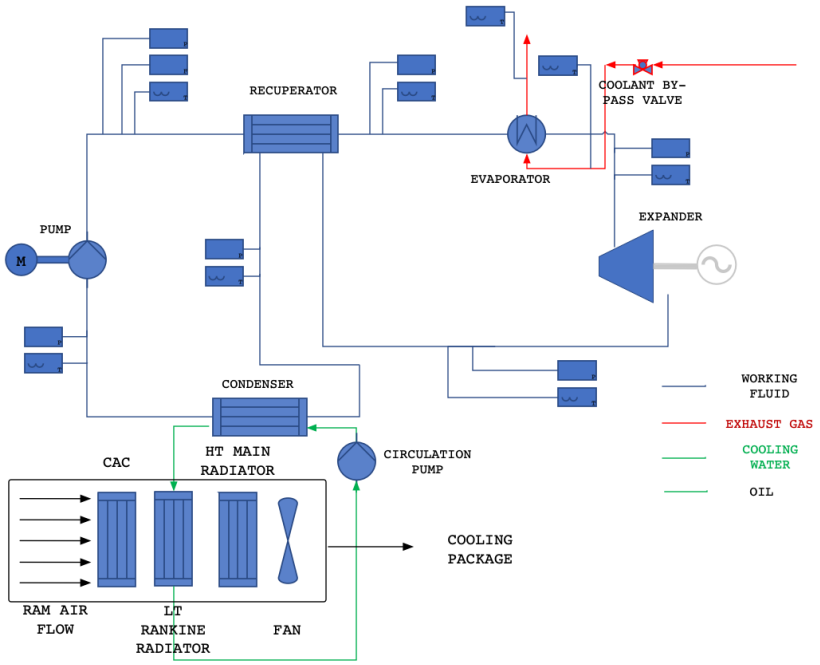

Figure C.9 – Disposition de l'architecture Rankine du condenseur indirect, caractérisée par une boucle de refroidissement supplémentaire pour le système Rankine et, par conséquent, un radiateur basse température supplémentaire dans le groupe de refroidissement.

Cela implique que pour chaque configuration de système et objectif de performance, la procédure de sélection de fluide fournit des résultats différents. Pour les deux architectures Rankine de Sec. 3.1, un premier criblage sur les fluides de travail disponibles pour l'application actuelle est réalisé à partir de la littérature, conduisant à l'éthanol, au R1233zd, au Novec649 et au cyclopentane comme quatre fluides de travail à étudier. Les résultats de l'analyse dans Preißinger et al. 2017 montrent que l'éthanol est le fluide le mieux classé dans l'ensemble car il est applicable à tous les points de fonctionnement étudiés et, dans le même temps, il n'est pas toxique et n'a pas de GWP. Le R1233zd et le Novec649 ont des performances thermodynamiques similaires et un GWP inférieur par rapport au R245fa, qui est considéré comme une référence courante, mais il est caractérisé par un GWP de 1030. Marlok et al. 2019 montre l'avantage d'utiliser le cyclopentane à la place de l'éthanol dans un condenseur en aluminium, il a donc été ajouté dans l'analyse actuelle. Les quatre fluides de travail, ainsi que leurs principales caractéristiques, sont répertoriés dans le Tab. C.1.

Fluide	Type	Point d'ébullition (°C)	$\Delta H_{vap}(\frac{kJ}{kg})$	$P_{crit}(bar)$
Cyclopentane	Dry	49	389	45.15
Ethanol	Wet	78	850	61.48
*Novec*649	Dry	49	88	18.69
*R*1233*zd*	Dry-Isentropic	14	195	36.23

Table C.1 – Principales caractéristiques des différents fluides.

Comme il est possible de le remarquer à partir de la Tab. C.1, les fluides de travail peuvent être comparés au préalable en fonction de la pente de la courbe de vapeur saturée (type), du point d'ébullition, de la chaleur latente de vaporisation et du point critique.
L'utilisation d'éthanol sur des composants en aluminium conduit à la corrosion, dans des conditions de fonctionnement comparables aux valeurs de pression et de température qu'il est possible

de rencontrer lors de la condensation de l'éthanol. Pour cette raison, la sélection du fluide de travail, dans le cas d'une architecture à condensation directe, est limitée au cyclopentane, Novec649 et R1233zd. Le fluide R1233zd est pénalisé en raison de la pression de condensation élevée qui a été réglée afin d'assurer une condensation complète du fluide de travail, impactant de manière dramatique la production d'énergie de la machine d'expansion. Le fluide Novec649 est également pénalisé en raison de sa faible pression critique (16 bars). Une remarque importante sur l'utilisation du Novec649 est qu'il semble plus adapté aux sources de chaleur thermique de faible qualité; cette déclaration sera vérifiée au Chap. 4, où les performances du Novec649 et du R1233zd sont comparées dans un système Rankine qui récupère l'énergie du flux de liquide de refroidissement. La Fig. 3.8 montre que le cyclopentane est le meilleur fluide, en termes de performances, pour cette architecture spécifique; malgré la forte demande de puissance du ventilateur, la puissance nette est plus élevée que l'utilisation des fluides restants, en raison du rapport de pression plus élevé à l'entrée et à la sortie du expanseur qu'il est possible d'atteindre. Novec649 et R1233zd entraînent également une demande de puissance de pompe plus élevée par rapport au cyclopentane, ce qui a un impact sur le bilan énergétique du système Rankine. La même étude peut être réalisée sur l'architecture Rankine caractérisée par la condensation indirecte; dans ce cas, l'éthanol est pris en compte dans l'analyse, car aucun problème de compatibilité des matériaux n'est signalé entre l'éthanol et l'acier inoxydable. Le tableau 3.4 montre une comparaison entre les quatre fluides de travail différents, fonctionnant dans un système de Rankine à condensation indirecte. L'utilisation d'éthanol implique à la pression de condensation la plus basse parmi les fluides de travail analysés en raison du point d'ébullition le plus élevé; Le R1233zd, en raison de son point d'ébullition normal le plus bas, implique une pression de condensation la plus élevée, ce qui a un impact sur la production d'énergie de l'expanseur et, par conséquent, sur la production nette d'énergie. La fig. 3.9 montre que la contribution de la demande de puissance de la pompe de liquide de refroidissement, de la demande de puissance de la pompe d'alimentation et de la puissance brute de l'expanseur pour chaque fluide de travail; le cyclopentane est à nouveau le meilleur fluide en termes de production nette d'énergie, par contre, l'éthanol présente la possibilité de ne pas pressuriser (ou faiblement pressuriser) le côté froid du Rankine, avec des performances comparables au cyclopentane; cet aspect doit être pris en compte, car l'adoption de la pression atmosphérique du côté froid du système Rankine est une forte simplification en termes de contrôle (le contrôle de la pression de condensation n'est pas nécessaire) et d'équipement (la vanne qui régule la pression de l'air sous pression utilisé pour pressuriser le côté froid du système Rankine n'est pas nécessaire).

Dans ce travail, une approche de commande basée sur un modèle linéaire, identifiée à partir des résultats expérimentaux du banc d'essai moteur, est proposée. Comme pour des raisons pratiques, liées au coût et à la disponibilité de la cellule d'essai, il n'est pas possible de manipuler et de tester tous les points de fonctionnement du moteur, une méthodologie de sélection des points de fonctionnement du moteur est également proposée afin de réaliser les expériences qui sont nécessaires pour récupérer les modèles linéaires utilisés pour une conception de commande ultérieure. L'architecture caractérisée par la condensation directe est choisie pour l'implémentation du modèle et de la commande pour la suite du travail.

Une fois les points de fonctionnement à tester trouvés, une campagne expérimentale basée sur des réponses échelons est réalisée dans la cellule de test du site Renault Trucks, Saint Priest, France. La variable manipulée (MV) dans les expériences est la vitesse de la pompe N_{pump}, qui entraîne une modification du débit massique délivré; la variable contrôlée (CV) est une propriété importante dans notre étude : la surchauffe à la sortie de l'évaporateur. La surchauffe $SH_{ex,ev}$ est définie comme la différence de la température du fluide de travail et de la température de saturation correspondant à sa pression à la sortie de l'évaporateur.

Pour un modèle du premier ordre à retard considéré sur chaque point opératoire, le gain statique G change dans un rapport de un à six, tandis que la constante de temps τ et le retard θ changent dans un rapport de un à cinq et de un à deux, respectivement. De plus, le gain et le retard sont assez similaires pour les deux machines de détente, tandis que la constante de temps liée à la deuxième machine de détente est plus élevée: selon le fait que le deuxième expanseur impose une pression plus

faible du côté haute pression du système Rankine, la constante de temps diminue à une pression plus basse. Cela peut amener à un comportement différent de la réponse car SH est fonction de la pression d'évaporation. Cette analyse statistique, montrant les fortes variations des paramètres du modèle le long de la campagne expérimentale, suggère que l'utilisation d'un modèle unique pour une conception de contrôle supplémentaire de la surchauffe à la sortie de l'évaporateur n'est pas appropriée.

Trois contrôleurs différents pour la surchauffe sont utilisés et comparés; le but du contrôleur est de suivre un point de consigne de la surchauffe à l'entrée de l'expanseur et d'assurer une variation douce de l'actionneur (vitesse de la pompe) qui peut indirectement influencer le contrôle d'une autre variable dans le système (par exemple la valeur de consigne de la pression d'évaporation est directement liée au débit massique du fluide de travail). Les trois stratégies comparées dans cette section sont :

- Un régulateur PID, basé sur le modèle FOPTD unique correspondant au point de fonctionnement le plus récurrent (Fig. 3.13), réglé au moyen de la technique de contrôle interne du modèle (IMC)
- Un contrôleur à multiples modèles PID (MMPID), qui a été réglé à l'aide des 37 modèles FOPTD récupérés en Sec. 3.3 et un schéma de pondération qui calcule un ensemble unique de paramètres du modèle (gain statique, constante de temps et retard) à chaque pas de temps à utiliser dans le contrôleur (schéma de pondération bayésien, Aufderheide and Bequette 2003)
- Un contrôleur à multiples modèle PID (MMPID), qui a été réglé à l'aide des 37 modèles FOPTD récupérés en Sec. 3.3 et un schéma de pondération qui a été introduit dans Grelet et al. 2016 pour réduire le nombre de paramètres de réglage (schéma de pondération développé).

Les ensembles de paramètres (gain statique, constante de temps et retard) qui ont été trouvés en appliquant les deux algorithmes au problème de surchauffe sont présentés sur la Fig. 3.20. Les algorithmes bayésien et développé identifient un seul ensemble de paramètres FOPTD qui est calculé en ligne, au moyen du poids $w_{i,k}$, spécifique à chaque estimateur de pondération; dans Fig. 3.6 on trouve l'ensemble équivalent de paramètres G_{eq}, τ_{eq} et θ_{eq}.

C.4 Récupération liquide de refroidissement moteur

La récupération de chaleur perdue disponible dans le flux de liquide de refroidissement dans le système de refroidissement du véhicule représente une partie non négligeable de l'énergie qui n'est pas convertie en énergie utile dans le véhicule et est donc gaspillée. Comme déjà mentionné dans la Sec. 1.2, 22% de l'énergie du camion lourd est gaspillée via le système de refroidissement (en tenant en compte également du refroidisseur EGR). Bien que ce pourcentage soit au peu près équivalent au pourcentage des pertes attribuées aux gaz d'échappement, l'énergie thermique dans le système de refroidissement est disponible à une température plus basse que le débit d'échappement. La source de chaleur est le flux de liquide de refroidissement qui refroidit la chaleur du moteur et éventuellement de l'EGR; la chaleur excessive dans le liquide de refroidissement est évacuée dans un radiateur placé dans la face avant du camion, au moyen du flux d'air RAM. Selon le véhicule et la conception du système de refroidissement et du radiateur lui-même, en cas de charge élevée, le ventilateur du système de refroidissement est activé et fournit un flux d'air supplémentaire au radiateur (dans la section 4.3, les détails du système de refroidissement ainsi que le système Rankine associé sont fournis).

Compte tenu des limites avantageuses de la récupération de l'énergie thermique du flux de fluide caloporteur et, dans le même temps, des simplifications liées aux contraintes thermiques réduites du système et aux régulateurs plus simples, la récupération de chaleur perdue du flux de fluide caloporteur est considérée comme une solution compacte et économique (Leduc et al. 2017). Les avantages de la récupération de l'énergie thermique du flux de liquide de refroidissement, qui ont été présentés amènent à une étude plus approfondie, est réalisée dans ce chapitre au moyen de la mise en œuvre de modèles de simulation et d'expériences.
Une analyse de haut niveau des fluides de travail, qui ont déjà été étudiés dans la Sec. 3.2, met en évidence que l'éthanol ne convient pas à une telle application, car à la température de 90 ° C, il s'évapore à 1.58 bar, réduisant considérablement le rapport de pression disponible mesuré entre l'entrée et la sortie de l'expanseur. Le Novec649 et le cyclopentane s'évaporent à une pression similaire (3.47 et 3.24 bar respectivement), tandis que le R123zd s'évapore à la pression la plus élevée parmi ces candidats, 8.33 bar. Dans le même temps, le R1233zd est caractérisé par le point d'ébullition normal le plus bas; ceci conduit à l'augmentation de la pression à la sortie du expanseur, limitant le rapport de pression.
L'application cible de la récupération de la chaleur résiduelle du liquide de refroidissement du moteur est le transport sur véhicule poids lourd, moteur 13 litres non EGR, 35 tonnes; l'architecture étudiée pour un tel système est illustrée dans la Fig.4.9 et les expériences sont réalisées au Laboratoire de Thermodynamique de l'Université de Liège. Le banc d'essai a été dimensionné en fonction du point de conception (Tab. 4.6) qui a été identifié par IFPEN, sur la base des données fournies par Volvo. Comme un moteur de poids lourd n'est pas disponible pendant la campagne expérimentale, un brûleur électrique à huile est utilisé pour mettre à disposition la source de chaleur caractérisée par le débit massique et les valeurs de température rencontrées dans le système de refroidissement du véhicule de l'application actuelle. Le débit massique et la température de la source de chaleur peuvent être réglés manuellement et mesurés via un débitmètre et un thermocouple T. Des capteurs tels que thermocouples T et des capteurs de pression, ainsi qu'un débitmètre sont utilisés pour mesurer la température, la pression et le débit massique du fluide de travail à l'entrée et à la sortie de chaque composant. L'eau de refroidissement qui circule dans le condenseur est de l'eau courante, disponible dans une plage de température comprise entre 7 et 10 ° C, selon les conditions météorologiques. L'architecture actuelle utilise une pompe d'alimentation centrifuge, un échangeur de chaleur à plaques et ailettes comme évaporateur, condenseur et récupérateur et une turbine d'entrée radiale comme machine de détente. Le récupérateur est contourné, comme il a été constaté expérimentalement, car il impose des chutes de pression trop importantes. Un code LabView a été développé afin d'assurer le contrôle des actionneurs comme la vitesse de la pompe d'alimentation et de visualiser en temps réel les valeurs mesurées dans le système; la vitesse de la pompe est ajustée pour assurer une surchauffe du fluide moteur à l'entrée de la turbine de 5 K. La vitesse de la turbine est contrôlée manuellement via le skid fourni par ENOGIA et l'écran incorporé montre la puissance électrique réelle produite. En fonction des conditions d'utilisation et de l'application et du temps disponible limité pour réaliser les expériences, 11 points de fonctionnement ont été testés; les expériences, en termes de débit massique et de température de la source de chaleur sont listées dans le tableau 4.7; comme on peut le constater, l'injection de la turbine est variée au cours de la campagne expérimentale. Pour un débit volumétrique donné du fluide de travail, la variation de la section d'injection a de l'influence sur la pression à l'entrée de la turbine.

C.5 Optimisation

Dans le chapitre 3, la consigne de pression de condensation a été calculée en fixant le rapport de pression entre l'amont et l'aval de la machine de détente. Ici, une stratégie de commande optimale qui emmène à un compromis entre l'engagement du ventilateur et la pression du côté basse pression du système est présentée. Sur la base d'un modèle de Rankine analytique simplifié,

une optimisation locale est effectuée pour améliorer la puissance nette du système dans deux cycles routiers différents avec des conditions environnementales différentes. Les résultats ont été publiés en 2021 (Galuppo et al. 2021). Le modèle développé aux chapitres 2 et 3 est considéré comme une référence de système physique (le modèle est validé et peut remplacer des essais routiers coûteux) et un modèle réduit est mis en œuvre afin d'évaluer la fonction objectif de l'optimisation comme fonction quadratique, avec contraintes quadratiques. Dans un premier temps, le modèle réduit est validé selon le modèle complet et un problème d'optimisation basé sur un modèle local est développé pour générer la valeur de pression de condensation appropriée et le point de consigne de sous-refroidissement optimal. Dans le Tab. 5.1, les signaux contrôlables sont répertoriés, avec les limites supérieures et inférieures correspondantes et le type de contrôleur utilisé pour chaque actionneur. La pompe d'alimentation et la vitesse de l'expanseur sont contrôlées par le contrôleur présenté au Chap. 3, tandis que la pression de condensation et le contrôle de la vitesse du ventilateur font l'objet de l'optimisation en temps réel qui est mise en œuvre dans cette section et s'adresse au contrôle optimal de la basse pression. La fonction objectif de l'optimisation est donnée par (5.2). Le modèle analytique simple qui doit être développé est la base pour l'optimisation qui a comme but celui d'améliorer la puissance nette du système, par rapport à un ensemble de résultats de base défini, consommant peu de mémoire et fonctionnant en temps réel. Afin d'assurer cette tâche, le modèle a été développé via des équations de bilan énergétique; les coefficients utilisés dans les fonctions d'ajustement sont constants et présentés à l'annexe B. L'approche proposée est de calculer chaque terme de la fonction objectif (5.2) puis de rassembler les équations. Les chutes de pression dans la boucle de fluide de travail sont négligées, par conséquent la pression mesurée à l'entrée de la machine de détente et de la pompe est considérée comme la pression pour l'ensemble du côté haute pression et basse pression respectivement.
Une fois que les équations du modèle et les contraintes sont toutes définies, il est possible de définir que le problème d'optimisation d'une fonction quadratique J soumise à des contraintes d'inégalité quadratique (C.13) .

$$J = \min_{u}(\frac{1}{2}u^T Q u + f^T u + c), \tag{C.13}$$

Avec les contraintes (C.14).

$$\frac{1}{2}u^T H_i u + k_i^T u + D_i \leq 0. \tag{C.14}$$

L'étude sur l'amélioration de la production nette d'énergie du système est réalisée en considérant deux cycles routiers, correspondant à deux types de missions différents. Tab.3.10 souligne que les cycles routiers FK et CC représentent deux types de missions très différents. Comme la température de l'air à l'entrée du condenseur dépend de la vitesse du véhicule (pour détails Tab. 3.11), il est nécessaire d'appliquer l'algorithme d'optimisation et de fournir une interprétation des résultats des deux cycles routiers. Pour les deux cycles routiers, 3 valeurs de température ambiante constante de 0, 20, 40 ° C ont été prises en compte et l'algorithme d'optimisation est exécuté pour l'ensemble des cycles routiers; les résultats sont comparés aux résultats de simulation caractérisés par une pression de condensation constante et une pression de condensation calculée imposant un rapport de pression optimale. Le temps d'échantillonnage du calcul faisant intervenir l'algorithme d'optimisation est de 0.3 seconde; ce choix a réduit le temps de calcul sans affecter la précision de la solution. Le problème d'optimisation est résolu, en moyenne, en 0.12 seconde à l'aide d'un MacBook Air, d'un processeur Intel Core i5 1.6 GHz, d'une mémoire RAM de 8 Go.
La figure 5.5 montre le comportement des deux actionneurs impliqués dans l'algorithme d'optimisation sur le cycle routier FK, pour chaque température ambiante, en considérant la référence (pression de condensation calculée imposant un rapport de pression constant optimal) et la stratégie optimisée; en analysant la figure, il est possible de constater que le compromis entre l'utilisation des deux actionneurs diffère selon la température ambiante. Quant à la température ambiante de 0 et 20 ° C, la stratégie optimisée impose une utilisation plus forte du ventilateur par rapport à la pressurisation du côté condensation du système par rapport à la référence; quant à la température ambiante de 40 ° C, la stratégie optimisée impose une pressurisation plus forte du côté condensation du système par

rapport à la référence. Ce résultat est physiquement logique, car pour une température plus élevée de l'air à l'entrée du condenseur, l'échange thermique dans le condenseur est moins performant et il est plus pratique de pressuriser le côté condensation du système. Les résultats sont confirmés en utilisant le cycle routier CC, mais, compte tenu de la nature du cycle routier, qui impose une faible vitesse du véhicule, la température du flux d'air à l'entrée du condenseur est toujours supérieure aux valeurs rencontrées dans le cycle routier FK, par conséquent la stratégie optimisée impose toujours une augmentation de la pression de condensation et une réduction de la vitesse du ventilateur par rapport à la référence.
La figure 5.6 montre les résultats de l'analyse d'optimisation utilisant le cycle routier FK, pour différentes températures ambiantes annoncées. La figure 5.6 (en haut) montre la comparaison par rapport à la référence caractérisée par une pression de condensation constante, qui est fixée à 2,5 bar, tandis que la figure 5.6 (en bas) montre la comparaison par rapport à la référence caractérisée par la pression de condensation calculée par rapport à un rapport de pression optimal. La stratégie optimisée améliore toujours la puissance de sortie nette; dans le cas de $T_{amb} = 20$ ° C, par rapport à la pression de condensation calculée imposant un rapport de pression optimal, l'amélioration est très faible; dans tous les autres cas, l'amélioration est significative. La stratégie de pression de condensation constante est loin d'être optimisée car la pression de condensation pourrait être réduite dans les phases du cycle routier caractérisées par des régimes bas et donc améliorer la production nette d'électricité. Les résultats confirment en outre que l'architecture de condensation directe actuelle, utilisant le cyclopentane comme fluide de travail, doit inclure le contrôle de la pression de condensation pour atteindre un niveau de performance plus élevé.
La figure 5.7, en plus, montre les résultats globaux exécutant la stratégie optimisée dans le cycle routier CC, mettant en évidence le fait que le pourcentage de l'amélioration de la puissance nette dans le cycle routier CC est plus élevé par rapport au FK. En effet, compte tenu du même rapport de pression optimal utilisé dans le cycle FK, la pression de condensation obtenue dans le cycle routier CC est plus faible, en raison de la pression d'évaporation plus faible, ce qui fait que le cycle routier est caractérisé par une puissance thermique récupérée plus faible. Cela implique que la condensation est obtenue via l'action du ventilateur, qui fournit de l'air plus chaud par rapport au cycle routier FK, du fait que la vitesse du véhicule dans le cycle CC route est réduite. La méthodologie proposée améliore la puissance nette produite par le cycle routier FK. En effet, le pourcentage de l'amélioration nette de la puissance est de 13.4% avec le cycle routier CC et $T_{amb} = 20$ ° mais, il est de 0.5% avec le cycle routier FK et $T_{amb} = 20$ ° C. Compte tenu de l'amélioration sensible qu'il est possible d'obtenir avec cette méthodologie, notamment en cas de conditions de conduite qui s'éloignent de la mission habituelle d'un poids lourd long-courrier (urbain au lieu d'un cycle routier) et de températures ambiantes plus extrêmes (0 °C ou 40°C au lieu de 20°C), l'utilisation des stratégies qui ont été présentées est fortement recommandée. De plus, l'algorithme peut fonctionner en temps réel et peut être facilement implémenté dans le contrôleur embarqué. En revanche, un effort particulier doit être consacré à l'étalonnage du modèle analytique simplifié, pour tenir compte de la température de l'air à l'entrée du condenseur. Dans les sections précédentes de cette thèse, il a été constaté que les performances de l'architecture de condensation directe, utilisant le cyclopentane comme fluide de travail, est fortement impactée par le côté froid du système. La section actuelle montre qu'un meilleur compromis peut être trouvé entre l'action des deux actionneurs impliqués dans la commande de sous-refroidissement, la vitesse du ventilateur N_{fan} et la pression de p_{cond}; en particulier, le compromis est influencé par la température de l'air ambiant et, par conséquent, la température de l'air de refroidissement à l'entrée du condenseur. Plus la température de l'air de refroidissement est basse, plus la vitesse du ventilateur est élevée et, par conséquent, plus la pression de condensation doit être réglée. La solution du problème d'optimisation apporte une amélioration de la puissance nette, par rapport aux résultats obtenus en utilisant une pression de condensation variable selon une pression fixe PR, dans toutes les conditions ambiantes considérées et dans les deux cycles routiers qui ont été pris en compte (FK autoroute et cycle routier urbain CC), les résultats répondent donc aux attentes annoncées au début de ce chapitre.

C.6 Conclusion

La technologie de récupération de la chaleur perdue basée sur cycle de Rankine Organique a attiré des nombreux chercheurs dans la dernière décennie, suivie de l'intérêt industriel croissant de la technologie. La nouvelle législation européenne concernant l'émissions de CO_2 des véhicules poids lourd a accéléré la nécessité de mettre en œuvre des solutions appropriées pour réduire la consommation de carburant et, par conséquent, la nouvelle limite d'émission en 2025. Dans nos jours, plus que dans le passé, l'intégration du système sans le véhicule, ainsi que son coûts, est crucial pour une commercialisation future de la technologie, la majeure partie de l'industrie s'intéresse à une solution compacte qui implique l'utilisation d'une seule source de chaleur. La récupération du gaz d'échappement est toujours considérée comme la source de chaleur préférée pour un système de récupération de chaleur perdue dans les camions lourds, car il contient 22% de l'énergie de carburant d'origine à la température entre-entre environ 250 et 450 ° C (à l'exception du turbo-compound, caractérisé par une réduction de la température du gaz d'échappement, qui implique une réduction de l'efficacité du cycle de Rankine), qui peut fournir entre 3 et 4 kW de la production moyenne moyenne de puissance nette dans le cycle routier de l'autoroute. Cependant, l'utilisation d'autres sources de chaleur, comme le flux EGR et le flux de liquide de refroidissement, est toujours exploré: la récupération de l'énergie perdue dans le flux de liquide de refroidissement peut notamment entraîner une solution convenable, qui peut apporter entre 1 et 1,5 kW de la production de puissance nette moyenne dans le cycle routier à grande échelle. Les contributions présentées dans cette thèse sont consacrées à l'utilisation de flux de gaz d'échappement et de liquide de refroidissement comme source de chaleur unique d'un système de récupération de chaleur perdue basé sur Rankine, dans un moteur long-courrier robuste, moteur non-EGR. Pour la récupération de la chaleur perdue de flux de gaz d'échappement, deux architectures différentes ont été examinées; une architecture de condensation directe caractérisée par une solution qui évacue la chaleur du condenseur à l'aide de ventilateurs à entraînement électrique et une solution indirecte, qui utilise une pompe d'eau supplémentaire et un radiateur dans une pièce séparée. Pour les deux architectures, une sélection de fluide de travail a été effectuée, sur la base de la compatibilité et de la compatibilité des performances. Le cyclopentane et l'éthanol ont été sélectionnés pour l'architecture directe et indirecte respectivement. La thèse se concentre sur les problèmes de contrôle et d'intégration rencontrés dans l'architecture directe, choisie comme architecture pour la suite de l'étude, grâce à l'absence d'impact du rejet de chaleur dans le système de refroidissement du véhicule. Cette fonctionnalité a récemment gagné une grande importance, car elle permet l'intégration du système Rankine sans modification du système de refroidissement du véhicule, il convient donc à une installation plus facile du véhicule. Une importance particulière est donnée au contrôle de la surchauffe et du sous-refroidissement; dans les deux cas, l'utilisation d'un contrôleur unique, avec un seul ensemble de paramètres, n'est pas suffisant, en raison de la variabilité large des paramètres du modèle linéaire localement considéré de la surchauffe et du sous-refroidissement, en ce qui concerne la pompe et la vitesse du ventilateur respectivement. De plus, il a été mis en évidence que la manipulation de la pression de condensation est nécessaire à l'utilisation du cyclopentane dans l'architecture de condensation directe, en raison de la différence de température limitée entre les profiles de température de chaleur et de température du fluide. La possibilité de manipuler la pression de condensation et de l'utiliser comme une variable supplémentaire est cruciale pour mieux exploiter le potentiel de la source de chaleur et limiter l'optimisation de la vanne de by-pass en raison d'une capacité de refroidissement réduite. De plus, l'impossibilité de manipuler la pression de condensation conduit à des valeurs extrêmement élevées de sous-refroidissement dans des phases de charge faibles (dans ces phases, la pression de condensation doit être réduite) et, par conséquent, à une production de puissance de plus basse. Dans la récupération des gaz d'échappement, le vitesse du ventilateur et la pression de condensation sont les deux variables manipulées utilisées afin de contrôler le sous-refroidissement. La vitesse du ventilateur est la variable manipulée d'un contrôleur MMPID, la condensation, comme première approche, est manipulée en imposant un rapport de pression constant entre l'entrée et la sortie de

l'extension. Cette solution assure le suivi du point de consigne du sous-refroidissement, mais, en termes de puissance nette produite, elle peut ne pas représenter la meilleure solution. En deuxième approche, un problème d'optimisation, basé sur un modèle analytique simplifié, est résolu, afin de trouver une pression de condensation optimale en temps réel. Les résultats montrent que, en ce qui concerne la température ambiante de 0 et 20 ° C, la stratégie optimale suggère d'augmenter la vitesse du ventilateur et de réduire la condensation par rapport aux résultats de la première approche. Pour ce qui concerne la température ambiante de 40 ° C, la stratégie optimale suggère de réduire la vitesse du ventilateur et d'augmenter la pression de condensation avec les résultats de la première approche. Dans la récupération de la chaleur de refroidissement du moteur également, la manipulation de la pression de condensation est nécessaire car réduit l'utilisation du ventilateur du système de refroidissement, caractérisée par une grande consommation d'énergie à haute puissance, même à une vitesse de rotation faible. L'utilisation de la variable manipulée de condensation assure le suivi approprié du point de consigne de sous-refroidissement, réduit la prise en charge du ventilateur du système de refroidissement et empêche la production de systèmes d'alimentation.
Compte tenu du niveau de maturité que la technologie a gagné au cours des dernières années et le besoin imminent de solutions pouvant contribuer à la satisfaction des nouvelles émissions de la législation européenne des camions, des tests sur le véhicule et le cycle routier réel devraient être augmentés. La stratégie de contrôle a été mise en œuvre devrait être vérifiée dans divers circuits routiers et situations de circulation possibles, afin de garantir les conditions de fonctionnement appropriées de l'ORC et, dans le même temps, garantir la plus haute production d'énergie possible pendant les missions. De plus, l'introduction d'ECU plus performantes pourrait ouvrir l'utilisation à des contrôleurs plus complexes qui sont censés améliorer les performances avec des perturbations élevées rencontrées lors des missions du véhicule.
De plus, la fiabilité et la durabilité des composants, ainsi que la compatibilité des matériaux, devraient être vérifiées attentivement : les composants testés de nos jours sont des prototypes et ont besoin d'un développement plus poussé pour être portés à l'état de production en série. Une attention particulière devrait être accordée à la sécurité, car les fluides de travail organiques (comme le cyclopentane et l'éthanol) sont très inflammables. Différents scénarios d'accidents doivent être étudiés afin de mettre en place des mesures de sécurité pour éviter les incendies, l'explosion et, en général, la libération incontrôlée du fluide à haute pression et haute température. Le poids et le temps de développement sont d'autres aspects qui sont particulièrement importants dans le contexte industriel.
Pour conclure, le principal défi des fabricants est de développer un système ORC sans danger, avec un rapport d'utilisation élevé, réduisant ainsi le coût total de la propriété (TCO) du véhicule, afin d'être une solution précieuse qui diminue les dépenses liée au carburant par le propriétaire du véhicule et donc diminue l'impact sur l'environnement.